Green Energy and Technology



Integrated Absorption Refrigeration Systems

Comparative Energy and Exergy Analyses



Green Energy and Technology

More information about this series at http://www.springer.com/series/8059

Ibrahim Dincer Tahir Abdul Hussain Ratlamwala

Integrated Absorption Refrigeration Systems

Comparative Energy and Exergy Analyses



Ibrahim Dincer
Department of Automotive, Mechanical and Manufacturing Engineering
University of Ontario Institute of Technology
Oshawa, ON
Canada

Tahir Abdul Hussain Ratlamwala Department of Mechatronics Engineering Shaheed Zulfikar Ali Bhutto Institute of Science and Technology Karachi, Sindh Pakistan

ISSN 1865-3529 Green Energy and Technology ISBN 978-3-319-33656-5 DOI 10.1007/978-3-319-33658-9 ISSN 1865-3537 (electronic)

ISBN 978-3-319-33658-9 (eBook)

Library of Congress Control Number: 2016938410

© Springer International Publishing Switzerland 2016

This work is subject to copyright. All rights are reserved by the Publisher, whether the whole or part of the material is concerned, specifically the rights of translation, reprinting, reuse of illustrations, recitation, broadcasting, reproduction on microfilms or in any other physical way, and transmission or information storage and retrieval, electronic adaptation, computer software, or by similar or dissimilar methodology now known or hereafter developed.

The use of general descriptive names, registered names, trademarks, service marks, etc. in this publication does not imply, even in the absence of a specific statement, that such names are exempt from the relevant protective laws and regulations and therefore free for general use.

The publisher, the authors and the editors are safe to assume that the advice and information in this book are believed to be true and accurate at the date of publication. Neither the publisher nor the authors or the editors give a warranty, express or implied, with respect to the material contained herein or for any errors or omissions that may have been made.

Printed on acid-free paper

This Springer imprint is published by Springer Nature
The registered company is Springer International Publishing AG Switzerland

Preface

Originally, humankind used wood as their fuel source fuel and later discovered fossil fuels, bringing about the industrial revolution as a starting point of technology developments. Since then, humankind has striven for greater prosperity and better wealth.

Energy-hungry devices, ranging from airplanes to mobile phones, are introduced to the consumers at a brisk rate to meet their perceived need for better lifestyle need. The extensive use of fossil fuels has been influential in changing the weather patterns and climatic cycles, due to the enormously increasing CO_2 emissions, resulting in harsher summers and winters around the globe. The earth's average temperature has constantly been increasing at a constant rate over the past few decades due to the extensive use of fossil fuels. The use of air-conditioning systems for the provision of heating and cooling has also increased due to the harsher climates with the drawback of a dependency on the energy-hungry technology. This increase has resulted in a sudden surge in peak electricity demand and government and private sector alike are unable to meet this demand. Extensive fossil fuel usage and environmental problems have drawn researcher focus to new refrigeration technology that can offset the use of fossil fuels and provide heating and cooling in a comparatively environmentally friendly manner.

The current book presents an overview of all the alternative refrigeration technologies that are either available on the market or are in the research phase, with a focus on an absorption refrigeration systems. An absorption refrigeration system is an attractive alternative to the conventional air-conditioning system, as it is mainly waste heat or low-grade heat dependent. However, as with all other technologies, absorption refrigeration systems also have some drawbacks that cannot be ignored.

The present book consists of eight chapters. Absorption refrigeration system background, components, operating principles, usage, and fundamentals are presented in Chap. 1. Also, the comparison of absorption refrigeration systems with other innovative refrigeration systems is presented in this chapter. Chapter 2 aims at helping the reader understand how to perform an in-depth energy, exergoeconomic, exergoenvironmental, and optimization analyses of a basic absorption

vi Preface

refrigeration system. Detailed system description, energy, exergy, exergoeconomic, exergoenvironmental, and optimization studies of the single effect absorption refrigeration system with numerical values are presented in Chap. 3. Chapter 4 offers comprehensive system description alongside numerical energy, exergy, exergoeconomic, exergoenvironmental, and optimization analyses of the double effect absorption refrigeration system. A thorough system description of more advanced triple effect absorption refrigeration system with numerical energy, exergy, exergoeconomic, exergoenvironmental, and optimization analyses is presented in Chap. 5. The system description with numerical energy, exergy, exerging exerging the system of the syste goeconomic, exergoenvironmental, and optimization studies of the most advanced and novel quadruple effect absorption refrigeration system is provided in Chap. 6. Chapter 7 presents different case studies related to the integrated absorption refrigeration system. This chapter also presents analysis and results of the multigeneration systems shedding light on the usage of absorption refrigeration systems in different walks of life. Chapter 8 highlights recent developments in an area of absorption refrigeration systems. Also presented in this chapter are different energy sources based absorption refrigeration systems, novel designs, advanced numerical and optimization models, and unique working mixtures of the absorption refrigeration systems.

Detailed references are provided to direct the readers that require more information in the correct direction. We sincerely hope that this book provides an in-depth knowledge in the area of absorption refrigeration systems so that the world can move towards more environmentally friendly, cost-efficient, and sustainable heating and cooling technologies in near future. The book is written in a way that it can be helpful to undergraduate students, postgraduate students, as well as people requiring advanced knowledge, governmental organizations, and industries alike.

Ontario, Canada Sindh, Pakistan Ibrahim Dincer Tahir Abdul Hussain Ratlamwala

Acknowledgments

We are greatly thankful to our parents, Hasan Dincer and Fatma Dincer, and Abdul Hussain Ratlamwala and Nafisa Abdul Hussain Ratlamwala, and our wives, Gulsen Dincer and Zahrah Tahir, and our children Meliha, Miray, Ibrahim Eren, Zeynep and Ibrahim Emir Dincer, and Amatullah Tahir. Tahir Abdul Hussain Ratlamwala would also like to thank his siblings, Hussain Abdul Hussain, Naquiya Abdul Hussain, and Fatima Abdul Hussain, and in-laws Yousuf Ezzi, Tasneem Ezzi, Fatima Ezzi and Amatullah Ezzi. They have been extremely patient, supportive, and motivating throughout the book writing process and we greatly appreciate it.

Contents

1	Fund	amental	s of Absorption Refrigeration Systems	1
	1.1	Introdu	ction	1
	1.2	Absorp	tion Process	2
	1.3	Absorb	ents and Refrigerants	2
	1.4	Classifi	cation of Absorption Refrigeration Systems	4
	1.5	Compo	nents of Absorption Refrigeration Systems	5
		1.5.1	Generator	5
		1.5.2	Absorber	7
		1.5.3	Condenser	8
		1.5.4	Evaporator	8
		1.5.5	Pump	9
		1.5.6	Expansion Valve	9
	1.6	Operati	ing Principle	10
	1.7	Types of	of Absorption Refrigeration Systems	10
		1.7.1	Single Effect Absorption Refrigeration System	11
		1.7.2	Double Effect Absorption Refrigeration System	12
		1.7.3	Triple Effect Absorption Refrigeration System	13
		1.7.4	Multiple Effect Absorption Refrigeration System	15
	1.8	Heat So	ources	17
	1.9	Advant	ages and Disadvantages	18
	1.10	Compa	rison with Other Cooling Systems	18
		1.10.1	Solar PV Cooling System	19
		1.10.2	Solar Thermoelectric Cooling System	20
		1.10.3		21
		1.10.4	Desiccant Cooling Systems	21
		1.10.5	Adsorption Cooling System	22
	1.11	Absorp	tion Heat Pumps	23
	1 12		Remarks	24

x Contents

2	Ther	modynamic Analysis
	2.1	Introduction
	2.2	Energy and Exergy Analyses
		2.2.1 Pump
		2.2.2 Generator
		2.2.3 Condenser
		2.2.4 Evaporator
		2.2.5 Absorber
		2.2.6 Expansion Valve
		2.2.7 Coefficient of Performance
	2.3	Exergoeconomic Analysis
	2.4	Exergoenvironmental Analysis
		2.4.1 Exergoenvironmental Impact Factor 41
		2.4.2 Exergoenvironmental Impact Coefficient 42
		2.4.3 Exergoenvironmental Impact Index 42
		2.4.4 Exergoenvironmental Impact Improvement 42
		2.4.5 Exergetic Stability Factor
		2.4.6 Exergetic Sustainability Index
	2.5	Optimization
	2.6	Closing Remarks
	Refer	ences
3	Singl	e Effect Absorption Refrigeration System 47
	3.1	Introduction
	3.2	System Description
	3.3	Energy and Exergy Analyses
	3.4	Exergoeconomic Analysis
	3.5	Exergoenvironmental Analysis
	3.6	Optimization
	3.7	Illustrative Example
	3.8	Closing Remarks
4		le Effect Absorption Refrigeration System
	4.1	Introduction
	4.2	System Description
	4.3	Energy and Exergy Analyses
	4.4	Exergoeconomic Analysis
	4.5	Exergoenvironmental Analysis
	4.6	Optimization
	4.7	Illustrative Example
	4.8	Closing Remarks
5	Tripl	e Effect Absorption Refrigeration System
	5.1	Introduction
	5.2	System Description
	5.3	Energy and Exergy Analyses

Contents xi

	5.4	Exergoeconomic Analysis	119
	5.5	Exergoenvironmental Analysis	120
	5.6	Optimization	121
	5.7	Illustrative Example	121
	5.8	Closing Remarks	148
6	Quad	Iruple Effect Absorption Refrigeration System	149
	6.1	Introduction	149
	6.2	System Description	150
	6.3	Energy and Exergy Analyses	152
	6.4	Exergoeconomic Analysis	163
	6.5	Exergoenvironmental Analysis	164
	6.6	Optimization Study	165
	6.7	Illustrative Example	166
	6.8	Closing Remarks	196
7	Integ	rated Absorption Refrigeration Systems: Case Studies	197
	7.1	Introduction	197
	7.2	Case Study 1: Geothermal-Based Power, Cooling,	
		and Liquefied Hydrogen Generation System	197
	7.3	Case Study 2: Solar-Based Integrated Absorption	
		Refrigeration and Desalination System for Cooling	
		and Fresh Water Production	207
	7.4	Case Study 3: Geothermal-Based Multigeneration System	219
	7.5	Case Study 4: Geothermal-Based Integrated System for	
		Standalone Building Needs	228
	7.6	Closing Remarks	239
8	Deve	lopments in Absorption Refrigeration Systems	241
	8.1	Introduction	241
	8.2	Advanced Solar-Based Absorption Refrigeration Systems	242
	8.3	Solid Oxide Fuel Cell-Based Multigeneration Systems	246
	8.4	Biomass-Based Multigeneration Systems	248
	8.5	Fossil Fuels-Based Multigeneration System	251
	8.6	Novel ARS-Based Combined Heating and Power	
		Generation Systems	251
	8.7	Novel ARS Designs	253
	8.8	Advanced Numerical and Optimization Studies of ARS	255
	8.9	Novel Working Mixtures	256
	8.10	Closing Remarks	257
Re	ferenc	ees	259
In	dex		265

Nomenclature

A	Area of PV module, m ²
b	Breadth of PV module, m
c	Cost, USD
C	Coefficient
\dot{C}	Cost rate, USD/s
COP	Coefficient of performance
cp	Specific heat capacity, kJ/kg K
ex	Specific exergy, kJ/kg
Ėn	Rate of energy, kW
Ėx	Rate of exergy, kW
f	Factor
h	Specific enthalpy, kJ/kg
h_{ba}	Heat transfer coefficient from black surface to air, W/m ² K
h_{t}	Heat transfer coefficient from black surface to air through glass,
	$W/m^2 K$
$h_{ m p1G}$	Penalty factor due to the presence of solar cell material, glass and
	EVA for glass to glass PV/T system, W/m ² K
$h_{ m p2G}$	Penalty factor due to presence of interface between glass and working
	fluid through absorber plate for glass to glass PV/T system, W/m ² K
HHV	Higher heating value, kJ/kg
İ	Incident solar flux, W/m ²
L	Length of the PV module, m
m	Mass flow rate, kg/s
MW	Molecular weight, kg/kmol
P	Pressure, kPa
\dot{Q}	Heat transfer rate, kW
Qu	Quality
R	Gas constant, kJ/kg K
RH	Relative humidity, %
S	Specific entropy, kJ/kg K

xiv Nomenclature

T	Temperature, K
t	Time, s
$U_{ m b}$	Overall heat transfer coefficient from bottom to ambient, W/m ² K
$U_{ m L}$	Overall heat transfer coefficient from solar cell to ambient through top and back surface of insulation, W/m ² K
U_{t}	Overall heat transfer coefficient from solar cell to ambient through glass cover, W/m ² K
$U_{ m tb}$	Overall heat transfer coefficient from glass to black surface through solar cell, W/m ² K
v	Specific volume, m ³ /kg
w	Specific work, kJ/kg
\dot{W}	Power, kW
x	Concentration
у	Ratio of the work output from the power plant to the work input to the liquefaction cycle

Greek Letters

Ż

η	Efficiency
Σ	Summation
Θ	Index
$\alpha_{ m c}$	Absorptance of solar cell
$\alpha_{ m b}$	Absorptance of painted black surface
$\beta_{\rm c}$	Packing factor of solar cell
$ au_{ m g}$	Transmittance of glass
ε	Utilization factor
ω	Humidity ratio

Equipment cost rate, USD

Subscript

a	Absorber; air
abs	Absorber; absorption system
ai	Air inlet
aux	Auxiliary
b	Binary power plant; painted black surface
bs	Back surface of PV/T
c	Condenser; solar cell
ch	Chemical
con	Condenser
comp	Compressor
cool	Cooling
d	Desalination; air-drying process; double

Nomenclature xv

dest Destruction

df Double flash power plant

dp Desalination pump

e Evaporator

ei Exergoenvironmental impact

eii Exergoenvironmental impact improvement

el Electrical
elec Electrolyzer
en Energy
eq Equipment

es Exergetic stability
est Exergetic sustainability
ev Expansion valve

eva Evaporator

evr Refrigerant expansion valve evw Weak solution expansion valve

ex Exergy f Flash system fw Freshwater

G Subscript for glass to glass PV/T system

g Generator; glass geo Geothermal h Hextuple

HHX High temperature heat exchanger

hw Hot water
H₂ Hydrogen
i Any state; inlet

in Inlet

irr Irreversible iso Isobutane liq Liquefied

LHX Low temperature heat exchanger LTG Low temperature generator

MHX Medium temperature heat exchanger MTG Medium temperature generator

o Outlet

OPM Operation and maintenance

out Outlet

p Pump; pentupleph Physicalq Quadruple

qf Quadruple flash system
QFPP Quadruple flash power plant

req Required rev Reversible

xvi Nomenclature

s Single
sw Seawater
t Triple
th Thermal
tot Total
turb Turbine
uu Unused fuel

VHHX Very high temperature heat exchanger VHTG Very high temperature generator

w Water
II Second law
1...41 State numbers

O Ambient: reference state

Abbreviations

abs Absorber

AC Alternate current

ACAR Auto-cascade absorption refrigeration ARS Absorption refrigeration system

BFB Bubbling fluidized bed CaCl Calcium chloride

CCHP Combined cooling, heating and power generation

CFB Circulating fluidized bed CHX Condenser heat exchanger

con Condenser

COP Coefficient of performance

DC Direct current

DEARS Double effect absorption refrigeration system

DFB Dual fluidized bed

EES Engineering equations solver

EVA Ethyl vinyl acetate

eva Evaporator

GAX Generator absorber heat recovery heat exchanger

HHX High temperature heat exchanger HTG High temperature generator

IR Internal reforming

LEC Levelized electricity cost

LH Linde-Hampson

LHX Low temperature heat exchanger

LiBr Lithium bromide LiCl Lithium chloride

LINMAP Linear programming technique for multidimensional analysis

LTG Low temperature generator

Nomenclature xvii

MHX Medium temperature heat exchanger MTG Medium temperature generator

ORS Organic Rankine cycle PV/T Photovoltaic thermal

PV Photovoltaic

QEARS Quadruple effect absorption refrigeration system

QFPP Quadruple flash power plant

SC Subcooled

SEARS Single effect absorption refrigeration system

SH Superheated

SOFC Solid oxide fuel cell

TEARS Triple effect absorption refrigeration system
TRI ThermoChem bubbling fluidized bed gasifier

TSVCS Two-stage vapor compression system
USD United States of America dollar
VCAS Vapor compression—absorption system
VHHX Very high temperature heat exchanger
VHTG Very high temperature generator

Chapter 1 Fundamentals of Absorption Refrigeration Systems

1.1 Introduction

Since the industrial revolution, humankind's demand for a better lifestyle and greater comfort has increased considerably. In order to meet such demands, an increasing number of energy-consuming technological devices and products are being introduced almost daily. In countries around the globe, the demand for energy required for cooling and heating applications has risen dramatically and it is expected to increase exponentially every day, making it difficult for countries to meet the growing demand. At present, the majority of power plants run on fossil fuels, including coal, oil, and natural gas, due to their easy availability and low cost in certain countries, especially in the Gulf region. However, such systems release toxic gases, such as CO₂ and NO₃, etc., which are harmful not only to the environment, but to all living things. The maximum amount of energy available in the grid of countries situated in either hot or cold regions is used to provide cooling or heating, respectively, by installing conventional energy-hungry vapor-compression cycles. These cycles use an ample amount of energy to run the compressor to achieve the required cooling or heating rate of the system. This high energy consumption not only affects the environment but also affects the individual in terms of running cost. Therefore, it has become more crucial to design air-conditioning, cooling, and refrigeration systems that are more cost-effective, more eco-friendly, and can be operated using low-grade heat sources, such as solar, geothermal, biomass, as well as process/waste heat. The performance of such a cooling cycle is represented by the coefficient of performance (COP) which is the ratio of cooling rate provided to the energy input to the system. This chapter sheds light on fundamental and conceptual aspects of absorption refrigeration systems for various applications, ranging from the residential sector to the industrial sector, using various sources of low-grade heat.

1.2 Absorption Process

Absorption is defined as a process in which two fluids entering at different states such as a gas or liquid are combined to leave at a single state, as either a gas or liquid as shown in Fig. 1.1. A cooling system that works on the principle of absorption is known as an absorption refrigeration system. It is important to differentiate between air-conditioning and refrigeration systems. Air-conditioning systems are used to provide cooling above 0 °C, whereas refrigeration systems are used to provide cooling both below and above 0 °C. A common example of an air-conditioning system is a cooling unit in a house and an example of a refrigeration system is a food storage unit. The absorption refrigeration system was first introduced in 1846 with the concept of producing ice while using heat as an energy input. The introduction of the absorption process in the cooling industry resulted in the ability to produce cooling using less electrical energy than conventional vapor-compression cooling systems. Absorption refrigeration technology is among the best alternatives to vapor-compression cooling with respect to energy diversification and environmental protection. Since absorption refrigeration technology is used extensively in practical applications, a number of high-performance absorption refrigeration cycles have been introduced for both residential and industrial applications.

1.3 Absorbents and Refrigerants

The word "absorbent' or "refrigerant' in an absorption refrigeration system refers to the working fluid of the system. As the name "absorption refrigeration system' implies, the absorbent or refrigerant is a mixture of two fluids, which are used in such a way that the saturation temperature of one fluid is lower than the other. The fluid with lower saturation temperature is selected based on the mixture used and the working environment. This lower saturation temperature fluid acts as a refrigerant

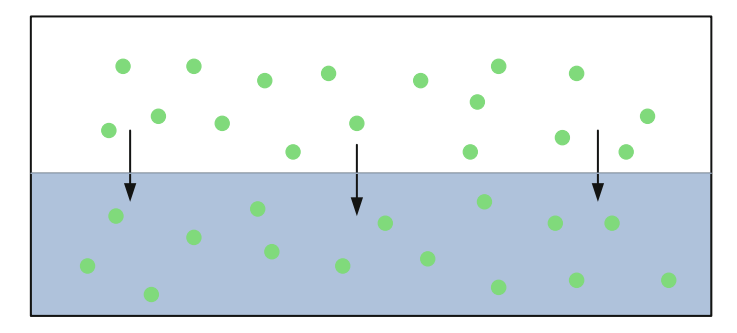


Fig. 1.1 Schematic illustration of an absorption process

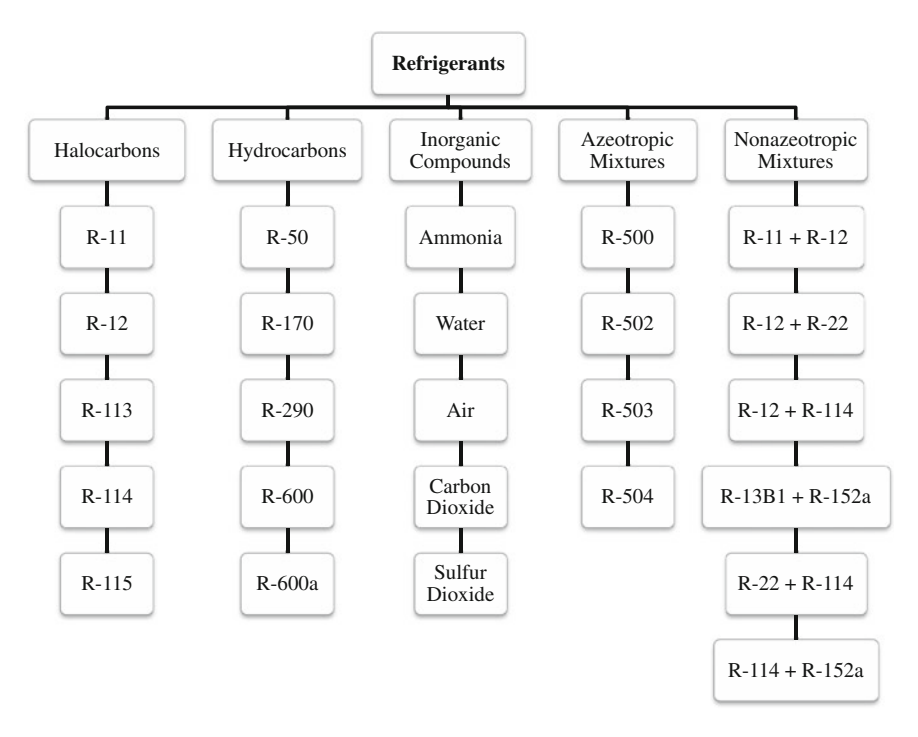


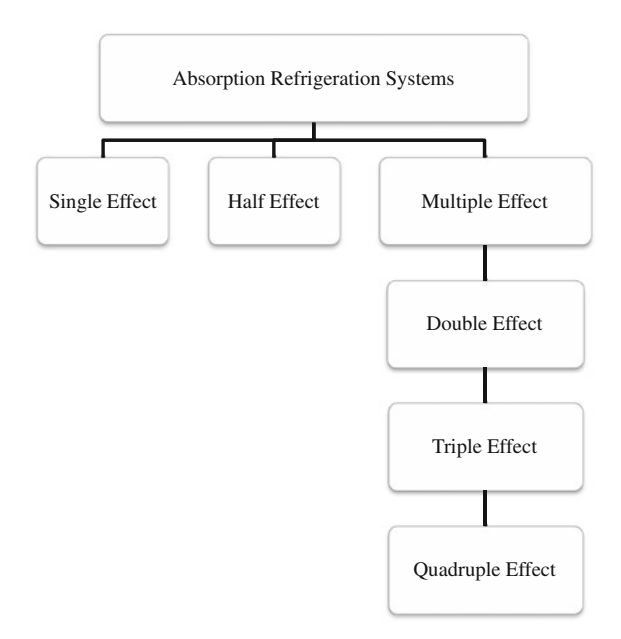
Fig. 1.2 Classification of refrigerants for various applications

and the other fluid acts as an absorbent that absorbs the refrigerant in an absorber. The refrigerants used in absorption refrigeration systems are classified into five categories namely halocarbons, hydrocarbons, inorganic compounds, azeotropic mixtures, and nonazeotropic mixtures as shown in Fig. 1.2. Different types of absorbents used in these systems include water, LiBr, LiCl, ZnCl₂, Li₂ZnCl₄, Li₂CaCl₄, and CaZnCl₄. Several working fluids are used in an absorption refrigeration system which include ammonia-water, lithium-bromide-water, Tridroxidewater, and Alkitrate-water. The most commonly used among them are ammoniawater and lithium-bromide-water. For residential air-conditioning applications, the lithium-bromide-water solution is preferred due to its high coefficient of performance and easy management. However, a major drawback to the LiBr-water system is the high operational costs that arise because of corrosion that occurs with working temperatures above 473.15 K as well as crystallization issues. The working temperature restriction in lithium-bromide-water working fluid prevents it from being used on a large scale, and the salt used in the system to solve the corrosion problem is expensive, which drives the operation cost of the system high. On the other hand, the ammonia-water system is preferred for industrial use as it can run at high temperatures without the problem of crystallization. Although the ammonia-water absorption refrigeration system also faces the problem of corrosion, the cure for this problem is sea salt which helps to reduce the operational costs. Other proposed working fluids are still in the testing phase and are not able to compete with the COP or operation cost of the conventional LiBr-water and ammonia-water absorption refrigeration systems.

1.4 Classification of Absorption Refrigeration Systems

Concerns related to the harmful effects of using fossil fuels for power generation have resulted in a push for the development of a cooling system that can run on low-grade energy and can minimize the use of power in the cooling or heating process. One such technology to provide cooling is the absorption refrigeration system. Absorption refrigeration systems can be classified into several categories which are single effect absorption refrigeration systems, half effect absorption refrigeration systems, and multiple effect absorption refrigeration systems as shown in Fig. 1.3. This classification is made based on the number of generators used and the way they are connected to each other. A single effect absorption refrigeration system is the simplest form and consists of a generator, a condenser, an absorber, an evaporator, a pump, and expansion valves. These components can be arranged either in series or in parallel depending on the application and the provided space. An enhanced form of single effect absorption refrigeration system is the half effect absorption refrigeration system which makes it possible to provide cooling while using a heat source at relatively lower temperature than the single effect absorption

Fig. 1.3 Classification of absorption refrigeration systems



refrigeration system. A half effect absorption refrigeration system consists of two generators, two absorbers, two pumps, three expansion valves, a condenser, and an evaporator. In the half effect absorption refrigeration system, heat is supplied to both generators from a single source. The drawback to using a half effect absorption refrigeration system is that it has very low COP compared to the single effect absorption refrigeration system. In order to enhance the COP of the absorption refrigeration system, researchers have introduced multiple effect absorption refrigeration systems varying from double effect to quadruple effect.

Although the increasing the number of effects drastically enhances the COP of the system from 0.7 for single effect to 2.5 for quadruple effect, it does so at the cost of a higher temperature heat source requirement compared to a lower effect absorption refrigeration system. A recent advancement in energy recovery from the cycle also led to the advancement of absorption refrigeration system working on the concept of internal heat recovery. The absorption refrigeration systems working on the concept of the heat recovery consist of an additional heat exchanger and are classified as absorption refrigeration systems with agenerator absorber heat exchanger (GAX). The addition of GAX in the cycle helps recovery of heat from the weak solution returning from the generator in the form of preheating of the strong solution going toward the generator.

1.5 Components of Absorption Refrigeration Systems

Absorption refrigeration systems are cooling generating devices that rely more on thermal energy than electrical energy to provide the desired output. An absorption refrigeration system generally comprises six basic subsystems which are generator, absorber, condenser, evaporator, pump, and an expansion valve as shown in Fig. 1.4. Each of these subsystems has a specific task to perform in order successfully to run the absorption refrigeration system.

1.5.1 Generator

Generator is a subsystem of the absorption refrigeration system whose job is to separate the refrigerant from the working fluid mixture using heat as an energy source. A generator of the absorption refrigeration system has the structure of a shell–and– tube heat exchanger with two inlets and three outlets as shown in Fig. 1.5. In the generator, the strong solution (a mixture of refrigerant and absorbent) from the absorber enters from the bottom where it is heated from the high temperature fluid from the heat source. As the strong solution boils, the refrigerant

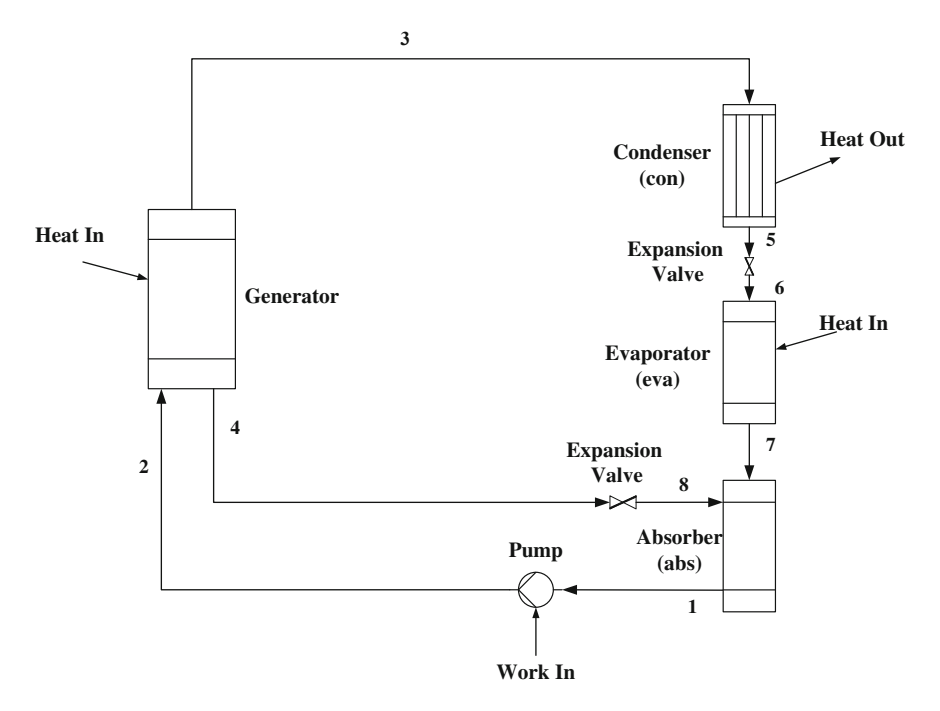
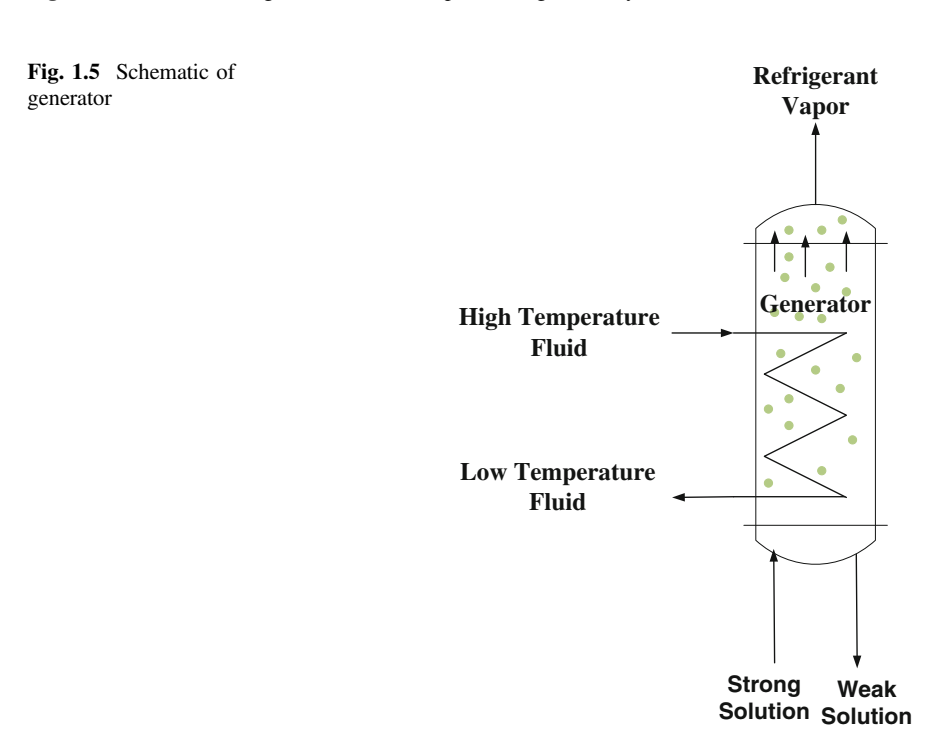


Fig. 1.4 A schematic diagram of basic absorption refrigeration system

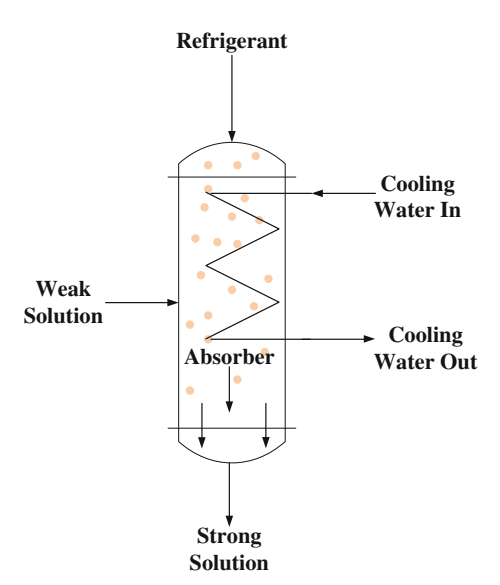


with comparitively lower boiling temperature than the absorbent leaves the generator from the top in superheated vapor form. The mixture containing a smaller amount of refrigerant compared to the strong solution leaves the generator as a weak solution to be recirculated back to the absorber.

1.5.2 Absorber

An absorber is a sub-system of the absorption refrigeration system, whose task is to mix together the refrigerant from the evaporator and the weak solution from the generator. An absorber is a simple mixing chamber in which two fluids enter the chamber to leave as a single fluid as shown in Fig. 1.6. The refrigerant from the evaporator first gains heat from the cooled space then enters the absorber from the top. The weak solution from the generator first passes through the expansion valve, where its pressure drops to that of the absorber before it enters the absorber. The use of an expansion valve before the absorber is necessary to ensure that both fluids entering the absorber are at the same pressure for mixing to take place. The refrigerant and the weak solution mix together in the absorber and release heat to the cooling water. After mixing and releasing heat in the absorber, the mixture leaves as a strong solution to be supplied to the generator.

Fig. 1.6 Schematic of absorber



1.5.3 Condenser

The condenser of an absorption refrigeration system acts as a heat exchanger whose job is to cool the refrigerant from the generator. In the condenser, the vaporized refrigerant from the generator ejects heat to the cooling water as shown in Fig. 1.7. The cooled refrigerant leaving the condenser then passes through the expansion valve to enter the evaporator. The cooling water used to cool the refrigerant leaves the condenser at a relatively higher temperature that can be further used for domestic heating purposes.

1.5.4 Evaporator

An evaporator of the absorption refrigeration system is a simple heat exchanger, tasked with cooling the space by absorbing heat from the cooled space as shown in Fig. 1.8. The refrigerant leaving the condenser passes through the expansion valve before entering the evaporator. In the expansion valve, the pressure of the refrigerant is suddenly drops which results in a saturated mixture of refrigerant that is high in vapor content. This high vapor content refrigerant then enters the evaporator where it absorbs heat from the cooled space and leaves as a saturated mixture refrigerant. This saturated mixture refrigerant then enters the absorber to be absorbed in the weak solution.

Fig. 1.7 Schematic of condenser

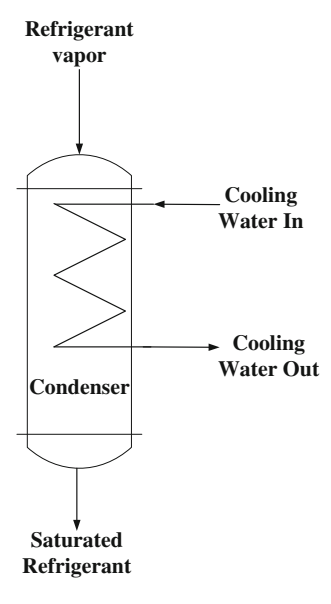


Fig. 1.8 Schematic of evaporator

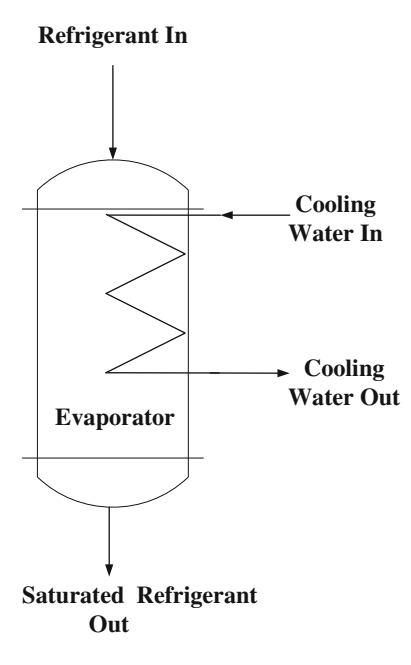
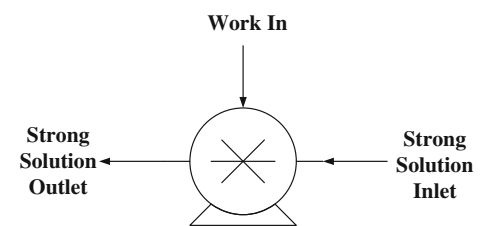


Fig. 1.9 Schematic of positive displacement pump



1.5.5 Pump

The pump used in an absorption refrigeration system is a positive displacement pump. The pump is used to increase the pressure of the strong solution to be supplied to the generator as shown in Fig. 1.9.

1.5.6 Expansion Valve

In an absorption refrigeration system, at least two expansion valves are used, one for the weak solution and one for the refrigerant as shown in Fig. 1.10. The expansion valve used for the weak solution is tasked with reducing the pressure of the weak solution to that of the absorber. The expansion valve used for the

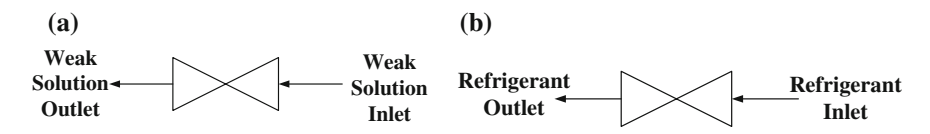


Fig. 1.10 Schematic of expansion valve for a weak solution and b refrigerant

refrigerant acts as a throttling valve in which the pressure of the refrigerant is suddenly dropped to increase the vapor content in the saturated mixture entering the evaporator.

1.6 Operating Principle

A basic absorption refrigeration system consists of a generator, an absorber, a condenser, an evaporator, a pump, and two expansion valves as shown in Fig. 1.4. Heat is supplied to the generator where strong solution enters at state 2. This strong solution is heated to in order to separate the refrigerant from the solution on the basis of saturation temperature difference between refrigerant and absorbent. The vaporized refrigerant leaves the generator at state 3 and the weak solution leaves the generator at state 4. The vaporized refrigerant at state 3 then enters the condenser where it rejects heat to the cooling fluid to leave at state 5 as a saturated mixture. The saturated mixture then passes through the expansion valve where its pressure drops suddenly to increase the vapor content in the saturated mixture and leaves at state 6 to enter the evaporator. In the evaporator, the saturated refrigerant mixture of the refrigerant gains heat from the cooled space and leaves at state 7 to enter the absorber. The weak solution returning from the generator passes through the expansion valve where its pressure drops to leave at state 8 to enter the absorber. The weak solution and the refrigerant then mix together in the absorber and reject heat to the cooling fluid to leave as a strong solution in liquid form at state 1. The strong solution leaving the absorber at state 1 first passes through the pump, where the pressure of the strong solution increases before it enters the generator at state 2, respectively.

1.7 Types of Absorption Refrigeration Systems

An absorption refrigeration system can be designed in several different ways based on generator arrangement. A simple absorption refrigeration system, also known as single effect absorption refrigeration system, consists of a generator, an absorber, a condenser, an evaporator, a pump, and two expansion valves. The present work considers, several absorption refrigeration designs including single effect, double effect, triple effect, and multiple effect absorption refrigeration systems.

1.7.1 Single Effect Absorption Refrigeration System

A single effect absorption refrigeration system is the simplest form of absorption refrigeration system. It is made up of a generator, an absorber, a condenser, an evaporator, a heat recovery heat exchanger, a pump, and two expansion valves as shown in Fig. 1.11. The process starts when the strong solution leaves the absorber at state 1 to enter the pump. In the pump, the pressure of the strong solution increases to the generator pressure and it leaves at state 2. The strong solution then enters the heat recovery heat exchanger at state 2, where it gains heat from the returning weak solution to leave at a slightly higher temperature at state 3. The strong solution at state 3 then enters the generator, where it gains heat from the heat source and starts boiling. The refrigerant mixed with the strong solution vaporizes before the absorbent and leaves at state 7. Once the refrigerant vaporizes from the strong solution, what is left in the generator is a weak solution which leaves at state 4. The vaporized refrigerant leaving at state 7 later enters the condenser, where it rejects heat to the surroundings to leave at a relatively lower temperature at state 8. The precooled refrigerant then enters the expansion valve, where it experiences a sudden pressure drop to leave at state 9 as a vapor-heavy saturated mixture. This vapor-heavy saturated mixture later enters the evaporator, where it gains heat from the cooled space to leave at state 10. The refrigerant leaving at state 10 then enters

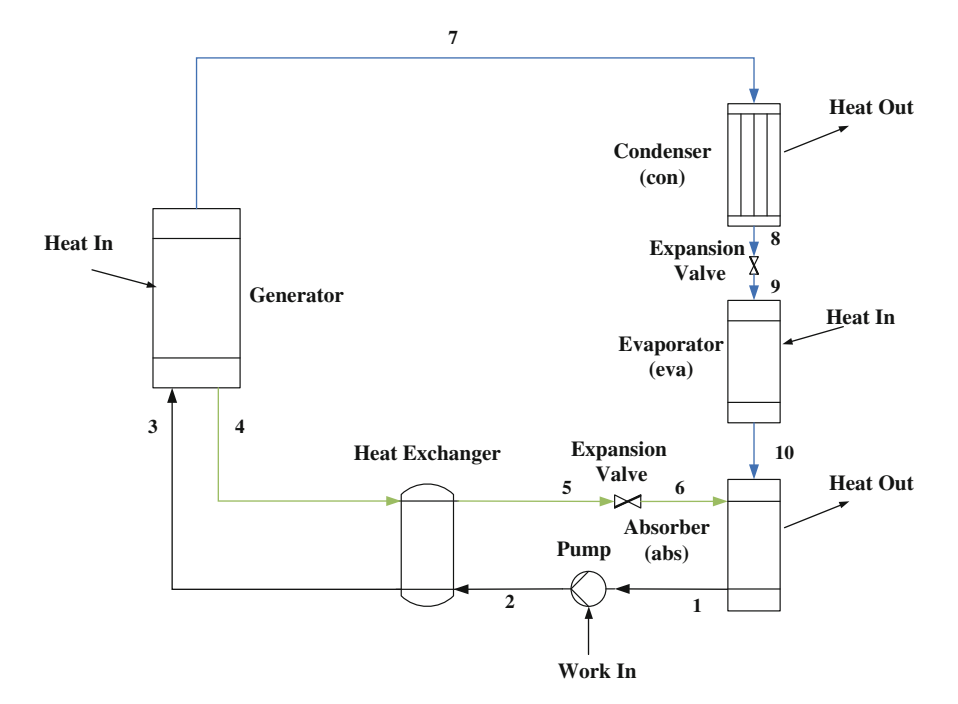


Fig. 1.11 Schematic of single effect absorption refrigeration system

the absorber. The weak solution exiting the generator at state 4 enters the heat recovery heat exchanger, where it loses heat to the incoming strong solution to leave at state 5 at comparatively lower temperature. The weak solution at state 5 then enters the expansion valve, where its pressure drops to the absorber pressure before entering the absorber at state 6. In the absorber, the weak solution and the refrigerant mix together and release heat to leave as a strong solution at state 1.

1.7.2 Double Effect Absorption Refrigeration System

A double effect absorption refrigeration system differs from a single effect absorption refrigeration system in that it double effect absorption refrigeration system has two generators and three heat recovery heat exchangers as shown in Fig. 1.12. In the double effect absorption refrigeration system, a strong solution leaves the absorber at state 1 to enter the solution pump. In the pump, the pressure of the strong solution increases and leaves at state 2. The strong solution at state 2 is then separated into two streams for energy recovery purposes. One strong solution stream at state 3 enters the low temperature heat exchanger, where it gains heat from the returning weak solution to leave at state 4 as a preheated stream. This preheated strong solution then divides into two streams from which one is directed

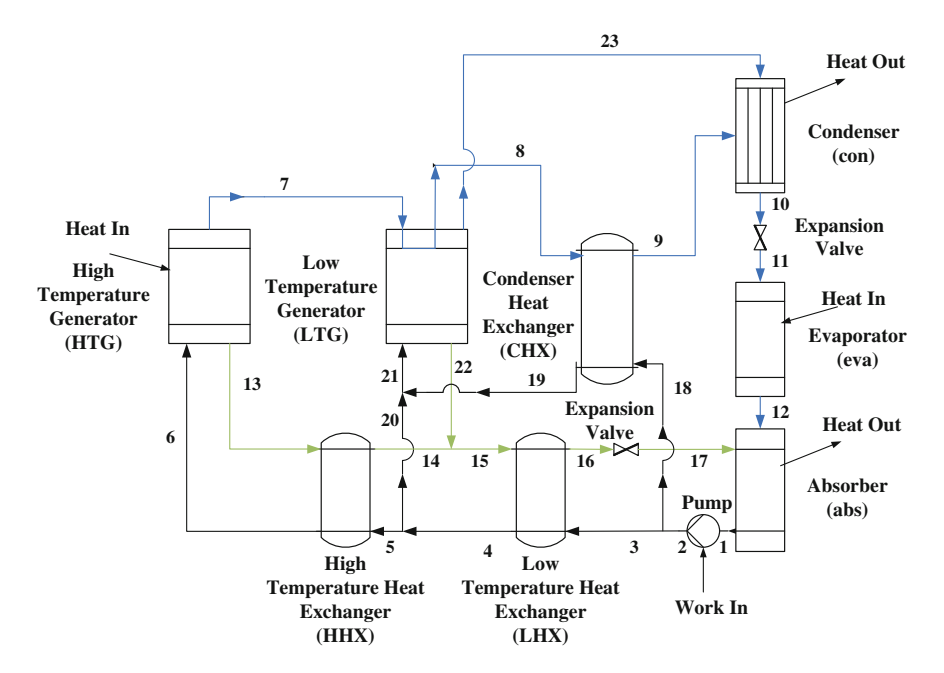


Fig. 1.12 Schematic of double-effect absorption refrigeration system

toward the low temperature generator (state 20) and the other one toward the high temperature heat exchanger (state 5). The strong solution at state 5 then enters the high temperature heat exchanger, where it gains heat from the returning fluid to leave at state 6 at a comparatively higher temperature than state 4. The strong solution at state 6 then enters the high temperature generator where high temperature heat from a heat source is supplied. This supplied high temperature heat helps in breaking the strong solution into weak solution and refrigerant vapor due to the difference in the saturation temperature of the refrigerant and absorbent. The vaporized refrigerant leaves the high temperature generator at state 7 to enter the low temperature generator. The high temperature vapor entering the low temperature generator at state 7 releases heat to the incoming strong solution at state 21. The release of heat from high temperature vapor helps to break thestrong solution into refrigerant vapor and weak solution. The refrigerant entering at state 7 leaves at state 8 and the refrigerated vapor generated in the low temperature generator leaves at state 23 to enter the condenser. The refrigerant vapor at state 8 enters the condenser heat exchanger, where it releases heat to the incoming strong solution at state 18 leaving at a relatively lower temperature to enter condenser at state 9. The strong solution entering at state 18 leaves the condenser heat exchanger at state 19 mixing with the strong solution at state 20 to enter the low temperature generator at state 21. In the condenser, the refrigerant vapor from state 23 and state 9 releases heat to leave at state 10 at a relatively lower temperature. The refrigerant at state 10 then enters the expansion valve where its pressure is dropped suddenly to leave at state 11. The low pressure refrigerant at state 11 then enters the evaporator, where it gains heat from the cooling space before entering the absorber at state 12. The weak solution leaving the high temperature generator at state 13 passes through the high temperature heat exchanger to release heat to the incoming strong solution before leaving at state 14. The weak solution at state 14 then combines with the weak solution returning from the low temperature generator at state 22 to leave at state 16. The weak solution at state 15 then enters the low temperature heat exchanger, where it releases heat to the strong solution before leaving at a relatively lower temperature at state 16. The weak solution at state 16 enters the expansion valve, where its pressure drops to the pressure of the absorber before entering the absorber at state 17. In the absorber, the refrigerant from state 12 and weak solution from state 17 mix together and release heat to leave at state 1 in the form of a strong solution.

1.7.3 Triple Effect Absorption Refrigeration System

A triple effect absorption refrigeration system consists of three generators, an absorber, a condenser, an evaporator, two expansion valves, a pump, and four energy recovery heat exchangers as shown in Fig. 1.13. Heat from an external source is supplied to the high temperature generator to produce cooling. In the high temperature generator, the strong solution from the absorber at state 29 is heated to

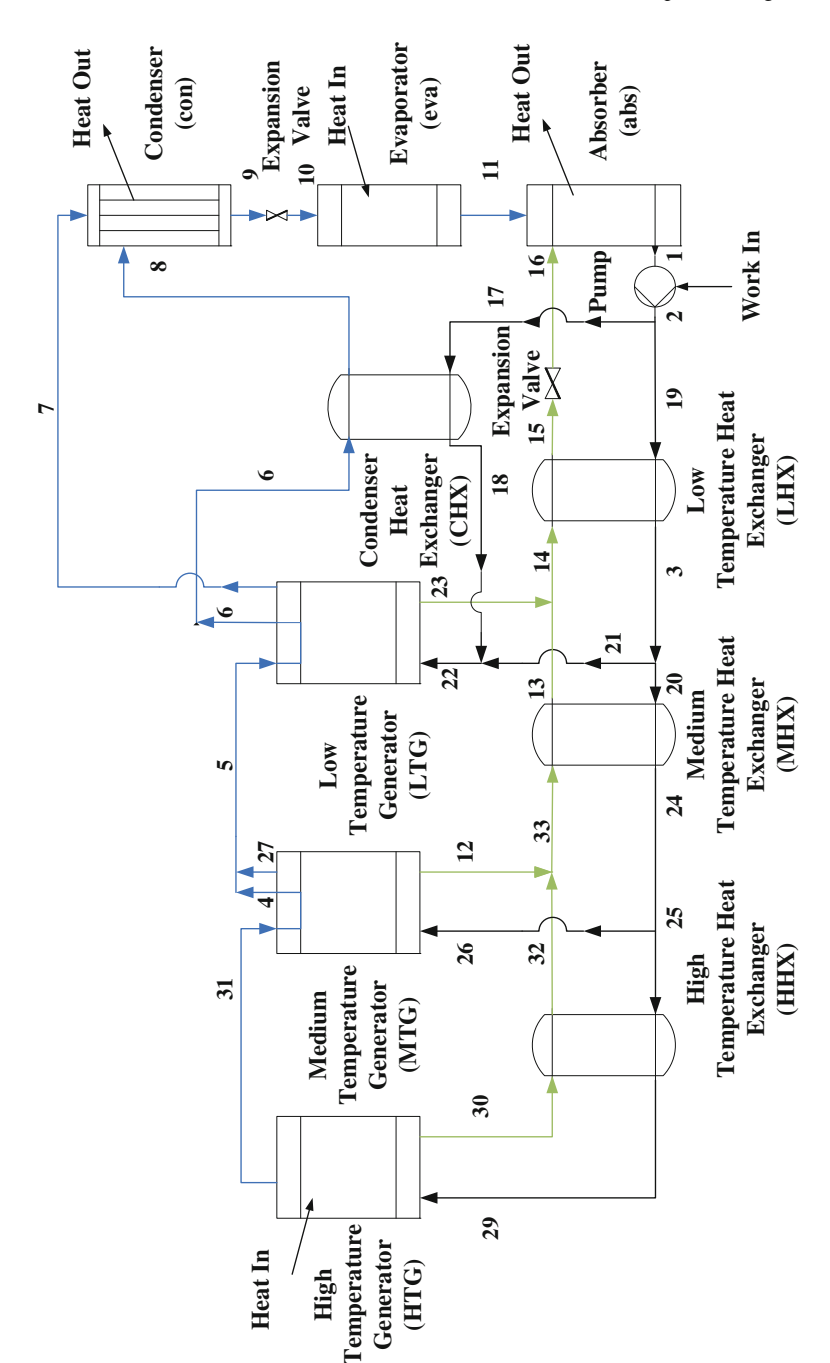


Fig. 1.13 Schematic of triple effect absorption refrigeration system

leave as a weak solution at state 30 and refrigerant vapor at state 31. The weak solution leaving the high temperature generator at state 30 then rejects heat in the high temperature heat exchanger before combining with the weak solution from the medium temperature generator at state 12 to leave at state 33. This weak solution from state 33 then rejects heat in the medium temperature heat exchanger and combines with the weak solution from state 23 to leave at state 14. This weak solution then enters the low temperature heat exchanger where it heats up the strong solution from state 19. After rejecting heat, the weak solution at state 15 enters the expansion valve where its pressure and temperature decrease before entering the absorber at state 16. The vapor at state 31 enters the medium temperature generator where it heats the strong solution from state 26 and leaves the medium temperature generator in two streams as refrigerant vapor at state 4 and state 27. These two refrigerant vapor streams are then combined together at state 5 before entering the low temperature generator. In the low temperature generator, the strong solution coming from state 22 is heated and leaves the low temperature generator as refrigerant vapor at state 6 and state 7. The vapor stream at state 7 is directed to the condenser while the vapor stream at state 6 is directed to the condenser heat exchanger to reject heat to the strong solution from state 17 and leaves at state 18. The refrigerant vapor stream leaving the condenser heat exchanger at state 8 enters the condenser where it rejects heat and leaves at state 9. This stream then passes through the expansion valve where its pressure drops to that of the evaporator and leaves at state 10. In the evaporator, heat is gained by the refrigerant from the production of chilled water production and the heated mixture leaves the evaporator at state 11 before entering the absorber. In the absorber, all three streams mix together and reject heat to the cooling fluid before entering the solution pump at state 1.

1.7.4 Multiple Effect Absorption Refrigeration System

A new advancement in the area of absorption refrigeration systems has led to the study of multiple effect absorption refrigeration systems beyond triple effect. One such system is the quadruple effect absorption refrigeration system which consists of four generators, an absorber, a condenser, an evaporator, two expansion valves, a pump, and five heat recovery heat exchangers as shown in Fig. 1.14. In a very high temperature generator, the strong solution from the absorber at state 14 is heated to leave as a weak solution at state 16 and refrigerant vapor at state 15. The weak solution exiting at state 34 after releasing heat in the very high temperature heat exchanger mixes with the weak solution from state 20 to leave at state 35. This weak solution from state 35 then releases heat in the high temperature heat exchanger and combines with the weak solution from state 24 to leave at state 37. This weak solution from state 37 then releases heat in the the medium temperature heat exchanger and combines with the weak solution from state 29 to leave at state 39. This weak solution then enters low temperature heat exchanger, where it heats

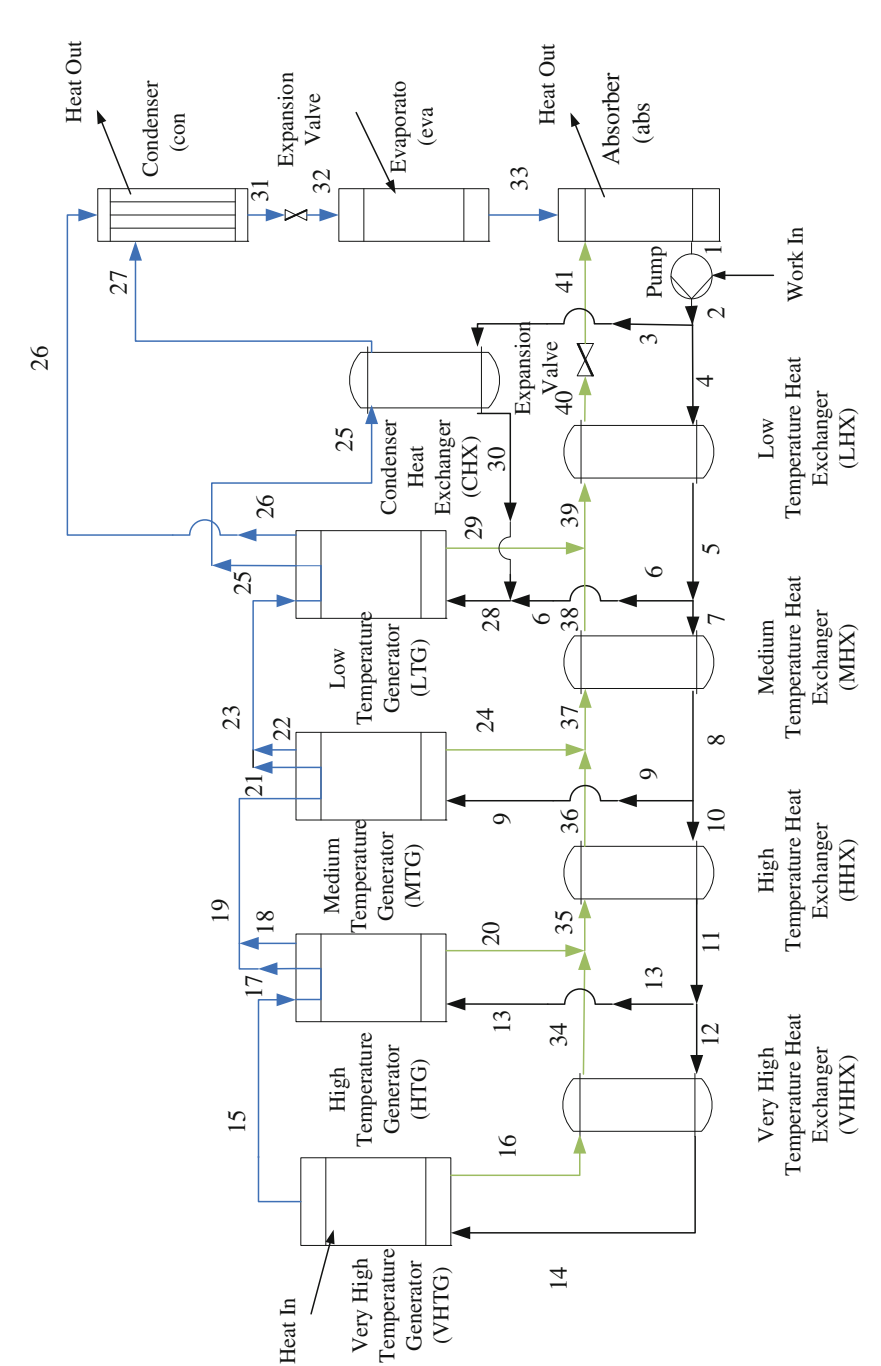


Fig. 1.14 Schematic of quadruple effect absorption refrigeration system

the strong solution from state 4. After releasing heat, the weak solution at state 40 enters the expansion valve where its pressure and temperature decrease before entering an absorber at state 41. The refrigerant vapor from state 15 then enters the high temperature generator, where it heats the strong solution from state 13 and leaves as refrigerant vapor at state 17 and state 18. These two refrigerant vapor streams mix together and leave at state 19 to enter the medium temperature generator, where it heats the strong solution from state 9 and leaves as refrigerant vapor at state 21 and state 22. These two refrigerant vapors are then combined together before leaving at state 23. The refrigerant vapor at state 23 enters the low temperature generator heats the strong solution from state 28, and leaves as refrigerant vapor at state 25 and state 26. The stream at state 26 goes directly into the condenser while the stream at state 25 is directed to the condenser heat exchanger to lose heat to part of the strong solution that is fed backward by the pump at state 3. The strong solution gains heat and leaves the condenser heat exchanger at state 30. The refrigerant vapor leaving condenser heat exchanger at state 27 enters the condenser, releases heat, and then leaves at state 31. The refrigerant stream then passes through the expansion valve and leaves at state 32 to enter the evaporator. In the evaporator, heat is gained by the refrigerant from the cooled space. The refrigerant is heated in the evaporator and leaves at state 33 to enter the absorber. In the absorber, all three streams mix together and release heat to the surrounding and leave at state 1 in liquid form to enter the pump.

1.8 Heat Sources

An absorption refrigeration system is mainly a low-grade heat-driven cooling system, which means that the operating temperature of the system determines the amount of cooling it can produce. A single effect absorption refrigeration system can run in the temperature range of 80–150 °C and is capable of producing cooling ranging from 1 to 100 tons. A double effect absorption refrigeration system requires a slightly higher working temperature than single effect ranging from 120 to 230 °C and is capable of producing cooling ranging from 1 to 1000 tons. A more advanced absorption refrigeration system, still under lab scale experimental investigation is the triple effect absorption refrigeration system which requires a working temperature range of 150–230 °C.

The triple effect absorption refrigeration system can cater to large industrial applications with expected capabilities of a cooling capacity greater than 1000 tons. The very low-grade heat-dependent characteristic of absorption refrigeration system makes them good contenders for integration with renewable energy sources as well as waste energy. The most attractive source of energy for absorption refrigeration systems is solar energy. Almost all types of solar thermal systems such as concentrated flat plate, evacuated tube, parabolic trough, and parabolic dish are capable of providing the required working temperature for absorption refrigeration systems which makes them very attractive source of energy for absorption refrigeration

systems. Geothermal energy sources can also be used to provide heat to absorption refrigeration systems in places where the geothermal source temperature is above $90\,^{\circ}\text{C}$.

Apart from renewable energy sources, absorption refrigeration systems can also be integrated with power plants and other industrial plants for recovery of low-grade waste heat. A large-scale steam power plant capable of generating power in mega watts rejects heat from its condenser at high temperatures that can be used for providing low-grade heat to the absorption refrigeration system. Recovering low-grade waste heat from power plants to produce cooling capable of meeting the needs of its operation can help improve the efficiency and economy of the power plant by reducing electricity consumption. Another very attractive heat source for absorption refrigeration system is nuclear power plants that reject low-grade heat at considerably high temperatures, part of which can be used to generate enormous amounts of cooling from the triple effect and higher effects absorption refrigeration systems.

1.9 Advantages and Disadvantages

There are several advantages and disadvantages associated with absorption refrigeration systems. Some of the advantages associated with absorption refrigeration systems are

- Reduced operating costs as opposed to the conventional system;
- Eradicates use of harmful chlorofluorocarbons and other refrigerants;
- The operation is safer and quiet;
- The system has low maintenance cost;
- Provides a useful application for heat recovery from almost any system; and
- The payback period is short due to high impact on energy savings.

However, like any other system, absorption refrigeration systems also have some drawbacks including

- Coefficient of performance is lower than the conventional system;
- The start-up time is longer than the conventional system; and
- Leakage in the system can result in a foul smell caused by the use of ammonia.

1.10 Comparison with Other Cooling Systems

Absorption refrigeration systems are not the only cooling system that can use renewable energy for production of cooling. Other renewable energy-based cooling systems that are being researched are (a) solar photovoltaic (PV), (b) solar thermoelectric, (c) thermomechanical, (d) desiccant, and (e) adsorption cooling systems. Each of these cooling systems is briefly described below.

1.10.1 Solar PV Cooling System

PV cell technology is among of the first solar technologies put into commercial manufacturing. The extensive amount of research work done on solar PV technology has aided its advancement with the passage of time. PV cells are semiconductor devices made of n-band and p-band structure and use solar light to generate electrons. Since the realization of the harmful effects caused by use of fossil fuels, the demand for PV modules has increased exponentially. The negative aspect of the solar PV system is that it produces direct current (DC) electricity rather than alternative current (AC) electricity which is required by the majority of electrical appliances in use today. In order to have properly running solar PV cooling technology, one needs to have an integrated system consisting of four basic subsystems which are PV panels, an electrical storage battery, an inverter, and a conventional vapor-compression AC unit as shown in Fig. 1.15 (Otanicar et al. 2012). PV cells are used to convert solar light intensity into direct current electrical energy in the which is then supplied to the battery. The battery is used to store DC voltage during high solar light intensity hours as it acts in a charging mode. However, when solar light intensity is low or is not available, the battery supplies

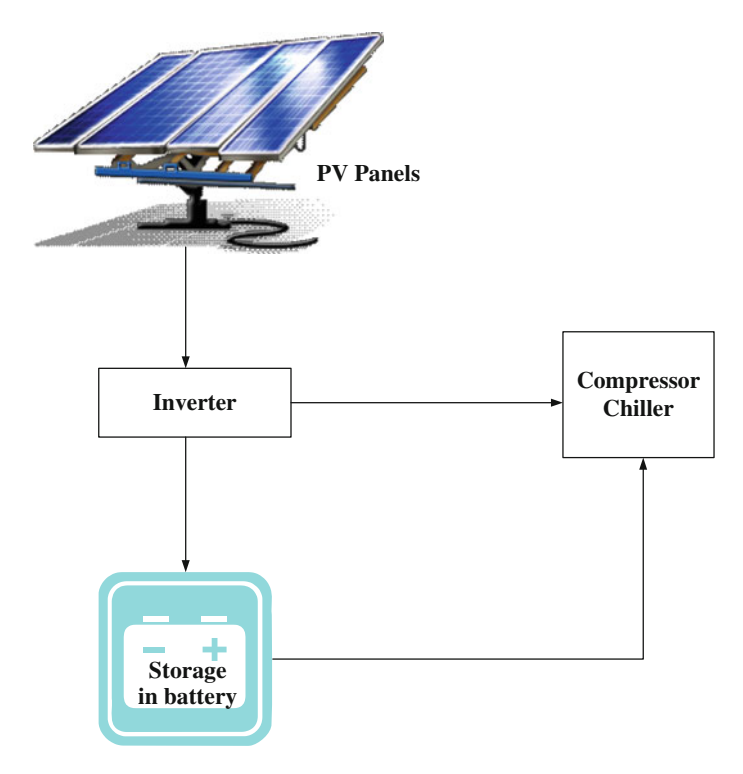


Fig. 1.15 Schematic of solar PV cooling system

the required energy input to the air-conditioning system. The voltage supplied by the battery is in DC form and is then passed through an inverter. An inverter is a device consisting of an electrical circuit which is used to convert direct current electrical power to alternating current electrical power and is then supplied to the air-conditioning unit. The conventional vapor-compression air-conditioning system is dependent on electrical energy to run the compressor in order to supply the required cooling load.

1.10.2 Solar Thermoelectric Cooling System

Solar thermoelectric cooling systems work on the principle of Peltier cooling, receiving energy from sunlight. In these systems, electrical energy from solar light is extracted by means of the thermoelectric effect, which is later used to produce cooling using the Peltier effect, as shown in Fig. 1.16. Thermoelectric devices consist of a series of thermocouples, which are used to generate high current thermoelectric power with the advantage of operating with a low level heat source. Research carried out by Vella et al. (1976) shows that thermoelectric generator which uses solar light intensity as the energy source, is of high interest for operation of a thermoelectric air-condition system. The theory of combined thermoelectric generator and refrigerator to determine the ratio of thermocouples needed for the two devices is also developed by Vella et al. (1976). The thermoelectric air-condition system uses electron gas as a working fluid which makes it very unique. Concerns about damage caused to the environment from the use of chlorofluorocarbons have given rise to alternative cooling technologies such as those using a Peltier system. Research efforts have been made to develop domestic

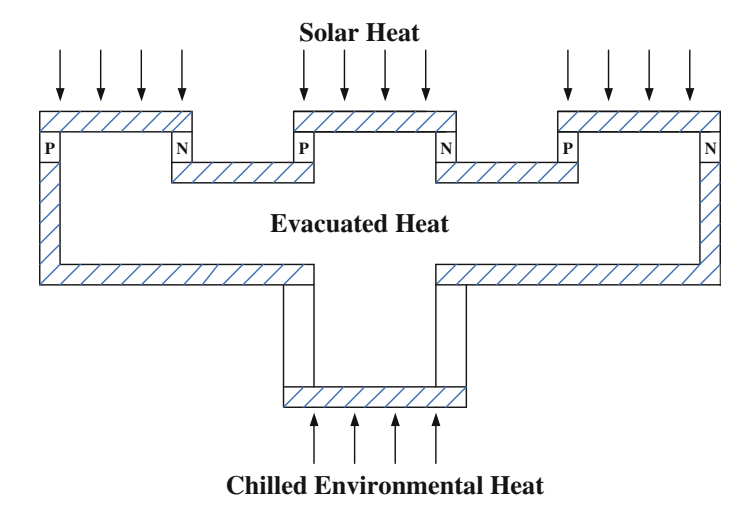


Fig. 1.16 Schematic of solar thermoelectric cooling system

thermoelectric cooling systems with COP comparable to conventional cooling systems in order to make use of this solid-state energy conversion technology.

1.10.3 Thermomechanical Cooling System

The thermomechanical cooling system transforms thermal energy to mechanical energy which is later used to produce the required amount of cooling. The steam ejector system is among the technologies that represent the thermomechanical cooling system. The integration of a steam ejector system with a solar thermal collector or geothermal source as shown in Fig. 1.17 makes the system environmentally benign as the energy need of the system is provided using renewable energy sources. In this system, steam extracted from the renewable energy source is supplied to the boiler, which then supplies high temperature steam to the ejector system where the pressure of the high temperature steam drops. The low pressure water—vapor mixture exiting the ejector then passes through the evaporator where it extracts heat from the water flowing through it. A benefit of the steam ejector system is that during the low cooling demand period it can also work as a turbine, producing electrical power. Table 1.1 shows the effect of working fluid on the performance of the steam ejector system.

1.10.4 Desiccant Cooling Systems

The concept of a renewable energy-based desiccant cooling system was first introduced by Lof (1955) in 1955. This makes use of heat supplied by the renewable energy source to decrease the moisture content of the ambient air flowing

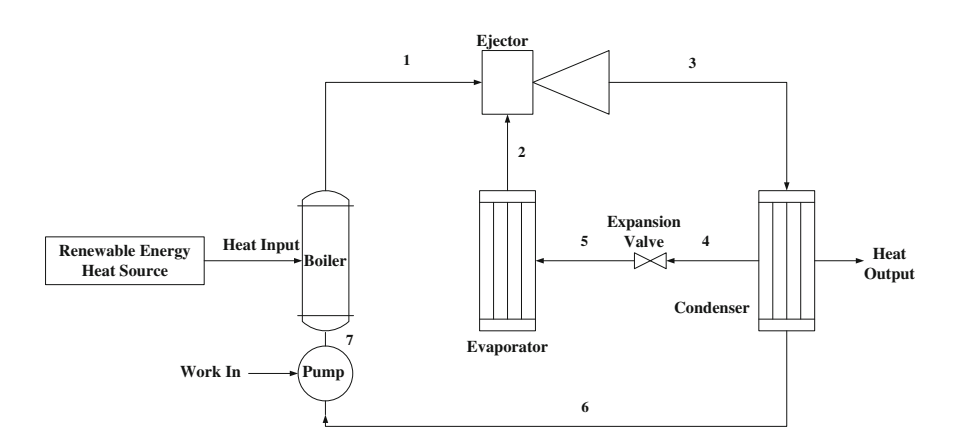


Fig. 1.17 Schematic of thermomechanical cooling system

Working fluid	Boiler temperature (°C)	Condenser temperature (°C)	Boiler pressure (kPa)	Evaporator pressure (kPa)	СОР
Water	85	37	392.2	0.88	0.913
Propane	85	37	2745	539	0.496
Butane	85	37	882.3	147	0.423
Ammonia	130	37	2157	520	0.348
R-134a	90	37	4900	980	0.25

Table 1.1 Effect of working fluid on performance of solar-steam ejector system

through the desiccant system. The temperature of this dry air is then reduced using direct or indirect evaporation. At present, most research in this area is focused on liquid desiccant cooling systems as they have the advantage of higher dehumidification of air, close to the same temperature as that of solid desiccant cooling systems and can also store high energy by using hygroscopic solutions. A comparative study carried out by Ameel et al. (1995) found that LiBr performs best among LiCl, CaCl, and LiBr solutions which are used as a working fluid in the renewable energy-based desiccant cooling systems.

1.10.5 Adsorption Cooling System

The first absorption cooling system was introduced in the early 1990s to meet the sudden increase in cooling demands due to industrial evolution. The adsorption process is a surface phenomenon in which a solid porous surface with large surface area and adsorptive capacity acts as a primary component of the system. The combination of working fluids used in the adsorption systems greatly affects the performance of the system. Working fluids used by different researchers are silica gel-water, activated-carbon-methanol, activated-carbon-ammonia, zeolite-water, activated-carbon-granular, and fiber adsorbent. A standard adsorption system consists of an adsorbent bed, an evaporator, and a condenser. Renewable energy-based thermal technologies can easily meet the thermal energy requirement of the adsorption cooling systems, hence making them environmental friendly. The COP of the renewable energy assisted adsorption system varies from 0.1 to 0.12 when zeolite-water working fluid is used. In another study, Critoph (1993) found that if activated-carbon-ammonia working fluid is used, the COP of the integrated system degrades to 0.05. A COP value of 0.096-0.13 was reported by Luo et al. (2007) when a renewable energy assisted adsorption cooling system was used for cold storage of grains. The effect of working fluid on the performance of the adsorption cooling systems is summarized in Table 1.2.

Table 1.2 Effect of working fluid on performance of solar assisted adsorption cooling system

Working fluids	COP	
Activated carbon/methanol	0.10-0.12	
Zeolite/water	0.10-0.12	
Activated carbon/ammonia	0.05	
Activated carbon/water	0.07	
Silica gel/water	0.20-0.30	

Table 1.3 Coefficient of performance of different cooling systems

Cooling system	COP
Solar PV cooling	0.7
Solar thermoelectric	0.3-0.5
Thermomechanical	0.49
Desiccant	0.35-0.94
Adsorption	0.05-0.3
Single effect absorption	0.5-0.7
Double effect absorption	0.8-1.2
Triple effect absorption	1.4–2.0
Quadruple effect absorption	1.7–2.5

However, among all the different renewable energy-based cooling technologies explained above, absorption refrigeration systems provide better coefficient of performance and operating temperature ranges. These benefits make absorption refrigeration systems an ideal replacement for conventional cooling systems. Table 1.3 summarizes the performance of all the renewable energy- based cooling systems.

1.11 Absorption Heat Pumps

Absorption heat pumps are the waste heat-driven systems capable of providing high temperature heat. They work in a similar manner to absorption refrigeration systems, with the only difference between the two systems being the replacement of an expansion valve between the condenser and an evaporator with the pump. The major benefit to using an absorption heat pump is that it allows the transformation of low temperature heat to high temperature heat at the expense of some work input required to maintain the flow of the working fluid as shown in Fig. 1.18. In an absorption heat pump, low-grade heat is supplied to the generator for the separation of refrigerant from the strong solution entering at state 2. The refrigerant vapor leaves the generator at state 3 and the weak solution exits at state 4. The refrigerant vapor then enters the condenser, where it releases heat to the environment before

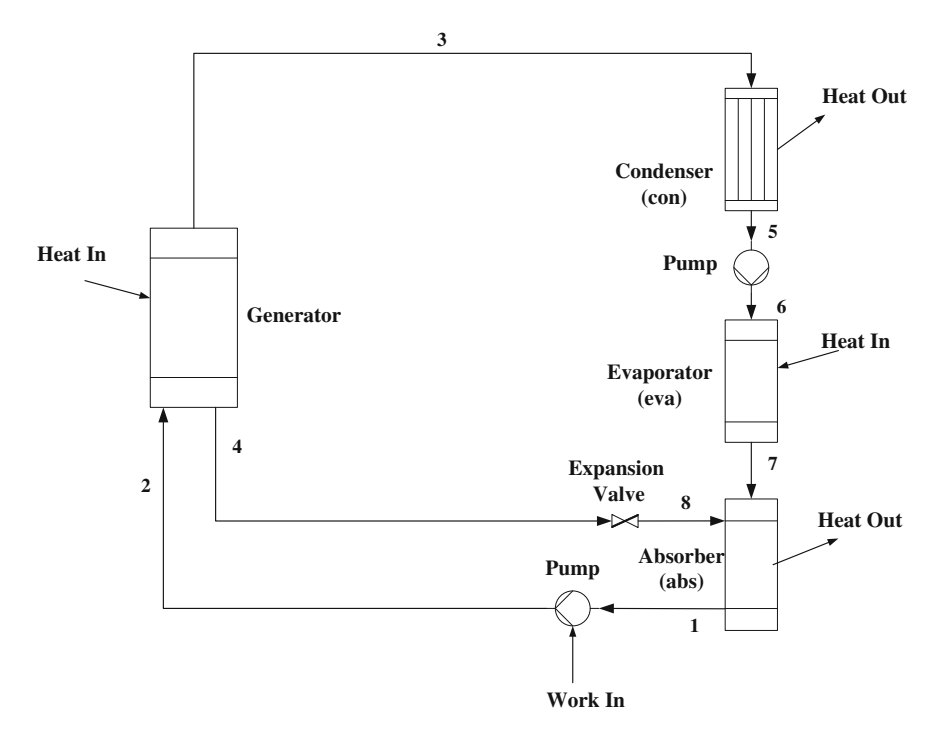


Fig. 1.18 Schematic of absorption heat pump

entering the pump at state 5. The pump helps to maintain the flow of the system and the refrigerant enters the evaporator at state 6. Low-grade heat is supplied, to the evaporator, same as the generator, in order to vaporize the refrigerant. It is worth noting that absorption heat pumps work in a manner such that the generator and evaporator are at the same temperature. The vaporized refrigerant then enters the absorber at state 7. In the absorber, the refrigerant vapour is absorbed into the weak solution entering at state 8. This absorption process results in release of high-temperature heat which is then supplied to the heated space as a useful output.

1.12 Closing Remarks

There has been an increasing interest to find more environmentally benign options for air-conditioning, cooling, and refrigeration applications in various sectors ranging from residential to commercial and from agricultural to industrial, in order to achieve comfortable conditions and storage atmospheres for safe storage of foodstuff and other products/materials. Its importance is also more recognized when we deal with renewables as low-grade heat is available from, for example, solar and

geothermal sources. Some other types of low-grade heat are process and waste heat available through various procedures and applications where we can make use of them. This chapter, in this regard, discusses the fundamentals, basic aspects, main concepts, key system types, main components, and operating principle of absorption refrigeration systems for various applications, ranging from human comfort to safe storage of foodstuff. Comparisons with some conventional types of cooling/refrigeration systems are presented with some features and advantages as well as some possible drawbacks.

Chapter 2 Thermodynamic Analysis

2.1 Introduction

The use of thermodynamic analysis plays a pivotal role in performance assessment and evaluation of any system under study. Thermodynamic analysis branches into two concepts, the first-law of thermodynamics and the second-law of thermodynamics, which are recognized as energy and exergy analyses. These are essentially applicable to all the engineering and science problems at large. The present chapter sheds light on the important aspects of energy and exergy analyses for absorption refrigeration systems. Also, presented are the general energy and exergy analyses of individual components of absorption refrigeration systems. The chapter also discusses the modeling of the absorption refrigeration systems from exergoeconomic and exergoenvironment perspectives, which are helpful in determining the overall effect of using absorption refrigeration systems on society. A brief introduction to optimization is also provided to show how an absorption refrigeration system can be optimized by considering energy, exergy, exergoenvironmental and exergoeconomic parameters.

2.2 Energy and Exergy Analyses

Thermodynamics can be defined as the science of energy (from the first-law of thermodynamics) and exergy (from the second-law of thermodynamics). Energy is the branch of thermodynamics that is derived from the law of conservation of energy according to which energy can be neither created nor destroyed but can transfer from one form to another. Performing energy analysis of a system is the first step in determining the overall performance of the system, as it is based on the basic conservation law. Energy analysis is important, but not sufficient since it does not account for irreversibility, inefficiency and exergy destruction. It is necessary to

proceed one more step to focus on exergy analysis which can further be enhanced for cost accounting and environmental impact assessment under exergoeconomic and exergoenvironmental analyses.

The drawback to using only energy analysis is that it only provides the quantity of energy and does not specify the quality of it. On the other hand, exergy analysis takes the concept of energy analysis forward by specifying the quality of energy carried by the system. Any process that is not in equilibrium with the surrounding is capable of doing work in one direction or another. Exergy analysis states that it is impossible to have a system that can work at 100% efficiency because no matter what every system has losses occurring. For example, it is known that heat transfer takes place from a hot body to a cold body but what if heat transfer is to take place from a cold body to a hot body?. Based on energy analysis it is possible to transfer heat from a cold body to a hot body without supplying any external work but it is known that this cannot happen in reality This is when exergy comes into play to provide quality to the quantity obtained from energy analysis. Exergy analysis can also be viewed as an inequality in thermodynamic analysis as it says that if a process is taking place, the total energy at the termination of a process will either be greater than or equal to the starting point of the process. The equality holds only for hypothetical reversible processes. The following subsections present energy and exergy formulations of each component of the ARS. Also presented, is an example for each component of the ARS.

2.2.1 Pump

The mass balance equation across the pump as shown in Table 2.1 can be written as

$$\dot{m}_{\rm in} = \dot{m}_{\rm out} = \dot{m}_{\rm p} \tag{2.1}$$

where \dot{m} represents mass flow rate.

The specific power consumed by the pump can be calculated using

$$w_{\rm p} = \frac{v(P_{\rm out} - P_{\rm in})}{\eta_{\rm p}} \tag{2.2}$$

where w, v, P and η represent specific power, specific volume, pressure and efficiency, respectively.

The total power consumed by the pump is defined as

$$\dot{W}_{\rm p} = \dot{m}_{\rm p} w_{\rm p} \tag{2.3}$$

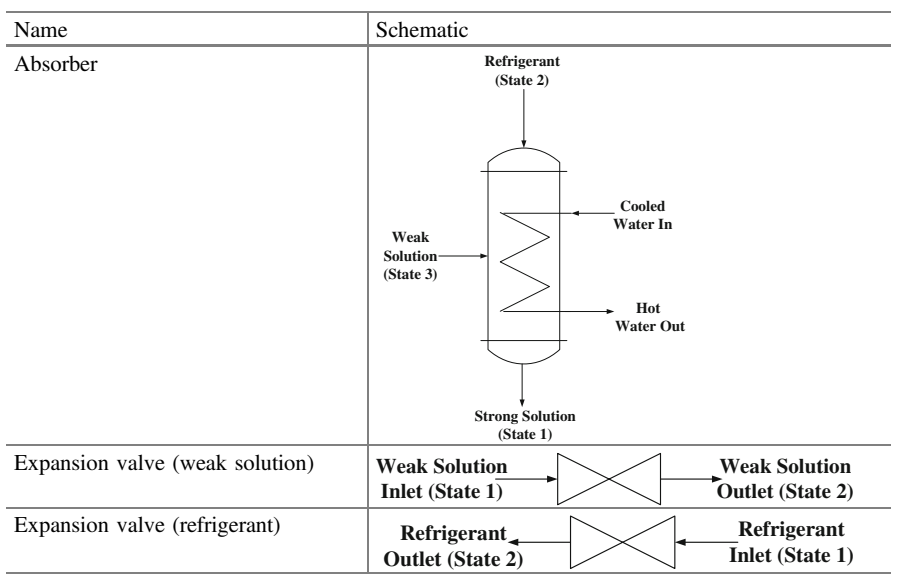
where \dot{W} represents total power consumed by the pump.

Table 2.1 Name and schematic of essential components of ARS

Name	Schematic
Pump	Strong Solution Outlet (State 2) Work In Strong Solution Inlet (State 1)
Generator	Refrigerant Vapor (State 3)
	High Temperature Fluid Low Temperature Fluid
	Strong Weak Solution Solution (State 1) (State 2)
Condenser	Refrigerant vapor (State 1) Cooled Water In Hot Water Out
Evaporator	Saturated Refrigerant (State 2) Refrigerant In (State 1)
	Hot Water In Cooled Water Out
	Refrigerant Out (State 2)

(continued)

Table 2.1 (continued)



The overall energy balance equation of the pump is given as

$$\sum (\dot{m}h)_{\rm in} + \sum \dot{W}_{\rm p} = \sum (\dot{m}h)_{\rm out}$$
 (2.4)

where h represents specific enthalpy of the state.

The specific exergy at any state is defined as

$$ex_i = (h_i - h_0) - T_0(s_i - s_0)$$
(2.5)

where ex, T and s represent specific exergy, temperature, and specific entropy. The same equations can be written at every state of the cycle.

The overall exergy balance equation of the pump is given as

$$\sum (\dot{m} \times ex)_{in} + \dot{W}_{pump} = \sum (\dot{m} \times ex)_{out} + \dot{E}x_{dest,p}$$
 (2.6)

where $\dot{E}x_{dest,p}$ represents exergy destruction rate in the pump.

Example 2.1 Let us consider an ARS, a solution pump in which is a strong solution of an ammonia—water mixture with a concentration of 0.6 is supplied at 250 kPa with a mass flow rate of 1 kg/s. The pump is used to raise the pressure of the strong solution to 400 kPa. Consider the isentropic efficiency of the pump to be 85 % and ambient temperature and pressure to be 25 °C and 100 kPa, respectively. Calculate the power consumed by the pump and the total exergy rate destruction inside the pump.

Solution

$$P_1 = 250 \,\text{kPa} \\ x_1 = 0.6 \\ Qu_1 = 0.00 \end{cases} \begin{cases} h_1 = 199.5 \,\text{kJ/kg} \\ s_1 = 0.06834 \,\text{kJ/kg} \,\text{K} \\ v_1 = 0.001247 \,\text{m}^3/\text{kg} \end{cases}$$

$$w_p = \frac{0.001247(400 - 250)}{0.85} = 0.002201 \,\text{kW/kg}$$

$$h_2 = h_1 + w_p = 199.5 + 0.002201 = 199.5002201 \,\text{kJ/kg}$$

$$P_2 = 400 \,\text{kPa} \\ x_2 = 0.6 \\ h_2 = 199.5002201 \end{cases} s_2 = 0.06945 \,\text{kJ/kg} \,\text{K}$$

$$\dot{W}_p = \mathbf{1}.(\mathbf{0.002201}) = \mathbf{0.002201} \,\text{kW}$$

$$P_0 = 100 \,\text{kPa} \\ T_0 = 298.15 \,\text{K} \end{cases} s_0 = 2.554 \,\text{kJ/kg} \,\text{K}$$

$$\dot{E}x_1 = 1(|(199.5 - 524.3) - 298.15(0.06834 - 2.554)|) = 457 \,\text{kW}$$

$$\dot{E}x_2 = 1(|(199.5002201 - 524.3) - 298.15(0.06945 - 2.554)|) = 457.3 \,\text{kW}$$

$$457 + 0.002201 = 457.3 + \dot{E}x_{\text{dest,p}}$$

$$\dot{E}x_{\text{dest,p}} = \mathbf{0.327} \,\text{kW}$$

2.2.2 Generator

The mass balance equations of the generator as displayed in Table 2.1 can be written as

$$\sum \dot{m}_{\rm in} = \sum \dot{m}_{\rm out} \tag{2.7}$$

and

$$\sum (\dot{m}x)_{\rm in} = \sum (\dot{m}x)_{\rm out} \tag{2.8}$$

where x represents concentration of the solution.

The energy balance equation of the generator is given as

$$\sum (\dot{m}h)_{\rm in} + \sum \dot{Q}_{\rm g} = \sum (\dot{m}h)_{\rm out}$$
 (2.9)

where \dot{Q}_{g} represents rate of heat required by the generator.

The thermal exergy rate supplied to the generator is defined as

$$\dot{\mathbf{E}}\mathbf{x}_{\mathsf{th},\mathsf{g}} = \left(1 - \frac{T_0}{T_\mathsf{g}}\right) \dot{Q}_\mathsf{g} \tag{2.10}$$

where $\dot{E}x_{th,g}$ represents thermal exergy rate of generator.

The exergy balance equation of the generator is given as

$$\sum (\dot{m} \times ex)_{\rm in} + \dot{E}x_{\rm th,g} = \sum (\dot{m} \times ex)_{out} + \dot{E}x_{\rm dest,g}$$
 (2.11)

where $\dot{E}x_{dest,g}$ represents rate of exergy destruction in the generator.

Example 2.2 A strong solution of an ammonia-water mixture at 400 K and 400 kPa with a concentration of 0.6 enters the ARS generator. In the generator, 250 kW of heat is supplied to vaporize the ammonia refrigerant from the strong solution. The weak solution and ammonia refrigerant leaves the generator with a mass concentration of 0.4 and 0.999, respectively. The temperature of the weak solution leaving the generator is taken to be 15 °C higher than the strong solution temperature. Calculate the exit temperature of the refrigerant vapor, mass flow rate of the refrigerant and strong solution and total destroyed exergy rate in the generator. Assume ambient temperature and pressure to be 25 °C and 100 kPa, respectively.

Solution

Solving two equations simultaneously will give us

$$\dot{m}_{2} = 0.6661 \text{ and } \dot{m}_{3} = 0.3339 \text{ kg}$$

$$\dot{m}_{1}h_{1} + \dot{Q}_{g} = \dot{m}_{2}h_{2} + \dot{m}_{3}h_{3}$$

$$1(2022) + 250 = 0.6661(2282) + 0.3339h_{3}$$

$$h_{3} = 2252 \text{ kJ/kg}$$

$$P_{3} = 400 \text{ kPa}$$

$$x_{3} = 0.999$$

$$h_{3} = 2252 \text{ kJ/kg}$$

$$\dot{E}x_{1} = 1[(2022 - 524.3) - 298.15(6.387 - 2.554)] = 355.2 \text{ kW}$$

$$\dot{E}x_{2} = 0.6661[(2282 - 80.87) - 298.15(6.718 - 0.9197)] = 314.9 \text{ kW}$$

$$\dot{E}x_{3} = 0.3339[(2252 - 1353) - 298.15(6.877 - 5.621)] = 175.1 \text{ kW}$$

$$\dot{E}x_{4} = \left(1 - \frac{298.15}{662.7}\right) 250 = 137.5 \text{ kW}$$

$$355.2 + 137.5 = 314.9 + 175.1 + \dot{E}x_{dest,g}$$

$$\dot{E}x_{dest,g} = 2.77 \text{ kW}$$

2.2.3 Condenser

The mass balance equation for the condenser as portrayed in Table 2.1 is defined as

$$\sum \dot{m}_{\rm in} = \sum \dot{m}_{\rm out} \tag{2.12}$$

The overall energy balance equation of the condenser is given as

$$\sum (\dot{m}h)_{\rm in} = \sum (\dot{m}h)_{\rm out} + \sum \dot{Q}_{\rm c}$$
 (2.13)

where \dot{Q}_{c} represents the rate of heat rejected by the refrigerant flowing through the condenser.

The thermal exergy rate rejected by the condenser is defined as

$$\dot{\mathbf{E}}\mathbf{x}_{th,c} = \left(1 - \frac{T_0}{T_c}\right)\dot{Q}_c \tag{2.14}$$

where $\dot{E}x_{th,c}$ represents thermal exergy rate of condenser.

The overall exergy balance equation of the condenser is given as

$$\sum (\dot{m} \times ex)_{in} = \sum (\dot{m} \times ex)_{out} + \dot{E}x_{th,c} + \dot{E}x_{dest,c}$$
 (2.15)

where $\dot{E}x_{dest,c}$ represents rate of exergy destruction in the condenser.

Example 2.3 In a condenser, ammonia vapor enters at 400 kPa, 400 K with a concentration of 0.999. The ammonia vapor leaves the condenser at 313.5 K with a mass flow rate of 1 kg/s. Calculate the rate of heat rejected by the condenser and total destroyed exergy rate in the condenser. Take ambient temperature and pressure to be 25 °C and 100 kPa, respectively.

Solution

$$P_{1} = 400 \text{ kPa} \\ x_{1} = 0.999 \\ T_{1} = 400 \text{ K}$$

$$\begin{cases} h_{1} = 1571 \text{ kJ/kg} \\ s_{1} = 5.58 \text{ kJ/kg K} \end{cases}$$

$$P_{2} = 400 \text{ kPa} \\ x_{2} = 0.999 \\ T_{2} = 313.5 \text{ K}$$

$$\begin{cases} h_{2} = 1369 \text{ kJ/kg} \\ s_{2} = 5.011 \text{ kJ/kg K} \end{cases}$$

$$\dot{m}_{1}h_{1} = \dot{m}_{2}h_{2} + \dot{Q}_{c} \\ 1(1571) = 1(1369) + \dot{Q}_{c}$$

$$\dot{Q}_{c} = 202.2 \text{ kW}$$

$$\dot{E}x_{1} = 1[(1571 - 1353) - 298.15(5.58 - 5.621)] = 230.1 \text{ kW}$$

$$\dot{E}x_{2} = 1[(1369 - 1353) - 298.15(5.011 - 5.621)] = 197.7 \text{ kW}$$

$$\dot{E}x_{th,c} = \left(1 - \frac{298.15}{313.2}\right) 202.2 = 9.684 \text{ kW}$$

$$230.1 = 197.7 + 9.684 + \dot{E}x_{dest,c}$$

$$\dot{E}x_{dest,c} = 22.66 \text{ kW}$$

2.2.4 Evaporator

The mass balance equation for the evaporator as shown in Table 2.1 is written as

$$\sum \dot{m}_{\rm in} = \sum \dot{m}_{\rm out} \tag{2.16}$$

The overall energy balance equation of the evaporator is given as

$$\sum (\dot{m}h)_{\rm in} + \sum \dot{Q}_{\rm e} = \sum (\dot{m}h)_{\rm out}$$
 (2.17)

where \dot{Q}_{e} represents rate of heat gained by the refrigerant flowing through the evaporator.

The thermal exergy rate gained by the evaporator is defined as

$$\dot{\mathbf{E}}\mathbf{x}_{\text{th,e}} = \left(1 - \frac{T_0}{T_e}\right)\dot{Q}_e \tag{2.18}$$

where $\dot{E}x_{\text{th,e}}$ represents thermal exergy rate of evaporator.

The overall exergy balance equation of the evaporator is given as

$$\sum (\dot{m} \times ex)_{in} + \dot{E}x_{th,e} = \sum (\dot{m} \times ex)_{out} + \dot{E}x_{dest,e}$$
 (2.19)

where Exdest,e represents rate of exergy destruction in the evaporator.

Example 2.4 An ammonia refrigerant enters the evaporator at 250 kPa, 259.6 K with a concentration of 0.999. The refrigerant leaves the evaporator at 259.7 K with a mass flow rate of 1 kg/s. Calculate the cooling rate and total destroyed exergy rate in the evaporator. Assume ambient temperature and pressure to be 25 °C and 100 kPa, respectively.

• Solution

$$P_1 = 250 \text{ kPa} \atop x_1 = 0.999 \atop T_1 = 259.6 \text{ K}$$

$$\begin{cases} h_1 = 965.2 \text{ kJ/kg} \\ s_1 = 3.724 \text{ kJ/kg K} \end{cases}$$

$$P_2 = 250 \text{ kPa} \atop x_2 = 0.999 \atop T_2 = 259.7 \text{ K}$$

$$\begin{cases} h_2 = 1058 \text{ kJ/kg} \\ s_2 = 4.0891 \text{ kJ/kg K} \end{cases}$$

$$\begin{aligned} \dot{m}_1 h_1 + \dot{Q}_e &= \dot{m}_2 h_2 \\ 1(965.2) + \dot{Q}_e &= 1(1058) \\ \dot{Q}_e &= 93.14 \text{ kW} \end{cases}$$

$$\begin{split} \dot{E}x_1 &= 1[(965.2 - 1353) - 298.15(3.724 - 5.621)] = 177.7 \, kW \\ \dot{E}x_2 &= 1[(1058 - 1353) - 298.15(4.081 - 5.621)] = 164.4 \, kW \\ \dot{E}x_{th,e} &= \left| \left(1 - \frac{298.15}{259.6} \right) 93.14 \right| = 13.83 \, kW \\ 177.7 + 13.83 &= 164.4 + \dot{E}x_{dest,e} \\ \dot{E}x_{dest,e} &= 27.16 \, kW \end{split}$$

2.2.5 Absorber

The mass balance equation for the absorber as displayed in Table 2.1 is written as

$$\sum \dot{m}_{\rm in} = \sum \dot{m}_{\rm out} \tag{2.20}$$

The overall energy balance equation of the absorber is given as

$$\sum (\dot{m}h)_{\rm in} = \sum (\dot{m}h)_{out} + \sum \dot{Q}_{\rm a}$$
 (2.21)

where \dot{Q}_a represents rate of heat rejected by the refrigerant and the weak solution when they mix together in the absorber.

The thermal exergy rate rejected by the absorber is calculated as

$$\dot{\mathbf{E}}\mathbf{x}_{\text{th,a}} = \left(1 - \frac{T_0}{T_a}\right)\dot{Q}_a \tag{2.22}$$

where $\dot{E}x_{th,a}$ represents thermal exergy rate of absorber.

The overall exergy balance equation of the absorber is given as

$$\sum (\dot{m} \times ex)_{in} = \sum (\dot{m} \times ex)_{out} + \dot{E}x_{th,a} + \dot{E}x_{dest,a}$$
 (2.23)

where $\dot{E}x_{dest,a}$ represents rate of exergy destruction in the absorber.

Example 2.5 In an absorber of the absorption refrigeration system, ammonia refrigerant enters at 250 kPa and 259.7 K with a mass flow rate and concentration of 0.5 kg/s and 0.999, respectively. The weak solution enters the absorber at 250 kPa and 314 K with a concentration and mass flow rate of 0.25 and 0.5 kg/s, respectively. The weak solution leaves the absorber as a saturated liquid with a concentration of 0.35. Calculate the heat rate rejected by the absorber and total destroyed exergy rate in the absorber. Assume ambient temperature and pressure to be 25 °C and 100 kPa, respectively.

Solution

$$P_1 = 250 \,\mathrm{kPa} \\ x_1 = 0.35 \\ Q_1 = 0 \\ \begin{cases} h_1 = -16.77 \,\mathrm{kJ/kg} \\ s_1 = 0.5451 \,\mathrm{kJ/kg} \,\mathrm{K} \end{cases}$$

$$P_2 = 250 \,\mathrm{kPa} \\ x_2 = 0.999 \\ T_2 = 259.7 \,\mathrm{K} \\ \end{cases} \begin{cases} h_2 = 1058 \,\mathrm{kJ/kg} \\ s_1 = 4.081 \,\mathrm{kJ/kg} \,\mathrm{K} \end{cases}$$

$$P_3 = 250 \,\mathrm{kPa} \\ x_3 = 0.25 \\ T_3 = 314 \,\mathrm{K} \\ \end{cases} \begin{cases} h_3 = 10.58 \,\mathrm{kJ/kg} \\ s_3 = 0.5496 \,\mathrm{kJ/kg} \,\mathrm{K} \end{cases}$$

$$\dot{m}_1 h_1 + \dot{Q}_a = \dot{m}_2 h_2 + \dot{m}_3 h_3 \\ 1(-16.77) + \dot{Q}_a = 0.5(1058) + 0.5(10.58) \\ \dot{Q}_a = 551.2 \,\mathrm{kW} \\ \dot{E}x_1 = 1[(-16.77 - (-29.98)) - 298.15(0.5451 - 5.112)] = 36.64 \,\mathrm{kW} \\ \dot{E}x_2 = 1[(1058 - 1353) - 298.15(4.081 - 5.621)] = 82.18 \,\mathrm{kW} \\ \dot{E}x_3 = 1[(10.58 - (-57.23)) - 298.15(0.5496 - 0.3285)] = 0.9507 \,\mathrm{kW} \\ \dot{E}x_{th,a} = \left| \left(1 - \frac{298.15}{314} \right) 551.2 \right| = 27.83 \,\mathrm{kW} \\ 36.64 + 27.83 = 82.18 + 09507 + \dot{E}x_{dest,a} \\ \dot{E}x_{dest,a} = 18.67 \,\mathrm{kW} \end{cases}$$

2.2.6 Expansion Valve

The mass balance equation for the expansion valve as shown in Table 2.1 is written as

$$\dot{m}_{\rm in} = \dot{m}_{\rm out} \tag{2.24}$$

The overall energy balance equation of the expansion valve is defined as

$$(\dot{m}h)_{\rm in} = (\dot{m}h)_{\rm out} \tag{2.25}$$

The overall exergy balance equation of the expansion valve is defined as

$$\sum (\dot{m} \times ex)_{\rm in} = \sum (\dot{m} \times ex)_{\rm out} + \dot{E}x_{\rm dest,ev}$$
 (2.26)

where $\dot{E}x_{dest,ev}$ represents rate of exergy destruction in the expansion valve.

Example 2.6 In an expansion valve, a weak solution with a concentration of 0.113 enters at 443.2 K and 1548 kPa. The weak solution leaves at 478.4 kPa with a mass flow rate of 1 kg/s. Calculate the exit temperature of the expansion valve and total destructed exergy rate. Assume ambient temperature and pressure to be 25 °C and 100 kPa, respectively.

Solution

$$P_1 = 1548 \text{ kPa} \\ x_1 = 0.4 \\ T_1 = 443.2 \text{ K} \end{cases} h_1 = 654.2 \text{ kJ/kg} \\ s_1 = 2.103 \text{ kJ/kg K} \end{cases}$$

$$P_2 = 478.4 \text{ kPa} \\ x_2 = x_1 \\ h_2 = h_1 \end{cases} T_2 = 402.2 \text{ K} \\ s_2 = 2.132 \text{ kJ/kg K} \end{cases}$$

$$\dot{E}x_1 = 1[(654.2 - 28.46) - 298.15(2.103 - 0.4027)] = 118.7 \text{ kW}$$

$$\dot{E}x_2 = 1[(654.2 - 28.46) - 298.15(2.132 - 0.4027)] = 110.1 \text{ kW}$$

$$118.7 = 110.1 + \dot{E}x_{\text{dest,ev}}$$

$$\dot{E}x_{\text{dest,ev}} = 8.578 \text{ kW}$$

2.2.7 Coefficient of Performance

The performance of an absorption refrigeration system is measured using the coefficient of performance. The energetic coefficient of performance of is defined as

$$COP_{en} = \frac{\dot{Q}_e}{\sum \dot{Q}_{in} + \dot{W}_p}$$
 (2.27)

The exergetic COP is defined as

$$COP_{ex} = \frac{\dot{E}x_{th,e}}{\sum \dot{E}x_{th,in} + \dot{W}_{p}}$$
 (2.28)

Example 2.7 An absorption refrigeration system is capable of producing 220 kW of cooling while consuming 150 kW of heat in the generator. The solution pump consumes 1 kW of power to pump the solution from 250 to 400 kPa. Calculate the energy and exergy coefficients of performance for this absorption refrigeration system. Assume evaporator, generator and ambient temperatures to be 260, 520, and 298 K, respectively.

Solution

$$COP_{en} = \frac{220}{150 + 1} = 1.46$$

$$COP_{ex} = \frac{\left|1 - \frac{298}{260}\right|220}{\left(1 - \frac{298}{570}\right)150 + 1} = 0.49$$

2.3 Exergoeconomic Analysis

Exergoeconomic analysis opens a new front in cost analysis of the energy systems by bridging the gap between the exergy and the cost of the system. Exergoeconomic analysis takes into consideration the cost of the equipment, operational costs, the cost of working fluid, and costs related to the exergy destruction of the system.

The exergoeconomic equation of the absorption refrigeration system is written as

$$\dot{Z}_{eq} + \dot{C}_{OPM} = \dot{C}_{Cool} \tag{2.29}$$

where \dot{Z}_{eq} , \dot{C}_{OPM} , and \dot{C}_{Cool} represent cost associated with equipments, operation and maintenance, and cooling, respectively.

The cost linked with the equipment is calculated as

$$\dot{Z}_{eq} = \dot{C}_a + \dot{C}_g + \dot{C}_c + \dot{C}_e + \dot{C}_P + \dot{C}_{ev}$$
 (2.30)

where \dot{C}_a , \dot{C}_g , \dot{C}_c , \dot{C}_e , \dot{C}_P and \dot{C}_{ev} represent the cost of the absorber, generator, condenser, evaporator, pump and expansion valve, respectively.

The cost associated with the operation and maintenance is defined as

$$\dot{C}_{\text{OPM}} = c_{\text{OPM}} \times \dot{E}x_{\text{OPM}} \tag{2.31}$$

where c_{OPM} and $\dot{\text{E}}x_{\text{OPM}}$ represent operation and maintenance cost and exergy carried by the heat and power, respectively.

The cost related to the cooling produced is defined as

$$\dot{C}_{\text{Cool}} = c_{\text{Cool}} \times \dot{E}_{\text{XCool}} \tag{2.32}$$

where c_{Cool} and $\dot{\text{E}}x_{\text{Cool}}$ represent cost of cooling produced and the exergy related to the cooling produced, respectively.

Thus the above equation can be written as

$$(c \times \dot{E}x)_{OPM} + \dot{Z}_{eq} = (c \times \dot{E}x)_{Cool}$$
 (2.33)

The cost of cooling can then be calculated by rearranging the above mentioned equation and rewriting it as

$$c_{\text{Cool}} = \frac{(c \times \dot{\text{Ex}})_{\text{OPM}} + \dot{Z}_{\text{eq}}}{\dot{\text{Ex}}_{\text{cool}}}$$
(2.34)

The problems, which have more unknowns than equations can be simplified by replacing exergy terms with mass flow rate terms. Figure 2.1 displays a flowchart for exergoeconomic analysis.

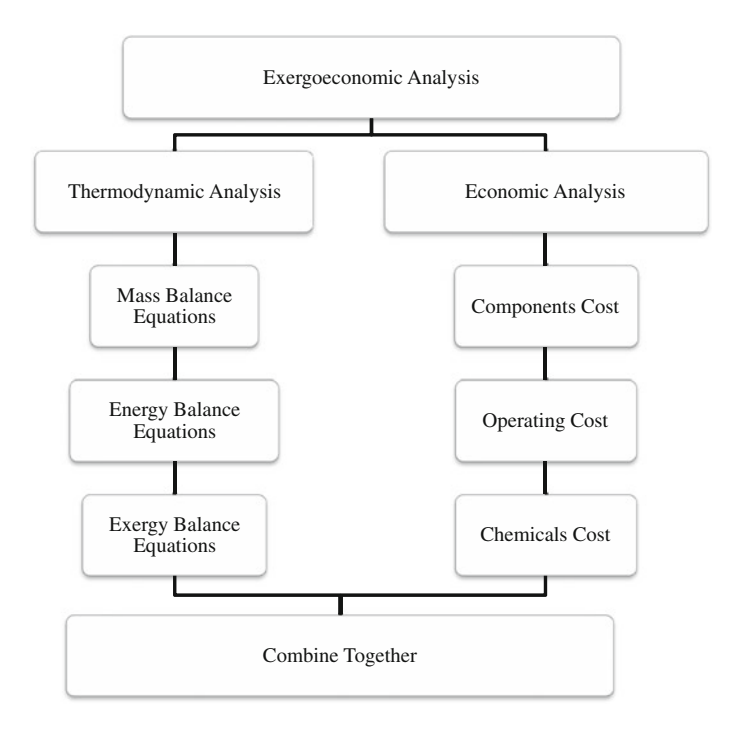


Fig. 2.1 Flowchart of exergoeconomic analysis

Example 2.8 An absorption refrigeration system is capable of producing 220 kW of cooling. The solution pump consumes 1 kW of power to pump the solution from 250 to 400 kPa. Calculate the cooling cost of this absorption refrigeration system. Assume evaporator and ambient temperatures to be 260 and 298 K, respectively. Note: the equipment cost of absorption refrigeration system can be estimated using $\dot{Z}_{eq}(\$) = 1144.3(\dot{Q}_{cool})^{0.67}$ and consider operation and maintenance cost to be 3 % of the total investment cost.

Solution

$$\begin{split} \dot{Z}_{eq} &= 1144.3(220)^{0.67} = \$42458 \\ \dot{C}_{OPM} &= 0.03 * 42458 = \$1274 \\ \dot{E}x_{Cool} &= \left(\left|1 - \frac{298}{260}\right|\right) 220 = 32.15 \, kW \\ c_{Cool} &= \frac{1274 + 42458}{32.15} = 1360 \, \$/kW \end{split}$$

2.4 Exergoenvironmental Analysis

In the present era, it is necessary to conduct an environmental analysis of a system under investigation to ensure that it has a minimal or no effect on the environment. This section of the chapter combines exergy and environmental analyses to present a new type of study namely exergoenvironmental analysis. Exergoenvironmental analysis is based on exergy analysis and it takes into account exergy destruction and efficiency to provide a measure of its impact on the environment. Exergoenvironmental analysis consists of six parameters which are an impact factor, impact coefficient, impact index impact improvement, exergetic stability factor, and exergetic sustainability index.

2.4.1 Exergoenvironmental Impact Factor

The exergoenvironmental impact factor determines the positive effect of the investigated system on the environment. The purpose of studying this parameter is that it helps to reduce the environmental impact of the system by decreasing the irreversibility in the system.

The reference value of this factor is "zero" which shows that the system has no irreversibility. The exergoenvironmental impact factor is defined as

$$f_{\rm ei} = \frac{\dot{\rm E}x_{\rm dest,tot}}{\sum \dot{\rm E}x_{\rm in}} \tag{2.35}$$

where $f_{\rm ei}$, $\dot{\rm E}x_{\rm dest,tot}$ and $\dot{\rm E}x_{\rm in}$ represent exergoenvironmental impact factor, total exergy destruction rate in the system and total exergy rate supplied to the system, respectively.

2.4.2 Exergoenvironmental Impact Coefficient

The exergoenvironmental impact coefficient is related to the exergetic efficiency of the system. In the ideal case, its value should be one, indicating that the system is working under an ideal condition with no exergy destruction. This coefficient is defined as

$$C_{\rm ei} = \frac{1}{\eta_{\rm ex}/100} \tag{2.36}$$

where C_{ei} and η_{ex} represent exergoenvironmental impact coefficient and exergetic efficiency, respectively.

2.4.3 Exergoenvironmental Impact Index

The exergoenvironmental impact index is an important parameter to study as it indicates whether or not the system under investigation damages the environment due to its unusable waste exergy output and exergy destruction. The desired value of the exergoenvironmental impact index should be as small as possible. The exergoenvironmental impact index is calculated by multiplying exergoenvironmental impact factor with exergoenvironmental impact coefficient and is defined as

$$\theta_{\rm ei} = f_{\rm ei} \times C_{\rm ei} \tag{2.37}$$

where θ_{ei} represents exergoenvironmental impact index.

2.4.4 Exergoenvironmental Impact Improvement

The exergoenvironmental impact improvement parameter helps in finding the environmental appropriateness of the investigated system. In order to improve the environmental appropriateness of the system, its exergoenvironmental impact index should be minimized. A high value of exergoenvironmental impact improvement means system is more useful for the environment and it is defined as

$$\theta_{eii} = \frac{1}{\theta_{ei}} \tag{2.38}$$

where θ_{eii} represents exergoenvironmental impact improvement.

2.4.5 Exergetic Stability Factor

The exergetic stability factor is a function of the desired output exergy, total exergy destruction, and exergy carried by unused fuel. The desired value of this factor should be as close to "one" as possible. This factor is defined as

$$f_{\rm es} = \frac{\dot{E}x_{\rm tot,out}}{\dot{E}x_{\rm tot,out} + \dot{E}x_{\rm dest,tot} + \dot{E}x_{\rm uu}}$$
(2.39)

where $f_{\rm es}$ and $\dot{\rm E}x_{\rm uu}$ represent exergetic stability factor and exergy rate carried by unused fuel.

2.4.6 Exergetic Sustainability Index

The exergetic sustainability index is the multiplication of exergetic stability factor and exergoenvironmental impact improvement of the system. This desired value of the exergetic sustainability index should be as high as possible. This index is defined as

$$\theta_{\rm est} = f_{\rm es} \times \theta_{\rm eii}$$
 (2.40)

where θ_{est} represents exergetic sustainability index.

Example 2.9 The rate of exergy supplied to the absorption refrigeration system through the generator, evaporator and pump are 48.39, 16.42, and 1.971 kW, respectively. The rate of exergy released by the condenser and absorber are 3.595 and 16.27 kW, respectively. Calculate all the exergoenvironmental parameters defined in the above section. The exergetic COP of absorption refrigeration system is 0.326.

Solution

$$\begin{split} \dot{\text{Ex}}_{\text{in}} &= 48.39 + 16.42 + 1.971 = 66.78 \, \text{kW} \\ \dot{\text{Ex}}_{\text{out}} &= 16.27 + 3.595 = 19.86 \, \text{kW} \\ \dot{\text{Ex}}_{\text{dest,tot}} &= 66.78 - 19.86 = 46.92 \, \text{kW} \\ \dot{f}_{\text{ei}} &= \frac{46.92}{66.78} = 0.70 \\ C_{\text{ei}} &= \frac{1}{0.326} = 3.07 \\ \theta_{\text{ei}} &= 0.70 \times 3.07 = 2.16 \\ \theta_{\text{eii}} &= \frac{1}{2.16} = 0.46 \\ f_{\text{es}} &= \frac{19.86}{19.86 + 46.92} = 0.29 \\ \theta_{\text{est}} &= 0.29 \times 0.46 = 0.13 \end{split}$$

2.5 Optimization

In designing any system, it is important to perform an optimization study in order to attain the best possible operating parameters. The optimization carried out using multi-objective optimization theory help to find the best possible set of design values needed to attain the preset objectives. There are many multi-objective optimization techniques available in the literature, but the most robust one is the genetic algorithm technique as shown in Fig. 2.2. The genetic algorithm technique can provide the best possible result for any desired output based on several inputs. The genetic method is a vigorous optimization algorithm that is designed to reliably locate a global optimum even in the presence of local minima/maxima. The genetic method intends to mimic the processes occurring in biological evolution. Initially, sample points are chosen at random from the range specified by the bounds of the independent variables. The sample points are then surveyed to determine the values of the objective function as quantified by the value of the variable that is to be minimized or maximized. A new generation of sample points is then generated in a stochastic manner by combining selected points of the current sample points. The characteristics of a point that are passed on to the next generation are represented by encoded values of its independent variables. The probability that a point out of the current sample point will be selected for breeding the next generation is an increasing function of its value. This process continues untill the best points are recorded.

There is much software available that can perform optimization studies but the most prominent are Matlab developed by Moler (2014) and Engineering Equation

2.5 Optimization 45

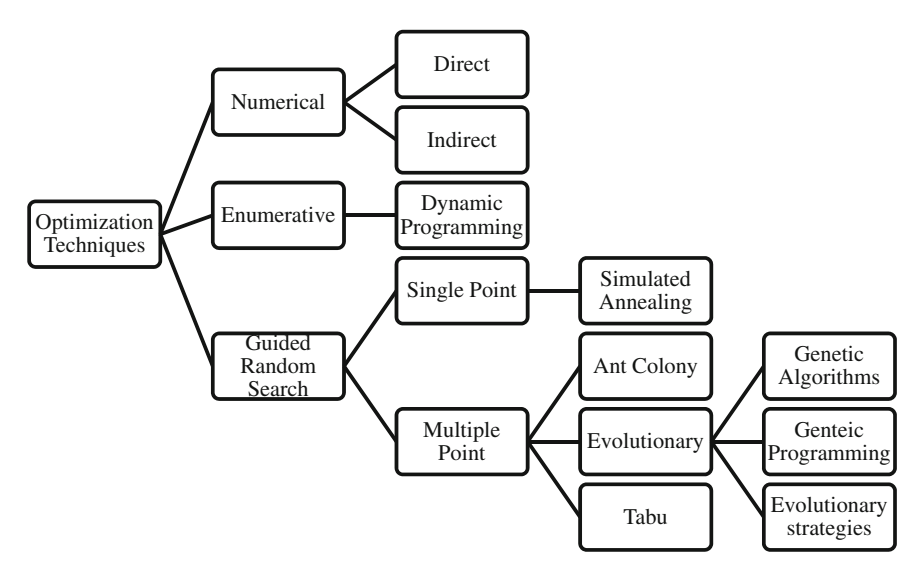


Fig. 2.2 Flowchart of optimization techniques

Solver developed by Klein (2014). While performing multi-objective optimization, first define the objective functions . The objective functions are those that should either maximized or minimized based on the requirement. An example for objective functions in absorption refrigeration systems is exergy COP (to be maximized) and cost of cooling (to be minimized). The second step in performing optimization study is the to define the independent variables also known as constraints. Independent variables are variables that the designer wishes to use to optimize the desired objective functions. Examples of independent variables in optimization study of an absorption refrigeration system are the concentration of weak and strong solutions and evaporator temperature. While selecting the independent variables, the designer should ensure that they are within the acceptable range or else the optimized results obtained will be hypothetical.

Example 2.10 Reconsider Example 2.2 in order to optimize the performance of the generator by minimizing the exergy destruction rate. The constraints to this problem are the concentration of the strong solution, the concentration of the weak solution and inlet temperature to the generator which varies between 0.45–0.6, 0.35–0.45, and 350–400 K, respectively. Use Nelder–Mead Simplex method optimization routine in an engineering equation solver to carry out this optimization.

Table 2.2 Constraints and best values for the optimization study

Name	Constraints	Best value	
Strong solution concentration	0.45-0.6	0.5518	
Weak solution concentration	0.35-0.45	0.4042	
Inlet temperature	350–400 K	378 K	

Solution

The objective function for this problem is written as

$$\dot{E}x_1 + \dot{E}x_{th,g} = \dot{E}x_2 + \dot{E}x_3 + \dot{E}x_{dest,g}$$

The optimized exergy destruction rate obtained for the present analysis is 0.001251 kW. The parameters at which this exergy destruction rate is achieved are presented in Table 2.2.

2.6 Closing Remarks

The use of absorption refrigeration systems, instead of the conventional vapor-compression refrigeration systems, to provide cooling offers a potential solution when process/waste heat or renewable heat is available. This helps to reduce environmental impact and increasing sustainability. Studying such systems energetically and exergetically is essential for their design, analysis, assessment, evaluation, and improvement. In this regard, this chapter presents comprehensive energy and exergy analyses of ARSs and their components with numerous illustrative examples. It also covers the use of exergoeconomic and exergoenvironmental analyses, instead of conventional economic and environmental studies, in terms of effect on cost and the environment because exergy provides more realistic results as compared to energy. Furthermore, it presents an optimization study before commissioning any system. The optimization study based on genetic algorithm provides best possible results, as this optimization technique can easily locate the global optimum even in the presence of local maximum and minimum. An example for each section is also provided to enhance the understanding of the material.

References

Klein, S. A. (2014). Engineering equation solver (EES): Academic commercial. F-Chart Software. www.fChart.com

Moler, C. (2014). Matlab: Acadmic. Mathworks. www.mathworks.com

Chapter 3 Single Effect Absorption Refrigeration System

3.1 Introduction

Humanity today faces environmental problems spanning a growing range of pollutants, hazards, and ecosystem degradation over increasing areas. The most significant problems include global climate change, stratospheric ozone depletion, and acid precipitation. The former stems from increasing atmospheric concentrations of greenhouse gases, which trap heat radiated from the earth's surface. Global climate change increases the surface temperature of the earth and raises sea levels, and is potentially the most important environmental problem related to energy use. Renewable energy systems, in this regard, appear to be strong candidates to help reduce the emissions and provide sustainable energy options. Conventional mechanical compression refrigeration systems rely on electricity only. If electricity comes from power plants where fossil fuels are employed, they contribute to environmental issues by emitting greenhouse gases. It is then important to use heat sources to drive refrigeration systems. Is this possible? Yes, it is possible with absorption refrigeration systems, where heat is supplied to the generator to drive the system to provide the refrigeration effect through an evaporator.

In the present chapter, the single effect absorption refrigeration system is introduced and discussed for its basic operation and thermodynamic analyses. In addition, the performance of the single effect absorption refrigeration system (SEARS) is discussed through energetic and exergetic-based coefficients of performance. At first, a description of the SEARS is provided to ensure understanding of the working principle. Second, energy, exergy, exergoenvironmental, exergoe-conomic, and optimization methodologies of the SEARS are provided in detail for assessment and evaluation as well as comparison. Finally, an illustrative example is provided to ensure that the readers understand how the respective balance equations are used to generate numerical results from the SEARS.

3.2 System Description

The SEARS is the simplest of all the absorption refrigeration systems studied or employed physically as shown in Fig. 3.1. In the SEARS, a strong solution of ammonia—water leaves the absorber at state 1 and enters the pump in a saturated liquid phase. In the pump, the pressure of the strong solution increases before it leaves at state 2. The strong solution at state 2 then enters the heat recovery heat exchanger, where it gains heat from the returning fluid to leave at state 3 at comparatively higher temperature. This strong solution at state 3 then enters the generator. In the generator, heat is supplied from an external source to boil the strong solution of ammonia-water. The boiling helps to separate ammonia from the mixture because ammonia boils at much lower temperature than water. The ammonia vapor is then extracted from the generator at state 7 and the remaining weak ammonia-water solution is extracted at state 4. This weak solution then enters the heat recovery heat exchanger, where it releases heat into the incoming strong solution to leave at a relatively lower temperature at state 5. The weak solution then enters the expansion valve, where its pressure drops suddenly to that of the absorber before it enters the absorber at state 6. The ammonia vapor extracted at state 7 then passes through the condenser, where it releases heat into the environment and leaves as a relatively cooled ammonia stream at state 8. This ammonia at state 8 later enters the expansion valve where it experiences a sudden pressure drop to that of the evaporator before entering the evaporator

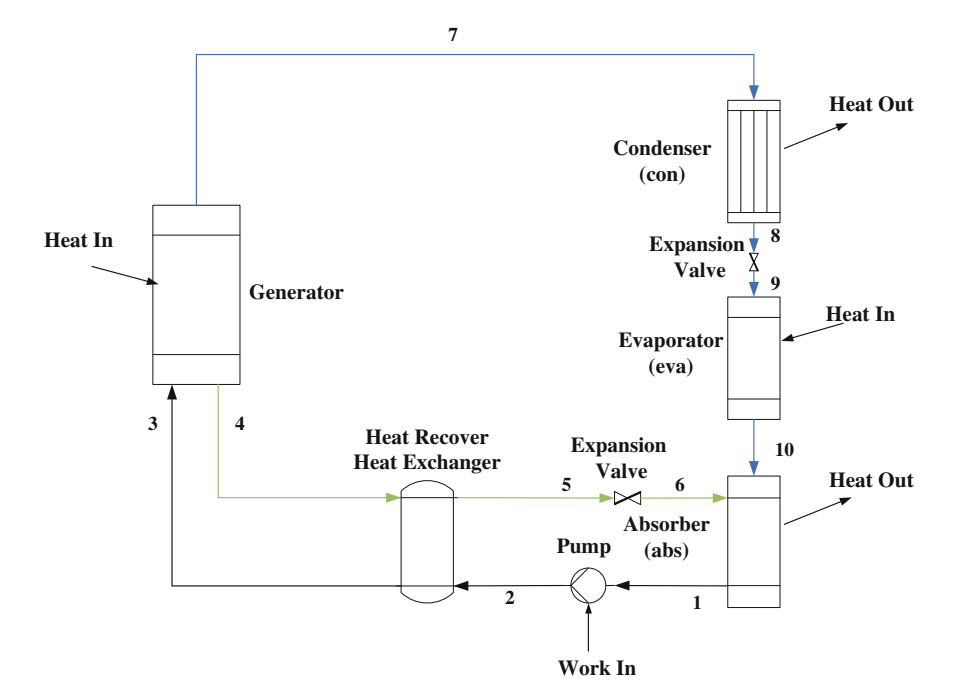


Fig. 3.1 Schematic of the SEARS

at state 9. In the evaporator, ammonia gains heat from the cooling space and leaves at state 10 to enter the absorber. The absorber acts as a mixing chamber, where ammonia from state 10 and the weak solution from state 6 mix together and release heat before leaving as a strong solution mixture at state 1.

3.3 Energy and Exergy Analyses

This section provides energy and exergy balance equations for each components of the SEARS.

• Pump:

The mass balance equation across the pump as shown in Fig. 3.1 can be written as

$$\dot{m}_1 = \dot{m}_2 = \dot{m}_p \tag{3.1}$$

where \dot{m} represents the mass flow rate.

The specific power consumed by the pump can be calculated using

$$w_{\rm p} = \frac{v(P_2 - P_1)}{\eta_{\rm p}} \tag{3.2}$$

where w, v, P and η represent specific power, specific volume, pressure and efficiency, respectively.

The total power consumed by the pump is defined as

$$\dot{W}_{\rm p} = \dot{m}_{\rm p} w_{\rm p} \tag{3.3}$$

where \dot{W} represents total power consumed by the pump.

The overall energy balance equation of the pump is given as

$$(\dot{m}h)_1 + \dot{W}_p = (\dot{m}h)_2 \tag{3.4}$$

where h represents specific enthalpy of the state.

The specific exergies at states 1 and 2 are defined as

$$ex_1 = (h_1 - h_0) - T_0(s_1 - s_0)$$
(3.5)

$$ex_2 = (h_2 - h_0) - T_0(s_2 - s_0)$$
(3.6)

where ex, T and s represent specific exergy, temperature, and specific entropy.

The overall exergy balance equation of the pump is given as

$$\dot{m}_1 ex_1 + \dot{W}_p = \dot{m}_2 ex_2 + \dot{E}x_{dest,p}$$
 (3.7)

where $\dot{E}x_{dest,p}$ represents the exergy destruction rate in the pump.

• Heat recovery heat exchanger:

The mass balance equations for the heat recovery heat exchanger as shown in Fig. 3.1 can be written as

$$\dot{m}_2 = \dot{m}_3 \tag{3.8}$$

$$\dot{m}_4 = \dot{m}_5 \tag{3.9}$$

The energy balance equation is given as

$$\dot{m}_2 h_2 + \dot{m}_4 h_4 = \dot{m}_3 h_3 + \dot{m}_5 h_5 \tag{3.10}$$

The specific exergies at states 3-5 are defined as

$$ex_3 = (h_3 - h_0) - T_0(s_3 - s_0)$$
(3.11)

$$ex_4 = (h_4 - h_0) - T_0(s_4 - s_0)$$
(3.12)

$$ex_5 = (h_5 - h_0) - T_0(s_5 - s_0)$$
(3.13)

The exergy balance equation is given as

$$\dot{m}_2 ex_2 + \dot{m}_4 ex_4 = \dot{m}_3 ex_3 + \dot{m}_5 ex_5 + \dot{E}x_{dest,HX}$$
 (3.14)

where $\dot{E}x_{dest,HX}$ represents the exergy destruction rate in the heat recovery heat exchanger.

Generator:

The mass balance equations of the generator, as shown in Fig. 3.1 can be written as

$$\dot{m}_3 = \dot{m}_4 + \dot{m}_7 \tag{3.15}$$

and

$$\dot{m}_3 x_3 = \dot{m}_4 x_4 + \dot{m}_7 x_7 \tag{3.16}$$

where x represents the concentration of the solution.

The energy balance equation is given as

$$\dot{m}_3 h_3 + \dot{Q}_g = \dot{m}_4 h_4 + \dot{m}_7 h_7 \tag{3.17}$$

where \dot{Q}_{g} represents the rate of heat required by the generator.

The specific exergies at states 6 and 7 are defined as

$$ex_6 = (h_6 - h_0) - T_0(s_6 - s_0)$$
(3.18)

$$ex_7 = (h_7 - h_0) - T_0(s_7 - s_0)$$
(3.19)

The thermal exergy rate supplied to the generator is defined as

$$\dot{\mathbf{E}}\mathbf{x}_{\text{th,g}} = \left(1 - \frac{T_0}{T_g}\right) \dot{Q}_g \tag{3.20}$$

where $\dot{E}x_{th,g}$ represents the thermal exergy rate of the generator.

The exergy balance equation is given as

$$\dot{m}_3 \text{ex}_3 + \dot{E}x_{\text{th.g}} = \dot{m}_4 \text{ex}_4 + \dot{m}_7 \text{ex}_7 + \dot{E}x_{\text{dest.g}}$$
 (3.21)

where $\dot{E}x_{dest,g}$ represents the rate of exergy destruction in the generator.

Condenser:

The mass balance equation for the condenser as shown in Fig. 3.1 is defined as

$$\dot{m}_7 = \dot{m}_8 \tag{3.22}$$

The energy balance equation is given as

$$\dot{m}_7 h_7 = \dot{m}_8 h_8 + \dot{Q}_c \tag{3.23}$$

where \dot{Q}_{c} represents the rate of heat rejected by the refrigerant flowing through the condenser.

The specific exergy at state 8 is defined as

$$ex_8 = (h_8 - h_0) - T_0(s_8 - s_0)$$
(3.24)

The thermal exergy rate released by the condenser is calculated as

$$\dot{\mathbf{E}}\mathbf{x}_{th,c} = \left(1 - \frac{T_0}{T_c}\right)\dot{Q}_c \tag{3.25}$$

where $\dot{E}x_{th,c}$ represents the thermal exergy rate.

The exergy balance equation is given as

$$\dot{m}_7 \text{ex}_7 = \dot{m}_8 \text{ex}_8 + \dot{E}x_{\text{th.c}} + \dot{E}x_{\text{dest.c}}$$
 (3.26)

where $\dot{E}x_{dest,c}$ represents the rate of exergy destruction in the condenser.

Evaporator:

The mass balance equation for the evaporator as shown in Fig. 3.1 is written as

$$\dot{m}_9 = \dot{m}_{10} \tag{3.27}$$

The energy balance equation is given as

$$\dot{m}_9 h_9 + \dot{Q}_e = \dot{m}_{10} h_{10} \tag{3.28}$$

where $\dot{Q}_{\rm e}$ represents the rate of heat gained by the refrigerant flowing through the evaporator.

The specific exergy at states 9 and 10 are defined as

$$ex_9 = (h_9 - h_0) - T_0(s_9 - s_0)$$
(3.29)

$$ex_{10} = (h_{10} - h_0) - T_0(s_{10} - s_0)$$
(3.30)

The thermal exergy rate supplied to the evaporator is calculated as

$$\dot{\mathbf{E}}\mathbf{x}_{\text{th,e}} = \left(1 - \frac{T_0}{T_e}\right)\dot{Q}_e \tag{3.31}$$

where $Ex_{th,e}$ represents the thermal exergy rate of the evaporator.

The exergy balance equation is given as

$$\dot{m}_9 \text{ex}_9 + \dot{E}x_{\text{th.e}} = \dot{m}_{10} \text{ex}_{10} + \dot{E}x_{\text{dest.e}}$$
 (3.32)

where Exdest,e represents the rate of exergy destruction in the evaporator.

• Absorber:

The mass balance equation for the absorber as shown in Fig. 3.1 is written as

$$\dot{m}_{10} + \dot{m}_6 = \dot{m}_1 \tag{3.33}$$

The energy balance equation is given as

$$\dot{m}_{10}h_{10} + \dot{m}_6h_6 = \dot{m}_1h_1 + \dot{Q}_a \tag{3.34}$$

where $\dot{Q}_{\rm a}$ represents the rate of heat rejected by the absorber.

The thermal exergy rate released by the absorber is calculated as

$$\dot{\mathbf{E}}\mathbf{x}_{\text{th,a}} = \left(1 - \frac{T_0}{T_a}\right)\dot{Q}_a \tag{3.35}$$

where $\dot{E}x_{\text{th,a}}$ represents the thermal exergy rate of the absorber.

The exergy balance equation is given as

$$\dot{m}_{10} ex_{10} + \dot{m}_{6} ex_{6} = \dot{m}_{1} ex_{1} + \dot{E}x_{th,a} + \dot{E}x_{dest,a}$$
 (3.36)

where $\dot{E}x_{dest,a}$ represents the rate of exergy destruction in the absorber.

• Expansion valve (for weak solution)

The mass balance equation for the weak solution expansion valve as shown in Fig. 3.1 is written as

$$\dot{m}_5 = \dot{m}_6 \tag{3.37}$$

The energy balance equation is defined as

$$\dot{m}_5 h_5 = \dot{m}_6 h_6 \tag{3.38}$$

The exergy balance equation of the weak solution expansion valve is given as

$$\dot{m}_5 \text{ex}_5 = \dot{m}_6 \text{ex}_6 + \dot{\text{E}} \text{x}_{\text{dest.evw}} \tag{3.39}$$

where $\dot{E}x_{dest,evw}$ represents the rate of exergy destruction in the weak solution expansion valve.

• Expansion valve (for refrigerant):

The mass balance equation for the refrigerant expansion valve as shown in Fig. 3.1 is written as

$$\dot{m}_8 = \dot{m}_9 \tag{3.40}$$

The energy balance equation is defined as

$$\dot{m}_8 h_8 = \dot{m}_9 h_9 \tag{3.41}$$

The exergy balance equation is given as

$$\dot{m}_8 \text{ex}_8 = \dot{m}_9 \text{ex}_9 + \dot{E} x_{\text{dest,evr}} \tag{3.42}$$

where $\dot{E}x_{dest,evr}$ represents the rate of exergy destruction in the refrigerant expansion valve.

The performance of an absorption refrigeration system is measured using the coefficient of performance. The energetic and exergetic coefficients of performances of absorption refrigeration system are defined as

$$COP_{en} = \frac{\dot{Q}_e}{\dot{Q}_g + \dot{W}_p} \tag{3.43}$$

$$COP_{ex} = \frac{\dot{E}x_{th,e}}{\dot{E}x_{th,g} + \dot{W}_{p}}$$
(3.44)

where COP_{en} and COP_{ex} represent energetic COP and exergetic COP, respectively.

3.4 Exergoeconomic Analysis

This section presents the exergoeconomic analysis equations of the single effect absorption refrigeration system. The overall exergoeconomic equation of the SEARS is written as

$$\dot{Z}_{eq} + \dot{C}_{OPM} = \dot{C}_{Cool} \tag{3.45}$$

where \dot{Z}_{eq} , \dot{C}_{OPM} and \dot{C}_{Cool} represent the cost associated with the equipments, operation and maintenance, and cooling, respectively.

The cost linked to the equipment is defined as

$$\dot{Z}_{eq} = \dot{C}_a + \dot{C}_g + \dot{C}_c + \dot{C}_e + \dot{C}_P + \dot{C}_{ev}$$
 (3.46)

where \dot{C}_a , \dot{C}_g , \dot{C}_c , \dot{C}_e , \dot{C}_P and \dot{C}_{ev} represent cost of absorber, generator, condenser, evaporator, pump and expansion valve, respectively.

However, the total equipment cost can also be calculated using a relation between the equipment cost and cooling load as provided below.

$$\dot{Z}_{\text{eq}}(\$) = 1144.3(\dot{Q}_{\text{cool}})^{0.67}$$
 (3.47)

The cost associated with the operation and maintenance is defined as

$$\dot{C}_{\text{OPM}} = c_{\text{OPM}} \times \dot{E}x_{\text{OPM}} \tag{3.48}$$

where $c_{\rm OP}$ and $\dot{\rm E}x_{\rm OPM}$ represent operation and maintenance cost, and exergy carried by the energy consumed in terms of heat and power, respectively. The operation and maintenance can also be assumed to be 3 % of the total equipment cost.

The cost related to the cooling produced is defined as

$$\dot{C}_{\text{Cool}} = c_{\text{Cool}} \times \dot{E}_{\text{XCool}} \tag{3.49}$$

where c_{Cool} and $\dot{\text{Ex}}_{\text{Cool}}$ represent the cost of cooling produced and the exergy related to the cooling produced, respectively.

Thus the above equation can be written as

$$(c \times \dot{E}x)_{OPM} + \dot{Z}_{eq} = (c \times \dot{E}x)_{Cool}$$
 (3.50)

The cost of cooling can then be calculated by rearranging the above-mentioned equation and rewriting it as

$$c_{\text{Cool}} = \frac{\left(c \times \dot{\text{Ex}}\right)_{\text{OPM}} + \dot{Z}_{\text{eq}}}{\dot{\text{Ex}}_{\text{cool}}}$$
(3.51)

3.5 Exergoenvironmental Analysis

In this section, we present an exergoenvironmental formulation for single effect absorption refrigeration system.

The total exergy supplied to the SEARS is calculated as

$$\dot{\mathbf{E}}\mathbf{x}_{in} = \dot{\mathbf{E}}\mathbf{x}_{th,g} + \dot{\mathbf{W}}_{p} + \dot{\mathbf{E}}\mathbf{x}_{th,e} \tag{3.52}$$

The total exergy rejected by the SEARS is defined as

$$\dot{\mathbf{E}}\mathbf{x}_{\text{out}} = \dot{\mathbf{E}}\mathbf{x}_{\text{th.a}} + \dot{\mathbf{E}}\mathbf{x}_{\text{th.c}} \tag{3.53}$$

The total exergy destroyed by the SEARS is calculated as

$$\dot{E}x_{dest,tot} = \dot{E}x_{in} - \dot{E}x_{out} \tag{3.54}$$

The exergoenvironmental impact factor is defined as

$$f_{ei} = \frac{\dot{E}x_{dest,tot}}{\dot{E}x_{in}}$$
 (3.56)

where $f_{\rm ei}$ represents exergoenvironmental impact factor.

The exergoenvironmental impact coefficient is calculated as

$$C_{ei} = \frac{1}{\text{COP}_{ex}} \tag{3.57}$$

where C_{ei} represents the exergoenvironmental impact coefficient.

The exergoenvironmental impact index is calculated as

$$\theta_{\rm ei} = f_{\rm ei} \times C_{\rm ei} \tag{3.58}$$

where θ_{ei} represents exergoenvironmental impact index.

Exergoenvironmental impact improvement is defined as

$$\theta_{eii} = \frac{1}{\theta_{ei}} \tag{3.59}$$

where θ_{eii} represents exergoenvironmental impact improvement.

The exergetic stability factor is defined as

$$f_{\rm es} = \frac{\dot{E}x_{\rm out}}{\dot{E}x_{\rm out} + \dot{E}x_{\rm dest\ tot}} \tag{3.60}$$

where $f_{\rm es}$ represents the exergetic stability factor.

The exergetic sustainability index is defined as

$$\theta_{\rm est} = f_{\rm es} \times \theta_{\rm eii} \tag{3.61}$$

where θ_{est} represents exergetic sustainability index.

3.6 Optimization

Common optimization problems for absorption refrigeration systems are maximizing exergetic COP, finding the exegetic sustainability index, and minimizing the cost of cooling. The three objective functions used for this study are presented in Eqs. 3.44, 3.51, and 3.61. The constraints for this study are the ambient temperature, the heat supplied to the generator, the concentration of the strong solution, and the concentration of the weak solution.

3.7 Illustrative Example

Consider a single effect absorption refrigeration system using ammonia—water as a working solution as shown in Fig. 3.1. The strong ammonia—water solution with a mass flow rate of 1 kg/s enters the pumpas a saturated liquid with concentration and pressure of 0.5 and 200 kPa, respectively. The strong solution leaves the pump at 700 kPa with a temperature increase of 0.4 °C. Heat is supplied to the generator at a rate of 150 kW which helps to boil the strong solution, and the weak solution and ammonia refrigerant vapor leaves the generator with concentrations of 0.3 and

0.999, respectively. Consider the condenser load and evaporator temperature to be 250 kW and -1.3.5 °C, respectively. Take ambient temperature and pressure to be 291.2 K and 100 kPa. Calculate the following:

- (a) the rate of cooling provided by the evaporator,
- (b) the power consumed by the pump,
- (c) the rate of heat rejected by the absorber,
- (d) the energetic and exergetic COPs,
- (e) the exergy destruction rate in each component,
- (f) the exergetic cost of cooling, and
- (g) exergoenvironmental parameters as discussed earlier in the chapter.

In addition, perform the following parametric studies to investigate

- (a) effects of generator load on cooling load, cost of cooling and energy and exergy COPs,
- (b) effects of strong solution concentration on cooling load, cost of cooling and energy and exergy COPs, and
- (c) effects of ambient temperature on energy and exergy COPs, and all exergoenvironmental parameters.

For parametric studies, use same ranges for data as defined below.

Also, perform an optimization study for the following scenarios:

- (a) maximizing exergetic COP and minimizing exergetic cost of cooling, and
- (b) maximizing exergetic sustainability index and minimizing exergetic cost of cooling.

For an optimization study consider generator heat load, strong solution concentration, weak solution concentration, and ambient temperature as constraints with the limits of 130–170 kW, 0.45–0.55, 0.2–0.3 and 290–310 K, respectively.

Solution

$$\begin{array}{l} P_1 = 200 \, \mathrm{kPa} \\ x_1 = 0.5 \\ Qu_1 = 0.00 \end{array} \right\} \quad \begin{array}{l} h_1 = -180.1 \, \mathrm{kJ/kg} \\ s_1 = 0.04011 \, \mathrm{kJ/kg} \, \mathrm{K} \\ v_1 = 0.001199 \, \mathrm{m^3/kg} \end{array}$$

$$\begin{array}{l} P_2 = 700 \, \mathrm{kPa} \\ x_2 = 0.5 \\ T_2 = 286.9 \, \mathrm{K} \\ \dot{m}_1 = 1 \, \mathrm{kg/s} \\ \dot{m}_2 = \dot{m}_1 \end{array} \right\} \quad \begin{array}{l} h_2 = -178.1 \, \mathrm{kJ/kg} \, \mathrm{K} \\ s_2 = 0.04481 \, \mathrm{kJ/kg} \, \mathrm{K} \end{array}$$

$$\begin{array}{l} \dot{W}_{\mathbf{p}} = 1((-178.1) - (-180.1)) = 1.971 \, \mathrm{kW} \end{array}$$

$$P_0 = 100 \,\mathrm{kPa} \\ T_0 = 291.2 \,\mathrm{K} \\ \end{pmatrix} \qquad h_0 = -150 \,\mathrm{kJ/kg} \\ S_0 = 0.1034 \,\mathrm{kJ/kg} \,\mathrm{K} \\ \dot{\mathrm{E}} x_1 = 1 ((-180.1 - (-150)) - 291.2 (0.04011 - 0.1034)) = -11.62 \,\mathrm{kW} \\ \dot{\mathrm{E}} x_2 = 1 ((-178.1 - (-150)) - 291.2 (0.04481 - 0.1034)) = -11.01 \,\mathrm{kW} \\ -11.62 + 1.971 = -11.01 + \dot{\mathrm{E}} x_{\mathrm{dest,p}} \\ \dot{\mathbf{E}} x_{\mathrm{dest,p}} = \mathbf{1.368 \,\mathrm{kW}} \\ P_3 = 700 \,\mathrm{kPa} \\ x_3 = 0.5 \\ T_3 = 363.9 \,\mathrm{K} \\ \end{pmatrix} \qquad h_3 = 647.4 \,\mathrm{kJ/kg} \\ s_3 = 2.505 \,\mathrm{kJ/kg} \,\mathrm{K} \\ P_4 = 700 \,\mathrm{kPa} \\ x_4 = 0.3 \\ T_4 = 378.9 \,\mathrm{K} \\ \end{pmatrix} \qquad h_4 = 461.5 \,\mathrm{kJ/kg} \\ s_4 = 1.853 \,\mathrm{kJ/kg} \,\mathrm{K} \\ \dot{m}_3 = \dot{m}_2 \\ \dot{m}_4 = \dot{m}_5 \\ \dot{m}_3 h_3 + \dot{m}_4 h_4 = \dot{m}_2 h_2 + \dot{m}_5 h_5 \\ 1 (647.4) + 0.7139 (461.5) = 1 (-178.1) + 0.2861 (h_5) \\ h_5 = -694.9 \,\mathrm{kJ/kg} \\ \dot{m}_2 h_2 + \dot{Q}_{\mathrm{HX}} = \dot{m}_3 h_3 \\ 1 (647.4) + \dot{Q}_{\mathrm{HX}} = \dot{m}_3 h_3 \\ 1 (647.4) + \dot{Q}_{\mathrm{HX}} = 1 (-178.1) \\ \dot{Q}_{\mathrm{HX}} = 825.5 \,\mathrm{kW} \\ \dot{\mathbf{E}} \mathbf{x}_{\mathrm{th,HX}} = \left(1 - \frac{291.2}{378.9}\right) \mathbf{825.5} = \mathbf{191.1 \,\mathrm{kW}}$$

$$\begin{split} \dot{E}x_3 &= 1((647.4 - (-150)) - 291.2(2.505 - 0.1034)) = 97.96 \, kW \\ \dot{E}x_4 &= 0.7139((461.5 - (-102.5)) - 291.2(1.853 - 0.1906)) = 57.08 \, kW \\ \dot{E}x_5 &= 0.7139((-694.9 - (-102.5)) - 291.2(-2.394 - 0.1906)) = 114.3 \, kW \\ &- 11.01 + 191.1 = 97.96 + \dot{E}x_{dest \, HX} \end{split}$$

$\dot{\mathbf{E}}\mathbf{x}_{\text{dest HX}} = 82.13\,\mathrm{kW}$

$$\dot{m}_3 = \dot{m}_4 + \dot{m}_7
\dot{m}_3 x_3 = \dot{m}_4 x_4 + \dot{m}_7 x_7
1 = \dot{m}_3 + \dot{m}_7
1(0.5) = \dot{m}_3(0.3) + \dot{m}_7(0.999)$$

Solving two equations simultaneously gives us $\dot{m}_4 = 0.7139$ kg/s and $\dot{m}_7 = 0.2861$ kg/s

$$\dot{m}_3 h_3 + \dot{Q}_g = \dot{m}_4 h_4 + \dot{m}_7 h_7$$

 $1(647.4) + 150 = 0.7139(461.5) + 0.2861 h_7$
 $h_7 = 1635 \,\text{kJ/kg}$

$$\left. \begin{array}{l} P_7 = 700 \, \mathrm{kPa} \\ x_7 = 0.999 \\ h_7 = 1635 \, \mathrm{kJ/kg} \end{array} \right\} \quad s_7 = 5.467 \, \mathrm{kJ/kg} \quad \mathrm{K}$$

$$\dot{E}x_7 = 0.2861[(1635 - 87.15) - 291.2(5.467 - 0.2708)] = 10.08 \,\mathrm{kW}$$

$$\dot{E}x_{th,g} = \left(1 - \frac{291.2}{429.8}\right)150 = 48.38 \, kW$$

$$97.96 + 48.38 = 57.08 + 10.08 + \dot{E}x_{dest,g}$$

$$\dot{E}x_{dest,g} = 79.17 \, kW$$

$$\dot{m}_8 = \dot{m}_7$$
 $\dot{m}_7 h_7 = \dot{m}_8 h_8 + \dot{Q}_c$
 $0.2861(1635) = 0.2861(h_8) + 250$
 $h_8 = 761.7 \text{ kJ/kg}$

$$\left. \begin{array}{l} P_8 = 700 \, \mathrm{kPa} \\ x_8 = 0.999 \\ h_8 = 761.7 \end{array} \right\} \quad s_8 = 2.663 \, \mathrm{kJ/kg} \, \mathrm{K}$$

$$\dot{E}x_8 = 0.2861[(761.7 - 87.15) - 291.2(2.663 - 0.2708)] = -6.349 \,\text{kW}$$

$$\dot{E}x_{th,c} = \left| \left(1 - \frac{291.2}{287} \right) 250 \right| = 3.638 \, kW$$

$$10.08 = -6.349 + 3.638 + \dot{E}x_{dest,c}$$

$$\dot{E}x_{dest.c} = 12.79 \, kW$$

$$\dot{m}_9 = \dot{m}_8$$

$$\left. \begin{array}{l}
 h_9 = h_8 \\
 P_9 = P_1 \\
 x_9 = x_8
 \end{array} \right\} \quad s_9 = 3.009 \,\text{kJ/kg K}$$

$$\begin{split} \dot{E}x_9 &= 0.2861[(761.7 - 87.15) - 291.2(3.009 - 0.2708)] = -35.13 \, kW \\ -6.349 &= -35.13 + \dot{E}x_{dest.evr} \end{split}$$

$\dot{E}x_{dest\,evr} = 28.78\,\mathrm{kW}$

$$\dot{m}_{10} = \dot{m}_9$$

$$\left. \begin{array}{l} P_{10} = P_9 \\ x_{10} = 0.999 \\ T_{10} = 259.7 \, \mathrm{K} \end{array} \right\} \quad \begin{array}{l} h_{10} = 1251 \, \mathrm{kJ/kg} \\ s_{10} = 4.922 \, \mathrm{kJ/kg} \, \mathrm{K} \end{array}$$

$$\dot{m}_9 h_9 + \dot{Q}_e = \dot{m}_{10} h_{10}$$

$$0.2861(761.7) + \dot{Q}_e = 0.2861(1251)$$

$$\dot{Q}_{\rm e}=140\,{\rm kW}$$

$$\dot{E}x_{10} = 0.2861[(1251 - 87.15) - 291.2(4.922 - 0.2708)] = -54.52 \,\mathrm{kW}$$

$$\dot{E}x_{th,e} = \left| \left(1 - \frac{291.2}{257} \right) 140 \right| = 16.44 \, kW$$

$$-35.13 + 16.44 = -54.52 + \dot{E}x_{dest,e}$$

$$\dot{E}x_{dest,e} = 35.83\,kW$$

$$\dot{m}_6 = \dot{m}_5$$

$$\left. \begin{array}{l}
 h_6 = h_5 \\
 P_6 = P_1 \\
 x_6 = x_5
 \end{array} \right\} \quad s_6 = -2.39 \,\text{kJ/kg K}$$

$$\dot{E}x_6 = 0.7139((-694.9 - (-102.5)) - 291.2(-2.39 - 0.1906)) = 113.6 \text{ kW}$$

$$114.3 = 113.6 + \dot{E}x_{\text{dest,evs}}$$

$$\dot{E}x_{dest\ evs} = 0.6824\ kW$$

$$\dot{m}_{1} = \dot{m}_{10} + \dot{m}_{6}
\dot{m}_{1}h_{1} + \dot{Q}_{a} = \dot{m}_{10}h_{10} + \dot{m}_{6}h_{6}
1(-180.1) + \dot{Q}_{a} = 0.2861(1251) + 0.7139(-694.9)
\dot{Q}_{a} = 41.96 \text{ kW}
\dot{E}x_{th,a} = \left| \left(1 - \frac{291.2}{178.3} \right) 41.96 \right| = 16.27 \text{ kW}$$

$$\dot{E}x_{dest,a} = 54.45 \text{ kW}$$

$$COP_{en} = \frac{140}{150 + 1.971} = 0.9211$$

 $-54.52 + 113.6 = -11.62 + 16.27 + \dot{E}x_{dest a}$

$$COP_{ex} = \frac{16.44}{48.38 + 1.971} = 0.3265$$

$$\dot{Z}_{eq}(\$) = 1144.3(140)^{0.67} = \$31363$$

$$\dot{C}_{OPM} = 0.03(31363) = \$940.9$$

$$c_{Cool} = \frac{940.9 + 31363}{16.44}$$

$$\mathbf{c}_{Cool} = \mathbf{1965} \$/\mathbf{kW}$$

$$\dot{E}x_{in} = 48.38 + 1.971 + 16.44 = 66.79\,kW$$

$$\dot{E}x_{out} = 16.27 + 3.638 = 19.91 \,\text{kW}$$

$$\dot{E}x_{dest,tot} = 66.79 - 19.91 = 46.88 \,\mathrm{kW}$$

$$f_{\rm ei} = \frac{46.88}{66.79} = 0.7019$$

$$C_{\rm ei} = \frac{1}{0.3265} = 3.063$$

$$\theta_{ei} = 0.7019 \times 3.063 = 2.15$$

$$\theta_{eii} = \frac{1}{2.15} = 0.4652$$

$$f_{\rm es} = \frac{19.91}{19.91 + 46.88} = 0.2981$$

State point	P (kPa)	T (K)	m (kg/s)	h (kJ/kg)	s (kJ/kg K)
0	100	291.2	_	-150	0.1034
1	200	286.5	1	-180.1	0.04011
2	700	286.9	1	-178.1	0.04481
3	700	363.9	1	647.4	2.505
4	700	378.9	0.7139	461.5	1.853
5	700	178.2	0.7139	-694.9	-2.394
6	200	178.3	0.7139	-694.9	-2.39
7	700	429.8	0.2861	1635	5.467
8	700	287	0.2861	761.7	2.663
9	200	254.4	0.2861	761.7	3.009
10	200	259.7	0.2861	1251	4.922

Table 3.1 Thermophysical properties at each state point of the SEARS

$$\theta_{est} = 0.2981 \times 0.4652 = 0.1387$$

The thermophyscial properties at each state point are presented in Table 3.1.

· Effects of generator load

The effects of generator load on the cooling capacity and cost of cooling are presented in Fig. 3.2. The cooling load is observed to be decreasing from 160 to 120 kW with an increase in generator load from 130 to 170 kW for a constant condenser load of 250 kW. The cost of cooling is noticed to be increasing from 1592 to 1755 \$/kW with the increase in generator load. This decreasing behavior of cooling load is because the increased generator load results in a higher exit temperature of the refrigerant vapor leaving the generator. This results in higher temperature refrigerant entering the evaporator due to fixed condenser load and because

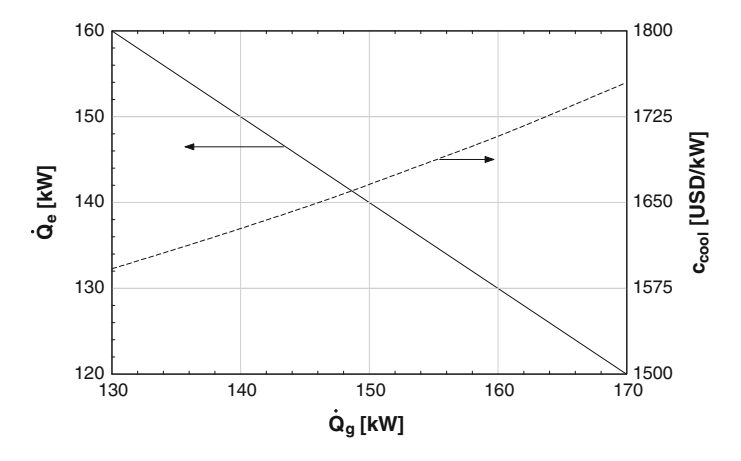


Fig. 3.2 Effects of generator load on cooling load and cost of cooling

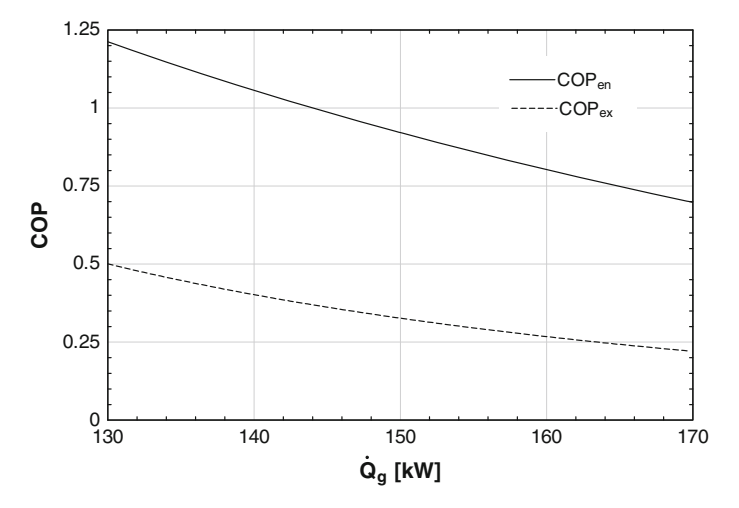


Fig. 3.3 Effects of generator load on energy and exergy COPs

of this the cooling capacity of the system decreases. The decrease in cooling load has adverse effects on the cost of cooling as seen in Fig. 3.2. This increasing cost of cooling is a result of lower cooling production from the system for the same system size. Figure 3.3 shows the effects of generator load on energy and exergy COPs of the SEARS. The energy and exergy COPs are observed to be decreasing from 1.2 to 0.7 and 0.5 to 0.2, respectively, with the rise in generator load. This decrease in the energy and exergy COPs is due to the decrease in the cooling capacity of the system.

Effects of strong solution concentration

The effects of strong solution concentration variation on the cooling load and cost of cooling are presented in Fig. 3.4. The rate of cooling is observed to be decreasing from 173 to 119.5 kW with an increase in concentration of the strong solution from 0.45 to 0.55. This behavior is because an increase in concentration adds more ammonia to the generator. This higher ammonia concentration requires a higher generator load in order to separate it from the solution. As the generator load remains constant, the higher amount of ammonia cannot separate from the strong solution and instead increases the temperature of ammonia refrigerant vapor leaving the generator. This higher temperature ammonia vapor requires releasing the higher amount of heat in the condenser to provide better cooling capacity. But with the restriction that the condenser load is fixed at 250 kW, the ammonia vapor cannot release the higher amount of heat and enters the evaporator at relatively higher temperature, in turn decreasing the cooling capacity of the system. As a result, the cost of cooling is observed to increase from 1548 to 1761 \$/kW with an increase in the strong solution concentration. Figure 3.5 displays the effects of strong solution concentration variation on energy and exergy COPs. Energy and exergy COPs are noted to decrease from 1.14 to 0.78 and 0.42 to 0.29, respectively, with an increase

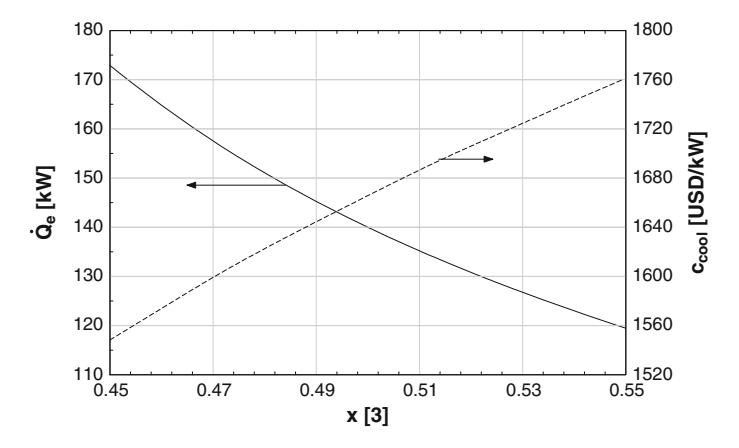


Fig. 3.4 Effects of strong solution concentration on cooling load and cost of cooling

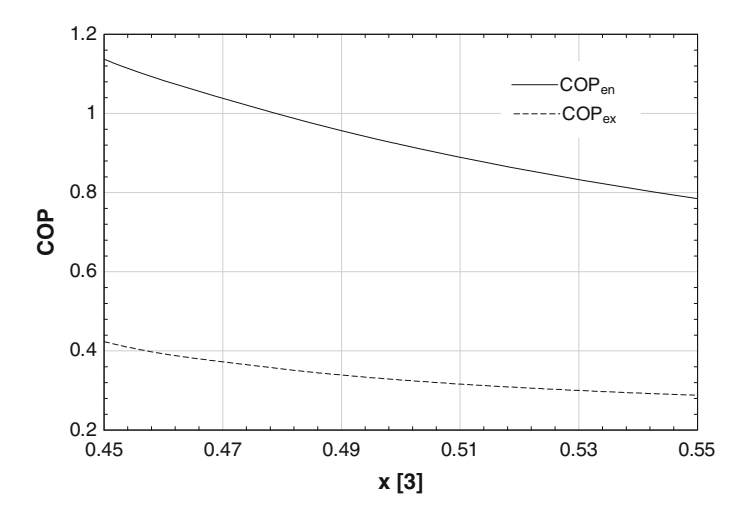


Fig. 3.5 Effects of strong solution concentration on energy and exergy COPs

in strong solution concentration. This trend of decreasing COPs is because SEARS COPs of the SEARS are directly related to the cooling capacity. As the cooling capacity of the system decreases the COPs of the system also decreases.

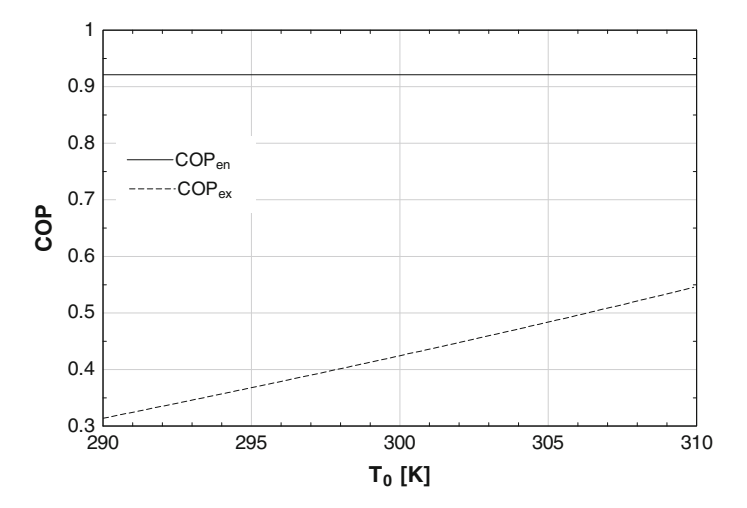


Fig. 3.6 Effects of ambient temperature on energy and exergy COPs

• Effects of ambient temperature

Figure 3.6 displays the effects of ambient temperature variation on the energy and exergy COPs of the SEARS. The energy COP is observed to remain constant at 0.92, whereas the exergy COP is noted to increase from 0.31 to 0.55 with an increase in ambient temperature from 290 to 310 K. The constant behavior of energy COP shows the importance of the exergy analysis. Energy analysis does not consider the losses, only quantity as opposed to quantity and quality covered by exergy analysis. In the real case scenario, the ambient temperature is expected to play a major role in systems performance because the temperature difference between the system and surrounding can lead to energy loss or energy gain from the system.

The exergy COP is noted to increase with an increase in ambient temperature because the absorption refrigeration systems are majorly heat driven and an increase in ambient temperature helps in decreasing the temperature difference between the system and the surrounding. This decrease in the temperature difference then helps in improving the performance of the systems due to the lesser rate of heat losses occurring.

Figure 3.7 portrays the effects of the rise in ambient temperature on the exergoenvironmental impact factors of the SEARS. The exergoenvironmental impact factor is noticed to be decreasing from 0.89 to 0.60 with rise in ambient temperature from 290 to 310 K. The decreasing behavior is because an increase in ambient temperature results in a smaller temperature difference between the system and the environment. Since the SEARS is heat driven, it benefits from this decreasing temperature difference because a decrease in temperature difference results in less heat loss from the system to the environment, which results in less total exergy destroyed by the system. The effects of the increase in ambient temperature on the

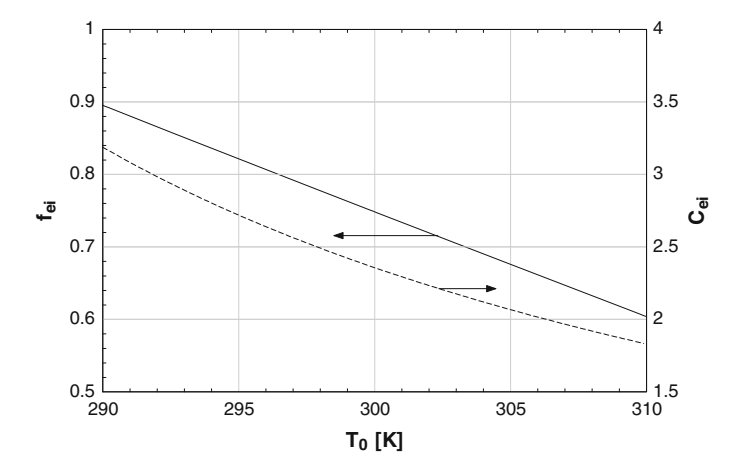


Fig. 3.7 Effects of ambient temperature on the exergoenvironmental impact factor and the exergoenvironmental impact coefficient

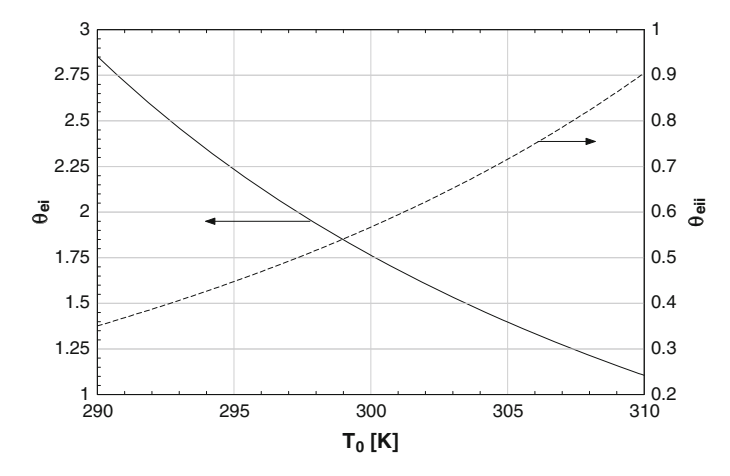


Fig. 3.8 Effects of ambient temperature on the exergoenvironmental impact index and the exergoenvironmental impact improvement

exergoenvironmental impact coefficient are shown in Fig. 3.7. The exergoenvironmental impact coefficient is observed to be decreasing from 3.19 to 1.83 with the increase in ambient temperature. This decreasing behavior indicates that the SEARS becomes more environmentally benign as the ambient temperature increases. This is because the increase in ambient temperature results in lesser amount of heat loss from the SEARS to the environment due to the lower temperature difference between the SEARS cycle and the environment.

Figure 3.8 shows the effects of the increase in ambient temperature on the exergoenvironmental impact index. The exergoenvironmental impact index is noted

to be decreasing from 2.85 to 1.10 with the increase in ambient temperature. This decreasing behavior that the waste exergy and the exergy destruction rate of the SEARS decrease with the increase in ambient temperature because the increased temperature helps to decrease the heat loss from the systems by lowering the temperature difference between the SEARS and the environment. Since the SEARS is mainly heat driven, it is greatly affected by the fluctuation in heat loss, and increasing the ambient temperature helps to save the SEARS heat energy from being lost to the environment. The effects of the increase in ambient temperature on exergoenvironmental impact improvement are also displayed in Fig. 3.8. The exergoenvironmental impact improvement factor is noted to increase from 0.35 to 0.90 with the increase in ambient temperature. This behavior shows that as the ambient temperature increases the environmental appropriateness of the SEARS increases due to less heat loss from the SEARS to the environment.

Figure 3.9 displays the effects of the rise in ambient temperature on exergetic stability factor and exergetic sustainability index. The exergetic stability factor and exergetic sustainability index are observed to increase from 0.1 to 0.39 and 0.04 to 0.36, respectively, with the increase in ambient temperature. Such increasing trends are because the increase in ambient temperature helps reducing the heat losses from the SEARS. As the heat losses decreases the rate of exergy destruction decreases which then makes the system more exergetically stable and sustainable at the same time.

Optimization

The constraints of the optimization study are presented in Table 3.2.

The results obtained from the optimization study of maximizing exergetic COP and minimizing exergetic cooling cost are presented in Fig. 3.10. The built-in

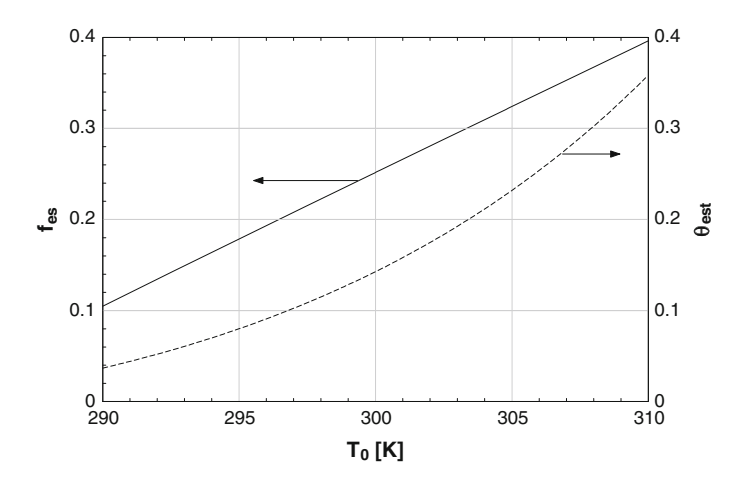


Fig. 3.9 Effects of ambient temperature on the exergetic stability and the exergetic sustainability index

Table 3.2 Constraints
associated with the
optimization study of the
SEARS

Parameter	Minimum value	Maximum value
$\dot{Q}_{ m g}$	130 kW	170 kW
T_0	290 K	310 K
<i>x</i> ₃	0.45	0.55
<i>X</i> ₄	0.2	0.3

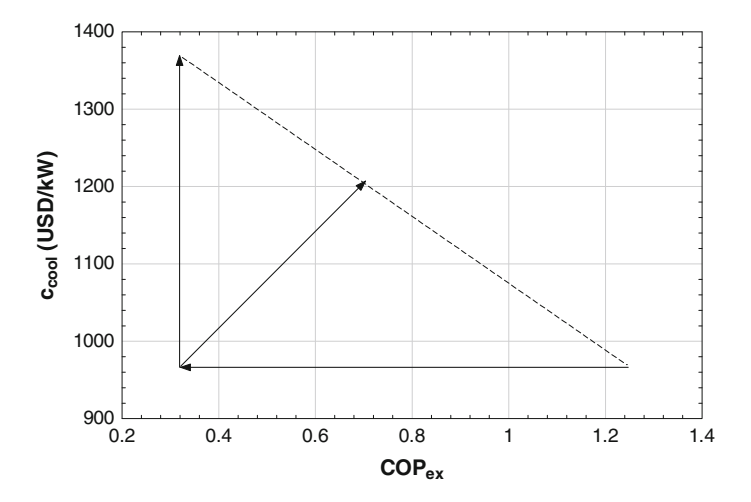


Fig. 3.10 Multi-objective optimization (exergetic COP vs. exergetic cooling cost)

Nelder-Mead simplex algorithm technique in the engineering equation solver software is used to perform multi-objective optimization. The algorithm uses N+1test points (where N is the number of dimensions [i.e., degrees of freedom], which is called a simplex. For example, a two-dimensional problem uses a triangle as its simplex. All points of the simplex are evaluated. The objective function is determined at each point. The worst point in the simplex is then thrown out and a new point is found by reflecting away from the worst point about the axis formed by the other test points. This process is repeated until one of the stopping criteria is met. The objective function of the best point is taken to be the optimum. The optimization study shows that the highest exergetic COP obtained is 1.25 and the lowest cooling cost achieved is 965 \$/kW for the given constraints. Although all points on the Pareto front are considered optimum, traditionally, linear programming technique for multidimensional analysis of preferences (LINMAP) is used to obtain the most desirable optimized points. LINMAP helps to identify a hypothetical point at which all the objective functions have their respective optimum point irrespective of other objective functions. The best exergetic COP and exergetic cooling cost obtained using LINMAP are 0.7056 and 1205.6 \$/kW, respectively. This multi-objective optimization shows that the exergetic COP is directly

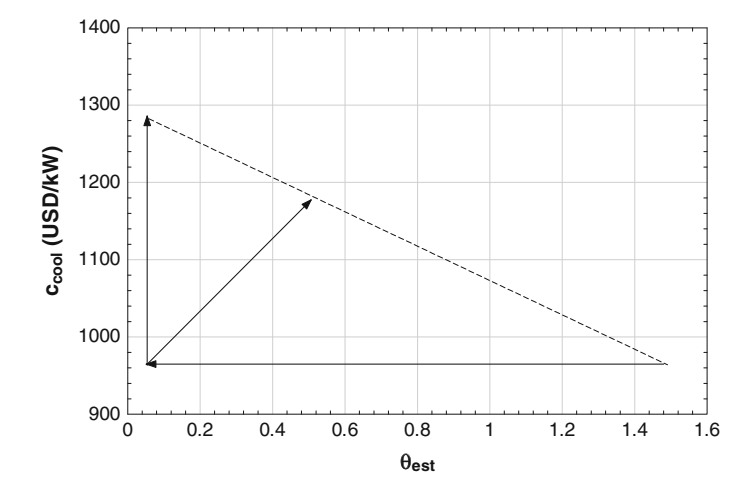


Fig. 3.11 Multi-objective optimization (exergetic sustainability index vs. exergetic cooling cost)

related to the cost of refrigeration. The results obtained from the optimization study for maximizing the exergetic sustainability index and minimizing the exergetic cost of cooling are presented in Fig. 3.11. LINMAP is used to obtain the hypothetically most desirable point. The values obtained for exergetic sustainability index and exergetic cost of refrigeration using LINMAP are 0.5184 and 1181.7 \$/kW, respectively.

3.8 Closing Remarks

The use of a single effect absorption refrigeration system, as compared to the conventional vapor-compression refrigeration systems, offers advantages regardingenergy, environment and sustainability. This chapter presents detailed energy and exergy analyses of the SEARS. The exergoeconomic and exergoenvironmental analyses and assessments are also presented to show how exergy can be integrated with cost and the environment. Furthermore, a comprehensive illustrative example is provided, which covers energy, exergy, exergoeconomic, exergoenvironmental, and optimization studies of the SEARS. The example provided in this chapter is intended to help readers modeling the SEARS.

Chapter 4 Double Effect Absorption Refrigeration System

4.1 Introduction

As discussed in earlier chapters, the use of absorption refrigeration systems compared to conventional vapor-compression refrigeration systems can provide numerous benefits in terms of reduced environmental impact and cost. However, this refrigeration system also requires innovative iterations in order to be more environmentally friendly and cost effective. The double effect absorption refrigeration system (DEARS) can be seen as an advanced single effect absorption refrigeration system which recovers energy within the system to enhance its performance. Of course, this additional heat recovery does not come for free but brings with it an additional equipment cost. In the long run, the additional equipment costis a good investment because of cost cuts provided in the form of additional cooling.

In this chapter, basic operation of the double effect absorption refrigeration system and its energy and exergy analyses are presented and discussed with an example. The chapter first presents the working principle of the DEARS in order to help the reader understand how it works. After that, energy, exergy, exergoenvironmental, exergoeconomic, and optimization modeling are presented for performance assessment and evaluation. Finally, a detailed illustrative example is provided to help readers understand how each equation is used to generate thermophysical properties at each state point and to obtain overall energy and exergy flow values of the double effect absorption refrigeration system.

4.2 System Description

The double effect absorption refrigeration system is a complex form of the single effect absorption refrigeration system as shown in Fig. 4.1. In the DEARS, a strong solution of ammonia-water leaving the absorber at state 1 enters the pump in a saturated liquid phase. In the pump, the pressure of the strong solution increases before it leaves at state 2. The strong solution at state 2 then divides into two streams, states 3 and 18. The stream at state 3 enters the low temperature heat exchanger, where it gains heat from the returning fluid from the generators to leave at state 4 at comparatively higher temperature. This strong solution at state 4 then divides into two streams, states 5 and 20. The strong solution at state 5 enters the high temperature heat exchanger where it extracts heat from the high temperature generator to leave at state 6 at relatively higher temperature before entering the high temperature generator. In the high temperature generator, heat is supplied by an external source to boil the strong ammonia—water solution. Boiling helps to separate ammonia from the mixture because it boils at a lower temperature than water. The ammonia vapor is then extracted from the generator at state 7, and the remaining weak ammonia-water solution is extracted at state 13. The ammonia vapor extracted at state 7 then enters the low temperature generator where it acts as a heat source. In the low temperature generator, a strong solution enters at state 21 where it receives heat from the ammonia vapor at state 7. The heat supplied to the low

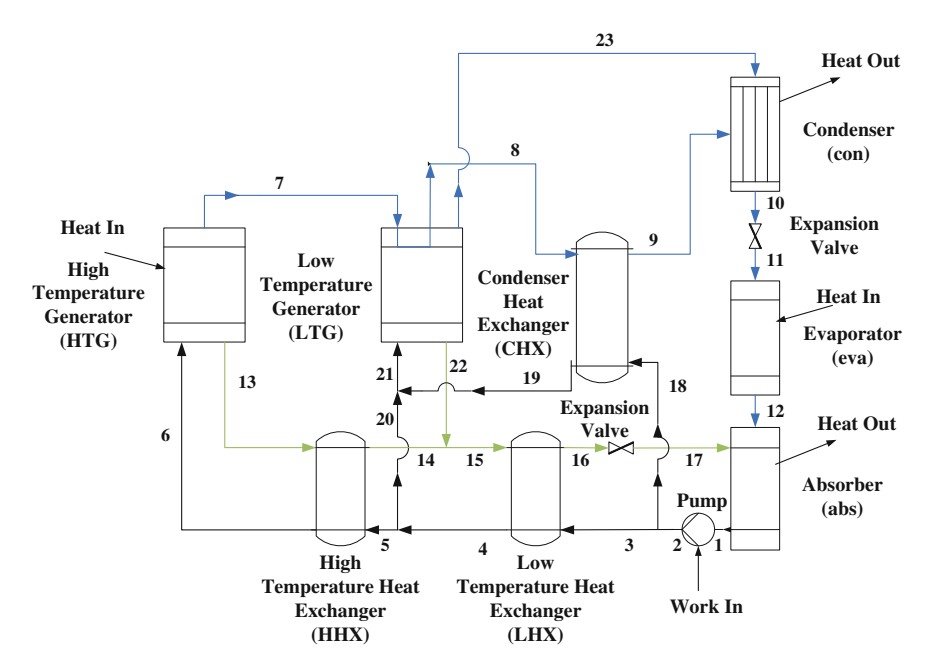


Fig. 4.1 Schematic of the DEARS

temperature generator helps to separate ammonia from the strong solution which leaves the low temperature generator at state 23. The remaining weak solution in the low temperature generator is then extracted at state 22. After releasing heat the ammonia vapor at state 7 leaves the low temperature generator at state 8 to enter the condenser heat exchanger. In the condenser heat exchanger, the strong solution entering at state 18 gains heat from the ammonia at state 8 and leaves at a higher temperature at state 19. The ammonia refrigerant leaves the condenser heat exchanger at state 9 after releasing heat to the strong solution. The strong solution exiting the condenser heat exchanger at state 19 mixes with the strong solution from state 20 to leave at state 21. The ammonia refrigerant at states 9 and 23 enter the condenser, where they release heat to the environment to leave as a relatively cooler refrigerant at state 10. This ammonia refrigerant at state 10 then passes through the refrigerant expansion valve where its pressure suddenly drops and leaves as a cooled ammonia refrigerant at state 11. The ammonia refrigerant at state 11 enters the evaporator and gains heat from the surrounding before leaving at a higher temperature at state 12. The weak solution exiting the high temperature generator at state 13 passes through the high temperature heat exchanger where it rejects heat to the incoming strong solution to leave at state 14. The weak solution at state 14 mixes with the weak solution returning from the low temperature generator at state 22 to leave at state 15. The weak solution at state 15 then enters the low temperature heat exchanger where it rejects heat and leaves at a cooler temperature at state 16. The weak solution at state 16 enters the weak solution expansion valve where its pressure suddenly drops before it enters the absorber at state 17. The weak solution at state 17 and ammonia refrigerant at state 12 then mix together in the absorber while rejecting heat to the environment to leave the absorber as a strong solution at state 1.

4.3 Energy and Exergy Analyses

This section of the chapter provides energy and exergy balance equations for each component of the DEARS.

• Pump:

The mass balance equation across the pump as shown in Fig. 4.1, can be written as

$$\dot{m}_1 = \dot{m}_2 = \dot{m}_p \tag{4.1}$$

where \dot{m} represents the mass flow rate.

The specific power consumed by the pump can be calculated using

$$w_{\rm p} = \frac{v(P_2 - P_1)}{\eta_{\rm p}} \tag{4.2}$$

where w, v, P, and η represent specific power, specific volume, pressure, and efficiency, respectively.

The total power consumed by the pump is defined as

$$\dot{W}_{\rm p} = \dot{m}_{\rm p} w_{\rm p} \tag{4.3}$$

where \dot{W} represents total power consumed by the pump.

The overall energy balance equation of the pump is given as

$$(\dot{m}h)_1 + \dot{W}_p = (\dot{m}h)_2 \tag{4.4}$$

where h represents specific enthalpy of the state.

The specific exergies at states 1 and 2 are defined as

$$ex_1 = (h_1 - h_0) - T_0(s_1 - s_0)$$
(4.5)

$$ex_2 = (h_2 - h_0) - T_0(s_2 - s_0)$$
(4.6)

where ex, T, and s represent specific exergy, temperature, and specific entropy. The overall exergy balance equation of the pump is given as

$$\dot{m}_1 e x_1 + \dot{W}_p = \dot{m}_2 e x_2 + \dot{E} x_{\text{dest},p}$$
 (4.7)

where $\dot{E}x_{\text{dest},p}$ represents the exergy destruction rate.

• Low temperature heat exchanger:

The mass balance equations for the low temperature heat exchanger can be written as

$$\dot{m}_4 = \dot{m}_3 \tag{4.8}$$

$$\dot{m}_{16} = \dot{m}_{15} \text{ and}$$
 (4.9)

$$\dot{m}_{14} + \dot{m}_{22} = \dot{m}_{15} \tag{4.10}$$

The energy balance equation is given as

$$\dot{m}_3 h_3 + \dot{m}_{15} h_{15} = \dot{m}_4 h_4 + \dot{m}_{16} h_{16} \tag{4.11}$$

The specific exergies at states 3, 4, 15, and 16 are defined as

$$ex_3 = (h_3 - h_0) - T_0(s_3 - s_0)$$
(4.12)

$$ex_4 = (h_4 - h_0) - T_0(s_4 - s_0)$$
(4.13)

$$ex_{15} = (h_{15} - h_0) - T_0(s_{15} - s_0)$$
(4.14)

$$ex_{16} = (h_{16} - h_0) - T_0(s_{16} - s_0)$$
(4.15)

The exergy balance equation is given as

$$\dot{m}_3 \text{ex}_3 + \dot{m}_{15} \text{ex}_{15} = \dot{m}_4 \text{ex}_4 + \dot{m}_{16} \text{ex}_{16} + \dot{E}_{x_{\text{dest}, \text{LHX}}}$$
 (4.16)

where $\dot{E}x_{dest,LHX}$ represents the exergy destruction rate.

• Medium temperature heat exchanger:

The mass balance equations for the medium temperature heat exchanger can be written as

$$\dot{m}_6 = \dot{m}_5 \tag{4.17}$$

$$\dot{m}_{14} = \dot{m}_{13} \text{ and}$$
 (4.18)

$$\dot{m}_5 + \dot{m}_{20} = \dot{m}_4 \tag{4.19}$$

The energy balance equation is given as

$$\dot{m}_5 h_5 + \dot{m}_{13} h_{13} = \dot{m}_6 h_6 + \dot{m}_{14} h_{14} \tag{4.20}$$

The specific exergies at states 5, 6, 13, and 14 are defined as

$$ex_5 = (h_5 - h_0) - T_0(s_5 - s_0) (4.21)$$

$$ex_6 = (h_6 - h_0) - T_0(s_6 - s_0) (4.22)$$

$$ex_{13} = (h_{13} - h_0) - T_0(s_{13} - s_0)$$
(4.23)

$$ex_{14} = (h_{14} - h_0) - T_0(s_{14} - s_0)$$
(4.24)

The exergy balance equation is given as

$$\dot{m}_5 \text{ex}_5 + \dot{m}_{13} \text{ex}_{13} = \dot{m}_6 \text{ex}_6 + \dot{m}_{14} \text{ex}_{14} + \dot{\text{E}}_{\text{dest,HHX}}$$
 (4.25)

where $\dot{E}x_{dest,HHX}$ represents the exergy destruction rate.

• High temperature generator:

The mass balance equations of the high temperature generator can be written as

$$\dot{m}_6 = \dot{m}_{13} + \dot{m}_7 \tag{4.26}$$

and

$$\dot{m}_6 x_6 = \dot{m}_{13} x_{13} + \dot{m}_7 x_7 \tag{4.27}$$

where x represents the concentration of the solution.

The energy balance equation is given as

$$\dot{m}_6 h_6 + \dot{Q}_{\rm HTG} = \dot{m}_{13} h_{13} + \dot{m}_7 h_7 \tag{4.28}$$

where $\dot{Q}_{\rm HTG}$ represents the rate of heat required by the high temperature generator. The specific exergy at state 7 is defined as

$$ex_7 = (h_7 - h_0) - T_0(s_7 - s_0)$$
(4.29)

The thermal exergy rate supplied to the high temperature generator is defined as

$$\dot{\mathbf{E}}\mathbf{x}_{\text{th,HTG}} = \left(1 - \frac{T_0}{T_{\text{HTG}}}\right) \dot{Q}_{\text{HTG}} \tag{4.30}$$

where $\dot{E}x_{th,HTG}$ represents the thermal exergy rate.

The exergy balance equation of the high temperature generator is given as

$$\dot{m}_6 \text{ex}_6 + \dot{\text{E}}_{\text{xth HTG}} = \dot{m}_{13} \text{ex}_{13} + \dot{m}_7 \text{ex}_7 + \dot{\text{E}}_{\text{xdest HTG}}$$
 (4.31)

where $\dot{E}x_{dest,HTG}$ represents the rate of exergy destruction.

• Low temperature generator:

The mass balance equations of the low temperature generator can be written as

$$\dot{m}_{21} = \dot{m}_{22} + \dot{m}_{23} \tag{4.32}$$

$$\dot{m}_{21}x_{21} = \dot{m}_{22}x_{22} + \dot{m}_{23}x_{23} \tag{4.33}$$

$$\dot{m}_8 = \dot{m}_7 \text{ and} \tag{4.34}$$

$$\dot{m}_{21} = \dot{m}_{20} + \dot{m}_{19} \tag{4.35}$$

where x represents the concentration of the solution.

The energy balance equation is given as

$$\dot{m}_7 h_7 + \dot{m}_{21} h_{21} = \dot{m}_8 h_8 + \dot{m}_{22} h_{22} + \dot{m}_{23} h_{23}$$
 and (4.36)

$$\dot{m}_7 h_7 = \dot{m}_8 h_8 + \dot{Q}_{\rm LTG} \tag{4.37}$$

where $\dot{Q}_{\rm LTG}$ represents the rate of heat required by the low temperature generator. The specific exergies at states 8 and 20–23 are defined as

$$ex_8 = (h_8 - h_0) - T_0(s_8 - s_0) (4.38)$$

$$ex_{20} = (h_{20} - h_0) - T_0(s_{20} - s_0)$$
(4.39)

$$ex_{21} = (h_{21} - h_0) - T_0(s_{21} - s_0)$$
(4.40)

$$ex_{22} = (h_{22} - h_0) - T_0(s_{22} - s_0)$$
(4.41)

$$ex_{23} = (h_{23} - h_0) - T_0(s_{23} - s_0)$$
(4.42)

The thermal exergy rate supplied to the low temperature generator is defined as

$$\dot{\mathbf{E}}\mathbf{x}_{\text{th,LTG}} = \left(1 - \frac{T_0}{T_{\text{LTG}}}\right) \dot{Q}_{\text{LTG}} \tag{4.43}$$

where $\dot{E}x_{th,LTG}$ represents the thermal exergy rate.

The exergy balance equation of the low temperature generator is given as

$$\dot{m}_{21} ex_{21} + \dot{E}x_{th,LTG} = \dot{m}_{22} ex_{22} + \dot{m}_{23} ex_{23} + \dot{E}x_{dest,LTG}$$
 (4.44)

where $\dot{E}x_{dest,LTG}$ represents the rate of exergy destruction.

• Condenser:

The mass balance equation for the condenser is defined as

$$\dot{m}_{10} = \dot{m}_9 + \dot{m}_{23} \tag{4.45}$$

The energy balance equation of the condenser is given as

$$\dot{m}_9 h_9 + \dot{m}_{23} h_{23} = \dot{m}_{10} h_{10} + \dot{Q}_c \tag{4.46}$$

where \dot{Q}_c represents the rate of heat rejected by the refrigerant flowing through the condenser.

The specific exergy at state 10 is defined as

$$ex_{10} = (h_{10} - h_0) - T_0(s_{10} - s_0)$$
(4.47)

The thermal exergy rate released by the condenser is calculated as

$$\dot{\mathbf{E}}\mathbf{x}_{\text{th,c}} = \left(1 - \frac{T_0}{T_c}\right)\dot{Q}_c \tag{4.48}$$

where $\dot{E}x_{th,c}$ represents the thermal exergy rate.

The exergy balance equation of the condenser is given as

$$\dot{m}_9 \text{ex}_9 + \dot{m}_{23} \text{ex}_{23} = \dot{m}_{10} \text{ex}_{10} + \dot{E}x_{\text{th.c}} + \dot{E}x_{\text{dest.c}}$$
 (4.49)

where $\dot{E}x_{dest,c}$ represents the rate of exergy destruction.

Evaporator:

The mass balance equation for the evaporator is written as

$$\dot{m}_{12} = \dot{m}_{11} \tag{4.50}$$

The energy balance equation of the evaporator is given as

$$\dot{m}_{11}h_{11} + \dot{Q}_{e} = \dot{m}_{12}h_{12} \tag{4.51}$$

where \dot{Q}_{e} represents the rate of heat gained by the refrigerant flowing through the evaporator.

The specific exergies at states 11 and 12 are defined as

$$ex_{11} = (h_{11} - h_0) - T_0(s_{11} - s_0)$$
(4.52)

$$ex_{12} = (h_{12} - h_0) - T_0(s_{12} - s_0)$$
(4.53)

The thermal exergy rate supplied to the evaporator is calculated as

$$\dot{\mathbf{E}}\mathbf{x}_{\text{th,e}} = \left(1 - \frac{T_0}{T_e}\right)\dot{Q}_e \tag{4.54}$$

where $\dot{E}x_{th,e}$ represents the thermal exergy rate.

The exergy balance equation of the evaporator is given as

$$\dot{m}_{11} e x_{11} + \dot{E} x_{th,e} = \dot{m}_{12} e x_{12} + \dot{E} x_{dest,e}$$
 (4.55)

where $\dot{E}x_{dest,e}$ represents the rate of exergy destruction in the evaporator.

• Absorber:

The mass balance equation for the absorber is written as

$$\dot{m}_{12} + \dot{m}_{17} = \dot{m}_1 \tag{4.56}$$

The energy balance equation of the absorber is given as

$$\dot{m}_{12}h_{12} + \dot{m}_{17}h_{17} = \dot{m}_1h_1 + \dot{Q}_a \tag{4.57}$$

where $\dot{Q}_{\rm a}$ represents the rate of heat rejected by the absorber.

The specific exergy at state 17 is defined as

$$ex_{17} = (h_{17} - h_0) - T_0(s_{17} - s_0)$$
(4.58)

The thermal exergy rate released by the absorber is calculated as

$$\dot{\mathbf{E}}\mathbf{x}_{\text{th,a}} = \left(1 - \frac{T_0}{T_a}\right) \dot{Q}_a \tag{4.59}$$

where $\dot{E}x_{th,a}$ represents the thermal exergy rate.

The exergy balance equation of the absorber is given as

$$\dot{m}_{12} ex_{12} + \dot{m}_{17} ex_{17} = \dot{m}_1 ex_1 + \dot{E}x_{th,a} + \dot{E}x_{dest,a}$$
 (4.60)

where $\dot{E}x_{dest,a}$ represents the rate of exergy destruction in the absorber.

• Expansion valve (for weak solution)

The mass balance equation for the weak solution expansion valve is written as

$$\dot{m}_{17} = \dot{m}_{16} \tag{4.61}$$

The energy balance equation of the weak solution expansion valve is defined as

$$\dot{m}_{16}h_{16} = \dot{m}_{17}h_{17} \tag{4.62}$$

The exergy balance equation of the weak solution expansion valve is given as

$$\dot{m}_{16} \text{ex}_{16} = \dot{m}_{17} \text{ex}_{17} + \dot{E}_{x_{\text{dest,evw}}}$$
 (4.63)

where $\dot{E}x_{dest,evw}$ represents the rate of exergy destruction.

• Expansion valve (for refrigerant):

The mass balance equation for the refrigerant expansion valve is written as

$$\dot{m}_{11} = \dot{m}_{10} \tag{4.64}$$

The energy balance equation of the refrigerant expansion valve is defined as

$$\dot{m}_{10}h_{10} = \dot{m}_{11}h_{11} \tag{4.65}$$

The exergy balance equation of the refrigerant expansion valve is given as

$$\dot{m}_{10} \text{ex}_{10} = \dot{m}_{11} \text{ex}_{11} + \dot{E}x_{\text{dest,evr}}$$
 (4.66)

where $\dot{E}x_{dest,evr}$ represents the rate of exergy destruction.

• Condenser heat exchanger:

The mass balance equations for the condenser heat exchanger can be written as

$$\dot{m}_9 = \dot{m}_8 \tag{4.67}$$

$$\dot{m}_{19} = \dot{m}_{18} \text{ and}$$
 (4.68)

$$\dot{m}_2 = \dot{m}_3 + \dot{m}_{18} \tag{4.69}$$

The energy balance equation is given as

$$\dot{m}_{18}h_{18} + \dot{m}_8h_8 = \dot{m}_9h_9 + \dot{m}_{19}h_{19} \tag{4.70}$$

The specific exergies at states 9, 18, and 19 are defined as

$$ex_9 = (h_9 - h_0) - T_0(s_9 - s_0) (4.71)$$

$$ex_{18} = (h_{18} - h_0) - T_0(s_{18} - s_0)$$
(4.72)

$$ex_{19} = (h_{19} - h_0) - T_0(s_{19} - s_0)$$
(4.73)

The exergy balance equation is given as

$$\dot{m}_{18} ex_{18} + \dot{m}_{8} ex_{8} = \dot{m}_{9} ex_{9} + \dot{m}_{19} ex_{19} + \dot{E}x_{\text{dest CHX}}$$
 (4.74)

where $\dot{E}x_{dest,CHX}$ represents the exergy destruction rate in the condenser heat exchanger.

The performance of an absorption refrigeration system is measured using the coefficient of performance. The energetic and exergetic coefficient of performances of absorption refrigeration system are defined as

$$COP_{en} = \frac{\dot{Q}_e}{\dot{Q}_{HTG} + \dot{W}_p} \tag{4.75}$$

$$COP_{ex} = \frac{\dot{E}x_{th,e}}{\dot{E}x_{th,HTG} + \dot{W}_{p}}$$
(4.76)

where COPen and COPex represent energetic COP and exergetic COP, respectively.

4.4 Exergoeconomic Analysis

This section presents the exergoeconomic analysis equations of the double effect absorption refrigeration system. The overall exergoeconomic equation of the DEARS is written as

$$\dot{Z}_{eq} + \dot{C}_{OPM} = \dot{C}_{Cool} \tag{4.77}$$

where \dot{Z}_{eq} , \dot{C}_{OPM} and \dot{C}_{Cool} represent the cost associated with the equipment, operation and maintenance, and cooling, respectively.

The cost linked with the equipment is defined as

$$\dot{Z}_{eq} = \dot{C}_{a} + \dot{C}_{g} + \dot{C}_{c} + \dot{C}_{e} + \dot{C}_{P} + \dot{C}_{ev}$$
 (4.78)

where \dot{C}_a , \dot{C}_g , \dot{C}_c , \dot{C}_e , \dot{C}_p , and \dot{C}_{ev} represent the cost of the absorber, generator, condenser, evaporator, pump, and expansion valve, respectively.

However, the total equipment cost can also be calculated using a relation between the equipment cost and cooling load, as provided below:

$$\dot{Z}_{eq}(\$) = 1144.3(\dot{Q}_{Cool})^{0.67}$$
 (4.79)

The cost associated with the operation and maintenance is defined as

$$\dot{C}_{\rm OPM} = c_{\rm OPM} \times \dot{E}x_{\rm OPM} \tag{4.80}$$

where $c_{\rm OPM}$ and $\dot{\rm Ex}_{\rm OPM}$ represent operation and maintenance cost, and exergy carried by the energy consumed in terms of heat and power, respectively. The operation and maintenance can also be assumed to be 3 % of the total equipment cost.

The cost related to the cooling produced is defined as

$$\dot{C}_{\text{Cool}} = c_{\text{Cool}} \times \dot{E}_{\text{XCool}} \tag{4.81}$$

where c_{Cool} and $\dot{\text{E}}x_{\text{Cool}}$ represent the cost of cooling and the exergy related to cooling, respectively.

Thus, the above equation can be written as

$$(c \times \dot{E}x)_{OPM} + \dot{Z}_{eq} = (c \times \dot{E}x)_{Cool}$$
 (4.82)

The cost of cooling can then be calculated by rearranging the above-mentioned equation and re-writing it as

$$c_{\text{Cool}} = \frac{(c \times \dot{E}x)_{\text{OPM}} + \dot{Z}_{\text{eq}}}{\dot{E}x_{\text{Cool}}}$$
(4.83)

4.5 Exergoenvironmental Analysis

In this section, we present an exergoenvironmental formulation for double effect absorption refrigeration system.

The total exergy supplied to the double effect absorption refrigeration system is calculated as

$$\dot{\mathbf{E}}\mathbf{x}_{in} = \dot{\mathbf{E}}\mathbf{x}_{th,HTG} + \dot{W}_{p} + \dot{\mathbf{E}}\mathbf{x}_{th,e} \tag{4.84}$$

The total exergy rejected by the double effect absorption refrigeration system is defined as

$$\dot{\mathbf{E}}\mathbf{x}_{\text{out}} = \dot{\mathbf{E}}\mathbf{x}_{\text{th.a}} + \dot{\mathbf{E}}\mathbf{x}_{\text{th.c}} \tag{4.85}$$

The total exergy destroyed by the DEARS is calculated as

$$\dot{E}x_{dest,tot} = \dot{E}x_{in} - \dot{E}x_{out} \tag{4.86}$$

The exergoenvironmental impact factor is defined as

$$f_{\rm ei} = \frac{\dot{\rm E}x_{\rm dest,tot}}{\dot{\rm E}x_{\rm in}} \tag{4.87}$$

where f_{ei} represents the exergoenvironmental impact factor.

This exergoenvironmental impact coefficient is calculated as

$$C_{ei} = \frac{1}{\text{COP}_{ex}} \tag{4.88}$$

where $C_{\rm ei}$ represents the exergoenvironmental impact coefficient.

The exergoenvironmental impact index is calculated as

$$\theta_{\rm ei} = f_{\rm ei} \times C_{\rm ei} \tag{4.89}$$

where θ_{ei} represents the exergoenvironmental impact index.

Exergoenvironmental impact improvement is defined as

$$\theta_{\rm eii} = \frac{1}{\theta_{\rm ei}} \tag{4.90}$$

where θ_{eii} represents the exergoenvironmental impact improvement.

The exergetic stability factor is defined as

$$f_{\rm es} = \frac{\dot{E}x_{\rm out}}{\dot{E}x_{\rm out} + \dot{E}x_{\rm dest.tot}} \tag{4.91}$$

where $f_{\rm es}$ represents exergetic stability factor.

The exergetic sustainability index is defined as

$$\theta_{\rm est} = f_{\rm es} \times \theta_{\rm eii}$$
 (4.92)

where θ_{est} represents the exergetic sustainability index.

4.6 Optimization

A common optimization problem in absorption refrigeration system is that of maximizing the exergetic COP and the exergetic sustainability index and minimizing the cost of cooling. The three objective functions used for this study are presented in Eqs. 4.76, 4.83, and 4.92. The constraints are ambient temperature, the heat supplied to the high temperature generator, the concentration of the strong solution and the concentration of the weak solution.

4.7 Illustrative Example

Consider a double effect absorption refrigeration system using ammonia—water as a working fluid as shown in Fig. 4.1. The strong ammonia—water solution with a mass flow rate of 1 kg/s enters the pumpas a saturated liquid with concentration and pressure of 0.5 and 200 kPa, respectively. The strong solution leaves the pump at 700 kPa with a temperature difference of 0.4 °C. The heat is supplied to the generator at a rate of 150 kW, which helps to boil the strong solution, and the weak solution and ammonia refrigerant vapor leaves the generator with concentrations of 0.3 and 0.999, respectively. Assume a temperature difference of 77 °C between the inlet and exit of the heat exchangers. Take the temperature difference between the

strong solution entering the generators and weak solution exiting the generators to be 10 $^{\circ}$ C. Consider the condenser load and evaporator temperature to be 250 kW and -1.3.5 $^{\circ}$ C, respectively. Take ambient temperature and pressure to be 291.2 K and 100 kPa. Calculate the following

- (a) the rate of cooling provided by the evaporator,
- (b) the power consumed by the pump,
- (c) the rate of heat rejected by the absorber,
- (d) energetic and exergetic COPs,
- (e) the exergy destruction rate in each component,
- (f) the exergetic cost of cooling, and
- (g) exergoenvironmental parameters as discussed earlier in the chapter.

In addition, perform the following parametric studies to investigate

- (a) effects of generator load on the cooling load, the cost of cooling, and the energy and exergy COPs;
- (b) effects of strong solution concentration on the cooling load, the cost of cooling and the energy and exergy COPs; and
- (c) effects of ambient temperature on the energy and exergy COPs, and all the exergoenvironmental parameters.

For parametric studies, use the same data ranges as defined below.

Also, perform an optimization study for the following scenarios:

- (a) maximizing the exergetic COP and minimizing the exergetic cost of cooling, and
- (b) maximizing the exergetic sustainability index and minimizing the exergetic cost of cooling.

For an optimization study, consider generator heat load, strong solution concentration, weak solution concentration, and ambient temperature as constraints with limits of 130–170 kW, 0.45–0.55, 0.2–0.3, and 290–310 K, respectively.

Solution

The pump inlet properties are considered by assuming pressure, strong solution concentration, and quality.

$$\left. \begin{array}{l} P_1 = 200 \mathrm{kPa} \\ x_1 = 0.5 \\ Qu_1 = 0.00 \end{array} \right\} \quad \begin{array}{l} h_1 = -180.1 \; \mathrm{kJ/kg} \\ s_1 = 0.04011 \; \mathrm{kJ/kg} \; \mathrm{K} \\ v_1 = 0.001199 \; \mathrm{m^3/kg} \\ T_1 = 286.5 \; \mathrm{K} \end{array}$$

It is assumed that at the exit of the pump, the temperature would be $0.4\ ^{\circ}\mathrm{C}$ higher than the inlet temperature.

$$\left. \begin{array}{l} P_2 = 700 \, \mathrm{kPa} \\ x_2 = 0.5 \\ T_2 = 286.9 \, \mathrm{K} \end{array} \right\} \quad \begin{array}{l} h_2 = -178.1 \, \mathrm{kJ/kg} \\ s_2 = 0.04481 \, \mathrm{kJ/kg} \, \mathrm{K} \\ \\ \dot{m}_1 = 1 \, \mathrm{kg/s} \\ \\ \dot{m}_2 = \dot{m}_1 \end{array}$$

The power required by the pump to increase the pressure of 1 kg/s of strong solution from 200 kPa to 700 kPa is calculated as

$$\dot{W}_{\rm p} = 1((-178.1) - (-180.1)) = 1.971 \text{ kW}$$

The ambient conditions to calculate specific exergy at each point are

$$\left. \begin{array}{l} P_0 = 100 \, \mathrm{kPa} \\ T_0 = 291.2 \, \, \mathrm{K} \\ x_0 = 0.5 \end{array} \right\} \quad \begin{array}{l} h_0 = -150 \, \mathrm{kJ/kg} \\ s_0 = 0.1034 \, \mathrm{kJ/kg} \, \, \mathrm{K} \end{array}$$

These ambient conditions can only be used for strong solution streams.

$$\dot{E}x_1 = 1((-180.1 - (-150)) - 291.2(0.04011 - 0.1034)) = -11.62 \text{ kW}$$

 $\dot{E}x_2 = 1((-178.1 - (-150)) - 291.2(0.04481 - 0.1034)) = -11.01 \text{ kW}$

The exergy destruction in the pump is then calculated as

$$-11.62 + 1.971 = -11.01 + \dot{E}x_{dest,p}$$

 $\dot{E}x_{dest,p} = 1.368 \text{ kW}$

It is assumed that 20 % of the flow rate from the pump is supplied to the condenser heat exchanger and the remaining 80 % is supplied to the low temperature heat exchanger. The temperature, pressure, and strong solution concentration remains the same at states 2, 3, and 18.

$$h_3 = h_2$$
 $s_3 = s_2$
 $T_3 = T_2$
 $h_{18} = h_2$
 $s_{18} = s_2$
 $T_{18} = T_2$

The mass balance equations for the low temperature heat exchanger are written as

$$\dot{m}_{18} = 0.2(\dot{m}_2) = 0.2 \,\mathrm{kg/s}$$
 $\dot{m}_3 = 0.8(\dot{m}_2) = 0.8 \,\mathrm{kg/s}$
 $\dot{m}_4 = \dot{m}_3$
 $\dot{m}_{15} = \dot{m}_{16}$

The temperature of the strong solution leaving the low temperature heat exchanger is assumed to be 77 °C higher than the inlet temperature.

$$\left. \begin{array}{l}
 P_4 = P_2 \\
 x_4 = x_2 \\
 T_4 = T_2 + 77
 \end{array} \right\} \quad \begin{array}{l}
 h_4 = 647.4 \,\text{kJ/kg} \\
 s_4 = 2.505 \,\text{kJ/kg K}
 \end{array}$$

The energy balance equation of the low temperature heat exchanger can be written as

$$\dot{m}_3 h_3 + \dot{m}_{15} h_{15} = \dot{m}_4 h_4 + \dot{m}_{16} h_{16}$$

$$0.8(-178.1) + 0.7139(343.4) = 0.8(647.4) + 0.7139(h_{16})$$
 $h_{16} = -581.7 \text{ kJ/kg}$

Using specific enthalpy at state 16 calculated using energy balance and knowing the pressure and weak solution concentration, one can find the specific entropy and temperature at state 16 as follows:

$$\left. \begin{array}{l} P_{16} = P_2 \\ x_{16} = 0.3 \\ h_{16} = -581.7 \end{array} \right\} \quad \begin{array}{l} T_{16} = 195.3 \text{ K} \\ s_{16} = -1.787 \text{ kJ/kg K} \end{array}$$

The rate of heat transfer taking place inside the low temperature heat exchanger can be calculated as

$$\dot{m}_3 h_3 + \dot{Q}_{LHX} = \dot{m}_4 h_4$$
 $0.8(-178.1) + \dot{Q}_{LHX} = 0.8(647.4)$
 $\dot{Q}_{LHX} = 660.4 \text{ kW}$

The thermal exergy rate of the low temperature heat exchanger can be calculated as

$$\dot{E}x_{th,LHX} = \left(1 - \frac{291.2}{363.9}\right) 660.4 = 132 \text{ kW}$$

The exergy flow rates at different states of the low temperature heat exchanger are calculated as

$$\begin{split} &\dot{E}x_3 = 0.8((-178.1 - (-150)) - 291.2(0.04481 - 0.1034)) = -8.811 \text{ kW} \\ &\dot{E}x_4 = 0.8((647.4 - (-150)) - 291.2(2.505 - 0.1034)) = 78.37 \text{ kW} \\ &\dot{E}x_{15} = 0.7139((343.4 - (-102.5)) - 291.2(1.539 - 0.1906)) = 37.88 \text{ kW} \\ &\dot{E}x_{16} = 0.7139((-581.7 - (-102.5)) - 291.2(-1.787 - 0.1906)) = 68.88 \text{ kW} \end{split}$$

The exergy destruction rate in the low temperature heat exchanger is calculated as

$$-8.811 + 132 = 78.37 + \dot{E}x_{dest,LHX}$$

 $\dot{E}x_{dest,LHX} = 44.79 \text{ kW}$

It is assumed that 20 % of the flow rate from state 4 is supplied to state 20 and the remaining 80 % is supplied to the high temperature heat exchanger. The temperature, pressure, and strong solution concentration remains the same at states 4, 5, and 20.

$$h_5 = h_4$$
 $s_5 = s_4$
 $T_5 = T_4$
 $h_{20} = h_4$
 $s_{20} = s_4$
 $T_{20} = T_4$

The mass balance equations for the high temperature heat exchanger are written as

$$\dot{m}_{20} = 0.2(\dot{m}_4) = 0.16 \,\mathrm{kg/s}$$
 $\dot{m}_5 = 0.8(\dot{m}_4) = 0.64 \,\mathrm{kg/s}$
 $\dot{m}_6 = \dot{m}_5$
 $\dot{m}_{14} = \dot{m}_{13}$

The temperature of the strong solution leaving the high temperature heat exchanger is assumed to be $10~^{\circ}\text{C}$ higher than the inlet temperature.

$$\left. \begin{array}{l}
 P_6 = P_2 \\
 x_6 = x_2 \\
 T_6 = T_5 + 10
\end{array} \right\} \quad h_6 = 807.1 \,\text{kJ/kg} \\
 s_6 = 2.936 \,\text{kJ/kg K}$$

The energy balance equation of the high temperature heat exchanger can be written as

$$\dot{m}_5 h_5 + \dot{m}_{13} h_{13} = \dot{m}_6 h_6 + \dot{m}_{14} h_{14}$$

$$0.64(647.4) + 0.4569(546.1) = 0.64(807.1) + 0.4569(h_{14})$$
 $h_{14} = 322.5 \text{ kJ/kg}$

Using specific enthalpy at state 14 calculated using the energy balance and knowing the pressure and weak solution concentration, one can find the specific entropy and temperature at state 14 as follows:

$$\begin{array}{l}
 P_{14} = P_2 \\
 x_{14} = x_{13} \\
 h_{14} = 322.5
 \end{array}
 \qquad
 \begin{array}{l}
 T_{14} = 370.3 \text{ K} \\
 s_{14} = 1.483 \text{ kJ/kg K}
 \end{array}$$

The rate of heat transfer taking place inside the high temperature heat exchanger can be calculated as

$$\dot{m}_5 h_5 + \dot{Q}_{\rm HHX} = \dot{m}_6 h_6$$
 $0.64(647.4) + \dot{Q}_{\rm HHX} = 0.64(807.1)$
 $\dot{Q}_{\rm HHX} = 102.2 \text{ kW}$

The thermal exergy rate of the high temperature heat exchanger can be calculated as

$$\dot{E}x_{th,HHX} = \left(1 - \frac{291.2}{373.9}\right)102.2 = 22.6 \; kW$$

The exergy flow rates at different states are calculated as

$$\begin{split} &\dot{E}x_5 = 0.64((647.4 - (-150)) - 291.2(2.505 - 0.1034)) = 62.69 \text{ kW} \\ &\dot{E}x_6 = 0.64((807.1 - (-150)) - 291.2(2.936 - 0.1034)) = 84.55 \text{ kW} \\ &\dot{E}x_{13} = 0.4569((546.1 - (-102.5)) - 291.2(2.074 - 0.1906)) = 45.8 \text{ kW} \\ &\dot{E}x_{14} = 0.4569((322.5 - (-102.5)) - 291.2(1.483 - 0.1906)) = 22.16 \text{ kW} \end{split}$$

The exergy destruction rate in the high temperature heat exchanger is calculated as

$$62.69 + 22.6 = 84.55 + \dot{E}x_{dest,HHX}$$

$$\dot{\mathbf{E}}\mathbf{x}_{\text{dest HHX}} = 0.7503 \text{ kW}$$

The mass balance equations of the high temperature generator are written as

$$\dot{m}_6 = \dot{m}_{13} + \dot{m}_7
\dot{m}_6 x_6 = \dot{m}_{13} x_{13} + \dot{m}_7 x_7
0.64 = \dot{m}_{13} + \dot{m}_7
0.64(0.5) = \dot{m}_{13}(0.3) + \dot{m}_7(0.999)$$

Solving two equations simultaneously gives us

$$\dot{m}_{13} = 0.4569 \text{ kg/s}$$
 and $\dot{m}_7 = 0.1831 \text{ kg/s}$

The temperature at state 13 is assumed to be 10 $^{\circ}$ C higher than the temperature at state 6.

$$\left. \begin{array}{l} P_{13} = P_2 \\ x_{13} = 0.3 \\ T_{13} = T_2 + 10 \end{array} \right\} \quad \left. \begin{array}{l} h_{13} = 546.1 \text{ kJ/kg} \\ s_{13} = 2.074 \text{ kJ/kg K} \end{array} \right.$$

The specific enthalpy at state 7 is calculated using the energy balance equation of the high temperature generator as defined below:

$$\dot{m}_6 h_6 + \dot{Q}_{HTG} = \dot{m}_{13} h_{13} + \dot{m}_7 h_7$$

$$0.64(807.1) + 150 = 0.4569(546.1) + 0.1831 h_7$$
 $h_7 = 2277 \text{ kJ/kg}$

Using specific enthalpy at state 7 and knowing pressure and concentration at this state, we can find the temperature and specific entropy at state 7 as follows:

$$\left. \begin{array}{l}
 P_7 = P_2 \\
 x_7 = 0.999 \\
 h_7 = 2277 \text{ kJ/kg}
 \end{array} \right\} \qquad T_7 = 672 \text{ K} \\
 s_7 = 6.643 \text{ kJ/kg K}$$

$$\dot{E}x_7 = 0.1831[(2277 - 87.15) - 291.2(6.643 - 0.2708)] = 61.28 \text{ kW}$$

The thermal exergy rate of the high temperature generator can be calculated by using average temperature as

$$\dot{E}x_{th,HTG} = \left(1 - \frac{291.2}{476.6}\right)150 = 58.35 \text{ kW}$$

Using the thermal exergy rate and rate of exergy at each state, we can find the total exergy destruction rate of the high temperature generator as

$$84.55 + 58.35 = 61.28 + 45.8 + \dot{E}x_{dest,HTG}$$

 $\dot{E}x_{dest,HTG} = 35.82 \text{ kW}$

The mass flow rates across the different streams entering and leaving the low temperature generator are calculated as

$$\dot{m}_{21} = \dot{m}_{20} + \dot{m}_{19}
\dot{m}_{19} = \dot{m}_{18} = 0.2 \text{ kg/s}
\dot{m}_{21} = 0.16 + 0.2 = 0.36 \text{ kg/s}
\dot{m}_{21} = \dot{m}_{22} + \dot{m}_{23}
\dot{m}_{21}x_{21} = \dot{m}_{22}x_{22} + \dot{m}_{23}x_{23}
0.36 = \dot{m}_{22} + \dot{m}_{23}
0.36(0.5) = \dot{m}_{22}(0.3) + \dot{m}_{23}(0.999)$$

Solving two equations simultaneously gives us

$$\dot{m}_{22} = 0.257 \text{ kg/s}$$
 and $\dot{m}_{23} = 0.103 \text{ kg/s}$
 $\dot{m}_8 = \dot{m}_7 = 0.1837 \text{ kg/s}$

The temperature at state 22 is assumed to be 10 °C higher than the temperature at state 21.

$$\left. egin{aligned} P_{22} &= P_2 \\ x_{22} &= x_{13} \\ T_{22} &= T_{21} + 10 \end{aligned}
ight\} \quad \left. egin{aligned} h_{22} &= 380.6 \text{ kJ/kg} \\ s_{22} &= 1.639 \text{ kJ/kg K} \end{aligned}
ight.$$

It is assumed that ammonia vapor at state 23 leaves with the same temperature as that of state 22.

$$\left. \begin{array}{l}
 P_{23} = P_2 \\
 x_{23} = x_7 \\
 T_{23} = T_{22}
 \end{array} \right\}$$
 $\left. \begin{array}{l}
 h_{23} = 1501 \text{ kJ/kg} \\
 s_{23} = 5.131 \text{ kJ/kg K}
 \end{array}$

The specific enthalpy at state 8 is calculated using the energy balance equation of the low temperature generator as defined below

$$\begin{split} \dot{m}_{21}h_{21} + \dot{m}_7h_7 &= \dot{m}_{23}h_{23} + \dot{m}_{22}h_{22} + \dot{m}_8h_8 \\ 0.36(647.4) + 0.1831(2277) &= 0.103(1501) + 0.257(380.6) + 0.1831h_8 \\ h_8 &= 2172 \text{ kJ/kg} \end{split}$$

Using specific enthalpy at state 8 and knowing pressure and concentration at this state, we can find the temperature and specific entropy at state 8 as follows:

$$\left. \begin{array}{l} P_8 = P_2 \\ x_8 = x_7 \\ h_8 = 2172 \text{ kJ/kg} \end{array} \right\} \quad \begin{array}{l} T_8 = 635.5 \text{ K} \\ s_8 = 6.481 \text{ kJ/kg K} \end{array}$$

$$\begin{split} \dot{E}x_8 &= 0.1831[(2172-87.15)-291.2(6.481-0.2708)] = 50.57 \text{ kW} \\ \dot{E}x_{21} &= 0.36((647.4-(-150))-291.2(2.55-0.1034)) = 35.27 \text{ kW} \\ \dot{E}x_{22} &= 0.257((380.6-(-102.5))-291.2(1.639-0.1906)) = 15.77 \text{ kW} \\ \dot{E}x_{23} &= 0.103((1501-(-102.5))-291.2(5.131-0.1906)) = -0.1836 \text{ kW} \end{split}$$

Using the exergyrate at each state, we can find the total exergy destruction rate of the low temperature generator as

$$35.27 + 61.28 = 15.77 + 50.57 - 0.1836 + \dot{E}x_{dest,LTG}$$

$$\dot{E}x_{dest\ LTG} = 30.39\ kW$$

The mass flow rates across the different streams entering and leaving the condenser heat exchanger are calculated as

$$\dot{m}_9 = \dot{m}_8 = 0.1831 \text{ kg/s}$$

The temperature at state 19 is assumed to be 77 $^{\circ}$ C higher than the temperature at state 18.

$$\begin{array}{l}
 P_{19} = P_2 \\
 x_{19} = x_6 \\
 T_{19} = T_{18} + 77
 \end{array}
 \qquad
 \begin{cases}
 h_{19} = 647.4 \text{ kJ/kg} \\
 s_{19} = 2.505 \text{ kJ/kg K}
 \end{cases}$$

The specific enthalpy at state 9 is calculated using the energy balance equation of the condenser heat exchanger as defined below

$$\dot{m}_8 h_8 + \dot{m}_{18} h_{18} = \dot{m}_9 h_9 + \dot{m}_{19} h_{19}$$

 $0.1831(2172) + 0.2(-178.1) = 0.1831(h_9) + 0.2(647.4)$
 $h_9 = 1270 \,\text{kJ/kg}$

Using specific enthalpy at state 9 and knowing pressure and concentration at this state, we can find the temperature and specific entropy at state 9 as follows:

$$\left. \begin{array}{l}
 P_9 = P_2 \\
 x_9 = x_{78} \\
 h_9 = 1270 \text{ kJ/kg}
 \end{array} \right\} \qquad T_9 = 289 \text{ K} \\
 s_9 = 4.426 \text{ kJ/kg K}$$

$$\begin{split} \dot{E}x_9 &= 0.1831[(1270 - 87.15) - 291.2(4.426 - 0.2708)] = -4.949 \text{ kW} \\ \dot{E}x_{19} &= 0.2((647.4 - (-150)) - 291.2(2.505 - 0.1034)) = 19.59 \text{ kW} \end{split}$$

Using the rate of exergy at each state, we can find the total exergy destruction rate of the condenser heat exchanger as

$$50.57 - 2.203 = -4.949 + 19.59 + \dot{E}x_{dest,CHX}$$

 $\dot{E}x_{dest,CHX} = 33.73 \text{ kW}$

The mass balance equation of the condenser can be written as

$$\dot{m}_9 + \dot{m}_{23} = \dot{m}_{10}$$

 $\dot{m}_{10} = 0.1831 + 0.103 = 0.2861$

The energy balance equation of the condenser capable of rejecting 250 kW of heat is written as

$$\dot{m}_9 h_9 + \dot{m}_{23} h_{23} = \dot{m}_{10} h_{10} + \dot{Q}_{c}$$

The above-mentioned equation is used to calculate the specific enthalpy at state 10 as

$$0.1831(1270) + 0.103(1501) = 0.2861h_{10} + 250$$

 $h_{10} = 479.4 \text{ kJ/kg}$

$$\left. \begin{array}{l} P_{10} = P_2 \\ x_{10} = x_7 \\ h_{10} = 479.4 \text{ kJ/kg} \end{array} \right\} \quad \begin{array}{l} T_{10} = 287 \text{ K} \\ s_{10} = 1.684 \text{ kJ/kg K} \end{array}$$

$$\dot{E}x_{10} = 0.2861[(479.4 - 87.15) - 291.2(1.684 - 0.2708)] = -5.521 \text{ kW}$$

The thermal exergy rate of the condenser can be calculated as

$$\dot{E}x_{th,c} = \left(1 - \frac{291.2}{287}\right)250 = 3.66 \text{ kW}$$

Using the exergy rate at each state and thermal rate of exergy, we can find the exergy destruction rate in the condenser as

$$-4.949 - 0.1836 = -5.521 - 3.66 + \dot{E}x_{dest,c}$$

$$\dot{E}x_{dest c} = 4.048 \text{ kW}$$

The mass balance equation of the refrigerant expansion valve is written as

$$\dot{m}_{11} = \dot{m}_{10} = 0.2861 \text{ kg/s}$$

$$\left. \begin{array}{l} h_{11} = h_{10} \\ P_{11} = P_1 \\ x_{11} = x_7 \end{array} \right\} \quad \begin{array}{l} T_{11} = 254.3 \text{ K} \\ s_{11} = 1.904 \text{ kJ/kg K} \end{array}$$

$$\dot{E}x_{11} = 0.2861[(479.4 - 87.15) + 291.2(1.904 - 0.2708)] = -23.84 \text{ kW}$$

- $5.521 = -23.84 + \dot{E}x_{dest,evr}$

$$\dot{\mathbf{E}}\mathbf{x}_{\text{dest evr}} = 18.32 \text{ kW}$$

The mass balance equation of the evaporator is written as

$$\dot{m}_{12} = \dot{m}_{11} = 0.2861 \text{ kg/s}$$

It is assumed that the refrigerant leaves the evaporator at a temperature of 259.7 K.

$$P_{12} = P_9$$
 $\begin{cases} h_{12} = 1251 \text{ kJ/kg} \\ s_{12} = 4.922 \text{ kJ/kg K} \end{cases}$

$$T_{12} = 259.7 \text{ K}$$

The energy balance equation to calculate the cooling load is defined as

$$\dot{m}_{11}h_{11} + \dot{Q}_e = \dot{m}_{12}h_{12}$$

 $0.2861(479.4) + \dot{Q}_e = 0.2861(1251)$

$$\dot{Q}_{\rm e}=220.8~{
m kW}$$

$$\dot{E}x_{12} = 0.2861[(1251 - 87.15) + 291.2(4.922 - 0.2708)] = \ -54.52 \ kW$$

The thermal exergy rate of the evaporator is calculated as

$$\dot{\mathbf{E}}\mathbf{x}_{\text{th,e}} = \left| \left(1 - \frac{291.2}{257} \right) 220.8 \right| = 25.93 \text{ kW}$$

$$-23.84 + 25.93 = -54.52 + \dot{\mathbf{E}}\mathbf{x}_{\text{dest,e}}$$

$$\dot{\mathbf{E}}\mathbf{x}_{\text{dest,e}} = \mathbf{56.61 \text{ kW}}$$

The mass balance equation of the weak solution expansion valve is written as

$$\dot{m}_{17} = \dot{m}_{16} = 0.7139 \text{ kg/s}$$
 $h_{17} = h_{16}$
 $P_{17} = P_1$
 $x_{17} = x_{13}$
 $rac{1}{3}$
 $$\dot{E}x_{17} = 0.7139((-581.7 - (-102.5)) + 291.2(-1.784 - 0.1906)) = 68.27 \text{ kW}$$

The exergy destruction rate of the weak solution expansion valve is calculated as

$$68.88 = 68.27 + \dot{E}x_{dest.evs}$$

$$\dot{E}x_{dest\ evs} = 0.61\ kW$$

The mass balance equation of the absorber is written as

$$\dot{m}_1 = \dot{m}_{12} + \dot{m}_{17}$$

The amount of heat rejected by the absorber is calculated using formula

$$\dot{m}_1 h_1 + \dot{Q}_a = \dot{m}_{12} h_{12} + \dot{m}_{17} h_{17}$$

$$1(-180.1) + \dot{Q}_a = 0.2861(1251) + 0.7139(-581.7)$$
 $\dot{Q}_a = 122.7 \text{ kW}$

The thermal exergy rate of the absorber is calculated as

$$\dot{E}x_{th,a} = \left| \left(1 - \frac{291.2}{286.5} \right) 122.7 \right| = 1.973 \text{ kW}$$

The rate of exergy destructed by the absorber is calculated as

$$-54.52 + 68.27 = -11.62 + 1.973 + \dot{E}x_{dest a}$$

$$\dot{E}x_{dest a} = 23.39 \text{ kW}$$

The weak solution at states 14 and 22 mix together to leave at state 15. The mass balance equation of this mixing process is written as

$$\dot{m}_{15} = \dot{m}_{14} + \dot{m}_{22}$$

 $\dot{m}_{15} = 0.4569 + 0.257 = 0.7139 \text{ kg/s}$

The energy balance equation of the mixing process is written as

$$\begin{array}{l} \dot{m}_{15}h_{15} = \dot{m}_{14}h_{14} + \dot{m}_{22}h_{22} \\ 0.7139h_{15} = 0.4569(322.5) + 0.257(380.6) \\ h_{15} = 343.4 \text{ kJ/kg} \\ h_{15} = 343.4 \text{ kJ/kg} \\ P_{15} = P_2 \\ x_{15} = x_{13} \end{array} \right\} \begin{array}{l} T_{15} = 371.6 \text{ K} \\ s_{15} = 1.539 \text{ kJ/kg K} \end{array}$$

$$\dot{E}x_{15} = 0.7139((343.4 - (-102.5)) + 291.2(1.539 - 0.1906)) = 37.88 \text{ kW}$$

The strong solution at states 19 and 20 mix together to leave at state 21. The energy balance equation of the mixing process is written as

$$\dot{m}_{21}h_{21} = \dot{m}_{19}h_{19} + \dot{m}_{20}h_{20}$$

 $0.36h_{21} = 0.2(647.4) + 0.2(0.16)$
 $h_{21} = 647.4 \text{ kJ/kg}$

$$\left. \begin{array}{l} h_{21} = 647.4 \text{ kJ/kg} \\ P_{21} = P_2 \\ x_{21} = x_6 \end{array} \right\} \quad \left. \begin{array}{l} T_{21} = 363.9 \text{ K} \\ s_{21} = 2.505 \text{ kJ/kg K} \end{array} \right.$$

$$\dot{E}x_{21} = 0.36((647.4 - (-150)) + 291.2(2.505 - 0.1034)) = 35.27 \text{ kW}$$

The energy and exergy COPs of the double effect absorption refrigeration systems are calculated as

$$\begin{split} COP_{en} &= \frac{220.8}{150 + 1.971} = 1.453 \\ COP_{ex} &= \frac{25.93}{58.35 + 1.971} = 0.4299 \end{split}$$

The equipment cost of the DEARS is found using

$$\dot{Z}_{\text{eq}}(\$) = 1144.3(220.8)^{0.67} = \$42556$$

The operation and maintenance cost of the DEARS is assumed to be 3 % of the equipment cost

$$\dot{C}_{\text{OPM}} = 0.03(42556) = \$1277$$

The exergetic cost of cooling can then be calculated by using equipment cost, cost of operation and maintenance, and the thermal exergy rate of the evaporator as

$$c_{\text{Cool}} = \frac{42556 + 1277}{25.93}$$
$$c_{\text{Cool}} = 1690 \text{ }\$/\text{kW}$$

The total rate of exergy entering the DEARS is calculated as

$$\dot{E}x_{in} = 58.35 + 1.971 + 25.93 = 86.26 \text{ kW}$$

The total rate of exergy exiting the DEARS is calculated as

$$\dot{E}x_{out} = 1.973 + 3.66 = 5.633 \text{ kW}$$

The total rate of exergy destroyed by the DEARS is calculated as

$$\dot{E}x_{dest.tot} = 86.26 - 5.633 = 80.62 \text{ kW}$$

The exergoenvironmental impact factor can then be calculated by dividing total exergy destruction rate by total exergy supplied to the DEARS as

$$f_{\rm ei} = \frac{80.62}{86.26} = 0.93$$

The exergoenvironmental impact coefficient is calculated by taking the inverse of the exergetic COP as

$$C_{\rm ei} = \frac{1}{0.4299} = 2.33$$

The exergoenvironmental impact index is found by multiplying exergoenvironmental impact factors as

$$\theta_{ei} = 0.93 \times 2.33 = 2.17$$

The exergoenvironmental impact improvement is then found by taking the inverse of the exergoenvironmental impact index as

$$\theta_{eii} = \frac{1}{2.17} = 0.4599$$

The exergetic stability factor is computed as

$$f_{\rm es} = \frac{5.633}{5.633 + 80.62} = 0.0653$$

The exergetic sustainability index is then calculated by the multiplying exergetic stability factor with exergoenvironmental impact improvement as

$$\theta_{est} = 0.0653 \times 0.4599 = 0.030$$

Note that the thermophysical properties at each state point are presented in Table 4.1.

• Effects of generator load

The variation in the heat rate supply to the generator can greatly affect the performance of the double effect absorption refrigeration system as shown in Fig. 4.2. The cooling load is observed todecrease from 240.8 to 200.8 kW with an increase in high temperature generator load from 130 to 170 kW. The cost of cooling is noted to increase from 1643 to 1744 \$/kW with the increase in high

Table 4.1	Thermophysical	properties at e	each state	points of the DEARS

State Point	P (kPa)	T (K)	m (kg/s)	h (kJ/kg)	s (kJ/kg K)
0	100	291.2	_	-150	0.1034
1	200	286.5	1	-180.1	0.04011
2	700	286.9	1	-178.1	0.04481
3	700	286.9	0.8	-178.1	0.04481
4	700	363.9	0.8	647.4	2.505
5	700	363.9	0.64	647.4	2.505
6	700	373.9	0.64	807.1	2.936
7	700	672	0.1831	2277	6.643
8	700	635.5	0.1831	2172	6.481
9	700	289	0.1831	1270	4.426
10	700	287	0.2861	479.4	1.684
11	200	254.3	0.2861	479.4	1.904
12	200	259.7	0.2861	1251	4.922
13	700	383.9	0.4569	546.1	2.074
14	700	370.3	0.4569	322.5	1.483
15	700	371.6	0.7139	343.4	1.539
16	700	195.3	0.7139	-581.7	-1.787
17	200	195.4	0.7139	-581.7	-1.784
18	700	286.9	0.2	-178.1	0.04481
19	700	363.9	0.2	647.4	2.505
20	700	363.9	0.16	647.4	2.505
21	700	363.9	0.36	647.4	2.505
22	700	373.9	0.257	380.6	1.639
23	700	373.9	0.103	1501	5.131

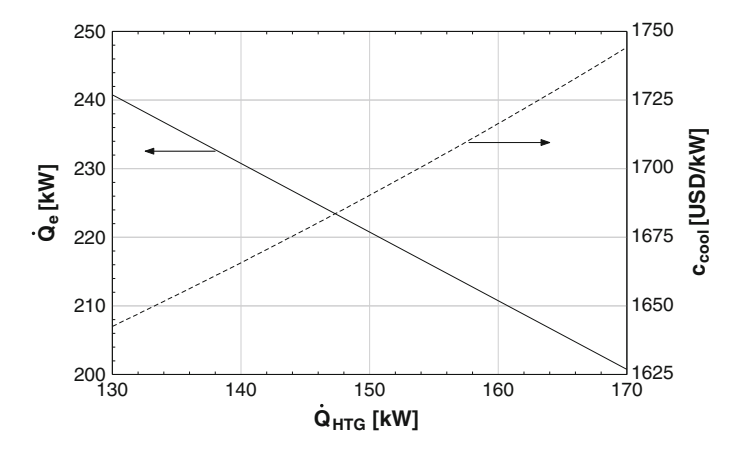


Fig. 4.2 Effects of generator load on cooling load and cost of cooling

temperature generator load. This decreasing behavior is seen because the increase in generator load results in an increased amount of energy being supplied to the strong solution. This strong solution then breaks into weak solution and ammonia vapor. The increase in energy supply results in a higher exit temperature of the ammonia refrigerant which then enters the fixed capacity condenser. With the fixed condenser load, the ammonia refrigerant leaves the condenser at relatively higher temperature to enter the evaporator. The higher temperature of the refrigerant adversely affects the performance of the evaporator as its capacity to carry heat from the cooled space decreases because the evaporator exit temperature is fixed. The decrease in cooling load for the fixed system size also has a negative impact on the cost of cooling. Cooling load is directly associated with the system size and displays an increasing trend with the increase in the generator load due to the comparatively lower cooling carrying ability of the refrigerant flowing in the evaporator. The effects of an increase in the high temperature generator load on the energy and exergy COPs are displayed in Fig. 4.3. The energy and exergy COPs are observed to decrease from 1.82 to 1.17 and 0.56 to 0.33, respectively, with an increase in the high temperature generator load. These decreasing behaviors of the energetic and exergetic COPs are directly related to the cooling carrying ability of the system. With increase in the refrigerant temperature entering the evaporator and decreasing in the cooling carrying capacity of the refrigerant; the performance of the system degrades as shown by the COP.

· Effects of strong solution concentration

The effects of variation in concentration of the strong solution on the cooling load and cost of cooling are presented in Fig. 4.4. The cooling rate is noted to decrease from 244.8 to 210.9 kW with an increase in the strong solution concentration from 0.45 to 0.55. On the other hand, the cost of cooling is observed to increase from 1633 to 1716 \$/kW, respectively, with an increase in the strong

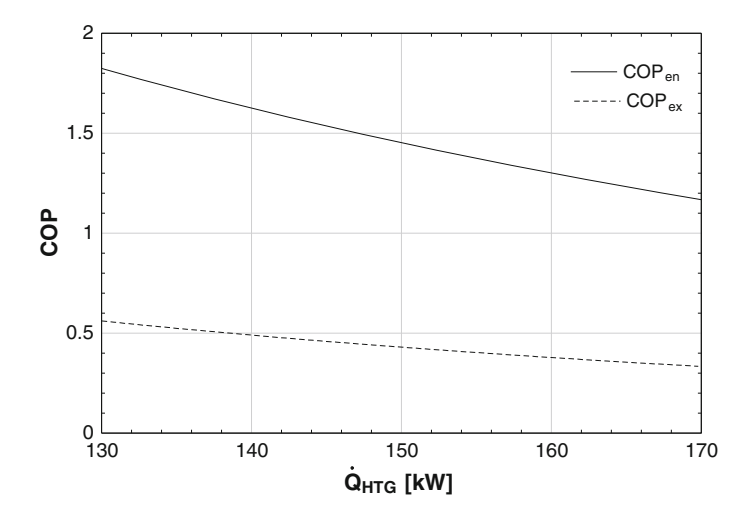


Fig. 4.3 Effects of generator load on energy and exergy COPs

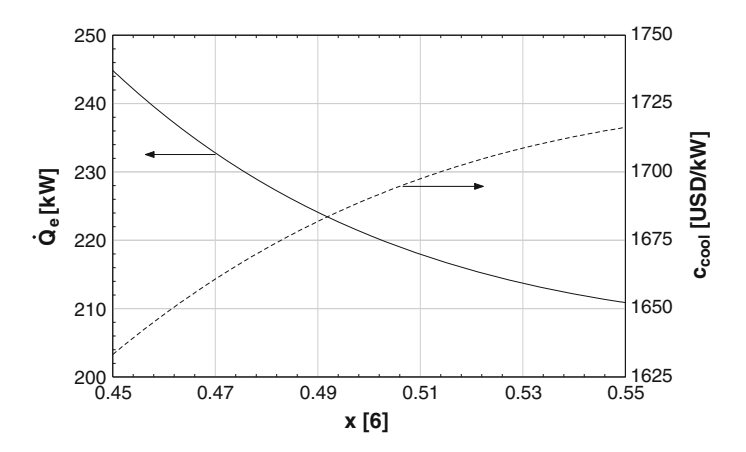


Fig. 4.4 Effects of strong solution concentration on cooling load and cost of cooling

solution concentration. This decreasing trend is because the increase in strong solution concentration brings a higher amount of ammonia refrigerant into the generator. For a fixed generator load, this excess ammonia refrigerant in the strong solution is not able to evaporate and leave as a refrigerant vapor. Thus, the alternative route available to the system in this scenario is increasing the temperature of ammonia refrigerant vapor leaving the generator. This relatively higher temperature refrigerant then brings with it the requirement of a larger size condenser, which is not met by the system as the systems condenser load is fixed at 250 kW. The fixed condenser load forces the refrigerant to enter the evaporator at a relatively higher temperature as it is not able to reject excess heat gained in the generator from the

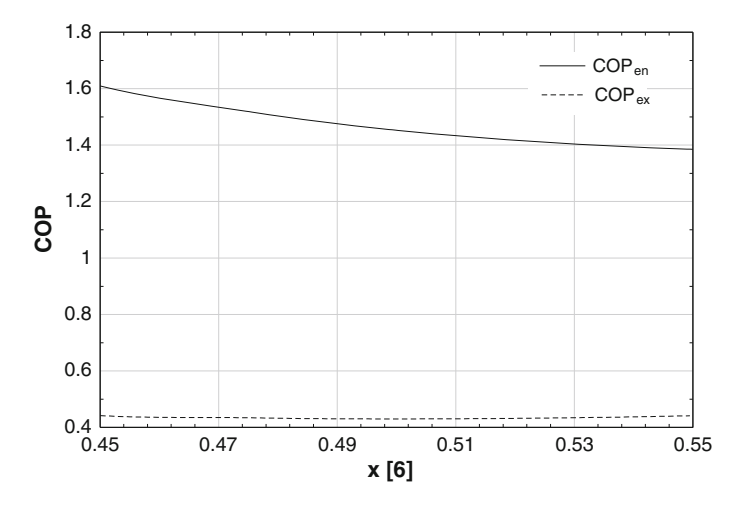


Fig. 4.5 Effects of strong solution concentration on energy and exergy COPs

condenser. The relatively higher temperature refrigerant is not able to carry enough cooling load in the evaporator due to the lower temperature difference between the inlet and exits of the temperature. The decrease in the cooling production capacity of the system results in the higher cooling cost. The cooling cost increases because the fixed size system in unable to transform higher refrigerant concentration into the higher cooling capacity. The effects of an increase in the strong solution concentration on the energy and exergy COPs are presented in Fig. 4.5. The energy and exergy COPs are observed to decrease from 1.61 to 1.38 and 0.44 to 0.43, respectively. The decreasing behavior of the COPs shows that the system performance degrades with an increase in the concentration of the strong solution. This degrading performance is directly related to the relatively lower cooling production capability of the system due to increase in the ammonia refrigerant vapor entering the evaporator of the system. This analysis shows that it is not necessary that providing excess refrigerant to the system will result in the better performance of the system. It is also noted that the energy COP decreases greatly whereas the exergy COP decreases with a very small amount displaying the importance of carrying out the exergy analysis because exergy analysis adds quality of the quantity provided by the energy analysis.

• Effects of ambient temperature

The variation in ambient temperature greatly hampers the performance of the system, especially those that are heat driven. The effects of variation in ambient temperature on the energy and exergy COPs are shown in Fig. 4.6. It can be seen in the figure that the energetic COP remains constant at 1.45 as the ambient temperature rises from 290 to 310 K.

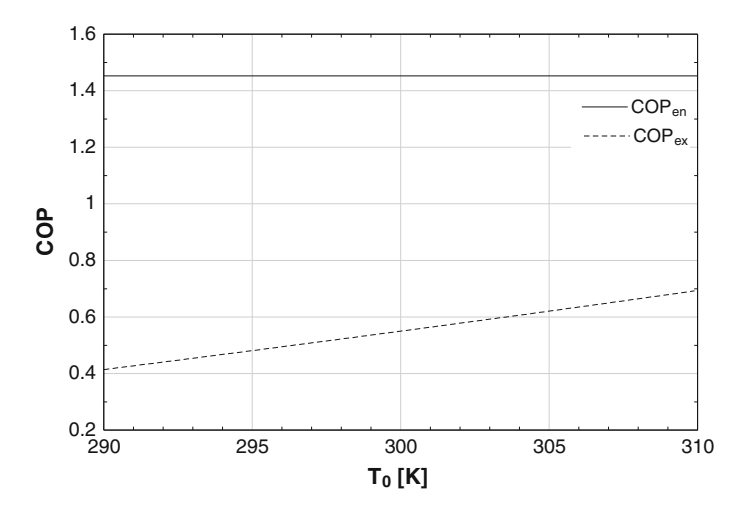


Fig. 4.6 Effects of ambient temperature on energy and exergy COPs

However, the exergetic COP is noted to increase from 0.41 to 0.7 with increase in ambient temperature. The first observation which can be made from the ambient temperature analysis is that it has no effect on the energetic performance of the system which is far from reality. In reality, the system performance varies greatly with change in ambient temperature because the rate of heat lostor gained by the system to or from the surrounding is dependent on the temperature difference between the surrounding and the system. The increase in exergetic COP is because the increase in ambient temperature results in a higher temperature difference between the DEARS and the surrounding. The DEARS is mainly heat driven, so it benefits from the increase in ambient temperature as losses from the system to the environment decrease because the temperature difference between the system and the environment is smaller. The effects of ambient temperature increase on the exergoenvironmental impact factor and the exergoenvironmental impact coefficient are shown in Fig. 4.7. The exergoenvironmental impact factor and the exergoenvironmental impact coefficient are observed to decrease from 0.95 to 0.68 and 2.42 to 1.44, respectively, with increase in ambient temperature from 290 to 310 K. The decreasing behavior of the exergoenvironmental impact factor shows that the DEARS becomes more environmentally friendly as the ambient temperature rises because of the relatively smaller irreversibility in the system. The ideal value for this parameter is zero, and the system approaches this ideal value as it becomes more environmentally benign. The exergoenvironmental impact coefficient is directly related to the exergetic COP of the system. The desired value should indicate that the system has no losses. The increase in ambient temperature helps to reach this ideal value because with an increase in ambient temperature the DEARS losses decrease and the system becomes more efficient.

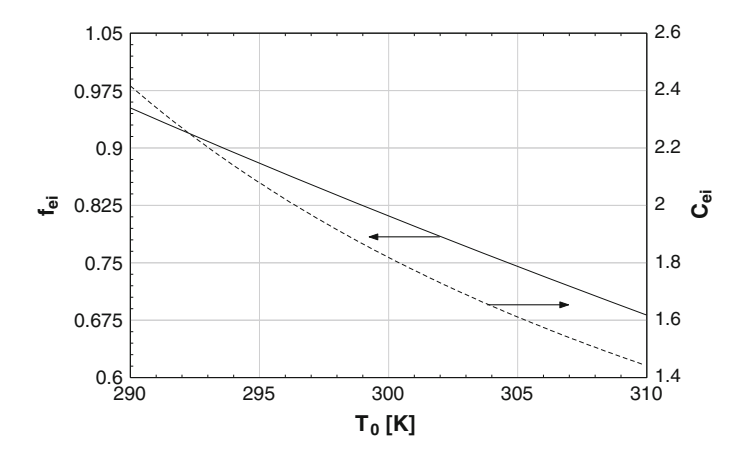


Fig. 4.7 Effects of ambient temperature on the exergoenvironmental impact factor and the exergoenvironmental impact coefficient

The effects of the increase in ambient temperature on the exergoenvironmental impact index and the exergoenvironmental impact improvement factor are shown in Fig. 4.8. The exergoenvironmental impact index is observed to decrease from 2.3 to 0.98, whereas the exergoenvironmental impact improvement factor is observed to increase from 0.43 to 1.0 with increase in ambient temperature from 290 to 310 K. The decreasing behavior of the exergoenvironmental impact index is a result of decrease in the waste exergy rate and the exergy destruction rate. The rise in ambient temperature helps to reduce the temperature difference between the

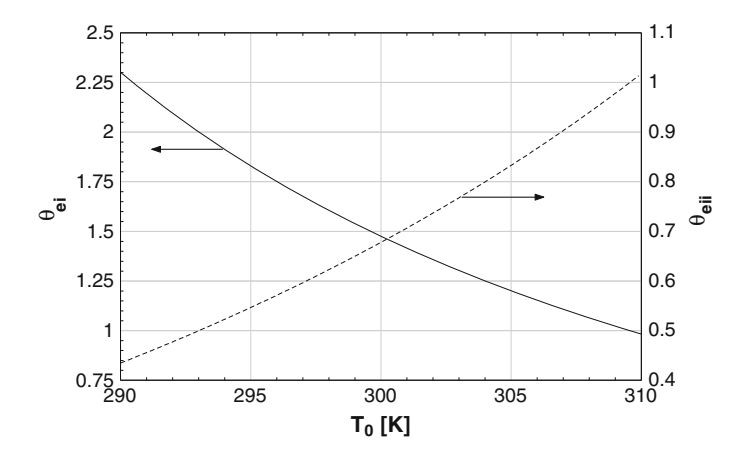


Fig. 4.8 Effects of ambient temperature on the exergoenvironmental impact index and the exergoenvironmental impact improvement

DEARS and the surrounding and as this temperature difference decreases the heat losses occurring from the DEARS to the surrounding decreases. The decrease in the value of the exergoenvironmental impact index indicates that with the increase in ambient temperature the DEARS becomes more environmentally friendly. On the other hand, the increasing exergoenvironmental impact improvement factor indicates that with increasing ambient temperature, the environmental appropriateness of the DEARS increases due to lower heat driven losses occurring from the system to the environment.

The last two exergoenvironmental parameters studies are the exergetic stability factor and the exergetic sustainability index and the effects of the increase in ambient temperature are shown in Fig. 4.9. The exergetic stability factor and the exergetic sustainability index are observed to increase from 0.05 to 0.32 and 0.02 to 0.32, respectively, with increasing ambient temperature from 290 to 310 K. Understanding these parameters is crucial as they indicate how stable and sustainable the system is from an exergoenvironment perspective. The increasing behavior of these parameters with increasing ambient temperature indicates that the system becomes more stable and sustainable with the increase in the temperature. This extra stability and sustainability are gained due to the lower heat losses occurring from the DEARS to the surrounding because of the lower temperature difference between the surrounding and the double effect absorption refrigeration system. The ambient temperature analysis reiterates the importance of performing exergy analysis, as the results show that the energy parameters are not affected by the ambient temperature; however, the exergetic parameters are greatly affected by the variation in ambient temperature.

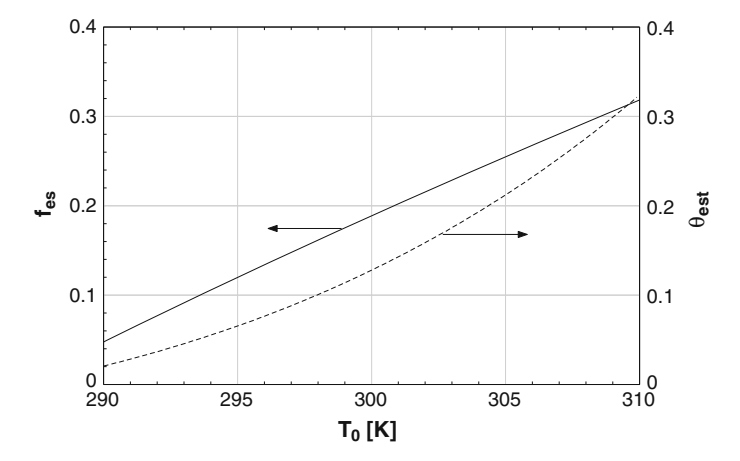


Fig. 4.9 Effects of ambient temperature on the exergetic stability and the exergetic sustainability index

Optimization

Table 4.2 presents the constraints associated with the optimization study of the double effect absorption refrigeration system. The first optimization study maximizes the exergetic COP and minimizes the exergetic cooling cost. The results obtained from the first optimization study are presented in Fig. 4.10. For optimization study, a built-in Nelder-Mead simplex algorithm routine in the engineering equation solver software is used. The Nelder-Mead simplex algorithm makes use of N + 1 test points (where N represents the degrees of freedom), which is called a simplex. For example, a two-dimensional problem uses a triangle as its simplex. The algorithm evaluates every single point of the simplex, and the objective function is found at each of the points. The worst point in the simplex is then thrown out and a new point is found by reflecting away from the worst point about the axis formed by the other test points. The process is repeated several times until one of the stopping criteria are met, and then the objective function of the best point is taken to be the optimum. The first optimization study reveals that the highest exergetic COP obtained is 1.0 and the lowest cooling cost obtained is 112.5 \$/kW for the given constraints. It is worth noting that although all the points

Parameter	Minimum value	Maximum value	
\dot{O}_{σ}	130 kW	170 kW	
T_0	290 K	310 K	
<i>x</i> ₃	0.45	0.55	
ν.	0.2	0.3	

Table 4.2 Constraints associated with the optimization study of the DEARS

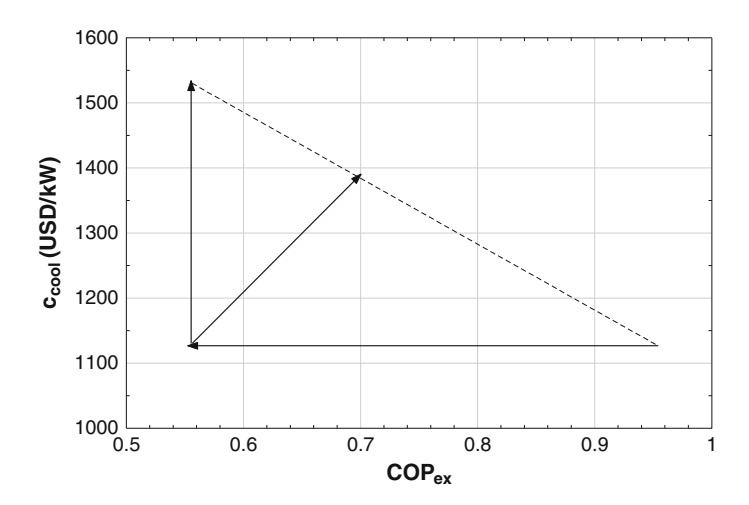


Fig. 4.10 Multi-objective optimization of the DEARS (exergetic COP versus exergetic cooling cost)

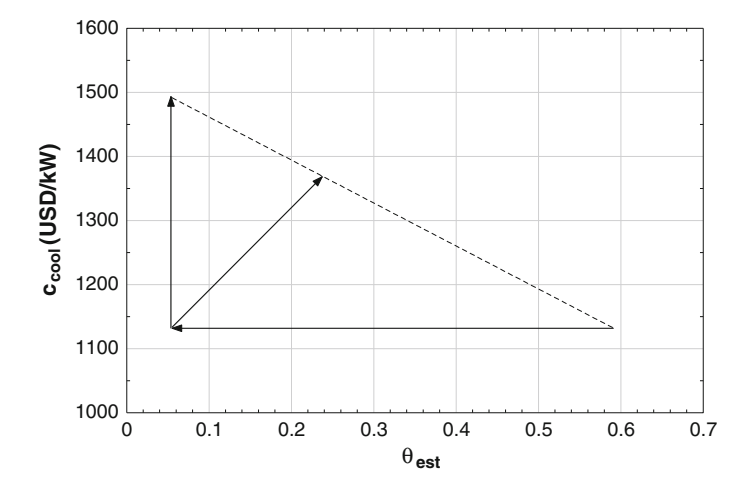


Fig. 4.11 Multi-objective optimization of the DEARS (exergetic sustainability index versus exergetic cooling cost)

on the Pareto front are considered optimum, traditionally LINMAP is used to obtain the most desirable optimized points. LINMAP helps to find an imaginary point at which all the objective functions have their respective optimum location irrespective of other objective functions. The best exergetic COP and exergetic cooling cost obtained on this basis are 0.70 and 1390.4 \$/kW, respectively. The results obtained from the second optimization study, maximizing exergetic sustainability index and minimizing the exergetic cost of cooling are presented in Fig. 4.11. The values obtained using LINMAP for exergetic sustainability index and exergetic cost of refrigeration are 0.24 and 1371.8 \$/kW, respectively.

4.8 Closing Remarks

The use of a double effect absorption refrigeration system provides an additional advantage in terms of energy, environment, and sustainability as compared to the use of a single effect absorption refrigeration system. Detailed energy, exergy, exergoeconomic, and exergoenvironmental analyses of the double effect absorption refrigeration system are presented in this chapter. Finally, a comprehensive example of the double effect absorption refrigeration system is presented, which shows how each thermophysical property can be found at each state point.

Chapter 5 Triple Effect Absorption Refrigeration System

5.1 Introduction

Absorption refrigeration systems have received renewed attention from researchers in the area of sustainable energy technologies because they use low-grade heat (renewable, process or waste heat) in a more environmentally benign manner. Thus, they are an attractive alternative to the conventional vapor-compression refrigeration system. An absorption refrigeration system provides a cooling effect using waste heat or solar heat and minimal power compared to a conventional refrigeration system where electrical power input is necessary to drive the system. Although an absorption refrigeration system has the capability to provide environmental-friendly cooling. One criticism is that its coefficient of performance is considerably smaller than the conventional refrigeration system. The introduction of a triple effect absorption refrigeration system (TEARS) presents better energy recovery as compared to the double effect absorption refrigeration system to show that the absorption refrigeration system an attractive alternative to the conventional refrigeration system from a performance perspective.

The present chapter discusses the basic operation of the TEARS in conjunction with its energy and exergy analyses. First, the working principle of the TEARS is explained in detail to help the reader understand how it works. Second, modeling studies for energy, exergy, exergoenvironmental, exergoeconomic, and optimization are offered for analysis, performance assessment and evaluation. Lastly, an in-depth illustrative example is provided to make sure that the reader understands how individual equations are employed to obtain thermophysical properties at each state point and acquire overall energy and exergy flow values.

5.2 System Description

The triple effect absorption refrigeration system is asophisticated form of the double effect absorption refrigeration system as shown in Fig. 5.1. In the TEARS, a strong solution of ammonia-water leaving the absorber at state 1 enters the pump in a saturated liquid phase. In the pump, the pressure of the strong solution increases before it leaves at state 2. The strong solution at state 2 then divides into two streams of states 17 and 19. The stream at state 19 enters the low temperature heat exchanger, where it gains heat from the fluid returning from the generators to leave at state 3 at relatively higher temperature. This strong solution at state 3 then divides into two streams of states 20 and 21. The strong solution at state 20 enters the medium temperature heat exchanger where it extracts heat from the streams returning from the generators to leave at state 24 at relatively higher temperature. This strong solution at state 24 then divides into two streams of states 25 and 26. The strong solution at state 25 enters the high temperature heat exchanger where it extracts heat from the streams returning from the high temperature generator to leave at state 29 at relatively higher temperature to enter the high temperature generator. In the high temperature generator, heat is supplied from the external 3333 source to increase the temperature of the strong ammonia-water solution above its boiling point. Boiling helps to separate ammonia from the mixture because ammonia boils at moderately lower temperature than water. The ammonia vapor is then extracted from the high temperature generator at state 31, and the remaining weak ammonia-water solution is extracted at state 30. The ammonia vapor extracted at state 31 then enters the medium temperature generator where it acts as a heat source. In the medium temperature generator, strong solution enters at state 26

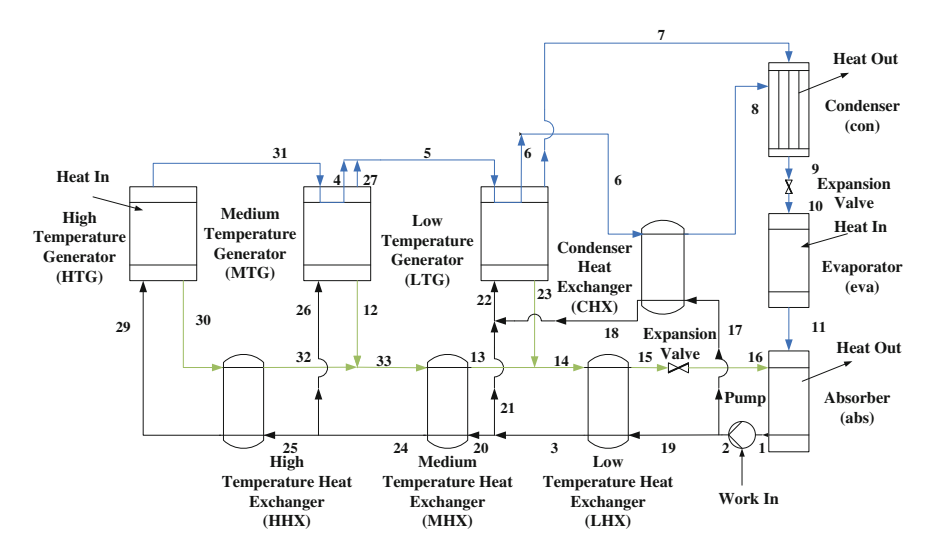


Fig. 5.1 Schematic of the TEARS

where it gains heat from the ammonia vapor entering at state 31. The heat supplied to the medium temperature generator helps to separate ammonia from the strong solution that leaves the medium temperature generator at state 27. The remaining weak solution in the medium temperature generator is then extracted at state 12. After releasing heat in the medium temperature generator, ammonia vapor leaves at state 4 to combine with the stream from state 27 before entering the low temperature generator at state 5. In the low temperature generator, strong solution enters at state 22 and gains heat from the ammonia vapor entering at state 5. The heat supplied to the low temperature generator helps to separate ammonia from the strong solution that leaves the low temperature generator at state 7. The remaining weak solution in the low temperature generator is then extracted at state 23. After releasing heat, ammonia vapor leaves the low temperature generator at state 6 to enter the condenser heat exchanger. In the condenser heat exchanger, the strong solution entering at state 17 gains heat from the ammonia stream and leaves at a relatively higher temperature at state 18. The ammonia refrigerant leaves the condenser heat exchanger at state 8 to enter the condenser. The strong solution exiting the condenser heat exchanger at state 18 mixes with the strong solution from state 21 to leave at state 22. The ammonia refrigerant streams release heat to the surrounding in the condenser to leave as a relatively cooler refrigerant at state 9. This ammonia refrigerant at state 9 then passes through the refrigerant expansion valve where its pressure suddenly drops and leaves as a cooled ammonia refrigerant at state 10. The ammonia refrigerant at state 10 enters the evaporator and gains heat from the surrounding before leaving at a relatively higher temperature at state 11. The weak solution exiting the high temperature generator at state 30 passes through the high temperature heat exchanger where it rejects heat to the incoming strong solution to leave at state 32. The weak solution at state 32 mixes with the weak solution returning from the medium temperature generator at state 12 to leave at state 33. The weak solution at state 33 then enters the medium temperature heat exchanger where it rejects heat and leaves at a relatively cooler temperature at state 13. The weak solution at state 13 mixes with the weak solution returning from the low temperature generator at state 23 to leave at state 14. The weak solution at state 14 then enters the low temperature heat exchanger where it rejects heat and leaves at a relatively cooler temperature at state 15. The weak solution at state 15 enters the weak solution expansion valve where its pressure drops before it enters the absorber at state 16. The weak solution at state 16 and ammonia refrigerant at state 11 then mix in the absorber while rejecting heat to the environment to leave the absorber as a strong solution in saturated liquid phase at state 1.

5.3 Energy and Exergy Analyses

This section provides energy and exergy balance equations for all components of the TEARS.

• Pump:

The mass balance equation across the pump can be written as

$$\dot{m}_1 = \dot{m}_2 = \dot{m}_p \tag{5.1}$$

where \dot{m} represents the mass flow rate.

The specific power consumed by the pump can be calculated using

$$w_{\rm p} = \frac{v(P_2 - P_1)}{\eta_{\rm p}} \tag{5.2}$$

where w, v, P, and η represent specific power, specific volume, pressure, and efficiency, respectively.

The total power consumed by the pump is defined as

$$\dot{W}_{\rm p} = \dot{m}_{\rm p} w_{\rm p} \tag{5.3}$$

where \dot{W} represents total power consumed by the pump.

The overall energy balance equation of the pump is given as

$$(\dot{m}h)_1 + \dot{W}_p = (\dot{m}h)_2 \tag{5.4}$$

where h represents specific enthalpy of the state.

The specific exergies at states 1 and 2 are defined as

$$ex_1 = (h_1 - h_0) - T_0(s_1 - s_0)$$
(5.5)

$$ex_2 = (h_2 - h_0) - T_0(s_2 - s_0)$$
(5.6)

where ex, T, and s represent specific exergy, temperature, and specific entropy. The overall exergy balance equation of the pump is given as

$$\dot{m}_1 e x_1 + \dot{W}_p = \dot{m}_2 e x_2 + \dot{E} x_{\text{dest},p}$$
 (5.7)

where $\dot{E}x_{dest,p}$ represents the exergy destruction rate in the pump.

• Low temperature heat exchanger:

The mass balance equations for the low temperature heat exchanger can be written as

$$\dot{m}_3 = \dot{m}_{19} \tag{5.8}$$

$$\dot{m}_{15} = \dot{m}_{14} \text{ and}$$
 (5.9)

$$\dot{m}_{17} + \dot{m}_{19} = \dot{m}_2 \tag{5.10}$$

The energy balance equation is given as

$$\dot{m}_{19}h_{19} + \dot{m}_{14}h_{14} = \dot{m}_3h_3 + \dot{m}_{15}h_{15} \tag{5.11}$$

The specific exergies at states 3, 14, 15, and 19 are defined as

$$ex_3 = (h_3 - h_0) - T_0(s_3 - s_0)$$
(5.12)

$$ex_{14} = (h_{14} - h_0) - T_0(s_{14} - s_0)$$
(5.13)

$$ex_{15} = (h_{15} - h_0) - T_0(s_{15} - s_0)$$
(5.14)

$$ex_{19} = (h_{19} - h_0) - T_0(s_{19} - s_0)$$
(5.15)

The exergy balance equation is given as

$$\dot{m}_{19} = x_{19} + \dot{m}_{14} = x_{14} = \dot{m}_{3} = x_{3} + \dot{m}_{15} = x_{15} + \dot{E}x_{\text{dest,LHX}}$$
 (5.16)

where $\dot{E}x_{dest,LHX}$ represents the exergy destruction rate in the low temperature heat exchanger.

• Medium temperature heat exchanger:

The mass balance equations for the medium temperature heat exchanger can be written as

$$\dot{m}_{24} = \dot{m}_{20} \tag{5.17}$$

$$\dot{m}_{13} = \dot{m}_{33} \text{ and}$$
 (5.18)

$$\dot{m}_{20} + \dot{m}_{21} = \dot{m}_3 \tag{5.19}$$

The energy balance equation is given as

$$\dot{m}_{20}h_{20} + \dot{m}_{33}h_{33} = \dot{m}_{13}h_{13} + \dot{m}_{24}h_{24} \tag{5.20}$$

The specific exergies at states 13, 20, 24, and 33 are defined as

$$ex_{13} = (h_{13} - h_0) - T_0(s_{13} - s_0)$$
(5.21)

$$ex_{20} = (h_{20} - h_0) - T_0(s_{20} - s_0)$$
(5.22)

$$ex_{24} = (h_{24} - h_0) - T_0(s_{24} - s_0)$$
(5.23)

$$ex_{33} = (h_{33} - h_0) - T_0(s_{33} - s_0)$$
(5.24)

The exergy balance equation is given as

$$\dot{m}_{20} ex_{20} + \dot{m}_{33} ex_{33} = \dot{m}_{13} ex_{13} + \dot{m}_{24} ex_{24} + \dot{E}x_{\text{dest,MHX}}$$
 (5.25)

where $\dot{E}x_{dest,MHX}$ represents the exergy destruction rate in the medium temperature heat exchanger.

• High temperature heat exchanger:

The mass balance equations for the high temperature heat exchanger can be written as

$$\dot{m}_{29} = \dot{m}_{25} \tag{5.26}$$

$$\dot{m}_{32} = \dot{m}_{30} \text{ and}$$
 (5.27)

$$\dot{m}_{25} + \dot{m}_{26} = \dot{m}_{24} \tag{5.28}$$

The energy balance equation is given as

$$\dot{m}_{25}h_{25} + \dot{m}_{30}h_{30} = \dot{m}_{29}h_{29} + \dot{m}_{32}h_{32} \tag{5.29}$$

The specific exergies at states 25, 29, 30, and 32 are defined as

$$ex_{25} = (h_{25} - h_0) - T_0(s_{25} - s_0)$$
(5.30)

$$ex_{29} = (h_{29} - h_0) - T_0(s_{29} - s_0)$$
 (5.31)

$$ex_{30} = (h_{30} - h_0) - T_0(s_{30} - s_0)$$
(5.32)

$$ex_{32} = (h_{32} - h_0) - T_0(s_{32} - s_0)$$
 (5.33)

The exergy balance equation is given as

$$\dot{m}_{25} ex_{25} + \dot{m}_{30} ex_{30} = \dot{m}_{29} ex_{29} + \dot{m}_{32} ex_{32} + \dot{E}x_{\text{dest,HHX}}$$
 (5.34)

where $\dot{E}x_{dest,HHX}$ represents the exergy destruction rate in the high temperature heat exchanger.

• High temperature generator:

The mass balance equations of the high temperature generator can be written as

$$\dot{m}_{29} = \dot{m}_{30} + \dot{m}_{31} \tag{5.35}$$

and

$$\dot{m}_{29}x_{29} = \dot{m}_{30}x_{30} + \dot{m}_{31}x_{31} \tag{5.36}$$

where x represents the solution concentration.

The energy balance equation is given as

$$\dot{m}_{29}h_{29} + \dot{Q}_{\rm HTG} = \dot{m}_{30}h_{30} + \dot{m}_{31}h_{31}$$
 (5.37)

where $\dot{Q}_{\rm HTG}$ represents the rate of heat required by the high temperature generator. The specific exergy at state 31 is defined as

$$ex_{31} = (h_{31} - h_0) - T_0(s_{31} - s_0)$$
(5.38)

The thermal exergy rate supplied to the high temperature generator is defined as

$$\dot{\mathbf{E}}\mathbf{x}_{th,HTG} = \left(1 - \frac{T_0}{T_{HTG}}\right)\dot{\mathbf{Q}}_{HTG} \tag{5.39}$$

where $\dot{E}x_{th,HTG}$ represents the thermal exergy rate of the high temperature generator. The exergy balance equation of the high temperature generator is given as

$$\dot{m}_{29} ex_{29} + \dot{E}x_{th,HTG} = \dot{m}_{30} ex_{30} + \dot{m}_{31} ex_{31} + \dot{E}x_{dest,HTG}$$
 (5.40)

where $\dot{E}x_{\text{dest,HTG}}$ represents the rate of exergy destruction in the high temperature generator.

• Medium temperature generator:

The mass balance equations of the medium temperature generator can be written as

$$\dot{m}_{26} = \dot{m}_{12} + \dot{m}_{27} \tag{5.41}$$

$$\dot{m}_{26}x_{26} = \dot{m}_{12}x_{12} + \dot{m}_{27}x_{27} \tag{5.42}$$

$$\dot{m}_4 = \dot{m}_{31} \text{ and}$$
 (5.43)

$$\dot{m}_5 = \dot{m}_4 + \dot{m}_{27} \tag{5.44}$$

where x represents the solution concentration.

The energy balance equation is given as

$$\dot{m}_{26}h_{26} + \dot{m}_{31}h_{31} = \dot{m}_4h_4 + \dot{m}_{12}h_{12} + \dot{m}_{27}h_{27}$$
 and (5.45)

$$\dot{m}_{31}h_{31} = \dot{m}_4h_4 + \dot{Q}_{\text{MTG}} \tag{5.46}$$

where \dot{Q}_{MTG} represents the rate of heat required by the medium temperature generator.

The specific exergies at states 4, 5, 12, 26, and 27 are defined as

$$ex_4 = (h_4 - h_0) - T_0(s_4 - s_0)$$
(5.47)

$$ex_5 = (h_5 - h_0) - T_0(s_5 - s_0)$$
(5.48)

$$ex_{12} = (h_{12} - h_0) - T_0(s_{12} - s_0)$$
(5.49)

$$ex_{26} = (h_{26} - h_0) - T_0(s_{26} - s_0)$$
(5.50)

$$ex_{27} = (h_{27} - h_0) - T_0(s_{27} - s_0)$$
(5.51)

The thermal exergy rate supplied to the medium temperature generator is defined as

$$\dot{\mathbf{E}}\mathbf{x}_{\text{th,MTG}} = \left(1 - \frac{T_0}{T_{\text{MTG}}}\right) \dot{Q}_{\text{MTG}} \tag{5.52}$$

where $\dot{E}x_{\text{th},MTG}$ represents the thermal exergy rate of the medium temperature generator.

The exergy balance equation is given as

$$\dot{m}_{26} \text{ex}_{26} + \dot{\text{E}}_{\text{xth,MTG}} = \dot{m}_{12} \text{ex}_{12} + \dot{m}_{27} \text{ex}_{27} + \dot{\text{E}}_{\text{xdest,MTG}}$$
 (5.53)

where $\dot{E}x_{dest,MTG}$ represents the rate of exergy destruction in the medium temperature generator.

• Low temperature generator:

The mass balance equations of the low temperature generator can be written as

$$\dot{m}_{22} = \dot{m}_7 + \dot{m}_{23} \tag{5.54}$$

$$\dot{m}_{22}x_{22} = \dot{m}_7x_7 + \dot{m}_{23}x_{23} \tag{5.55}$$

$$\dot{m}_6 = \dot{m}_5 \text{ and} \tag{5.56}$$

$$\dot{m}_{22} = \dot{m}_{18} + \dot{m}_{21} \tag{5.57}$$

where x represents the solution concentration.

The energy balance equation is given as

$$\dot{m}_5 h_5 + \dot{m}_{22} h_{22} = \dot{m}_6 h_6 + \dot{m}_7 h_7 + \dot{m}_{23} h_{23} \text{ and}$$
 (5.58)

$$\dot{m}_5 h_5 = \dot{m}_6 h_6 + \dot{Q}_{\rm LTG} \tag{5.59}$$

where \dot{Q}_{LTG} represents the rate of heat required by the low temperature generator. The specific exergies at states 6, 7, 22, and 23 are defined as

$$ex_6 = (h_6 - h_0) - T_0(s_6 - s_0) (5.60)$$

$$ex_7 = (h_7 - h_0) - T_0(s_7 - s_0)$$
(5.61)

$$ex_{22} = (h_{22} - h_0) - T_0(s_{22} - s_0)$$
(5.62)

$$ex_{23} = (h_{23} - h_0) - T_0(s_{23} - s_0)$$
(5.63)

The thermal exergy rate supplied to the low temperature generator is defined as

$$\dot{\mathbf{E}}\mathbf{x}_{th,LTG} = \left(1 - \frac{T_0}{T_{LTG}}\right)\dot{Q}_{LTG} \tag{5.64}$$

where $\dot{E}x_{th,LTG}$ represents the thermal exergy rate of the low temperature generator. The exergy balance equation of the low temperature generator is given as

$$\dot{m}_{22} ex_{22} + \dot{E}x_{th,LTG} = \dot{m}_7 ex_7 + \dot{m}_{23} ex_{23} + \dot{E}x_{dest,LTG}$$
 (5.65)

where $\dot{E}x_{\text{dest},LTG}$ represents the rate of exergy destruction.

· Condenser:

The mass balance equation for the condenser is defined as

$$\dot{m}_9 = \dot{m}_7 + \dot{m}_8 \tag{5.66}$$

The energy balance equation of the condenser is given as

$$\dot{m}_7 h_7 + \dot{m}_8 h_8 = \dot{m}_9 h_9 + \dot{Q}_c \tag{5.67}$$

where \dot{Q}_c represents the rate of heat rejected by the refrigerant flowing through the condenser.

The specific exergy at state 9 is defined as

$$ex_9 = (h_9 - h_0) - T_0(s_9 - s_0)$$
(5.68)

The thermal exergy rate released by the condenser is calculated as

$$\dot{\mathbf{E}}\mathbf{x}_{\text{th,c}} = \left(1 - \frac{T_0}{T_c}\right)\dot{Q}_c \tag{5.69}$$

where $\dot{E}x_{\text{th,c}}$ represents the thermal exergy rate of the condenser.

The exergy balance equation of the condenser is given as

$$\dot{m}_7 \text{ex}_7 + \dot{m}_8 \text{ex}_8 = \dot{m}_9 \text{ex}_9 + \dot{E}x_{\text{th.c}} + \dot{E}x_{\text{dest.c}}$$
 (5.70)

where Ex_{dest,c} represents the rate of exergy destruction in the condenser.

Evaporator:

The mass balance equation for the evaporator is written as

$$\dot{m}_{11} = \dot{m}_{10} \tag{5.71}$$

The energy balance equation of the evaporator is given as

$$\dot{m}_{10}h_{10} + \dot{Q}_{\rm e} = \dot{m}_{11}h_{11} \tag{5.72}$$

where \dot{Q}_{e} represents the rate of heat gained by the refrigerant flowing through the evaporator.

The specific exergies at states 10 and 11 are defined as

$$ex_{10} = (h_{10} - h_0) - T_0(s_{10} - s_0)$$
(5.73)

$$ex_{11} = (h_{11} - h_0) - T_0(s_{11} - s_0)$$
(5.74)

The thermal exergy rate supplied to the evaporator is calculated as

$$\dot{\mathbf{E}}\mathbf{x}_{\text{th,e}} = \left(1 - \frac{T_0}{T_e}\right)\dot{Q}_e \tag{5.75}$$

where $\dot{E}x_{th,e}$ represents the thermal exergy rate of the evaporator.

The exergy balance equation of the evaporator is given as

$$\dot{m}_{10}$$
ex₁₀ + \dot{E} x_{th,e} = \dot{m}_{11} ex₁₁ + \dot{E} x_{dest,e} (5.76)

where Exdest,e represents the rate of exergy destruction in the evaporator.

Absorber:

The mass balance equation for the absorber is written as

$$\dot{m}_{11} + \dot{m}_{16} = \dot{m}_1 \tag{5.77}$$

The energy balance equation of the absorber is given as

$$\dot{m}_{11}h_{11} + \dot{m}_{16}h_{16} = \dot{m}_1h_1 + \dot{Q}_a \tag{5.78}$$

where $\dot{Q}_{\rm a}$ represents the rate of heat rejected by the absorber.

The specific exergy at state 16 is defined as

$$ex_{16} = (h_{16} - h_0) - T_0(s_{16} - s_0)$$
(5.79)

The thermal exergy rate released by the absorber is calculated as

$$\dot{\mathbf{E}}\mathbf{x}_{\text{th,a}} = \left(1 - \frac{T_0}{T_a}\right) \dot{Q}_a \tag{5.80}$$

where $\dot{E}x_{th,a}$ represents the thermal exergy rate of the absorber.

The exergy balance equation of the absorber is given as

$$\dot{m}_{11} e x_{11} + \dot{m}_{16} e x_{16} = \dot{m}_{1} e x_{1} + \dot{E} x_{th a} + \dot{E} x_{dest a}$$
 (5.81)

where $\dot{E}x_{dest,a}$ represents the rate of exergy destruction in the absorber.

• Expansion valve (for weak solution)

The mass balance equation for the weak solution expansion valve is written as

$$\dot{m}_{16} = \dot{m}_{15} \tag{5.82}$$

The energy balance equation of the weak solution expansion valve is defined as

$$\dot{m}_{16}h_{16} = \dot{m}_{15}h_{15} \tag{5.83}$$

The exergy balance equation of the weak solution expansion valve is given as

$$\dot{m}_{16} \text{ex}_{16} = \dot{m}_{15} \text{ex}_{15} + \dot{E}_{x_{\text{dest,evw}}}$$
 (5.84)

where $\dot{E}x_{dest,evw}$ represents the rate of exergy destruction in the weak solution expansion valve.

• Expansion valve (for refrigerant):

The mass balance equation for the refrigerant expansion valve is written as

$$\dot{m}_9 = \dot{m}_{10} \tag{5.85}$$

The energy balance equation of the refrigerant expansion valve is defined as

$$\dot{m}_{10}h_{10} = \dot{m}_9 h_9 \tag{5.86}$$

The exergy balance equation of the refrigerant expansion valve is given as

$$\dot{m}_9 \text{ex}_9 = \dot{m}_{10} \text{ex}_{10} + \dot{\text{E}}_{\text{xdest.evr}}$$
 (5.87)

where $\dot{E}x_{dest,evr}$ represents the rate of exergy destruction in the refrigerant expansion valve.

• Condenser heat exchanger:

The mass balance equations for the condenser heat exchanger can be written as

$$\dot{m}_8 = \dot{m}_6 \tag{5.88}$$

$$\dot{m}_{18} = \dot{m}_{17} \tag{5.89}$$

The energy balance equation is given as

$$\dot{m}_{17}h_{17} + \dot{m}_6h_6 = \dot{m}_8h_8 + \dot{m}_{18}h_{18} \tag{5.90}$$

The specific exergies at states 17 and 18 are defined as

$$ex_{17} = (h_{17} - h_0) - T_0(s_{17} - s_0)$$
(5.91)

$$ex_{18} = (h_{18} - h_0) - T_0(s_{18} - s_0)$$
(5.92)

The exergy balance equation is given as

$$\dot{m}_{17} e x_{17} + \dot{m}_6 e x_6 = \dot{m}_{18} e x_{18} + \dot{m}_8 e x_8 + \dot{E} x_{\text{dest,CHX}}$$
 (5.93)

where $\dot{E}x_{dest,CHX}$ represents the exergy destruction rate in the condenser heat exchanger.

The performance of an absorption refrigeration system is measured using the coefficient of performance. The energetic and exergetic coefficients of performance of the absorption refrigeration system are defined as

$$COP_{en} = \frac{\dot{Q}_e}{\dot{Q}_{HTG} + \dot{W}_p} \tag{5.94}$$

$$COP_{ex} = \frac{\dot{E}x_{th,e}}{\dot{E}x_{th,HTG} + \dot{W}_{p}}$$
 (5.95)

where COPen and COPex represent energetic COP and exergetic COP, respectively.

5.4 Exergoeconomic Analysis

This section presents the exergoeconomic analysis equations of the triple effect absorption refrigeration system. The overall exergoeconomic equation of the TEARS is written as

$$\dot{Z}_{\rm eq} + \dot{C}_{\rm OPM} = \dot{C}_{\rm Cool} \tag{5.96}$$

where \dot{Z}_{eq} , \dot{C}_{OPM} , and \dot{C}_{Cool} represent the cost associated with the equipment, operation and maintenance, and cooling, respectively.

The cost linked to the equipment is defined as

$$\dot{Z}_{eq} = \dot{C}_a + \dot{C}_g + \dot{C}_c + \dot{C}_e + \dot{C}_P + \dot{C}_{ev}$$
 (5.97)

where \dot{C}_a , \dot{C}_g , \dot{C}_c , \dot{C}_e , \dot{C}_P , and \dot{C}_{ev} represent the cost of absorber, generator, condenser, evaporator, pump, and expansion valve, respectively.

However, the total equipment cost can also be calculated on the basis of a relation between the equipment cost and cooling load as provided below.

$$\dot{Z}_{\text{eq}}(\$) = 1144.3(\dot{Q}_{\text{cool}})^{0.67}$$
 (5.98)

The cost associated with the operation and maintenance is defined as

$$\dot{C}_{\text{OPM}} = c_{\text{OPM}} \times \dot{E}_{X\text{OPM}} \tag{5.99}$$

where c_{OPM} and $\dot{\text{E}}x_{\text{OPM}}$ represent operation and maintenance cost, and exergy carried by the energy consumed in terms of heat and power, respectively. The operation and maintenance is also assumed to be 3 % of the total equipment cost.

The cost related to the cooling produced is defined as

$$\dot{C}_{\text{Cool}} = c_{\text{Cool}} \times \dot{E}_{x_{\text{Cool}}} \tag{5.101}$$

where c_{Cool} and $\dot{\text{Ex}}_{\text{Cool}}$ represent the cost of cooling produced and the exergy related to the cooling produced, respectively.

Thus the above equation can be written as

$$(c \times \dot{E}x)_{OPM} + \dot{Z}_{eq} = (c \times \dot{E}x)_{Cool}$$
 (5.102)

The cost of cooling can then be calculated by rearranging the equation mentioned above and rewriting it as

$$c_{\text{Cool}} = \frac{(c \times \dot{\text{Ex}})_{\text{OPM}} + \dot{Z}_{\text{eq}}}{\dot{\text{Ex}}_{\text{cool}}}$$
(5.103)

5.5 Exergoenvironmental Analysis

In this section, we present an exergoenvironmental formulation for the TEARS.

The total exergy supplied to the triple effect absorption refrigeration system is calculated as

$$\dot{\mathbf{E}}\mathbf{x}_{in} = \dot{\mathbf{E}}\mathbf{x}_{th,HTG} + \dot{W}_{p} + \dot{\mathbf{E}}\mathbf{x}_{th,e} \tag{5.104}$$

The total exergy rejected by the triple effect absorption refrigeration system is defined as

$$\dot{\mathbf{E}}\mathbf{x}_{\text{out}} = \dot{\mathbf{E}}\mathbf{x}_{\text{th,a}} + \dot{\mathbf{E}}\mathbf{x}_{\text{th,c}} \tag{5.105}$$

The total exergy destroyed by the TEARS is calculated as

$$\dot{E}x_{dest,tot} = \dot{E}x_{in} - \dot{E}x_{out} \tag{5.106}$$

The exergoenvironmental impact factor is defined as

$$f_{\rm ei} = \frac{\dot{E}x_{\rm dest,tot}}{\dot{E}x_{\rm in}} \tag{5.107}$$

where f_{ei} represents exergoenvironmental impact factor.

This exergoenvironmental impact coefficient is calculated as

$$C_{ei} = \frac{1}{\text{COP}_{ex}} \tag{5.108}$$

where C_{ei} represents the exergoenvironmental impact coefficient.

The exergoenvironmental impact index is calculated as

$$\theta_{\rm ei} = f_{\rm ei} \times C_{\rm ei} \tag{5.109}$$

where θ_{ei} represents exergoenvironmental impact index.

The exergoenvironmental impact improvement is defined as

$$\theta_{\rm eii} = \frac{1}{\theta_{\rm ei}} \tag{5.110}$$

where θ_{eii} represents exergoenvironmental impact improvement.

The exergetic stability factor is defined as

$$f_{\rm es} = \frac{\dot{E}x_{\rm out}}{\dot{E}x_{\rm out} + \dot{E}x_{\rm dest,tot}}$$
 (5.111)

where $f_{\rm es}$ represents exergetic stability factor. The exergetic sustainability index is defined as

$$\theta_{\rm est} = f_{\rm es} \times \theta_{\rm eii} \tag{5.112}$$

where $\theta_{\rm est}$ represents exergetic sustainability index.

5.6 Optimization

Typical optimization problems for the absorption refrigeration system is maximizing exergetic COP and exergetic sustainability index and minimizing the cost of cooling. The three objective functions used for this study are presented in Eqs. 5.95, 5.103, and 5.112. The constraints for this study are ambient in temperature, the heat supplied to the high temperature generator, the concentration of the strong solution, and the concentration of the weak solution.

5.7 Illustrative Example

Consider a triple effect absorption refrigeration system using ammonia—water as a working fluid as shown in Fig. 5.1. The strong ammonia—water solution with a mass flow rate of 1 kg/s enters the pump as a saturated liquid with concentration and pressure of 0.5 and 200 kPa, respectively. The strong solution leaves the pump at 700 kPa with a temperature difference of 0.4 °C. The heat is supplied to the high temperature generator at a rate of 260 kW which helps to boil the strong solution, and the weak solution and ammonia refrigerant vapor leave the generator with concentrations of 0.3 and 0.999, respectively. Assume temperature differences of 30 and 3 °C, respectively, between the inlet and exit of the heat exchangers and the condenser heat exchanger. Take the temperature difference between the strong solution entering the generators and weak solution exiting the generators to be 15 °C. Consider the condenser load and evaporator temperature to be 200 kW and -1.3.5 °C, respectively. Take ambient temperature and pressure to be 291.2 K and 100 kPa. Calculate the following:

- (a) the rate of cooling provided by the evaporator,
- (b) the power consumed by the pump,
- (c) the rate of heat rejected by the absorber,

- (d) energetic and exergetic COPs,
- (e) the exergy destruction rate in each component,
- (f) the exergetic cost of cooling, and
- (g) exergoenvironmental parameters as discussed earlier in the chapter.

In addition, perform the following parametric studies to investigate

- (a) effects of the high temperature generator load on the cooling load, the cost of cooling, and the energy and exergy COPs,
- (b) effects of the strong solution concentration on the cooling load, the cost of cooling, and the energy and exergy COPs, and
- (c) effects of the ambient temperature on the energy and exergy COPs, and all the exergoenvironmental parameters.

For parametric studies, use the same data ranges as defined below.

Also, perform an optimization study for the following scenarios:

- (a) maximizing the exergetic COP and minimizing the exergetic cost of cooling, and
- (b) maximizing the exergetic sustainability index and minimizing the exergetic cost of cooling.

For an optimization study consider the high temperature generator heat load, strong solution concentration, weak solution concentration, and ambient temperature to be constraints with limits of 260–300 kW, 0.5–0.6, 0.2–0.3, and 280–300 K, respectively.

Solution

The pump inlet properties are considered by assuming pressure, strong solution concentration, and quality.

$$\left. \begin{array}{l} P_1 = 200 \; \mathrm{kPa} \\ x_1 = 0.5 \\ \mathrm{Qu}_1 = 0.00 \end{array} \right\} \qquad \begin{array}{l} h_1 = -180.1 \; \mathrm{kJ/kg} \\ s_1 = 0.04011 \; \mathrm{kJ/kg} \; \mathrm{K} \\ v_1 = 0.001199 \; \mathrm{m^3/kg} \\ T_1 = 286.5 \; \mathrm{K} \end{array}$$

It is assumed that at the exit of the pump, the temperature would be $0.4~^{\circ}\mathrm{C}$ higher than the inlet temperature.

$$P_2 = 700 \text{ kPa} x_2 = 0.5 T_2 = 286.9 \text{ K}$$

$$h_2 = -178.1 \text{ kJ/kg} s_2 = 0.04481 \text{ kJ/kg K} \dot{m}_1 = 1 \text{ kg/s} \dot{m}_2 = \dot{m}_1$$

The power required to increase the pressure of 1 kg/s of strong solution from 200 to 700 kPa for the pump is calculated as

$$\dot{W}_{\rm p} = 1((-178.1) - (-180.1)) = 1.971 \; {\rm kW}$$

The ambient conditions for calculating specific exergy at each point are calculated as

$$\left. \begin{array}{l} P_0 = 100 \text{ kPa} \\ T_0 = 291.2 \text{ K} \\ x_0 = 0.5 \end{array} \right\} \begin{array}{l} h_0 = -150 \text{ kJ/kg} \\ s_0 = 0.1034 \text{ kJ/kg K} \end{array}$$

These ambient conditions can only be used for strong solution streams.

$$\dot{E}x_1 = 1((-180.1 - (-150)) - 291.2(0.04011 - 0.1034)) = -11.62 \text{ kW}$$

 $\dot{E}x_2 = 1((-178.1 - (-150)) - 291.2(0.04481 - 0.1034)) = -11.01 \text{ kW}$

The exergy destruction in the pump is then calculated as

$$-11.62 + 1.971 = -11.01 + \dot{E}x_{dest,p}$$

 $\dot{E}x_{dest,p} = 1.368 \text{ kW}$

It is assumed that 20 % of the flow rate from the pump is supplied to the condenser heat exchanger and the remaining 80 % is supplied to the low temperature heat exchanger. The temperature, pressure, and strong solution concentration remains the same in states 2, 17, and 19.

$$h_{17} = h_2$$
 $s_{17} = s_2$
 $T_{17} = T_2$
 $h_{19} = h_2$
 $s_{19} = s_2$
 $T_{19} = T_2$

The mass balance equations for the low temperature heat exchanger are written as

$$\dot{m}_{17} = 0.2(\dot{m}_2) = 0.2 \text{ kg/s}$$

 $\dot{m}_{19} = 0.8(\dot{m}_2) = 0.8 \text{ kg/s}$
 $\dot{m}_3 = \dot{m}_{19}$
 $\dot{m}_{15} = \dot{m}_{14}$

The temperature of the strong solution leaving the low temperature heat exchanger is assumed to be 15 °C higher than the inlet temperature.

The energy balance equation of the low temperature heat exchanger can be written as

$$\dot{m}_{19}h_{19} + \dot{m}_{14}h_{14} = \dot{m}_3h_3 + \dot{m}_{15}h_{15}$$

$$0.8(-178.1) + 0.7139(-56.38) = 0.8(-110.8) + 0.7139(h_{15})$$

$$h_{15} = -131.9 \text{ kJ/kg}$$

On the basis of specific enthalpy at state 15 obtained using the energy balance equation and knowing the pressure and weak solution concentration at this state, one can find the specific entropy and temperature at state 15 as follows:

$$\left. \begin{array}{l}
 P_{15} = P_2 \\
 x_{15} = 0.3 \\
 h_{15} = -131.9
 \end{array} \right\} T_{15} = 286.5 \text{ K} \\
 s_{15} = 0.1247 \text{ kJ/kg K}$$

The rate of heat transfer occurring inside the low temperature heat exchanger can be calculated as

$$\dot{m}_{19}h_{19} + \dot{Q}_{LHX} = \dot{m}_3h_3$$
 $0.8(-178.1) + \dot{Q}_{LHX} = 0.8(-110.8)$
 $\dot{Q}_{LHX} = 53.88 \text{ kW}$

The thermal exergy rate of the low temperature heat exchanger can be calculated as

$$\dot{E}x_{th,LHX} = \left(1 - \frac{291.2}{301.9}\right)$$
53.88 = 1.913 kW

The exergy flow rates in states 3, 14, 15, and 19 of the low temperature heat exchanger are calculated as

$$\begin{split} \dot{E}x_3 &= 0.8((-110.8 - (-150)) - 291.2(0.2736 - 0.1034)) = -8.234 \text{ kW} \\ \dot{E}x_{19} &= 0.8((-178.1 - (-150)) - 291.2(0.04481 - 0.1034)) = -8.811 \text{ kW} \\ \dot{E}x_{14} &= 0.7139((-56.38 - (-102.5)) - 291.2(0.3804 - 0.1906)) = -6.548 \text{ kW} \\ \dot{E}x_{15} &= 0.7139((-131.9 - (-102.5)) - 291.2(0.1247 - 0.1906)) = -7.272 \text{ kW} \end{split}$$

The exergy destruction rate in the low temperature heat exchanger is calculated as

$$-8.811 + 1.913 = -8.234 + \dot{E}x_{dest,LHX}$$

$$\dot{E}x_{dest,LHX} = 1.336 \text{ kW}$$

It is assumed that 20 % of the flow rate from the state 3 is supplied to the state 21 and the remaining 80 % is supplied to the medium temperature heat exchanger at state 20. The temperature, pressure, and strong solution concentration remains same in states 3, 20, and 21.

$$h_{20} = h_3$$
 $s_{20} = s_3$
 $T_{20} = T_3$
 $h_{21} = h_3$
 $s_{21} = s_3$
 $T_{21} = T_3$

The mass balance equations for the medium temperature heat exchanger are written as

$$\dot{m}_{21} = 0.2(\dot{m}_3) = 0.16 \text{ kg/s}$$
 $\dot{m}_{20} = 0.8(\dot{m}_3) = 0.64 \text{ kg/s}$
 $\dot{m}_{24} = \dot{m}_{20}$
 $\dot{m}_{13} = \dot{m}_{33}$

The temperature of the strong solution leaving the medium temperature heat exchanger is assumed to be $15\ ^{\circ}\text{C}$ higher than the inlet temperature.

$$\left. \begin{array}{l}
P_{24} = P_2 \\
x_{24} = x_2 \\
T_{24} = T_{20} + 15
\end{array} \right\} \begin{array}{l}
h_{24} = -43.42 \text{ kJ/kg} \\
s_{24} = 0.4913 \text{ kJ/kg K}
\end{array}$$

The energy balance equation of the medium temperature heat exchanger can be written as

$$\begin{split} \dot{m}_{20}h_{20} + \dot{m}_{33}h_{33} &= \dot{m}_{13}h_{13} + \dot{m}_{24}h_{24} \\ 0.64(-110.8) + 0.4569(-29.75) &= 0.4569(h_{13}) + 0.64(-43.42) \\ h_{13} &= -124.1 \text{ kJ/kg} \end{split}$$

Using the specific enthalpy at state 13 calculated with the energy balance equation and knowing the pressure and weak solution concentration, one can find the specific entropy and temperature at state 13 as follows:

$$\left. \begin{array}{l}
 P_{13} = P_2 \\
 x_{13} = x_{33} \\
 h_{13} = -124.1
 \end{array} \right\} T_{13} = 288.3 \text{ K} \\
 s_{13} = 0.1517 \text{ kJ/kg K}$$

The rate of heat transfer taking place inside the medium temperature heat exchanger can be calculated as

$$\dot{m}_{20}h_{20} + \dot{Q}_{\text{MHX}} = \dot{m}_{24}h_{24}$$

$$0.64(-110.8) + \dot{Q}_{\text{MHX}} = 0.64(-43.42)$$
 $\dot{Q}_{\text{MHX}} = 43.11 \text{ kW}$

The thermal exergy rate of the medium temperature heat exchanger can be calculated as

$$\dot{E}x_{th,MHX} = \left(1 - \frac{291.2}{316.9}\right) 43.11 = 3.498 \text{ kW}$$

The exergy flow rates in states 13, 20, 24, and 33 of the medium temperature heat exchanger are calculated as

$$\begin{split} \dot{E}x_{20} &= 0.64((-110.8 - (-150)) - 291.2(0.2736 - 0.1034)) = -6.587 \text{ kW} \\ \dot{E}x_{24} &= 0.64((-43.42 - (-150)) - 291.2(0.4913 - 0.1034)) = -4.057 \text{ kW} \\ \dot{E}x_{13} &= 0.4569((-124.1 - (-102.5)) - 291.2(0.1517 - 0.1906)) = -4.7 \text{ kW} \\ \dot{E}x_{33} &= 0.4569((-29.75 - (-102.5)) - 291.2(0.4671 - 0.1906)) = -3.562 \text{ kW} \end{split}$$

The exergy destruction rate in the medium temperature heat exchanger is calculated as

$$-6.587 + 3.498 = -4.057 + \dot{E}x_{dest,MHX}$$

 $\dot{E}x_{dest,MHX} = 0.9672 \text{ kW}$

It is assumed that 20 % of the flow rate from the state 24 is supplied to the state 26 and remaining 80 % is supplied to the high temperature heat exchanger at state 25. The temperature, pressure, and strong solution concentration remains same as states 24, 25, and 26.

$$h_{25} = h_{24}$$
 $s_{25} = s_{24}$
 $T_{25} = T_{24}$
 $h_{26} = h_{24}$
 $s_{26} = s_{24}$
 $T_{26} = T_{24}$

The mass balance equations for the high temperature heat exchanger are written as

$$\dot{m}_{26} = 0.2(\dot{m}_{24}) = 0.128 \text{ kg/s}$$
 $\dot{m}_{25} = 0.8(\dot{m}_{24}) = 0.512 \text{ kg/s}$
 $\dot{m}_{29} = \dot{m}_{25}$
 $\dot{m}_{32} = \dot{m}_{30}$

The temperature of the strong solution leaving the high temperature heat exchanger is assumed to be 15 °C higher than the inlet temperature.

$$\left. \begin{array}{l}
 P_{29} = P_2 \\
 x_{29} = x_2 \\
 T_{29} = T_{25} + 15
 \end{array} \right\} h_{29} = 145.7 \text{ kJ/kg K}$$

The energy balance equation of the high temperature heat exchanger can be written as

$$\dot{m}_{25}h_{25} + \dot{m}_{30}h_{30} = \dot{m}_{29}h_{29} + \dot{m}_{32}h_{32}$$

$$0.512(-43.42) + 0.3655(195.5) = 0.3655(h_{32}) + 0.512(145.7)$$

$$h_{32} = -69.51 \text{ kJ/kg}$$

On the basis of specific enthalpy at state 32 calculated using the energy balance equation and knowing the pressure and weak solution concentration one can find the specific entropy and temperature at state 32 as follows:

$$\left. \begin{array}{l}
 P_{32} = P_2 \\
 x_{32} = x_{30} \\
 h_{32} = -69.51
 \end{array} \right\} \begin{array}{l}
 T_{32} = 300.9 \text{ K} \\
 s_{32} = 0.337 \text{ kJ/kg K}
 \end{array}$$

The rate of heat transfer taking place inside the high temperature heat exchanger can be calculated as

$$\dot{m}_{25}h_{25} + \dot{Q}_{HHX} = \dot{m}_{29}h_{29}$$
 $0.512(-43.42) + \dot{Q}_{HHX} = 0.512(145.7)$
 $\dot{Q}_{HHX} = 96.85 \text{ kW}$

The thermal exergy rate of the high temperature heat exchanger can be calculated as

$$\dot{E}x_{th,HHX} = \left(1 - \frac{291.2}{331.9}\right)96.85 = 11.88 \ kW$$

The exergy flow rates in states 25, 29, 30, and 32 of the high temperature heat exchanger are calculated as

$$\begin{split} &\dot{E}x_{25} = 0.512((-43.42 - (-150)) - 291.2(0.4913 - 0.1034)) = -3.245 \text{ kW} \\ &\dot{E}x_{29} = 0.512((145.7 - (-150)) - 291.2(1.068 - 0.1034)) = 7.653 \text{ kW} \\ &\dot{E}x_{30} = 0.3655((195.5 - (-102.5)) - 291.2(1.138 - 0.1906)) = 8.025 \text{ kW} \\ &\dot{E}x_{32} = 0.3655((-69.51 - (-102.5)) - 291.2(0.337 - 0.1906)) = -3.532 \text{ kW} \end{split}$$

The exergy destruction rate in the high temperature heat exchanger is calculated as

$$-3.245 + 11.88 = 7.653 + \dot{E}x_{dest,HHX}$$

 $\dot{E}x_{dest,HHX} = 0.983 \text{ kW}$

The mass balance equations of the high temperature generator are written as

$$\dot{m}_{29} = \dot{m}_{30} + \dot{m}_{31}
\dot{m}_{29}x_{29} = \dot{m}_{30}x_{30} + \dot{m}_{31}x_{31}
0.512 = \dot{m}_{30} + \dot{m}_{31}
0.512(0.5) = \dot{m}_{30}(0.3) + \dot{m}_{31}(0.999)$$

Solving two equations simultaneously gives us

$$\dot{m}_{30} = 0.3655 \text{ kg/s}$$
 and $\dot{m}_{31} = 0.1465 \text{ kg/s}$

The temperature at state 30 is assumed to be 30 °C higher than the temperature at state 29.

$$\left. \begin{array}{l}
 P_{30} = P_2 \\
 x_{30} = 0.3 \\
 T_{30} = T_{29} + 30
 \end{array} \right\} h_{30} = 195.5 \text{ kJ/kg K}$$

The specific enthalpy at state 31 is calculated using energy balance equation of the high temperature generator as defined below.

$$\dot{m}_{29}h_{29} + \dot{Q}_{\rm HTG} = \dot{m}_{30}h_{30} + \dot{m}_{31}h_{31}$$

$$0.512(145.7) + 260 = 0.3655(195.5) + 0.1465h_{31}$$
 $h_{31} = 1796 \text{ kJ/kg}$

Using specific enthalpy at state 31 and knowing pressure and concentration in this state, we can find the temperature and specific entropy at state 31 as follows:

$$\left. \begin{array}{l}
 P_{31} = P_2 \\
 x_{31} = 0.999 \\
 h_{31} = 1796 \text{ kJ/kg}
 \end{array} \right\} \begin{array}{l}
 T_{31} = 494.9 \text{ K} \\
 s_{31} = 5.815 \text{ kJ/kg K}
 \end{array}$$

$$\dot{E}x_{31} = 0.1465[(1796 - 87.15) - 291.2(5.815 - 0.2708)] = 13.88 \text{ kW}$$

The thermal exergy rate of the high temperature generator can be calculated using average temperature as

$$\dot{E}x_{th,HTG} = \left(1 - \frac{291.2}{396.3}\right)260 = 68.93 \text{ kW}$$

Using the thermal exergy rate and rate of exergy at each state, we can find the total exergy destruction rate of the high temperature generator as

$$7.653 + 68.93 = 8.025 + 13.88 + \dot{E}x_{dest,HTG}$$

 $\dot{E}x_{dest,HTG} = 54.68 \text{ kW}$

The mass flow rates of the different streams entering and leaving the medium temperature generator are calculated as

$$\dot{m}_4 = \dot{m}_{31} = 0.1465 \text{ kg/s}$$

$$\dot{m}_{26} = \dot{m}_{12} + \dot{m}_{27}$$

$$\dot{m}_{26}x_{26} = \dot{m}_{12}x_{12} + \dot{m}_{27}x_{27}$$

$$0.128 = \dot{m}_{12} + \dot{m}_{27}$$

$$0.128(0.5) = \dot{m}_{12}(0.3) + \dot{m}_{27}(0.999)$$

Solving two equations simultaneously gives us

$$\dot{m}_{12} = 0.09138 \text{ kg/s}$$
 and $\dot{m}_{27} = 0.03662 \text{ kg}$

The temperature at state 12 is assumed to be 30 $^{\circ}$ C higher than the temperature at state 26.

$$\left. \begin{array}{l} P_{12} = P_2 \\ x_{12} = x_{30} \\ T_{12} = T_{26} + 30 \end{array} \right\} h_{12} = 129.3 \text{ kJ/kg} \\ s_{12} = 0.9516 \text{ kJ/kg K}$$

It is assumed that ammonia vapor at state 27 leaves with the same temperature as that of state 12.

$$P_{27} = P_2 x_{27} = x_{31} T_{27} = T_{12}$$

$$h_{27} = 1435 \text{ kJ/kg K} s_{27} = 4.95 \text{ kJ/kg K}$$

The specific enthalpy at state 4 is calculated using energy balance equation of the medium temperature generator as defined below.

$$\dot{m}_{26}h_{26} + \dot{m}_{31}h_{31} = \dot{m}_{12}h_{12} + \dot{m}_{27}h_{27} + \dot{m}_4h_4$$

$$0.128(-43.42) + 0.1465(1796) = 0.09138(129.3) + 0.03662(1435) + 0.1465h_4$$

$$h_4 = 1319 \text{ kJ/kg}$$

Using specific enthalpy at state 4 and knowing pressure and concentration in this state, we can find the temperature and specific entropy at state 4 as follows:

$$P_4 = P_2 x_4 = x_{31} h_4 = 1319 \text{ kJ/kg}$$

$$T_4 = 301.3 \text{ K} s_4 = 4.591 \text{ kJ/kg K}$$

The exergy rate at states 26, 12, 4, and 27 are found as

$$\begin{split} &\dot{E}x_4 = 0.1465[(1319-87.15)-291.2(4.591-0.2708)] = -3.832 \text{ kW} \\ &\dot{E}x_{26} = 0.128((-43.42-(-150))-291.2(0.4913-0.1034)) = -0.8113 \text{ kW} \\ &\dot{E}x_{12} = 0.09138((129.3-(-102.5))-291.2(0.9516-0.1906)) = 0.9281 \text{ kW} \\ &\dot{E}x_{27} = 0.03662((1435-(87.15))-291.2(4.95-0.2708)) = -0.5249 \text{ kW} \end{split}$$

Using the rate of exergy at each state, we can find the total exergy destruction rate of the medium temperature generator as

$$-0.8113 + 13.88 = 0.9281 - 3.832 - 0.5249 + \dot{E}x_{dest,MTG}$$

 $\dot{E}x_{dest,MTG} = 16.5 \text{ kW}$

The ammonia vapor leaving the medium temperature generator at states 4 and 27 are combined to leave at state 5

$$\dot{m}_5 = \dot{m}_4 + \dot{m}_{27} = 0.1465 + 0.03662 = 0.1831 \text{ kg/s}$$
 $\dot{m}_5 h_5 = \dot{m}_4 h_4 + \dot{m}_{27} h_{27}$
 $0.1831 h_5 = 0.1465(1319) + 0.03662(1435)$
 $h_5 = 1342 \text{ kJ/kg}$

Using the specific enthalpy at state 5 and knowing the concentration and pressure, we can find the temperature and specific enthalpy at state 5 as follows:

$$\left. \begin{array}{l}
 P_5 = P_2 \\
 x_5 = x_{31} \\
 h_5 = 1342 \text{ kJ/kg}
 \end{array} \right\} T_5 = 309.5 \text{ K} \\
 s_5 = 4.667 \text{ kJ/kg K}$$

The exergy rate at state 5 can then be calculated as

$$\dot{E}x_5 = 0.1831[(1342 - 87.15) - 291.2(4.667 - 0.2708)] = -4.57 \text{ kW}$$

The mass flow rates of the different streams entering and leaving the low temperature generator are calculated as

$$\dot{m}_6 = \dot{m}_5 = 0.1831 \text{ kg/s}$$

$$\dot{m}_{22} = \dot{m}_{23} + \dot{m}_7$$

$$\dot{m}_{22}x_{22} = \dot{m}_{23}x_{23} + \dot{m}_7x_7$$

$$0.36 = \dot{m}_{23} + \dot{m}_7$$

$$0.36(0.5) = \dot{m}_{23}(0.3) + \dot{m}_7(0.999)$$

Solving two equations simultaneously gives us

$$\dot{m}_{23} = 0.257 \text{ kg/s}$$
 and $\dot{m}_7 = 0.103 \text{ kg/s}$
 $\dot{m}_{22} = \dot{m}_{21} + \dot{m}_{18} = 0.16 + 0.2 = 0.36 \text{ kg/s}$
 $\dot{m}_{22}h_{22} = \dot{m}_{21}h_{21} + \dot{m}_8h_8$
 $0.36h_{22} = 0.16(-110.8) + 0.2(0.2736)$
 $h_{22} = -110.8 \text{ kJ/kg}$

Using the specific enthalpy at state 22 and knowing the concentration and pressure, we can find the temperature and specific enthalpy at state 22 as follows:

$$\left. \begin{array}{l} P_{22} = P_2 \\ x_{22} = x_{29} \\ h_{22} = -110.8 \; \mathrm{kJ/kg} \end{array} \right\} \begin{array}{l} T_{22} = 301.9 \; \mathrm{K} \\ s_{22} = 0.2736 \; \mathrm{kJ/kg} \; \mathrm{K} \end{array}$$

The temperature at state 23 is assumed to be 30 $^{\circ}$ C higher than the temperature at state 22.

$$P_{23} = P_2 x_{23} = x_{30} T_{23} = T_{22} + 30$$

$$\begin{cases} h_{23} = 64.01 \text{ kJ/kg} \\ s_{23} = 0.7593 \text{ kJ/kg K} \end{cases}$$

It is assumed that ammonia vapor at state 7 leaves with the same temperature as that of state 23.

$$P_7 = P_2$$

 $x_7 = x_{31}$
 $T_7 = T_{23}$
 $h_7 = 1399 \text{ kJ/kg}$
 $s_7 = 4.842 \text{ kJ/kg K}$

The specific enthalpy at state 6 is calculated using energy balance equation of the low temperature generator as defined below.

$$\dot{m}_{22}h_{22} + \dot{m}_5h_5 = \dot{m}_{23}h_{23} + \dot{m}_7h_7 + \dot{m}_6h_6$$

 $0.36(-110.8) + 0.1831(1342) = 0.257(64.01) + 0.103(1399) + 0.1831h_6$
 $h_6 = 248 \text{ kJ/kg}$

Using specific enthalpy at state 6 and knowing pressure and concentration in this state, we can find the temperature and specific entropy at state 6 as follows:

$$\left. \begin{array}{l} P_6 = P_2 \\ x_6 = x_{31} \\ h_6 = 248 \text{ kJ/kg} \end{array} \right\} \begin{array}{l} T_6 = 287 \text{ K} \\ s_6 = 0.881 \text{ kJ/kg K} \end{array}$$

The exergy rate at states 22, 23, 6, and 7 are found as

$$\begin{split} &\dot{E}x_6 = 0.1831[(248 - 87.15) - 291.2(0.881 - 0.2708)] = -3.09 \text{ kW} \\ &\dot{E}x_7 = 0.103((1399 - (87.15)) - 291.2(4.842 - 0.2708)) = -2.019 \text{ kW} \\ &\dot{E}x_{22} = 0.36((-110.8 - (-150)) - 291.2(0.2736 - 0.1034)) = -3.705 \text{ kW} \\ &\dot{E}x_{23} = 0.257((64.01 - (-102.5)) - 291.2(0.7593 - 0.1906)) = 0.2287 \text{ kW} \end{split}$$

The rate of heat transfer taking place inside the low temperature generator can be calculated as

$$\dot{m}_5 h_5 + \dot{Q}_{LTG} = \dot{m}_6 h_6$$

$$0.1831(1342) + \dot{Q}_{LTG} = 0.1831(248)$$
 $\dot{Q}_{LTG} = 200.4 \text{ kW}$

The thermal exergy rate of the low temperature generator can be calculated as

$$\dot{E}x_{th,LTG} = \left(1 - \frac{291.2}{309.5}\right) 200.4 = 11.85 \text{ kW}$$

The total exergy destruction rate of the low temperature generator can be calculated as

$$-4.57 = -3.09 + 11.85 + \dot{E}x_{dest,LTG}$$

 $\dot{E}x_{dest,LTG} = 10.37 \text{ kW}$

The mass flow rates of the different streams entering and leaving the condenser heat exchanger are calculated as

$$\dot{m}_{18} = \dot{m}_{17} = 0.2 \text{ kg/s}$$

 $\dot{m}_8 = \dot{m}_6 = 0.1831 \text{ kg/s}$

The temperature at state 18 is assumed to be 30 $^{\circ}$ C higher than the temperature at state 17.

$$P_{18} = P_2 x_{18} = x_{29} T_{18} = T_{17} + 30$$

$$\begin{cases} h_{18} = -110.8 \text{ kJ/kg K} \\ s_{18} = 0.2736 \text{ kJ/kg K} \end{cases}$$

The specific enthalpy at state 8 is calculated using energy balance equation of the condenser heat exchanger as defined below.

$$\dot{m}_{17}h_{17} + \dot{m}_6h_6 = \dot{m}_8h_8 + \dot{m}_{18}h_{18}$$

$$0.2(-178.1) + 0.1831(248) = 0.1831(h_8) + 0.2(-110.8)$$
 $h_8 = 174.4 \text{ kJ/kg}$

Using specific enthalpy at state 8 and knowing pressure and concentration in this state, we can find the temperature and specific entropy at state 8 as follows:

$$\left. \begin{array}{l} P_8 = P_2 \\ x_8 = x_{31} \\ h_8 = 174.4 \; \text{kJ/kg} \end{array} \right\} \begin{array}{l} T_8 = 287 \; \text{K} \\ s_8 = 0.6258 \; \text{kJ/kg K} \end{array}$$

The rate of exergy at states 8 and 17 are calculated as

$$\begin{split} \dot{E}x_8 &= 0.1831[(174.4 - 87.15) - 291.2(0.6258 - 0.2708)] = -2.951 \text{ kW} \\ \dot{E}x_{17} &= 0.2((-178.1 - (-150)) - 291.2(0.04481 - 0.1034)) = -2.203 \text{ kW} \end{split}$$

The rate of heat transfer taking place inside the condenser heat exchanger can be calculated as

$$\dot{m}_{17}h_{17} + \dot{Q}_{\text{CHX}} = \dot{m}_{18}h_{18}$$

$$0.2(-178.1) + \dot{Q}_{\text{CHX}} = 0.2(-110.8)$$
 $\dot{Q}_{\text{CHX}} = 13.47 \text{ kW}$

The thermal exergy rate of the condenser heat exchanger can be calculated as

$$\dot{E}x_{th,CHX} = \left(1 - \frac{291.2}{301.9}\right) 13.47 = 0.4782 \; kW$$

The total exergy destruction rate of the condenser heat exchanger can be calculated as

$$-2.203 + 0.4782 = -2.059 + \dot{E}x_{dest,CHX}$$

 $\dot{E}x_{dest,CHX} = 0.3341 \text{ kW}$

The mass balance equation of the condenser can be written as

$$\dot{m}_7 + \dot{m}_8 = \dot{m}_9$$

 $\dot{m}_9 = 0.103 + 0.181 = 0.2861$

The energy balance equation of the condenser capable of rejecting 200 kW of heat is written as

$$\dot{m}_8h_8 + \dot{m}_7h_7 = \dot{m}_9h_9 + \dot{Q}_c$$

The equation mentioned above is used to calculate the specific enthalpy at state 9 as

$$0.1831(174.4) + 0.103(1399) = 0.2861h_9 + 200$$

 $h_9 = -83.85 \text{ kJ/kg}$

$$P_9 = P_2 x_9 = x_{31} h_9 = -83.85 \text{ kJ/kg}$$

$$T_9 = 254.8 \text{ K} s_9 = -0.3034 \text{ kJ/kg K}$$

$$\dot{E}x_9 = 0.2861[(-83.85 - 87.15) - 291.2(-0.3034 - 0.2708)] = -1.086 \text{ kW}$$

The thermal exergy rate of the condenser can be calculated as

$$\dot{E}x_{th,c} = \bigg(1 - \frac{291.2}{254.8}\bigg)200 = -28.58 \; kW$$

Using the exergy rate at each state and thermal rate of exergy, we can find the exergy destruction rate in the condenser as

$$-2.019 - 2.951 = -1.086 - 28.58 + \dot{E}x_{dest,c}$$

 $\dot{E}x_{dest,c} = 24.69 \text{ kW}$

The mass balance equation of the refrigerant expansion valve is written as

$$\dot{m}_{10} = \dot{m}_9 = 0.2861 \text{ kg/s}$$

$$h_{10} = h_9$$

$$P_{10} = P_1$$

$$x_{10} = x_{31}$$

$$T_{10} = 254.3 \text{ K}$$

$$s_{10} = -0.3004 \text{ kJ/kg K}$$

$$\begin{split} \dot{E}x_{10} &= 0.2861[(-83.85 - 87.15) + 291.2(-0.3004 - 0.2708)] = -1.341 \text{ kW} \\ &- 1.086 = -1.341 + \dot{E}x_{dest,evr} \end{split}$$

$$\dot{\mathbf{E}}\mathbf{x}_{\text{dest.evr}} = 2.43 \text{ kW}$$

The mass balance equation of the evaporator is written as

$$\dot{m}_{11} = \dot{m}_{10} = 0.2861 \text{ kg/s}$$

It is assumed that the refrigerant leaves the evaporator at a temperature of 259.7 K.

$$\begin{cases}
P_{11} = P_9 \\
x_{11} = x_{31} \\
T_{11} = 259.7 \text{ K}
\end{cases}
\begin{cases}
h_{11} = 1251 \text{ kJ/kg} \\
s_{11} = 4.922 \text{ kJ/kg K}
\end{cases}$$

The energy balance equation to calculate the cooling load is defined as

$$\dot{m}_{10}h_{10} + \dot{Q}_{e} = \dot{m}_{11}h_{11}$$

$$0.2861(-83.85) + \dot{Q}_{e} = 0.2861(1251)$$

$$\dot{\mathbf{Q}}_{e} = 381.9 \text{ kW}$$

$$\dot{E}x_{11} = 0.2861[(1251 - 87.15) + 291.2(4.922 - 0.2708)] = -54.52 \text{ kW}$$

The thermal exergy rate of the evaporator is calculated as

$$\begin{split} \dot{E}x_{th,e} &= \left| \left(1 - \frac{291.2}{257} \right) 381.9 \right| = 44.87 \text{ kW} \\ &- 1.341 + 44.87 = -54.52 + \dot{E}x_{dest,e} \\ \dot{E}x_{dest,e} &= 98.05 \text{ kW} \end{split}$$

The mass balance equation of the weak solution expansion valve is written as

$$\dot{m}_{16} = \dot{m}_{15} = 0.7139 \text{ kg/s}$$

$$h_{16} = h_{15}$$

$$P_{16} = P_1$$

$$x_{16} = x_{30}$$

$$T_{16} = 286.7 \text{ K}$$

$$s_{16} = 0.1266 \text{ kJ/kg K}$$

$$\dot{E}x_{16} = 0.7139((-131.9 - (-102.5)) + 291.2(0.1266 - 0.1906)) = -7.676 \text{ kW}$$

The exergy destruction rate of the weak solution expansion valve is calculated as

$$-7.272 = -7.676 + \dot{E}x_{dest,evs}$$

$$\dot{E}x_{dest\ evs} = 0.4\ kW$$

The mass balance equation of the absorber is written as

$$\dot{m}_1 = \dot{m}_{11} + \dot{m}_{16}$$

The amount of heat rejected by the absorber is calculated using formula

$$\begin{split} \dot{m}_1 h_1 + \dot{Q}_{\rm a} &= \dot{m}_{11} h_{11} + \dot{m}_{16} h_{16} \\ 1(-180.1) + \dot{Q}_{\rm a} &= 0.2861(1251) + 0.7139(-131.9) \\ \dot{Q}_{\rm a} &= 443.9 \; {\rm kW} \end{split}$$

The thermal exergy rate of the absorber is calculated as

$$\dot{E}x_{th,a} = \left(1 - \frac{291.2}{259.7}\right) 443.9 = 53.94 \text{ kW}$$

The rate of exergy destructed by the absorber is calculated as

$$-54.52 - 7.676 = -11.62 - 53.94 + \dot{E}x_{dest,a}$$

 $\dot{E}x_{dest,a} = 3.353 \text{ kW}$

The weak solution at states 12 and 32 mixes to leave at state 33. The mass balance equation of this mixing process is written as

$$\dot{m}_{33} = \dot{m}_{12} + \dot{m}_{32}$$

 $\dot{m}_{33} = 0.09138 + 0.3655 = 0.4569 \text{ kg/s}$

The energy balance equation of the mixing process is written as

$$\begin{aligned} \dot{m}_{33}h_{33} &= \dot{m}_{12}h_{12} + \dot{m}_{32}h_{32} \\ 0.4569h_{33} &= 0.09138(129.3) + 0.3655(-69.51) \\ h_{33} &= -29.75 \text{ kJ/kg} \\ h_{33} &= -29.75 \text{ kJ/kg} \\ P_{33} &= P_2 \\ x_{33} &= x_{30} \end{aligned} \right\} \begin{cases} T_{33} &= 310.2 \text{ K} \\ s_{33} &= 0.4671 \text{ kJ/kg K} \end{cases}$$

$$\dot{E}x_{33} = 0.4569((-29.75 - (-102.5)) + 291.2(0.4671 - 0.1906)) = -3.562 \text{ kW}$$

The weak solution at states 13 and 23 mixes to leave at state 14. The mass balance equation of this mixing process is written as

$$\dot{m}_{14} = \dot{m}_{13} + \dot{m}_{23}$$

 $\dot{m}_{14} = 0.4569 + 0.257 = 0.7139 \text{ kg/s}$

The energy balance equation of the mixing process is written as

$$\begin{aligned} \dot{m}_{14}h_{14} &= \dot{m}_{13}h_{13} + \dot{m}_{23}h_{23} \\ 0.7139h_{14} &= 0.4569(-124.1) + 0.257(64.01) \\ h_{14} &= -56.38 \text{ kJ/kg} \\ h_{14} &= -56.38 \text{ kJ/kg} \\ P_{14} &= P_2 \\ x_{14} &= x_{30} \end{aligned} \right\} \begin{aligned} T_{14} &= 304 \text{ K} \\ s_{14} &= 0.3804 \text{ kJ/kg K} \end{aligned}$$

$$\dot{E}x_{14} = 0.7139((-56.38 - (-102.5)) + 291.2(0.3804 - 0.1906)) = -6.548 \text{ kW}$$

The energy and exergy COPs of the triple effect absorption refrigeration systems are calculated as

$$\begin{split} COP_{en} &= \frac{381.5}{260 + 1.971} = 1.458 \\ COP_{ex} &= \frac{44.87}{68.93 + 1.368} = 0.6329 \end{split}$$

The equipment cost of the TEARS is found using

$$\dot{Z}_{eq}(\$) = 1144.3(381.9)^{0.67} = \$61440$$

The operation and maintenance cost of the TEARS is assumed to be 3 % of the equipment cost

$$\dot{C}_{\text{OPM}} = 0.03(61440) = \$1843$$

The exergetic cost of cooling can then be calculated using equipment cost, cost of operation and maintenance, and the thermal exergy rate of the evaporator as

$$c_{\text{Cool}} = \frac{61440 + 1843}{44.87}$$
 $c_{\text{Cool}} = 1410 \text{ } \text{/kW}$

The total rate of exergy entering the TEARS is calculated as

$$\dot{E}x_{in} = 68.93 + 1.971 + 44.87 = 115.8 \text{ kW}$$

The total rate of exergy exiting the TEARS is calculated as

$$\dot{E}x_{out} = 28.58 + 53.94 = 82.51 \text{ kW}$$

The total rate of exergy destructed by the TEARS is calculated as

$$\dot{E}x_{dest,tot} = 115.8 - 82.51 = 33.26 \text{ kW}$$

The exergoenvironmental impact factor can then be calculated by dividing total exergy destruction rate by total exergy supplied to the TEARS as

$$f_{\rm ei} = \frac{33.26}{115.8} = 0.2873$$

The exergoenvironmental impact coefficient is calculated by taking inverse of the exergetic COP as

$$C_{\rm ei} = \frac{1}{0.6329} = 1.58$$

The exergoenvironmental impact index is found by multiplying exergoenvironmental impact factor by exergoenvironmental impact factor as

$$\theta_{\rm ei} = 0.2873 \times 1.58 = 0.454$$

The exergoenvironmental impact improvement is then found by taking inverse of the exergoenvironmental impact index as

$$\theta_{\rm eii} = \frac{1}{0.454} = 2.203$$

The exergetic stability factor is computed as

$$f_{\rm es} = \frac{82.51}{82.51 + 33.26} = 0.7127$$

The exergetic sustainability index is then calculated by multiplying exergetic stability factor with exergoenvironmental impact improvement as

$$\theta_{\rm est} = 0.7127 \times 2.203 = 1.57$$

Note that the thermophysical properties at each state point of the TEARS are presented in Table 5.1.

Table 5.1 Thermophysical properties at each state point of the TEARS

State point	P (kPa)	T (K)	m (kg/s)	h (kJ/kg)	s (kJ/kg K)
0	100	291.2		-150	0.1034
1	200	286.5	1	-180.1	0.04011
2	700	286.9	1	-178.1	0.04481
3	700	301.9	0.8	-110.8	0.2736
4	700	301.3	0.1465	1319	4.591
5	700	309.5	0.1831	1342	4.667
6	700	287	0.1831	248	0.881
7	700	331.9	0.103	1399	4.842
8	700	287	0.1831	174.4	0.6258
9	700	254.8	0.2861	-83.85	-0.3034
10	200	254.3	0.2861	-83.85	-0.3004
11	200	259.7	0.2861	1251	4.922
12	700	346.9	0.09138	129.3	0.9516
13	700	288.3	0.4569	-124.1	0.1517
14	700	304	0.7139	-56.38	0.3804
15	700	286.5	0.7139	-131.9	0.1247

(continued)

State point	P (kPa)	T (K)	m (kg/s)	h (kJ/kg)	s (kJ/kg K)
16	200	286.7	0.7139	-131.9	0.1266
17	700	286.9	0.2	-178.1	0.04481
18	700	301.9	0.2	-110.8	0.2736
19	700	286.9	0.8	-178.1	0.04481
20	700	301.9	0.64	-110.8	0.2736
21	700	301.9	0.16	-110.8	0.2736
22	700	301.9	0.36	-110.8	0.2736
23	700	331.9	0.257	64.01	0.7593
24	700	316.9	0.64	-43.42	0.4913
25	700	316.9	0.512	-43.42	0.4913
26	700	316.9	0.128	-43.42	0.4913
27	700	346.9	0.03662	1435	4.95
29	700	331.9	0.512	145.7	1.068
30	700	361.9	0.3655	195.5	1.138
31	700	494.9	0.1465	1796	5.815
32	700	300.9	0.3655	-69.51	0.337
33	700	310.2	0.4569	-29.75	0.4671

Table 5.1 (continued)

• Effects of the high temperature generator load

The variation in the rate of energy supplied to the high temperature generator of the triple effect absorption refrigeration system (TEARS) can significantly affect its performance. The impact of variation in high temperature generator heat load on the rate of cooling produced and the cost of cooling are presented in Fig. 5.2. The rate of cooling is observed decrease from 382 to 342 kW with the increase in the high temperature generator load from 260 to 300 kW. The cost of cooling is noted to be increase from 1410 to 1463 USD/kW with the increase in the high temperature generator load. The decreasing behavior of cooling capacity is because the increase in high temperature generator load brings with it an excess amount of energy to the TEARS. With a constant condenser load of 200 kW, this higher load is not able to reflect its benefits in terms of higher cooling capacity. The cooling capacity decreases because the increase in high temperature generator load results in the relatively higher temperature of the ammonia refrigerant exiting the high temperature generator. This relatively higher temperature ammonia refrigerant is then constrained by fixed condenser load when it comes to decreasing its temperature and enters the evaporator at relatively higher temperature. This results in the lower temperature difference between the inlet of the evaporator and the exit of the evaporator and as a consequence of this the heat carrying capacity of the ammonia refrigerant stream decreases. This adverse effect of a rise in the high temperature generator load also reflects on the cost of cooling. The cost of cooling decreases because with the increase in the high temperature generator pushes the cooling

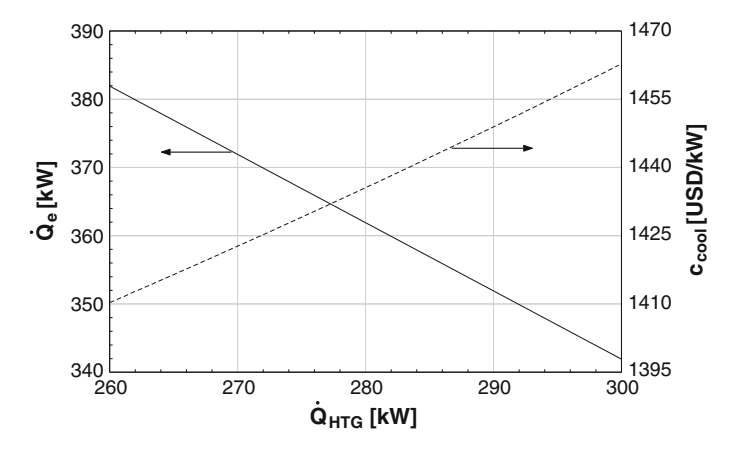


Fig. 5.2 Effects of the high temperature generator load on cooling load and cost of cooling

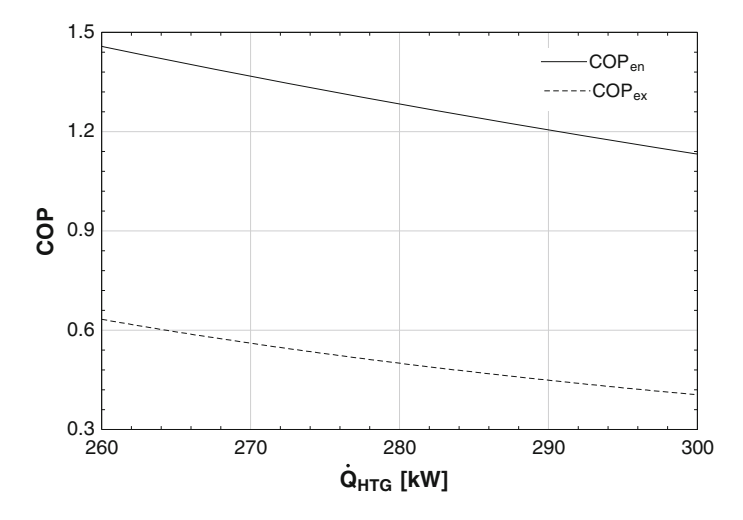


Fig. 5.3 Effects of the high temperature generator load on energy and exergy COPs

capacity downward and as the cooling capacity decreases for the same component size, the cost of cooling increases. Figure 5.3 depicts the effects of the increase in the high temperature generator load on the energy and exergy coefficient of performance. (COPs) of the TEARS. The energy and exergy COPs are observed to be decreasing from 1.46 to 1.13 and 0.63 to 0.41, respectively, with the rise in the high temperature generator load from 260 to 300 kW. This decline in the performance is directly related to the cooling production capacity of the system. As the cooling production capacity decreases with increase in the high temperature generator load

due to the relatively higher temperature ammonia refrigerant entering the evaporator, the energetic and exergetic performance of the system degrades.

• Effects of the strong solution concentration

The strong solution concentration plays a significant role in the performance of the absorption refrigeration system as it determines how ammonia can be vaporized to act as a refrigerant. The effects of the increase in concentration of the strong solution on cooling production rate and cost of cooling are presented in Fig. 5.4. The cooling production rate is noted to increase from 381.9 to 514.8 kW with the increase in the strong solution concentration from 0.5 to 0.6. On the other hand, the cost of cooling is observed to decrease from 1410 to 1278 USD/kW with the rise in the strong solution concentration. This increasing cooling production rate behavior is perceived because the increse in the strong solution concentration results in the higher amount of ammonia being vaporized from the high temperature generator for the fixed generator load of 260 kW. Since ammonia is the refrigerant of the system, the increase in the supply of the refrigerant to the evaporator results in the higher heat carrying capacity from the evaporator. This higher heat carrying capacity of the refrigerant in the evaporator is reflected in terms of the higher cooling production rate from the TEARS. The higher cooling production capacity also helps to decrease the cooling production cost of the system. The cooling production cost includes the equipment cost, operation and maintenance cost, and the thermal exergy rate of the evaporator. As the cooling production rate increases, the thermal exergy rate of the evaporator increases which in turn helps reducing the cooling cost of the TEARS. Figure 5.5 shows the effects of the rise in the strong solution concentration on the energy and exergy COPs of the TEARS. The energy and exergy COPs are noted to increase from 1.46 to 1.96 and 0.63 to 1.66, respectively, with the increase in the strong solution concentration from 0.5 to 0.6. The swelling behavior of both the COPs is because the increase in the strong solution

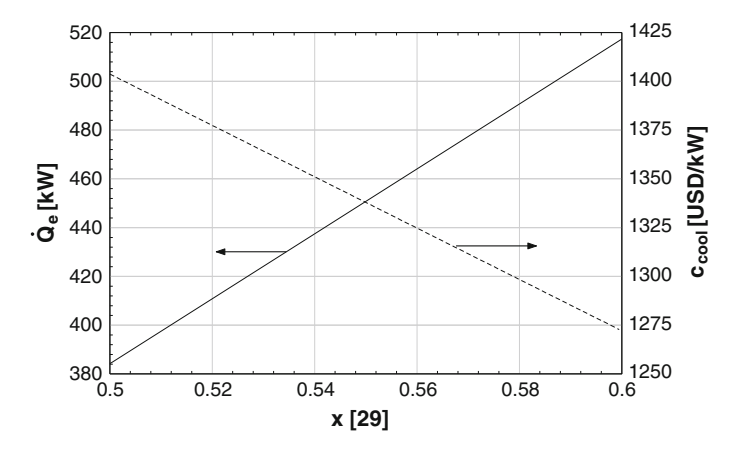


Fig. 5.4 Effects of strong solution concentration on cooling load and cost of cooling

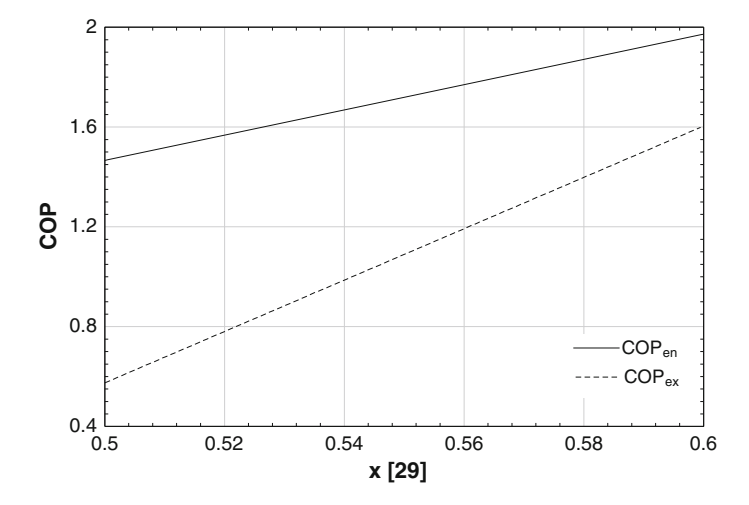


Fig. 5.5 Effects of strong solution concentration on energy and exergy COPs

concentration results in better cooling production rate from the TEARS. The performance of the cooling system is measured in terms of how much cooling a system can provide for certain amount of energy consumption. As the cooling capacity of the TEARS increases while having constant high temperature generator load, the energetic and exergetic performances of the TEARS increases.

• Effects of ambient temperature

The variation in ambient temperature plays a significant role in the performance determination of systems relying extensively on heat transfer. The impact of the increase in ambient in temperature on the energy and exergy COPs of the TEARS is presented in Fig. 5.6. The energy COP is observed to remain constant at 1.458 and exergy COP is noted to increase from 0.40 to 0.84 with increase in ambient temperature from 280 to 300 K. The constant behavior of energetic COP reflects the importance of performing exergy analysis, because it is logical that the systems that rely on temperature difference are easily affected by any difference change in. The increasing behavior of exergetic COP with the increase in ambient temperature is because the increase in ambient temperature helps in decreasing the overall temperature difference from the system to the surrounding. As this overall temperature decreases, the thermal exergy loss from the system to the surrounding decreases and as a consequence of this phenomenon, the exergetic COP increases. Figure 5.7 displays the effects of the rise in ambient temperature on the exergoenvironmental impact factor and the exergoenvironmental impact coefficient. The exergoenvironmental impact factor and the exergoenvironmental impact coefficient are observed to decrease from 0.5 to 0.13 and 2.49 to 1.18, respectively, with an increase in ambient temperature from 280 to 300 K. The optimal value for the

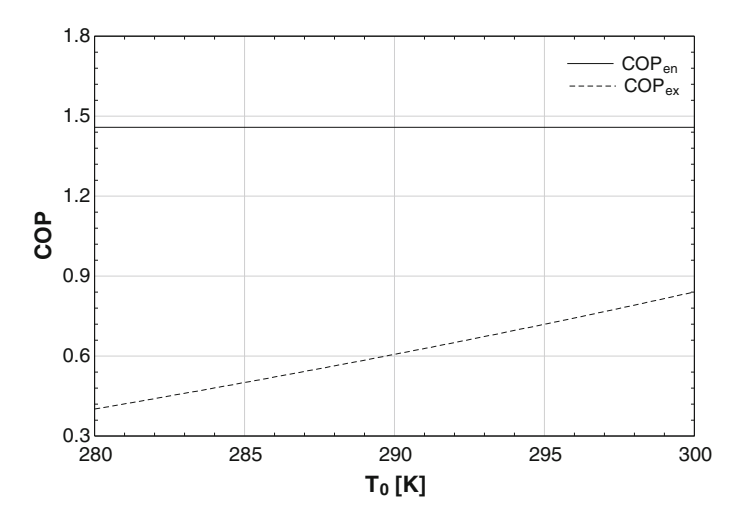


Fig. 5.6 Effects of ambient temperature on energy and exergy COPs

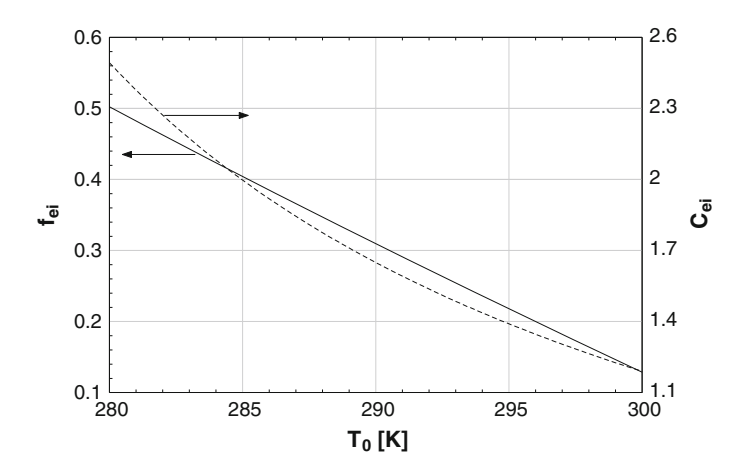


Fig. 5.7 Effects of ambient temperature on the exergoenvironmental impact factor and the exergoenvironmental impact coefficient

exergoenvironmental impact factor is zero which indicates that the system is completely environmentally neutral.

In Fig. 5.7, it can be seen that the exergoenvironmental impact factor is approaching its ideal value with the rise in the ambient temperature, and this indicates that the TEARS becomes more and more environmentally friendly as the ambient temperature rises. This decreasing trend of the exergoenvironmental impact factor is observed because the increase in the ambient temperature decreasing the exergetic heat loss from the system to the surrounding and as the exergetic heat loss

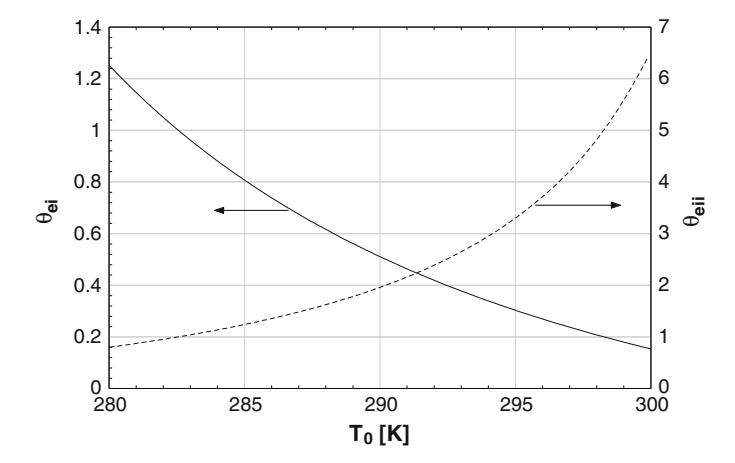


Fig. 5.8 Effects of ambient temperature on the exergoenvironmental impact index and the exergoenvironmental impact improvement

decreases the system performance increases. On the other hand, the ideal value for the exergoenvironmental impact coefficient is one which indicates that the system has no irreversibility. The exergoenvironmental impact coefficient is directly related to the exegetic COP of the TEARS, and as the exergetic COP increases with the rise in ambient temperature, the exergoenvironmental impact coefficient decreases to reach its ideal value of one.

Figure 5.8 displays the impact of the rise in ambient temperature on the exergoenvironmental impact index and the exergoenvironmental impact improvement factor. The exergoenvironmental impact index is observed to decrease from 1.25 to 0.15, whereas, the exergoenvironmental impact improvement factor is noted to increase from 0.79 to 6.53 with increase in ambient temperature from 280 to 300 K. The increase in ambient temperature helps reduce the overall temperature difference between the system and the surrounding, and as this temperature difference decreases, the performance of the TEARS increases. This enhancement in performance of the TEARS is also facilitated by the reduction in exergy destruction rate. However, the increase in the exergoenvironmental impact improvement factor with increase in ambient temperature is noticed because the rise in ambient temperature helps reduce the loss of useful energy in the form of heat to the surrounding. Also, the increase in the exergoenvironmental impact improvement factor shows that with the increase in the ambient temperature, the TEARS become more environmentally benign. The effects of the rise in ambient temperature on the exergetic stability factor and the exergetic sustainability index are shown in Fig. 5.9. The exergetic stability factor and the exergetic sustainability index are observed to increase from 0.49 to 0.87 and 0.39 to 5.69, respectively, with an increase in ambient temperature from 280 to 300 K. The growing trends of the exergetic stability factor and the exergetic sustainability index show that the TEARS becomes more and more stable and sustainable from the exergoenvironmental perspective with rise in the ambient

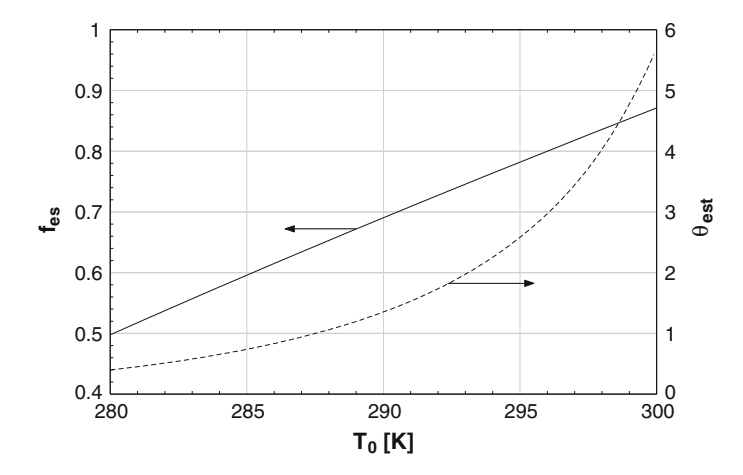


Fig. 5.9 Effects of ambient temperature on the exergetic stability and the exergetic sustainability index

temperature. Lower heat losses from the system to the surrounding causes again in exergetic stability and sustainability because of the relatively lower temperature difference between the system and the surrounding.

Optimization study results:

Table 5.2 presents the constraints associated with the optimization study of the triple effect absorption refrigeration system. The first optimization study performed is, maximizing the exergetic COP and minimizing the exergetic cooling cost. The results obtained from the first optimization study are presented in Fig. 5.10. A built-in Nelder–Mead simplex algorithm routine in the engineering equation solver software is used to perform multi-objective optimization study in this chapter. The Nelder–Mead simplex algorithm makes use of N+1 test points (where N represents the degrees of freedom), which is called a simplex. The algorithm evaluates every single point of the simplex, and the objective function is found at each of the points. The worst point in the simplex is then discarded, and a new point is found by reflecting away from the worst point about the axis formed by the other test points. The process is repeated several times until one of the stopping criteria is met, and then the objective function of the best point is taken to be the optimum. The first optimization study reveals that the highest exergetic COP obtained is 5.1 and the lowest cooling cost obtained is 964.2 k

Table 5.2 Constraints associated with the optimization study of the TEARS

Parameter	Minimum value	Maximum value
$\dot{Q}_{ m HTG}$	260 kW	300 kW
T_0	280 K	300 K
x ₂₉	0.5	0.6
x ₃₀	0.2	0.3

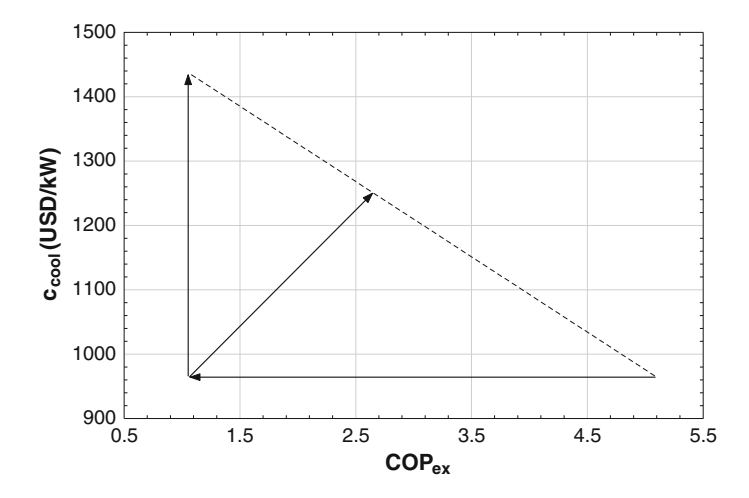


Fig. 5.10 Multi-objective optimization of the TEARS (exergetic COP vs. exergetic cooling cost)

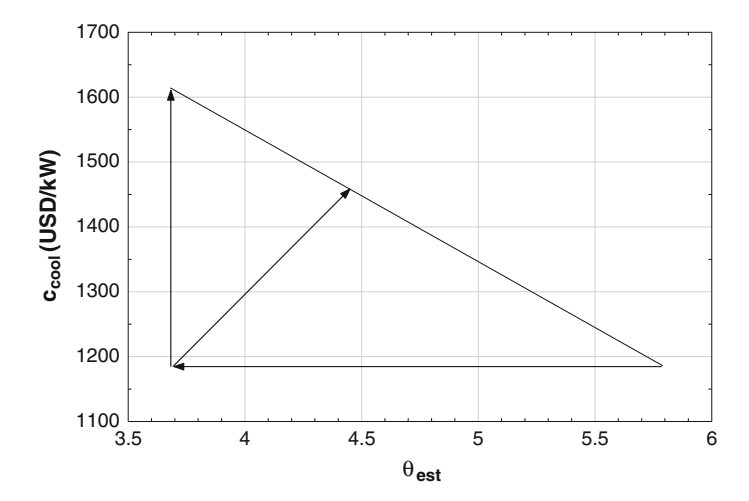


Fig. 5.11 Multi-objective optimization of the TEARS (exergetic sustainability index vs. exergetic cooling cost)

worth noting that although all the points on the Pareto front are considered optimum, traditionally LINMAP is used to obtain the most desirable optimized points. LINMAP helps to find an imaginary point at which all the objective functions have their respective optimum location irrespective of other objective functions. The best exergetic COP and exergetic cooling cost obtained with this basis are 2.64 and 1251.5 \$/kW, respectively. The results achieved from the second optimization study of maximizing exergetic sustainability index and minimizing the exergetic cost of cooling are presented in Fig. 5.11. The values obtained using LINMAP for

the exergetic sustainability index, and the exergetic cost of refrigeration are 4.45 and 1458.3 \$/kW, respectively.

5.8 Closing Remarks

The exploitation of the triple effect absorption refrigeration system provides an additional benefit as compared to a double effect absorption refrigeration system in terms of energy, exergy, environment, and sustainability. The present chapter provides in-depth energy, exergy, exergoeconomic and exergoenvironmental analyses of the TEARS. The chapter also provides a broad example of the TEARS showing how each thermophysical property can be calculated and how energy and exergy requirements of the TEARS can be calculated.

Chapter 6 Quadruple Effect Absorption Refrigeration System

6.1 Introduction

The introduction of absorption refrigeration systems to meet heating and cooling demands requirements has given impetus to moving toward environmentally friendly and sustainable applications. However, the introduction of new technology never comes without criticism. At present, absorption refrigeration systems are criticized because they have lower coefficients of performance (COPs) and cover larger floor space as compared to the conventional vapor–compression refrigeration system. The introduction of the quadruple effect absorption refrigeration system (QEARS) helps address the criticism providing higher COPs compared to the conventional refrigeration system. Also, the QEARS makes the absorption refrigeration system more environmentally friendly and sustainable as compared to other absorption and conventional refrigeration systems.

The current chapter focuses on the basic operation of the QEARS in conjunction with its energy and exergy analyses. First, the working principle of the QEARS is explained to help the reader understand how the QEARS works. Second, energy, exergy, exergoenvironment, exergoeconomic, and optimization modeling of the QEARS are presented for the performance assessment and evaluation. Lastly, a comprehensive illustrative example is provided to ensure that the reader understands how individual equations are used to attain thermophysical properties at each state point and to obtain overall energy and exergy flow values of the QEARS.

6.2 System Description

The OEARS appears to be the most complex form of absorption refrigeration system as shown in Fig. 6.1. A strong ammonia water solution leaving the absorber of the QEARS at state 1 enters the pump in a saturated liquid phase. In the pump, the pressure of the strong solution increases before it leaves at state 2. The strong solution at state 2 then divides into two streams of states 17 and 19. The stream at state 19 enters the low temperature heat exchanger, where it gains heat from the returning fluid from the generators to leave at state 3 at relatively higher temperature. This strong solution at state 3 then divides into two streams of states 20 and 21. The strong solution at state 20 enters the medium temperature heat exchanger where it extracts heat from the streams returning from the generators to leave at state 24 at relatively higher temperature. This strong solution at state 24 then divides into two streams of states 25 and 26. The strong solution at state 25 enters the high temperature heat exchanger where it extracts heat from the streams returning from the generators to leave at state 29 at relatively higher temperature. The strong solution stream at state 29 then further divides into two streams to leave at states 34 and 35. State 35 enters the very high temperature heat exchanger where it gains heat from the returning weak solution from the very high temperature generator to leave at a relatively higher temperature at state 36. The strong solution at state 36 then enters the very high temperature generator where heat is supplied from the external source to raise the temperature of the strong solution of ammoniawater above its boiling point. Boiling helps to separate ammonia from the mixture because ammonia boils at moderately lower temperature than water. The ammonia

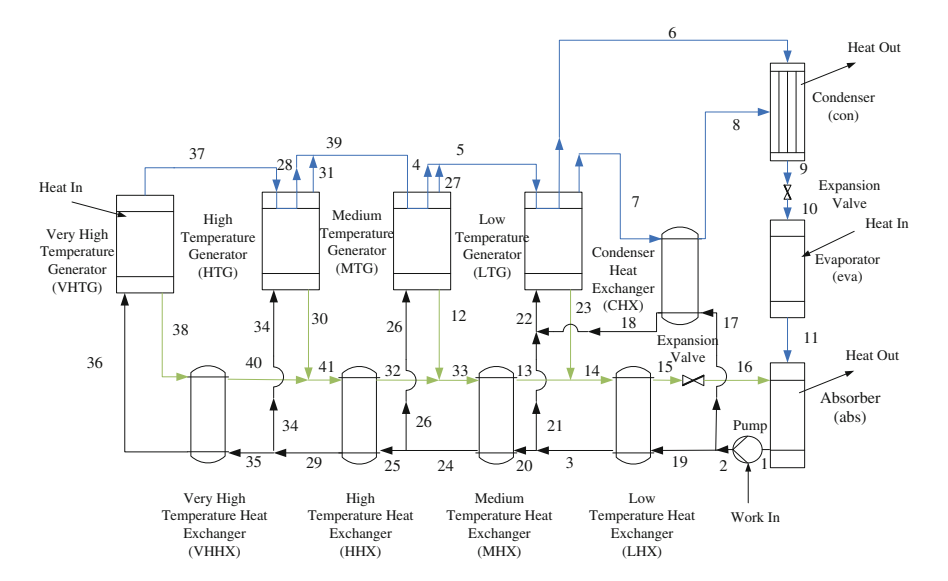


Fig. 6.1 Schematic of the QEARS

vapor is then extracted from the high temperature generator at state 37, and the remaining weak ammonia water solution is extracted at state 38. The ammonia vapor removed at state 37 enters the high temperature generator where it gives heat to the strong solution entering at state 34. The ammonia vapor leaves the high temperature generator at state 31, and the weak solution leave at state 30. The ammonia vapor provides heat to the high temperature generator at state 37 and leaves the generator at state 28 to mix with the ammonia vapor at state 31, leaving at a relatively lower temperature at state 39. The ammonia at state 39 then enters the medium temperature generator where it acts as a heat source. In the medium temperature generator, the strong solution approaches state 26 where it gains heat from the ammonia vapor entering at state 39. The heat supplied to the medium temperature generator helps to separate ammonia from the strong solution that leaves the medium temperature generator at state 27. The remaining weak solution in the medium temperature generator is then extracted at state 12. After releasing heat in the medium temperature generator, ammonia vapor leaves at state 4 to combine with a stream coming from state 27 before entering the low temperature generator at state 5. In the low temperature generator, the strong solution enters at state 22 and gains heat from the ammonia vapor entering at state 5. The heat supplied to the low temperature generator helps in separating ammonia from the strong solution that leaves the low temperature generator at state 7. The remaining weak solution in the low temperature generator is then extracted at state 23. After releasing heat, ammonia vapor leaves the low temperature generator at state 6 to enter the condenser, and the ammonia stream at state 7 enters the condenser heat exchanger. In the condenser heat exchanger, the strong solution entering at state 17 gains heat from the ammonia stream and leaves at a relatively higher temperature at state 18. The ammonia refrigerant leaves the condenser heat exchanger at state 8 to enter the condenser. The strong solution exiting the condenser heat exchanger at state 18 mixes with the strong solution from state 21 to leave at state 22. The ammonia refrigerant streams release heat to the surrounding in the condenser to leave as a relatively cooler refrigerant at state 9. This ammonia refrigerant at state 9 then passes through the refrigerant expansion valve where its pressure suddenly drops and leaves as a cooled ammonia refrigerant at state 10. The ammonia refrigerant at state 10 enters the evaporator and gains heat from the surrounding before leaving at a relatively higher temperature at state 11. The weak solution exiting the very high temperature generator at state 38 passes through the very high temperature heat exchanger where it releases heat to the strong solution to leave at state 40. The weak solution at state 40 mixes with the weak solution from state 30 to leave at state 41 before entering the high temperature heat exchanger. The weak solution at state 41 rejects heat to the incoming strong solution to leave at state 32. The weak solution at state 32 mixes with the weak solution returning from the medium temperature generator at state 12 to leave at state 33. The weak solution at state 33 then enters the medium temperature heat exchanger where it rejects heat and leaves at a relatively cooler temperature at state 13. The weak solution at state 13 mixes with the weak solution returning from the low temperature generator at state 23 to leave at state 14. The weak solution at state 14 then enters the low temperature heat exchanger where it rejects heat and leaves at a relatively cooler temperature at state 15. The weak solution at state 15 enters the weak solution expansion valve where its pressure suddenly drops before it enters the absorber at state 16. The weak solution at state 16 and ammonia refrigerant at state 11 then mix in the absorber while rejecting heat to the environment to leave the absorber as a strong solution in saturated liquid phase at state 1.

6.3 Energy and Exergy Analyses

Energy and exergy balance equations for all system components of the QEARS are presented in this section of the chapter.

• Pump:

The mass balance equation across the pump can be written as

$$\dot{m}_1 = \dot{m}_2 = \dot{m}_p \tag{6.1}$$

where \dot{m} represents the mass flow rate.

The specific power consumed by the pump can be calculated using

$$w_{\rm p} = \frac{v(P_2 - P_1)}{\eta_{\rm p}} \tag{6.2}$$

where w, v, P, and η represent specific power, specific volume, pressure, and efficiency, respectively.

The total power consumed by the pump is defined as

$$\dot{W}_{\rm p} = \dot{m}_{\rm p} w_{\rm p} \tag{6.3}$$

where \dot{W} represents total power consumed by the pump.

The overall energy balance equation of the pump is given as

$$(\dot{m}h)_1 + \dot{W}_p = (\dot{m}h)_2 \tag{6.4}$$

where h represents specific enthalpy of the state.

The specific exergies at states 1 and 2 are defined as

$$ex_1 = (h_1 - h_0) - T_0(s_1 - s_0)$$
(6.5)

$$ex_2 = (h_2 - h_0) - T_0(s_2 - s_0)$$
(6.6)

where ex, T and s represent specific exergy, temperature, and specific entropy.

The overall exergy balance equation of the pump is given as

$$\dot{m}_1 e x_1 + \dot{W}_p = \dot{m}_2 e x_2 + \dot{E} x_{\text{dest},p}$$
 (6.7)

where $\dot{E}x_{dest,p}$ represents the exergy destruction rate in the pump.

• Low temperature heat exchanger:

The mass balance equations for the low temperature heat exchanger can be written as

$$\dot{m}_3 = \dot{m}_{19} \tag{6.8}$$

$$\dot{m}_{15} = \dot{m}_{14} \tag{6.9}$$

and

$$\dot{m}_{17} + \dot{m}_{19} = \dot{m}_2 \tag{6.10}$$

The energy balance equation is given as

$$\dot{m}_{19}h_{19} + \dot{m}_{14}h_{14} = \dot{m}_3h_3 + \dot{m}_{15}h_{15} \tag{6.11}$$

The specific exergies at states 3, 14, 15, and 19 are defined as

$$ex_3 = (h_3 - h_0) - T_0(s_3 - s_0)$$
(6.12)

$$ex_{14} = (h_{14} - h_0) - T_0(s_{14} - s_0)$$
(6.13)

$$ex_{15} = (h_{15} - h_0) - T_0(s_{15} - s_0)$$
(6.14)

$$ex_{19} = (h_{19} - h_0) - T_0(s_{19} - s_0)$$
(6.15)

The exergy balance equation is given as

$$\dot{m}_{19} = x_{19} + \dot{m}_{14} = x_{14} = \dot{m}_{3} = x_{3} + \dot{m}_{15} = x_{15} + \dot{E}x_{\text{dest,LHX}}$$
 (6.16)

where $\dot{E}x_{dest,LHX}$ represents the exergy destruction rate in the low temperature heat exchanger.

• Medium temperature heat exchanger:

The mass balance equations for the medium temperature heat exchanger can be written as

$$\dot{m}_{24} = \dot{m}_{20} \tag{6.17}$$

$$\dot{m}_{13} = \dot{m}_{33} \tag{6.18}$$

and

$$\dot{m}_{20} + \dot{m}_{21} = \dot{m}_3 \tag{6.19}$$

The energy balance equation is given as

$$\dot{m}_{20}h_{20} + \dot{m}_{33}h_{33} = \dot{m}_{13}h_{13} + \dot{m}_{24}h_{24} \tag{6.20}$$

The specific exergies at states 13, 20, 24, and 33 are defined as

$$ex_{13} = (h_{13} - h_0) - T_0(s_{13} - s_0)$$
(6.21)

$$ex_{20} = (h_{20} - h_0) - T_0(s_{20} - s_0)$$
(6.22)

$$ex_{24} = (h_{24} - h_0) - T_0(s_{24} - s_0)$$
(6.23)

$$ex_{33} = (h_{33} - h_0) - T_0(s_{33} - s_0)$$
(6.24)

The exergy balance equation is given as

$$\dot{m}_{20} ex_{20} + \dot{m}_{33} ex_{33} = \dot{m}_{13} ex_{13} + \dot{m}_{24} ex_{24} + \dot{E}x_{\text{dest,MHX}}$$
 (6.25)

where $\dot{E}x_{dest,MHX}$ represents the exergy destruction rate in the medium temperature heat exchanger.

• High temperature heat exchanger:

The mass balance equations for the high temperature heat exchanger can be written as

$$\dot{m}_{29} = \dot{m}_{25} \tag{6.26}$$

$$\dot{m}_{32} = \dot{m}_{41} \tag{6.27}$$

and

$$\dot{m}_{25} + \dot{m}_{26} = \dot{m}_{24} \tag{6.28}$$

The energy balance equation is given as

$$\dot{m}_{25}h_{25} + \dot{m}_{41}h_{41} = \dot{m}_{29}h_{29} + \dot{m}_{32}h_{32}$$
 (6.29)

The specific exergies at states 25, 29, 41, and 32 are defined as

$$ex_{25} = (h_{25} - h_0) - T_0(s_{25} - s_0)$$
(6.30)

$$ex_{29} = (h_{29} - h_0) - T_0(s_{29} - s_0)$$
(6.31)

$$ex_{41} = (h_{41} - h_0) - T_0(s_{41} - s_0)$$
(6.32)

$$ex_{32} = (h_{32} - h_0) - T_0(s_{32} - s_0)$$
(6.33)

The exergy balance equation is given as

$$\dot{m}_{25} ex_{25} + \dot{m}_{41} ex_{41} = \dot{m}_{29} ex_{29} + \dot{m}_{32} ex_{32} + \dot{E}x_{\text{dest,HHX}}$$
 (6.34)

where $\dot{E}x_{dest,HHX}$ represents the exergy destruction rate in the high temperature heat exchanger.

• Very high temperature heat exchanger:

The mass balance equations for the very high temperature heat exchanger can be written as

$$\dot{m}_{36} = \dot{m}_{35} \tag{6.35}$$

$$\dot{m}_{38} = \dot{m}_{40} \tag{6.36}$$

and

$$\dot{m}_{34} + \dot{m}_{25} = \dot{m}_{29} \tag{6.37}$$

The energy balance equation is given as

$$\dot{m}_{35}h_{35} + \dot{m}_{38}h_{48} = \dot{m}_{36}h_{36} + \dot{m}_{40}h_{40} \tag{6.38}$$

The specific exergies at states 35, 36, 38, and 40 are defined as

$$ex_{35} = (h_{35} - h_0) - T_0(s_{35} - s_0)$$
(6.39)

$$ex_{36} = (h_{36} - h_0) - T_0(s_{36} - s_0)$$
(6.40)

$$ex_{38} = (h_{38} - h_0) - T_0(s_{38} - s_0)$$
(6.41)

$$ex_{40} = (h_{40} - h_0) - T_0(s_{40} - s_0)$$
(6.42)

The exergy balance equation is given as

$$\dot{m}_{25} ex_{25} + \dot{m}_{41} ex_{41} = \dot{m}_{29} ex_{29} + \dot{m}_{32} ex_{32} + \dot{E}x_{\text{dest,VHHX}}$$
 (6.43)

where $\dot{E}x_{\text{dest},\text{VHHX}}$ represents the exergy destruction rate in the very high temperature heat exchanger.

• Very high temperature generator:

The mass balance equations of the very high temperature generator can be written as

$$\dot{m}_{36} = \dot{m}_{37} + \dot{m}_{38} \tag{6.44}$$

and

$$\dot{m}_{36}x_{36} = \dot{m}_{37}x_{37} + \dot{m}_{38}x_{38} \tag{6.45}$$

where x represents the concentration of the solution.

The energy balance equation is given as

$$\dot{m}_{36}h_{36} + \dot{Q}_{\text{VHTG}} = \dot{m}_{37}h_{37} + \dot{m}_{38}h_{38} \tag{6.46}$$

where \dot{Q}_{VHTG} represents the rate of heat required by the very high temperature generator.

The specific exergy at state 37 is defined as

$$ex_{37} = (h_{37} - h_0) - T_0(s_{37} - s_0)$$
(6.47)

The thermal exergy rate supplied to the very high temperature generator is defined as

$$\dot{\mathbf{E}}\mathbf{x}_{\text{th,VHTG}} = \left(1 - \frac{T_0}{T_{\text{VHTG}}}\right) \dot{Q}_{\text{VHTG}} \tag{6.48}$$

where $\dot{E}x_{th,VHTG}$ represents the thermal exergy rate of the very high temperature generator.

The exergy balance equation of the very high temperature generator is given as

$$\dot{m}_{36} ex_{36} + \dot{E}x_{th,VHTG} = \dot{m}_{37} ex_{37} + \dot{m}_{38} ex_{38} + \dot{E}x_{dest,VHTG}$$
 (6.49)

where $\dot{E}x_{dest,VHTG}$ represents the rate of exergy destruction in the very high temperature generator.

• High temperature generator:

The mass balance equations of the high temperature generator can be written as

$$\dot{m}_{34} = \dot{m}_{30} + \dot{m}_{31} \tag{6.50}$$

$$\dot{m}_{34}x_{34} = \dot{m}_{30}x_{30} + \dot{m}_{31}x_{31} \tag{6.51}$$

$$\dot{m}_{28} = \dot{m}_{37} \tag{6.52}$$

and

$$\dot{m}_{39} = \dot{m}_{28} + \dot{m}_{31} \tag{6.53}$$

The energy balance equation is given as

$$\dot{m}_{34}h_{34} + \dot{m}_{37}h_{37} = \dot{m}_{28}h_{28} + \dot{m}_{30}h_{30} + \dot{m}_{31}h_{31} \tag{6.54}$$

and

$$\dot{m}_{37}h_{37} = \dot{m}_{28}h_{28} + \dot{Q}_{\rm HTG} \tag{6.55}$$

where $\dot{Q}_{\rm HTG}$ represents the rate of heat required by the high temperature generator. The specific exergies at states 28, 30, 31, 34, and 39 are then defined as

$$ex_{28} = (h_{28} - h_0) - T_0(s_{28} - s_0)$$
(6.56)

$$ex_{30} = (h_{30} - h_0) - T_0(s_{30} - s_0)$$
(6.57)

$$ex_{31} = (h_{31} - h_0) - T_0(s_{31} - s_0)$$
(6.58)

$$ex_{34} = (h_{34} - h_0) - T_0(s_{34} - s_0)$$
(6.59)

$$ex_{39} = (h_{39} - h_0) - T_0(s_{39} - s_0)$$
(6.60)

The thermal exergy rate supplied to the high temperature generator is defined as

$$\dot{\mathbf{E}}\mathbf{x}_{\text{th,HTG}} = \left(1 - \frac{T_0}{T_{\text{HTG}}}\right) \dot{Q}_{\text{HTG}} \tag{6.61}$$

where $\dot{E}x_{th,HTG}$ represents the thermal exergy rate of the high temperature generator. The exergy balance equation of the high temperature generator is given as

$$\dot{m}_{34} ex_{34} + \dot{E}x_{\text{th,HTG}} = \dot{m}_{30} ex_{30} + \dot{m}_{31} ex_{31} + \dot{E}x_{\text{dest,HTG}}$$
 (6.62)

where $\dot{E}x_{dest,HTG}$ represents the rate of exergy destruction in the high temperature generator.

• Medium temperature generator:

The mass balance equations of the medium temperature generator can be written as

$$\dot{m}_{26} = \dot{m}_{12} + \dot{m}_{27} \tag{6.63}$$

$$\dot{m}_{26}x_{26} = \dot{m}_{12}x_{12} + \dot{m}_{27}x_{27} \tag{6.64}$$

$$\dot{m}_4 = \dot{m}_{39} \tag{6.65}$$

and

$$\dot{m}_5 = \dot{m}_4 + \dot{m}_{27} \tag{6.66}$$

The energy balance equation is given as

$$\dot{m}_{26}h_{26} + \dot{m}_{39}h_{39} = \dot{m}_4h_4 + \dot{m}_{12}h_{12} + \dot{m}_{27}h_{27} \tag{6.67}$$

and

$$\dot{m}_{39}h_{39} = \dot{m}_4 h_4 + \dot{Q}_{\text{MTG}} \tag{6.68}$$

where \dot{Q}_{MTG} represents the rate of heat required by the medium temperature generator.

The specific exergies at states 4, 5, 12, 26, and 27 are defined as

$$ex_4 = (h_4 - h_0) - T_0(s_4 - s_0)$$
(6.69)

$$ex_5 = (h_5 - h_0) - T_0(s_5 - s_0)$$
(6.70)

$$ex_{12} = (h_{12} - h_0) - T_0(s_{12} - s_0)$$
(6.71)

$$ex_{26} = (h_{26} - h_0) - T_0(s_{26} - s_0)$$
(6.72)

$$ex_{27} = (h_{27} - h_0) - T_0(s_{27} - s_0)$$
(6.73)

The thermal exergy rate supplied to the medium temperature generator is defined as

$$\dot{\mathbf{E}}\mathbf{x}_{\text{th,MTG}} = \left(1 - \frac{T_0}{T_{\text{MTG}}}\right) \dot{Q}_{\text{MTG}} \tag{6.74}$$

where $\dot{E}x_{th,MTG}$ represents the thermal exergy rate of the medium temperature generator.

The exergy balance equation of the medium temperature generator is given as

$$\dot{m}_{26} ex_{26} + \dot{E}x_{th,MTG} = \dot{m}_{12} ex_{12} + \dot{m}_{27} ex_{27} + \dot{E}x_{dest,MTG}$$
 (6.75)

where $\dot{E}x_{dest,MTG}$ represents the rate of exergy destruction in the medium temperature generator.

• Low temperature generator:

The mass balance equations of the low temperature generator can be written as

$$\dot{m}_{22} = \dot{m}_7 + \dot{m}_{23} \tag{6.76}$$

$$\dot{m}_{22}x_{22} = \dot{m}_7x_7 + \dot{m}_{23}x_{23} \tag{6.77}$$

$$\dot{m}_6 = \dot{m}_5 \tag{6.78}$$

and

$$\dot{m}_{22} = \dot{m}_{18} + \dot{m}_{21} \tag{6.79}$$

The energy balance equation is given as

$$\dot{m}_5 h_5 + \dot{m}_{22} h_{22} = \dot{m}_6 h_6 + \dot{m}_7 h_7 + \dot{m}_{23} h_{23} \tag{6.80}$$

and

$$\dot{m}_5 h_5 = \dot{m}_6 h_6 + \dot{Q}_{\rm LTG} \tag{6.81}$$

where $\dot{Q}_{\rm LTG}$ represents the rate of heat required by the low temperature generator. The specific exergies at states 6, 7, 22, and 23 are defined as

$$ex_6 = (h_6 - h_0) - T_0(s_6 - s_0)$$
(6.82)

$$ex_7 = (h_7 - h_0) - T_0(s_7 - s_0)$$
(6.83)

$$ex_{22} = (h_{22} - h_0) - T_0(s_{22} - s_0)$$
(6.84)

$$ex_{23} = (h_{23} - h_0) - T_0(s_{23} - s_0)$$
(6.85)

The thermal exergy rate supplied to the low temperature generator is defined as

$$\dot{\mathbf{E}}\mathbf{x}_{\text{th,LTG}} = \left(1 - \frac{T_0}{T_{\text{LTG}}}\right) \dot{\mathbf{Q}}_{\text{LTG}} \tag{6.86}$$

where $\dot{E}x_{th,LTG}$ represents the thermal exergy rate of the low temperature generator. The exergy balance equation of the low temperature generator is given as

$$\dot{m}_{22} ex_{22} + \dot{E}x_{th,LTG} = \dot{m}_7 ex_7 + \dot{m}_{23} ex_{23} + \dot{E}x_{dest,LTG}$$
 (6.87)

where $\dot{E}x_{dest,LTG}$ represents the rate of exergy destruction in the low temperature generator.

Condenser:

The mass balance equation for the condenser is defined as

$$\dot{m}_9 = \dot{m}_6 + \dot{m}_8 \tag{6.88}$$

The energy balance equation of the condenser is given as

$$\dot{m}_6 h_6 + \dot{m}_8 h_8 = \dot{m}_9 h_9 + \dot{Q}_c \tag{6.89}$$

where \dot{Q}_c represents the rate of heat rejected by the refrigerant flowing through the condenser.

The specific exergy at state 9 is defined as

$$ex_9 = (h_9 - h_0) - T_0(s_9 - s_0)$$
(6.90)

The thermal exergy rate released by the condenser is calculated as

$$\dot{\mathbf{E}}\mathbf{x}_{\text{th,c}} = \left(1 - \frac{T_0}{T_c}\right)\dot{Q}_c \tag{6.91}$$

where $\dot{E}x_{\text{th,c}}$ represents the thermal exergy rate of the condenser.

The exergy balance equation of the condenser is given as

$$\dot{m}_6 ex_6 + \dot{m}_8 ex_8 = \dot{m}_9 ex_9 + \dot{E}x_{th,c} + \dot{E}x_{dest,c}$$
 (6.92)

where Exdest,c represents the rate of destruction in the condenser.

• Evaporator:

The mass balance equation for the evaporator is written as

$$\dot{m}_{11} = \dot{m}_{10} \tag{6.93}$$

The energy balance equation of the evaporator is given as

$$\dot{m}_{10}h_{10} + \dot{Q}_{e} = \dot{m}_{11}h_{11} \tag{6.94}$$

where $\dot{Q}_{\rm e}$ represents the rate of heat gained by the refrigerant flowing through the evaporator.

The specific exergies at states 10 and 11 are defined as

$$ex_{10} = (h_{10} - h_0) - T_0(s_{10} - s_0)$$
(6.95)

$$ex_{11} = (h_{11} - h_0) - T_0(s_{11} - s_0)$$
(6.96)

The thermal exergy rate supplied to the evaporator is calculated as

$$\dot{\mathbf{E}}\mathbf{x}_{\text{th,e}} = \left(1 - \frac{T_0}{T_e}\right)\dot{Q}_e \tag{6.97}$$

where $\dot{E}x_{\text{th.e}}$ represents the thermal exergy rate of the evaporator.

The exergy balance equation of the evaporator is given as

$$\dot{m}_{10} ex_{10} + \dot{E}x_{th,e} = \dot{m}_{11} ex_{11} + \dot{E}x_{dest,e}$$
 (6.98)

where Ex_{dest,e} represents the rate of exergy destruction in the evaporator.

Absorber:

The mass balance equation for the absorber is written as

$$\dot{m}_{11} + \dot{m}_{16} = \dot{m}_1 \tag{6.99}$$

The energy balance equation of the absorber is given as

$$\dot{m}_{11}h_{11} + \dot{m}_{16}h_{16} = \dot{m}_1h_1 + \dot{Q}_a \tag{6.100}$$

where $\dot{Q}_{\rm a}$ represents the rate of heat rejected by the absorber.

The specific exergy at state 16 is defined as

$$ex_{16} = (h_{16} - h_0) - T_0(s_{16} - s_0)$$
(6.101)

The thermal exergy rate released by the absorber is calculated as

$$\dot{\mathbf{E}}\mathbf{x}_{\text{th,a}} = \left(1 - \frac{T_0}{T_a}\right)\dot{Q}_a \tag{6.102}$$

where $\dot{E}x_{th,a}$ represents the thermal exergy rate of the absorber.

The exergy balance equation of the absorber is given as

$$\dot{m}_{11} e x_{11} + \dot{m}_{16} e x_{16} = \dot{m}_{1} e x_{1} + \dot{E} x_{th,a} + \dot{E} x_{dest,a}$$
 (6.103)

where $\dot{E}x_{dest,a}$ represents the rate of exergy destruction in the absorber.

• Expansion valve (for weak solution)

The mass balance equation for the weak solution expansion valve is written as

$$\dot{m}_{16} = \dot{m}_{15} \tag{6.104}$$

The energy balance equation of the weak solution expansion valve is defined as

$$\dot{m}_{16}h_{16} = \dot{m}_{15}h_{15} \tag{6.105}$$

The exergy balance equation of the weak solution expansion valve is given as

$$\dot{m}_{16} ex_{16} = \dot{m}_{15} ex_{15} + \dot{E}x_{\text{dest,evw}}$$
 (6.106)

where $\dot{E}x_{dest,evw}$ represents the rate of exergy destruction in the weak solution expansion valve.

• Expansion valve (for refrigerant):

The mass balance equation for the refrigerant expansion valve is written as

$$\dot{m}_9 = \dot{m}_{10} \tag{6.107}$$

The energy balance equation of the refrigerant expansion valve is defined as

$$\dot{m}_{10}h_{10} = \dot{m}_9 h_9 \tag{6.108}$$

The exergy balance equation of the refrigerant expansion valve is given as

$$\dot{m}_9 \text{ex}_9 = \dot{m}_{10} \text{ex}_{10} + \dot{E}x_{\text{dest.evr}}$$
 (6.109)

where $\dot{E}x_{dest,evr}$ represents the rate of exergy destruction in the refrigerant expansion valve.

• Condenser heat exchanger:

The mass balance equations for the condenser heat exchanger can be written as

$$\dot{m}_8 = \dot{m}_7$$
 (6.110)

$$\dot{m}_{18} = \dot{m}_{17} \tag{6.111}$$

The energy balance equation is given as

$$\dot{m}_{17}h_{17} + \dot{m}_7h_7 = \dot{m}_8h_8 + \dot{m}_{18}h_{18} \tag{6.112}$$

The specific exergies at states 17 and 18 are defined as

$$ex_{17} = (h_{17} - h_0) - T_0(s_{17} - s_0)$$
(6.113)

$$ex_{18} = (h_{18} - h_0) - T_0(s_{18} - s_0)$$
(6.114)

The exergy balance equation is given as

$$\dot{m}_{17} e x_{17} + \dot{m}_7 e x_7 = \dot{m}_{18} e x_{18} + \dot{m}_8 e x_8 + \dot{E} x_{\text{dest,CHX}}$$
 (6.115)

where $\dot{E}x_{dest,CHX}$ represents the exergy destruction rate in the condenser heat exchanger.

The performance of an absorption refrigeration system is measured using the coefficient of performance. The energetic and exergetic coefficient of performances of absorption refrigeration system are defined as

$$COP_{en} = \frac{\dot{Q}_e}{\dot{Q}_{VHTG} + \dot{W}_p} \tag{6.116}$$

$$COP_{ex} = \frac{\dot{E}x_{th,e}}{\dot{E}x_{th,VHTG} + \dot{W}_{p}}$$
 (6.117)

where COPen and COPex represent energetic COP and exergetic COP, respectively.

6.4 Exergoeconomic Analysis

This section presents the exergoeconomic analysis equations of the QEARS. The overall exergoeconomic balance equation of the QEARS is written as

$$\dot{Z}_{eq} + \dot{C}_{OPM} = \dot{C}_{Cool} \tag{6.118}$$

where $\dot{Z}_{\rm eq}$, $\dot{C}_{\rm OPM}$ and $\dot{C}_{\rm Cool}$ represent the cost associated with the equipment, operation and maintenance, and cooling, respectively.

The cost linked with the equipment is defined as

$$\dot{Z}_{eq} = \dot{C}_a + \dot{C}_g + \dot{C}_c + \dot{C}_e + \dot{C}_p + \dot{C}_{ev}$$
 (6.119)

where \dot{C}_a , \dot{C}_g , \dot{C}_c , \dot{C}_e , \dot{C}_P and \dot{C}_{ev} represent the cost of absorber, generator, condenser, evaporator, pump and expansion valve, respectively.

However, the total equipment cost can also be calculated on the basis of a relation between the equipment cost and cooling load as provided below.

$$\dot{Z}_{eq}(\$) = 1144.3(\dot{Q}_{cool})^{0.67}$$
 (6.120)

The cost associated with the operation and maintenance is defined as

$$\dot{C}_{\text{OPM}} = c_{\text{OPM}} \times \dot{E}_{X_{\text{OPM}}} \tag{6.121}$$

where $c_{\rm OPM}$ and $\dot{\rm Ex}_{\rm OPM}$ represent operation and maintenance cost, and exergy carried by the energy consumed in terms of heat and power, respectively. The operation and maintenance can also be assumed to be 3 % of the total equipment cost.

The cost related to the cooling produced is defined as

$$\dot{C}_{\text{Cool}} = c_{\text{Cool}} \times \dot{E}_{x_{\text{Cool}}} \tag{6.122}$$

where c_{Cool} and $\dot{\text{Ex}}_{\text{Cool}}$ represent the cost of cooling produced and the exergy related to the cooling produced, respectively.

In this regard, the above equation can be written as

$$(c \times \dot{E}x)_{OPM} + \dot{Z}_{eq} = (c \times \dot{E}x)_{Cool}$$
 (6.123)

The cost of cooling can then be calculated by rearranging the equation mentioned above and rewriting it as

$$c_{\text{cool}} = \frac{\left(c \times \dot{E}x\right)_{\text{OPM}} + \dot{Z}_{\text{eq}}}{\dot{E}x_{\text{cool}}}$$
(6.124)

6.5 Exergoenvironmental Analysis

In this section ,we present an exergoenvironmental formulation for the quadruple effect absorption refrigeration system.

The total exergy supplied to the QEARS is calculated as

$$\dot{\mathbf{E}}\mathbf{x}_{\text{in}} = \dot{\mathbf{E}}\mathbf{x}_{\text{th,VHTG}} + \dot{W}_{\text{p}} + \dot{\mathbf{E}}\mathbf{x}_{\text{th,e}} \tag{6.125}$$

The total exergy rejected by the QEARS is defined as

$$\dot{E}x_{out} = \dot{E}x_{th,a} + \dot{E}x_{th,c} \tag{6.126}$$

The total exergy destructed by the QEARS is calculated as

$$\dot{E}x_{dest,tot} = \dot{E}x_{in} - \dot{E}x_{out} \tag{6.127}$$

The exergoenvironmental impact factor is defined as

$$f_{\rm ei} = \frac{\dot{E}x_{\rm dest,tot}}{\dot{E}x_{\rm in}} \tag{6.128}$$

where $f_{\rm ei}$ represents exergoenvironmental impact factor.

This exergoenvironmental impact coefficient is calculated as

$$C_{\rm ei} = \frac{1}{\rm COP_{\rm ex}} \tag{6.129}$$

where $C_{\rm ei}$ represents the exergoenvironmental impact coefficient.

The exergoenvironmental impact index is calculated as

$$\theta_{\rm ei} = f_{\rm ei} \times C_{\rm ei} \tag{6.130}$$

where θ_{ei} represents exergoenvironmental impact index.

The exergoenvironmental impact improvement is defined as

$$\theta_{\rm eii} = \frac{1}{\theta_{\rm ei}} \tag{6.131}$$

where θ_{eii} represents exergoenvironmental impact improvement.

The exergetic stability factor is defined as

$$f_{\rm es} = \frac{\dot{E}x_{\rm out}}{\dot{E}x_{\rm out} + \dot{E}x_{\rm dest.tot}}$$
(6.132)

where $f_{\rm es}$ represents exergetic stability factor.

The exergetic sustainability index is defined as

$$\theta_{\rm est} = f_{\rm es} \times \theta_{\rm eii} \tag{6.133}$$

where $\theta_{\rm est}$ represents exergetic sustainability index.

6.6 Optimization Study

Two multi-objective optimization studies of the quadruple effect absorption refrigeration system are carried out with the goal of maximizing exergetic COP and exergetic sustainability index and minimizing the cost of cooling. The objective functions used for the study presented in Eqs. 6.117, 6.124 and 6.133, respectively. The constraints for this study are ambient in temperature, the heat supplied to the very high temperature generator, the concentration of the strong solution and the concentration of the weak solution.

6.7 Illustrative Example

Consider a QEARS using ammonia-water as a working fluid as shown in Fig. 6.1. The strong ammonia water solution with the mass flow rate of 1 kg/s enters the pump with concentration and pressure of 0.5 and 200 kPa, respectively. The strong solution leaves the pump at 700 kPa with a temperature difference of 0.4 °C. The heat is supplied to the very high temperature generator at a rate of 290 kW which helps to boil the strong solution, and the weak solution and ammonia refrigerant vapor leaves the generator with concentrations of 0.3 and 0.999, respectively. Assume a temperature difference of 7 °C between the inlet and exit of the heat exchangers and the condenser heat exchanger. Take the temperature difference between the strong solution entering the generators and weak solution exiting the generators to be 7 °C. Consider the condenser load and evaporator temperature to be 290 kW and -13.5 °C, respectively. Take ambient temperature and pressure to be 291.2 K and 100 kPa. Calculate the following:

- (a) the rate of cooling provided by the evaporator,
- (b) the power consumed by the pump,
- (c) the rate of heat rejected by the absorber
- (d) energetic and exergetic COPs,
- (e) the exergy destruction rate in each component,
- (f) the exergetic cost of cooling, and
- (g) exergoenvironmental parameters as discussed earlier in the chapter.

Also, perform the following parametric studies to investigate

- (a) effects of the very high temperature generator load on the cooling load, the cost of cooling and the energy and exergy COPs
- (b) effects of the strong solution concentration on the cooling capacity, the cost of cooling and the energy and exergy COPs, and
- (c) effects of the ambient temperature on the energy and exergy COPs, and all the exergoenvironmental parameters.

For parametric studies, use the same data ranges as defined below.

Also, perform an optimization study for the following scenarios:

- (a) maximizing the exergetic COP and minimizing the exergetic cost of cooling, and
- (b) maximizing the exergetic sustainability index and minimizing the exergetic cost of cooling

For the optimization study, consider the very high temperature generator heat load, strong solution concentration, weak solution concentration and ambient temperature as constraints with limits 290–340 kW, 0.45–0.5, 0.2–0.3 and 270–290 K, respectively.

Solution

The pump inlet properties are considered by assuming pressure, strong solution concentration and quality.

$$\left. \begin{array}{l} P_1 = 200 \; \mathrm{kPa} \\ x_1 = 0.5 \\ Qu_1 = 0.00 \end{array} \right\} \quad \left. \begin{array}{l} h_1 = -180.1 \; \mathrm{kJ/kg} \\ s_1 = 0.04011 \; \mathrm{kJ/kg} \, \mathrm{K} \\ v_1 = 0.001199 \; \mathrm{m^3/kg} \\ T_1 = 286.5 \; \mathrm{K} \end{array} \right.$$

It is assumed that at the exit of the pump, the temperature would be $0.4~^{\circ}\mathrm{C}$ higher than the inlet temperature.

$$\left. \begin{array}{l} P_2 = 700 \text{ kPa} \\ x_2 = 0.5 \\ T_2 = 286.9 \text{ K} \end{array} \right\} \quad \begin{array}{l} h_2 = -178.1 \text{ kJ/kg} \\ s_2 = 0.04481 \text{ kJ/kg K} \end{array}$$

$$\dot{m}_1 = 1 \text{ kg/s} \\ \dot{m}_2 = \dot{m}_1$$

The power required by the pump to increase the pressure of 1 kg/s of strong solution from 200 kPa to 700 kPa is calculated as

$$\dot{W}_{\rm p} = 1((-178.1) - (-180.1)) = 1.971 \text{ kW}$$

The ambient conditions for calculating specific exergy at each point are calculated as

$$\left. \begin{array}{l} P_0 = 100 \; \text{kPa} \\ T_0 = 291.2 \; \text{K} \\ x_0 = 0.5 \end{array} \right\} \quad \left. \begin{array}{l} h_0 = -150 \; \text{kJ/kg} \\ s_0 = 0.1034 \; \text{kJ/kg} \; \text{K} \end{array} \right.$$

These ambient conditions can only be used for strong solution streams.

$$\dot{E}x_1 = 1((-180.1 - (-150)) - 291.2(0.04011 - 0.1034)) = -11.62 \text{ kW}$$

 $\dot{E}x_2 = 1((-178.1 - (-150)) - 291.2(0.04481 - 0.1034)) = -11.01 \text{ kW}$

The exergy destruction in the pump is then calculated as

$$-11.62 + 1.971 = -11.01 + \dot{E}x_{dest,p}$$

 $\dot{E}x_{dest,p} = 1.368 \text{ kW}$

It is assumed that $20\,\%$ of the flow rate from the pump is supplied to the condenser heat exchanger and remaining $80\,\%$ is supplied to the low temperature

heat exchanger. The temperature, pressure, and strong solution concentration remains the same at states 2, 17, and 19.

$$h_{17} = h_2$$
 $s_{17} = s_2$
 $T_{17} = T_2$
 $h_{19} = h_2$
 $s_{19} = s_2$
 $T_{10} = T_2$

The mass balance equations for the low temperature heat exchanger are written as

$$\dot{m}_{17} = 0.2(\dot{m}_2) = 0.2 \text{ kg/s}$$
 $\dot{m}_{19} = 0.8(\dot{m}_2) = 0.8 \text{ kg/s}$
 $\dot{m}_3 = \dot{m}_{19}$
 $\dot{m}_{15} = \dot{m}_{14}$

The temperature of the strong solution leaving the low temperature heat exchanger is assumed to be 7 °C higher than the inlet temperature.

$$P_3 = P_2 x_3 = x_2 T_3 = T_{19} + 7$$

$$h_3 = -146.7 \text{ kJ/kg K} s_3 = 0.1532 \text{ kJ/kg K}$$

The energy balance equation of the low temperature heat exchanger can be written as

$$\dot{m}_{19}h_{19} + \dot{m}_{14}h_{14} = \dot{m}_3h_3 + \dot{m}_{15}h_{15}$$

$$0.8(-178.1) + 0.7139(-91.24) = 0.8(-146.7) + 0.7139(h_{15})$$
 $h_{15} = -126.5 \text{ kJ/kg}$

Using the specific enthalpy at state 15 obtained with the energy balance equation and knowing the pressure and weak solution concentration at this state, one can find the specific entropy and temperature at state 15 as follows:

$$\left. \begin{array}{l}
 P_{15} = P_2 \\
 x_{15} = 0.3 \\
 h_{15} = -126.5
 \end{array} \right\} \qquad T_{15} = 287.8 \text{ K} \\
 s_{15} = 0.1433 \text{ kJ/kg K}$$

The rate of heat transfer occurring inside the low temperature heat exchanger can be calculated as

$$\dot{m}_{19}h_{19} + \dot{Q}_{LHX} = \dot{m}_3h_3$$

$$0.8(-178.1) + \dot{Q}_{LHX} = 0.8(-146.7)$$
 $\dot{Q}_{LHX} = 25.17 \text{ kW}$

The thermal exergy rate of the low temperature heat exchanger can be calculated as

$$\dot{E}x_{th,LHX} = \left(1 - \frac{291.2}{293.9}\right) 25.17 = 0.2329 \; kW$$

The exergy flow rates in states 3, 14, 15, and 19 of the low temperature heat exchanger are calculated as

$$\begin{split} &\dot{E}x_3 = 0.8((-146.7 - (-150)) - 291.2(0.1532 - 0.1034)) = -8.88 \text{ kW} \\ &\dot{E}x_{19} = 0.8((-178.1 - (-150)) - 291.2(0.04481 - 0.1034)) = -8.811 \text{ kW} \\ &\dot{E}x_{14} = 0.7139((-91.24 - (-102.5)) - 291.2(0.2642 - 0.1906)) = -7.272 \text{ kW} \\ &\dot{E}x_{15} = 0.7139((-126.5 - (-102.5)) - 291.2(0.1433 - 0.1906)) = -7.326 \text{ kW} \end{split}$$

The exergy destruction rate in the low temperature heat exchanger is calculated as

$$-8.811 + 0.2329 = -8.88 + \dot{E}x_{dest,LHX}$$

 $\dot{E}x_{dest,LHX} = 0.302 \text{ kW}$

It is assumed that 20 % of the flow rate from state 3 is supplied to state 21 and remaining 80 % is supplied to the medium temperature heat exchanger at state 20. The temperature, pressure, and strong solution concentration remains same at states 3, 20 and 21.

$$h_{20} = h_3$$

 $s_{20} = s_3$
 $T_{20} = T_3$
 $h_{21} = h_3$
 $s_{21} = s_3$
 $T_{21} = T_3$

The mass balance equations for the medium temperature heat exchanger are written as

$$\dot{m}_{21} = 0.2(\dot{m}_3) = 0.16 \text{ kg/s}$$
 $\dot{m}_{20} = 0.8(\dot{m}_3) = 0.64 \text{ kg/s}$
 $\dot{m}_{24} = \dot{m}_{20}$
 $\dot{m}_{13} = \dot{m}_{33}$

The temperature of the strong solution leaving the medium temperature heat exchanger is assumed to be 7 °C higher than the inlet temperature.

$$P_{24} = P_2 x_{24} = x_2 T_{24} = T_{20} + 7$$

$$h_{24} = -115.3 \text{ kJ/kg} x_{24} = 0.2587 \text{ kJ/kg K}$$

The energy balance equation of the medium temperature heat exchanger can be written as

$$\dot{m}_{20}h_{20} + \dot{m}_{33}h_{33} = \dot{m}_{13}h_{13} + \dot{m}_{24}h_{24}$$

$$0.64(-146.7) + 0.4569(-59.43) = 0.4569(h_{13}) + 0.64(-115.3)$$

$$h_{13} = -103.4 \text{ kJ/kg}$$

Using the specific enthalpy at state 13 calculated with the energy balance equation and knowing the pressure and weak solution concentration, one can find the specific entropy and temperature at state 13 as follows:

$$P_{13} = P_2 x_{13} = x_{38} h_{13} = -103.4$$

$$T_{13} = 293.1 \text{ K} s_{13} = 0.2229 \text{ kJ/kg K}$$

The rate of heat transfer taking place inside the medium temperature heat exchanger can be calculated as

$$\dot{m}_{20}h_{20} + \dot{Q}_{\text{MHX}} = \dot{m}_{24}h_{24}$$

$$0.64(-146.7) + \dot{Q}_{\text{MHX}} = 0.64(-115.3)$$
 $\dot{Q}_{\text{MHX}} = 20.09 \text{ kW}$

The thermal exergy rate of the medium temperature heat exchanger can be calculated as

$$\dot{E}x_{th,MHX} = \left(1 - \frac{291.2}{300.9}\right) 20.09 = 0.6489 \text{ kW}$$

The exergy flow rates in states 20, 24, 13, and 33 of the medium temperature heat exchanger are calculated as

$$\begin{split} &\dot{E}x_{20} = 0.64((-146.7 - (-150)) - 291.2(0.1532 - 0.1034)) = -7.104 \text{ kW} \\ &\dot{E}x_{24} = 0.64((-115.3 - (-150)) - 291.2(0.2587 - 0.1034)) = -6.685 \text{ kW} \\ &\dot{E}x_{13} = 0.4569((-103.4 - (-102.5)) - 291.2(0.2229 - 0.1906)) = -4.717 \text{ kW} \\ &\dot{E}x_{33} = 0.4569((-59.43 - (-102.5)) - 291.2(0.3704 - 0.1906)) = -4.248 \text{ kW} \end{split}$$

The exergy destruction rate in the medium temperature heat exchanger is calculated as

$$-7.104 + 0.6489 = -6.685 + \dot{E}x_{dest,MHX}$$

 $\dot{E}x_{dest,MHX} = 0.2298 \text{ kW}$

It is assumed that 20 % of the flow rate from state 24 is supplied to state 26 and remaining 80 % is supplied to the high temperature heat exchanger at state 25. The temperature, pressure, and strong solution concentration remains same in states 24, 25, and 26.

$$h_{25} = h_{24}$$
 $s_{25} = s_{24}$
 $T_{25} = T_{24}$
 $h_{26} = h_{24}$
 $s_{26} = s_{24}$
 $T_{26} = T_{24}$

The mass balance equations for the high temperature heat exchanger are written as

$$\dot{m}_{26} = 0.2(\dot{m}_{24}) = 0.128 \text{ kg/s}$$
 $\dot{m}_{25} = 0.8(\dot{m}_{24}) = 0.512 \text{ kg/s}$
 $\dot{m}_{29} = \dot{m}_{25}$
 $\dot{m}_{32} = \dot{m}_{41}$

The temperature of the strong solution leaving the high temperature heat exchanger is assumed to be 7 °C higher than the inlet temperature:

$$\left. \begin{array}{l} P_{29} = P_2 \\ x_{29} = x_2 \\ T_{29} = T_{25} + 7 \end{array} \right\} \quad \left. \begin{array}{l} h_{29} = -83.87 \text{ kJ/kg} \\ s_{29} = 0.3618 \text{ kJ/kg K} \end{array} \right.$$

The energy balance equation of the high temperature heat exchanger can be written as

$$\dot{m}_{25}h_{25} + \dot{m}_{41}h_{41} = \dot{m}_{29}h_{29} + \dot{m}_{32}h_{32}$$

$$0.512(-115.3) + 0.3655(-20.45) = 0.3655(h_{32}) + 0.512(-83.87)$$

$$h_{32} = -64.42 \text{ kJ/kg}$$

Using the specific enthalpy at state 32 calculated with the energy balance equation and knowing the pressure and weak solution concentration, one can find the specific entropy and temperature at state 32 as follows:

$$\left. \begin{array}{l} P_{32} = P_2 \\ x_{32} = x_{38} \\ h_{32} = -64.42 \end{array} \right\} \quad \begin{array}{l} T_{32} = 302.1 \text{ K} \\ s_{32} = 0.3539 \text{ kJ/kg K} \end{array}$$

The rate of heat transfer taking place inside the high temperature heat exchanger can be calculated as

$$\dot{m}_{25}h_{25} + \dot{Q}_{HHX} = \dot{m}_{29}h_{29}$$

$$0.512(-115.3) + \dot{Q}_{HHX} = 0.512(-83.87)$$
 $\dot{Q}_{HHX} = 16.07 \text{ kW}$

The thermal exergy rate of the high temperature heat exchanger can be calculated as

$$\dot{E}x_{th,HHX} = \left(1 - \frac{291.2}{307.9}\right) 16.07 = 0.8726 \; kW$$

The exergy flow rates in states 25, 29, 32, and 41 of the high temperature heat exchanger are calculated as

$$\begin{split} &\dot{E}x_{25} = 0.512((-115.3 - (-150)) - 291.2(0.2587 - 0.1034)) = -5.348 \text{ kW} \\ &\dot{E}x_{29} = 0.512((-83.87 - (-150)) - 291.2(0.3618 - 0.1034)) = -4.651 \text{ kW} \\ &\dot{E}x_{32} = 0.3655((-64.42 - (-102.5)) - 291.2(0.3539 - 0.1906)) = -3.468 \text{ kW} \\ &\dot{E}x_{41} = 0.3655((-20.45 - (-102.5)) - 291.2(0.497 - 0.1906)) = -2.631 \text{ kW} \end{split}$$

The exergy destruction rate in the high temperature heat exchanger is calculated as

$$-5.348 + 0.8726 = -4.651 + \dot{E}x_{dest,HHX}$$

 $\dot{E}x_{dest\;HHX} = 0.1754\;kW$

It is assumed that 20 % of the flow rate from state 29 is supplied to state 34 and remaining 80 % is supplied to the very high temperature heat exchanger at state 35.

The temperature, pressure, and strong solution concentration remains same in states 29, 34, and 35.

$$h_{34} = h_{29}$$
 $s_{34} = s_{29}$
 $T_{34} = T_{29}$
 $h_{35} = h_{29}$
 $s_{35} = s_{29}$
 $T_{35} = T_{29}$

The mass balance equations for the very high temperature heat exchanger are written as

$$\dot{m}_{34} = 0.2(\dot{m}_{29}) = 0.1024 \text{ kg/s}$$
 $\dot{m}_{35} = 0.8(\dot{m}_{29}) = 0.4096 \text{ kg/s}$
 $\dot{m}_{35} = \dot{m}_{36}$
 $\dot{m}_{40} = \dot{m}_{38}$

The temperature of the strong solution leaving the very high temperature heat exchanger is assumed to be 7 °C higher than the inlet temperature.

$$P_{36} = P_2 x_{36} = x_2 T_{36} = T_{35} + 7$$

$$h_{36} = -52.42 \text{ kJ/kg K} s_{36} = 0.4628 \text{ kJ/kg K}$$

The energy balance equation of the very high temperature heat exchanger can be written as

$$\begin{split} \dot{m}_{35}h_{35} + \dot{m}_{38}h_{38} &= \dot{m}_{36}h_{36} + \dot{m}_{40}h_{40} \\ 0.4096(-83.87) + 0.2924(20.82) &= 0.2924(h_{40}) + 0.4096(-52.42) \\ h_{40} &= -23.23 \text{ kJ/kg} \end{split}$$

Using the specific enthalpy at state 40 calculated with the energy balance equation and knowing the pressure and weak solution concentration one can find the specific entropy and temperature at state 40 as follows:

$$\left. \begin{array}{l}
 P_{40} = P_2 \\
 x_{40} = x_{38} \\
 h_{40} = -23.23
 \end{array} \right\} \qquad T_{40} = 311.7 \text{ K} \\
 s_{40} = 0.4881 \text{ kJ/kg K}$$

The rate of heat transfer taking place inside the very high temperature heat exchanger can be calculated as

$$\dot{m}_{35}h_{35} + \dot{Q}_{VHHX} = \dot{m}_{36}h_{36}$$
 $0.4096(-83.87) + \dot{Q}_{VHHX} = 0.4096(-52.42)$
 $\dot{Q}_{VHHX} = 12.88 \text{ kW}$

The thermal exergy rate of the very high temperature heat exchanger can be calculated as

$$\dot{E}x_{th,VHHX} = \left(1 - \frac{291.2}{314.9}\right) 12.88 = 0.9701 \text{ kW}$$

The exergy flow rates in states 35, 36, 38, and 40 of the very high temperature heat exchanger are calculated as

$$\begin{split} &\dot{E}x_{35} = 0.4096((-83.87 - (-150)) - 291.2(0.3618 - 0.1034)) = -3.72 \text{ kW} \\ &\dot{E}x_{36} = 0.4096((-52.42 - (-150)) - 291.2(0.4628 - 0.1034)) = -2.885 \text{ kW} \\ &\dot{E}x_{38} = 0.2924((20.82 - (-102.5)) - 291.2(0.6271 - 0.1906)) = -1.119 \text{ kW} \\ &\dot{E}x_{40} = 0.2924((-23.23 - (-102.5)) - 291.2(0.4881 - 0.1906)) = -2.159 \text{ kW} \end{split}$$

The exergy destruction rate in the very high temperature heat exchanger is calculated as

$$-3.72 + 0.9701 = -2.885 + \dot{E}x_{dest,VHHX}$$

 $\dot{E}x_{dest,VHHX} = 0.1343 \text{ kW}$

The mass balance equations of the very high temperature generator are written as

$$\dot{m}_{36} = \dot{m}_{37} + \dot{m}_{38}$$

$$\dot{m}_{36}x_{36} = \dot{m}_{37}x_{37} + \dot{m}_{38}x_{38}$$

$$0.4096 = \dot{m}_{37} + \dot{m}_{38}$$

$$0.4096(0.5) = \dot{m}_{37}(0.3) + \dot{m}_{38}(0.999)$$

Solving two equations simultaneously gives us

$$\dot{m}_{37} = 0.1172 \text{ kg/s}$$
 and $\dot{m}_{38} = 0.2924 \text{ kg/s}$

The temperature at state 38 is assumed to be 7 $^{\circ}$ C higher than the temperature at state 36.

$$\left. \begin{array}{l} P_{38} = P_2 \\ x_{38} = 0.3 \\ T_{38} = T_{36} + 7 \end{array} \right\} \quad \left. \begin{array}{l} h_{36} = -52.42 \text{ kJ/kg} \\ s_{36} = 0.4628 \text{ kJ/kg K} \end{array} \right.$$

The specific enthalpy at state 37 is calculated using energy balance equation of the very high temperature generator as defined below:

$$\dot{m}_{36}h_{36} + \dot{Q}_{VHTG} = \dot{m}_{37}h_{37} + \dot{m}_{38}h_{38}$$

$$0.4096(-52.42) + 290 = 0.2924(20.82) + 0.1172h_{37}$$
 $h_{37} = 2239 \text{ kJ/kg}$

Using specific enthalpy at state 37 and knowing pressure and concentration in this state, we can find the temperature and specific entropy at state 37 as follows:

$$\left. \begin{array}{l}
 P_{37} = P_2 \\
 x_{37} = 0.999 \\
 h_{37} = 2239 \text{ kJ/kg}
 \end{array} \right\} \quad \begin{array}{l}
 T_{37} = 659 \text{ K} \\
 s_{37} = 6.586 \text{ kJ/kg K}
 \end{array}$$

$$\dot{E}x_{37} = 0.1172[(2239 - 87.15) - 291.2(6.586 - 0.2708)] = 36.72 \text{ kW}$$

The thermal exergy rate of the very high temperature generator can be calculated by using average temperature as

$$\dot{E}x_{th,VHTG} = \left(1 - \frac{291.2}{432}\right) 290 = 94.5 \; kW$$

Using the thermal exergy rate and rate of exergy at each state, we can find the total exergy destruction rate of the very high temperature generator as

$$-2.885 + 94.5 = 36.72 - 1.119 + \dot{E}x_{dest,VHTG}$$

 $\dot{E}x_{dest,VHTG} = 56.01 \text{ kW}$

The mass flow rates of the different streams entering and leaving the high temperature generator are calculated as

$$\dot{m}_{28} = \dot{m}_{37} = 0.1172 \text{ kg/s}
\dot{m}_{34} = \dot{m}_{30} + \dot{m}_{31}
\dot{m}_{34}x_{34} = \dot{m}_{30}x_{30} + \dot{m}_{31}x_{31}
0.1024 = \dot{m}_{30} + \dot{m}_{31}
0.1024(0.5) = \dot{m}_{30}(0.3) + \dot{m}_{31}(0.999)$$

Solving two equations simultaneously gives us

$$\dot{m}_{30} = 0.0731 \text{ kg/s}$$
 and $\dot{m}_{31} = 0.0293 \text{ kg/s}$

The temperature at state 30 is assumed to be 7 $^{\circ}$ C higher than the temperature at state 34.

$$P_{30} = P_2 x_{30} = x_{38} T_{30} = T_{34} + 7$$
 $h_{30} = -9.329 \text{ kJ/kg K}$

It is assumed that ammonia vapor at state 31 leaves with the same temperature as that of state 30.

$$\left.\begin{array}{l}
 P_{31} = P_2 \\
 x_{31} = x_{37} \\
 T_{31} = T_{30}
 \end{array}\right\}$$
 $\left.\begin{array}{l}
 h_{31} = 1356 \text{ kJ/kg} \\
 s_{31} = 4.711 \text{ kJ/kg K}
 \end{array}\right.$

The specific enthalpy at state 28 is calculated using energy balance equation of the high temperature generator as defined below:

$$\dot{m}_{34}h_{34} + \dot{m}_{37}h_{37} = \dot{m}_{30}h_{30} + \dot{m}_{31}h_{31} + \dot{m}_{28}h_{28}$$

 $0.1024(-83.87) + 0.1172(2239) = 0.0731(-9.329) + 0.0293(1356) + 0.1172h_{28}$
 $h_{28} = 1833 \text{ kJ/kg}$

Using specific enthalpy at state 28 and knowing pressure and concentration in this state, we can find the temperature and specific entropy at state 28 as follows:

$$\left. \begin{array}{l} P_{28} = P_2 \\ x_{28} = x_{37} \\ h_{28} = 1833 \text{ kJ/kg} \end{array} \right\} \quad \begin{array}{l} T_{28} = 509.3 \text{ K} \\ s_{28} = 5.888 \text{ kJ/kg K} \end{array}$$

The exergy rate at states 34, 30, 31, and 28 are found as

$$\begin{split} &\dot{E}x_{34} = 0.1024((-83.87 - (-150)) - 291.2(0.3618 - 0.1034)) = -0.9301 \text{ kW} \\ &\dot{E}x_{28} = 0.1172[(1833 - 87.15) - 291.2(5.888 - 0.2708)] = 12.89 \text{ kW} \\ &\dot{E}x_{30} = 0.0731((-9.329 - (-102.5)) - 291.2(0.5325 - 0.1906)) = -0.468 \text{ kW} \\ &\dot{E}x_{31} = 0.0293((11356 - (87.15)) - 291.2(4.711 - 0.2708)) = -0.7019 \text{ kW} \end{split}$$

Using the rate of exergy at each state, we can find the total exergy destruction rate of the high temperature generator as

$$-0.9301 + 36.72 = 12.89 - 0.468 - 0.7019 + \dot{E}x_{dest,HTG}$$

 $\dot{E}x_{dest,HTG} = 24.07 \text{ kW}$

The ammonia vapor leaving the high temperature generator at states 28 and 31 are combined to leave at state 39

$$\dot{m}_{39} = \dot{m}_{28} + \dot{m}_{31} = 0.1172 + 0.0293 = 0.1465$$
 $\dot{m}_{39}h_{39} = \dot{m}_{28}h_{28} + \dot{m}_{31}h_{31}$
 $0.1465h_{39} = 0.1172(1833) + 0.0293(1356)$
 $h_{39} = 1737 \text{ kJ/kg}$

Using the specific enthalpy at state 39 and knowing the concentration and pressure, we can find the temperature and specific enthalpy at state 39 as follows:

$$P_{39} = P_2$$

 $x_{39} = x_{37}$
 $h_{39} = 1737 \text{ kJ/kg}$

$$T_{39} = 471.4 \text{ K}$$

 $s_{39} = 5.693 \text{ kJ/kg K}$

The exergy rate at state 39 can then be calculated as

$$\dot{E}x_{39} = 0.1831[(1737 - 87.15) - 291.2(5.693 - 0.2708)] = 10.45 \text{ kW}$$

The mass flow rates of the different streams entering and leaving the medium temperature generator are calculated as

$$\dot{m}_4 = \dot{m}_{39} = 0.1465 \text{ kg/s}$$

$$\dot{m}_{26} = \dot{m}_{12} + \dot{m}_{27}$$

$$\dot{m}_{26}x_{26} = \dot{m}_{12}x_{12} + \dot{m}_{27}x_{27}$$

$$0.128 = \dot{m}_{12} + \dot{m}_{27}$$

$$0.128(0.5) = \dot{m}_{12}(0.3) + \dot{m}_{27}(0.999)$$

Solving two equations simultaneously gives us

$$\dot{m}_{12} = 0.09138 \text{ kg/s}$$
 and $\dot{m}_{27} = 0.03662 \text{ kg/s}$

The temperature at state 12 is assumed to be 7 $^{\circ}$ C higher than the temperature at state 26.

$$\left. \begin{array}{l} P_{12} = P_2 \\ x_{12} = x_{38} \\ T_{12} = T_{26} + 7 \end{array} \right\} \quad \begin{array}{l} h_{12} = -39.46 \text{ kJ/kg} \\ s_{12} = 0.4357 \text{ kJ/kg K} \end{array}$$

It is assumed that ammonia vapor at state 27 leaves with the same temperature as that of state 12.

$$\left. egin{array}{l} P_{27} = P_2 \\ x_{27} = x_{37} \\ T_{27} = T_{12} \end{array}
ight\} \quad \left. egin{array}{l} h_{27} = 1338 \ \mathrm{kJ/kg} \\ s_{27} = 4.654 \ \mathrm{kJ/kg} \ \mathrm{K} \end{array}
ight.$$

The specific enthalpy at state 4 is calculated using energy balance equation of the medium temperature generator as defined below

$$\begin{split} \dot{m}_{26}h_{26} + \dot{m}_{39}h_{39} &= \dot{m}_{12}h_{12} + \dot{m}_{27}h_{27} + \dot{m}_4h_4 \\ 0.128(-115.3) + 0.1465(1737) &= 0.09138(-39.46) + 0.03662(1338) + 0.1465h_4 \\ h_4 &= 1327 \text{ kJ/kg} \end{split}$$

Using specific enthalpy at state 4 and knowing pressure and concentration in this state, we can find the temperature and specific entropy at state 4 as follows:

$$P_4 = P_2 x_4 = x_{37} h_4 = 1327 \text{ kJ/kg}$$

$$T_4 = 303.8 \text{ K} s_4 = 4.617 \text{ kJ/kg K}$$

The exergy rate at states 26, 12, 4, and 27 are found as

$$\begin{split} \dot{E}x_4 &= 0.1465[(1327-87.15)-291.2(4.617-0.2708)] = -3.782 \text{ kW} \\ \dot{E}x_{26} &= 0.128((-115.3-(-150))-291.2(0.2587-0.1034)) = -1.337 \text{ kW} \\ \dot{E}x_{12} &= 0.09138((-39.46-(-102.5))-291.2(0.4357-0.1906)) = -0.7636 \text{ kW} \\ \dot{E}x_{27} &= 0.03662((1338-(87.15))-291.2(4.654-0.2708)) = -0.9232 \text{ kW} \end{split}$$

Using the rate of exergy at each state, we can find the total exergy destruction rate of the medium temperature generator as

$$-1.337 + 10.45 = -3.782 - 0.7636 - 0.9232 + \dot{E}x_{dest,MTG}$$

 $\dot{E}x_{dest,MTG} = 14.58 \text{ kW}$

The ammonia vapor leaving the medium temperature generator at states 4 and 27 are combined to leave at state 5

$$\dot{m}_5 = \dot{m}_4 + \dot{m}_{27} = 0.1465 + 0.03662 = 0.1831 \text{ kg/s}$$

$$\dot{m}_5 h_5 = \dot{m}_4 h_4 + \dot{m}_{27} h_{27}$$

$$0.1831 h_5 = 0.1465(1327) + 0.03662(1338)$$

$$h_5 = 1329 \text{ kJ/kg}$$

Using the specific enthalpy at state 5 and knowing the concentration and pressure, we can find the temperature and specific enthalpy at state 5 as follows:

$$P_5 = P_2 x_5 = x_{37} h_5 = 1329 \text{ kJ/kg}$$

$$T_5 = 304.5 \text{ K} s_5 = 4.624 \text{ kJ/kg K}$$

The exergy rate at state 5 can then be calculated as

$$\dot{E}x_5 = 0.1831[(1329 - 87.15) - 291.2(4.624 - 0.2708)] = -4.708 \text{ kW}$$

The mass flow rates of the different streams entering and leaving the low temperature generator are calculated as

$$\dot{m}_6 = \dot{m}_5 = 0.1831 \text{ kg/s}$$

$$\dot{m}_{22} = \dot{m}_{23} + \dot{m}_7$$

$$\dot{m}_{22}x_{22} = \dot{m}_{23}x_{23} + \dot{m}_7x_7$$

$$0.36 = \dot{m}_{23} + \dot{m}_7$$

$$0.36(0.5) = \dot{m}_{23}(0.3) + \dot{m}_7(0.999)$$

Solving two equations simultaneously gives us

$$\dot{m}_{23} = 0.257 \text{ kg/s}$$
 and $\dot{m}_7 = 0.103 \text{ kg/s}$
 $\dot{m}_{22} = \dot{m}_{21} + \dot{m}_{18} = 0.16 + 0.2 = 0.36 \text{ kg/s}$
 $\dot{m}_{22}h_{22} = \dot{m}_{21}h_{21} + \dot{m}_{18}h_{18}$
 $0.36h_{22} = 0.16(-146.7) + 0.2(-146.7)$
 $h_{22} = -146.7 \text{ kJ/kg}$

Using the specific enthalpy at state 22 and knowing the concentration and pressure, we can find the temperature and specific enthalpy at state 22 as follows:

$$\begin{array}{l} P_{22} = P_2 \\ x_{22} = x_{26} \\ h_{22} = -146.7 \text{ kJ/kg} \end{array} \right\} \quad \begin{array}{l} T_{22} = 293.9 \text{ K} \\ s_{22} = 0.1532 \text{ kJ/kg K} \end{array}$$

The temperature at state 23 is assumed to be 7 °C higher than the temperature at state 22.

$$P_{23} = P_2 x_{23} = x_{38} T_{23} = T_{22} + 7$$

$$h_{23} = -69.61 \text{ kJ/kg K} s_{23} = 0.3366 \text{ kJ/kg K}$$

It is assumed that ammonia vapor at state 7 leaves with the same temperature as that of state 23.

$$P_7 = P_2$$

 $x_7 = x_{37}$
 $T_7 = T_{23}$
 $h_7 = 1318 \text{ kJ/kg}$
 $s_7 = 4.587 \text{ kJ/kg K}$

The specific enthalpy at state 6 is calculated using energy balance equation of the low temperature generator as defined below

$$\dot{m}_{22}h_{22} + \dot{m}_5h_5 = \dot{m}_{23}h_{23} + \dot{m}_7h_7 + \dot{m}_6h_6$$

$$0.36(-146.7) + 0.1831(1329) = 0.257(-69.61) + 0.103(1318) + 0.1831h_6$$

$$h_6 = 397.2 \text{ kJ/kg}$$

Using specific enthalpy at state 6 and knowing pressure and concentration in this state, we can find the temperature and specific entropy at state 6 as follows:

$$\left. \begin{array}{l}
 P_6 = P_2 \\
 x_6 = x_{37} \\
 h_6 = 397.2 \text{ kJ/kg}
 \end{array} \right\} \quad \begin{array}{l}
 T_6 = 287 \text{ K} \\
 s_6 = 1.399 \text{ kJ/kg K}
 \end{array}$$

The exergy rate at states 22, 23, 6, and 7 are found as

$$\begin{split} \dot{E}x_6 &= 0.1831[(397.2 - 87.15) - 291.2(1.399 - 0.2708)] = -3.377 \text{ kW} \\ \dot{E}x_7 &= 0.103((1318 - (87.15)) - 291.2(4.587 - 0.2708)) = -2.7 \text{ kW} \\ \dot{E}x_{22} &= 0.36((-146.7 - (-150)) - 291.2(0.1532 - 0.1034)) = -3.996 \text{ kW} \\ \dot{E}x_{23} &= 0.257((-69.61 - (-102.5)) - 291.2(0.3366 - 0.1906)) = -2.484 \text{ kW} \end{split}$$

The rate of heat transfer taking place inside the low temperature generator can be calculated as

$$\dot{m}_5 h_5 + \dot{Q}_{LTG} = \dot{m}_6 h_6$$

$$0.1831(1329) + \dot{Q}_{LTG} = 0.1831(397.2)$$
 $\dot{Q}_{LTG} = 170.6 \text{ kW}$

The thermal exergy rate of the low temperature generator can be calculated as

$$\dot{E}x_{th,LTG} = \left(1 - \frac{291.2}{304.5}\right)170.6 = 7.459 \text{ kW}$$

The total exergy destruction rate of the low temperature generator can be calculated as

$$-3.996 + 7.459 = -2.484 - 2.7 + \dot{E}x_{dest,LTG}$$

 $\dot{E}x_{dest,LTG} = 8.647 \text{ kW}$

The mass flow rates of the different streams entering and leaving the condenser heat exchanger are calculated as

$$\dot{m}_{18} = \dot{m}_{17} = 0.2 \text{ kg/s}$$

 $\dot{m}_8 = \dot{m}_7 = 0.103 \text{ kg/s}$

The temperature at state 18 is assumed to be 7 °C higher than the temperature at state 17.

$$\left. \begin{array}{l} P_{18} = P_2 \\ x_{18} = x_{36} \\ T_{18} = T_{17} + 7 \end{array} \right\} \quad \begin{array}{l} h_{18} = -146.7 \text{ kJ/kg} \\ s_{18} = 0.1532 \text{ kJ/kg K} \end{array}$$

The specific enthalpy at state 8 is calculated using energy balance equation of the condenser heat exchanger as defined below

$$\dot{m}_{17}h_{17} + \dot{m}_7h_7 = \dot{m}_8h_8 + \dot{m}_{18}h_{18}$$

$$0.2(-178.1) + 0.103(1318) = 0.103(h_8) + 0.2(-146.7)$$

$$h_8 = 1257 \text{ kJ/kg}$$

Using specific enthalpy at state 8 and knowing pressure and concentration in this state, we can find the temperature and specific entropy at state 8 as follows:

$$\left. \begin{array}{l}
 P_8 = P_2 \\
 x_8 = x_{37} \\
 h_8 = 1257 \text{ kJ/kg}
 \end{array} \right\} \quad T_8 = 288.2 \text{ K} \\
 s_8 = 4.38 \text{ kJ/kg K}$$

The rate of exergy at states 8 and 17 are calculated as

$$\begin{split} \dot{E}x_8 &= 0.103[(1257-87.15)-291.2(4.38-0.2708)] = -2.779 \; kW \\ \dot{E}x_{17} &= 0.2((-178.1-(-150))-291.2(0.04481-0.1034)) = -2.203 \; kW \end{split}$$

The rate of heat transfer taking place inside the condenser heat exchanger can be calculated as

$$\dot{m}_{17}h_{17} + \dot{Q}_{\text{CHX}} = \dot{m}_{18}h_{18}$$

$$0.2(-178.1) + \dot{Q}_{\text{CHX}} = 0.2(-146.7)$$
 $\dot{Q}_{\text{CHX}} = 6.294 \text{ kW}$

The thermal exergy rate of the condenser heat exchanger can be calculated as

$$\dot{E}x_{th,CHX} = \left(1 - \frac{291.2}{293.9}\right) 6.294 = 0.4782 \; kW$$

The total exergy destruction rate of the condenser heat exchanger can be calculated as

$$-2.203 + 0.4782 = -2.22 + \dot{E}x_{dest,CHX}$$

 $\dot{E}x_{dest,CHX} = 0.2614 \text{ kW}$

The mass balance equation of the condenser can be written as

$$\dot{m}_6 + \dot{m}_8 = \dot{m}_9$$

$$\dot{m}_9 = 0.1831 + 0.103 = 0.2861$$

The energy balance equation of the condenser capable of rejecting 200 kW of heat is written as

$$\dot{m}_8 h_8 + \dot{m}_6 h_6 = \dot{m}_9 h_9 + \dot{Q}_c$$

The equation mentioned above is used to calculate the specific enthalpy at state 9 as

$$0.103(1257) + 0.1831(397.2) = 0.2861h_9 + 290$$

 $h_9 = -306.9 \text{ kJ/kg}$

$$P_9 = P_2 x_9 = x_{31} h_9 = -306.9 \text{ kJ/kg}$$

$$T_9 = 204.6 \text{ K} s_9 = -1.278 \text{ kJ/kg K}$$

$$\dot{E}x_9 = 0.2861[(-306.9 - 87.15) - 291.2(-1.278 - 0.2708)] = 16.32 \text{ kW}$$

The thermal exergy rate of the condenser can be calculated as

$$\dot{E}x_{th,c} = \bigg(1 - \frac{291.2}{204.6}\bigg)290 = -122.7 \; kW$$

Using the exergy rate at each state and thermal rate of exergy, we can find the exergy destruction rate in the condenser as

$$-3.377 - 2.779 = 16.32 - 122.7 + \dot{E}x_{dest,c}$$

 $\dot{E}x_{dest,c} = 100.3 \text{ kW}$

The mass balance equation of the refrigerant expansion valve is written as

$$\dot{m}_{10} = \dot{m}_9 = 0.2861 \text{ kg/s}$$

$$\left. \begin{array}{l}
 h_{10} = h_9 \\
 P_{10} = P_1 \\
 x_{10} = x_{37}
 \end{array} \right\} \qquad T_{10} = 204.7 \text{ K} \\
 s_{10} = -1.275 \text{ kJ/kg K}$$

$$\begin{split} \dot{E}x_{10} &= 0.2861[(-306.9 - 87.15) + 291.2(-1.275 - 0.2708)] = 16.03 \text{ kW} \\ 16.32 &= 16.03 + \dot{E}x_{dest,evr} \end{split}$$

 $\dot{\mathbf{E}}\mathbf{x}_{\text{dest.evr}} = 0.29 \text{ kW}$

The mass balance equation of the evaporator is written as

$$\dot{m}_{11} = \dot{m}_{10} = 0.2861 \text{ kg/s}$$

It is assumed that the refrigerant leaves the evaporator at a temperature of 259.7 K.

$$\begin{array}{l} P_{11} = P_9 \\ x_{11} = x_{31} \\ T_{11} = 259.7 \text{ K} \end{array} \right\} \quad \begin{array}{l} h_{11} = 1251 \text{ kJ/kg} \\ s_{11} = 4.922 \text{ kJ/kg K} \end{array}$$

The energy balance equation to calculated the cooling load is defined as

$$\dot{m}_{10}h_{10} + \dot{Q}_{e} = \dot{m}_{11}h_{11}$$

$$0.2861(-306.9) + \dot{Q}_{e} = 0.2861(1251)$$

$$\dot{\mathbf{Q}}_{e} = \mathbf{445.7 \ kW}$$

$$\dot{E}x_{11} = 0.2861[(1251 - 87.15) + 291.2(4.922 - 0.2708)] = -54.52 \text{ kW}$$

The thermal exergy rate of the evaporator is calculated as

$$\begin{split} \dot{E}x_{th,e} &= \left| \left(1 - \frac{291.2}{232.2} \right) 445.7 \right| = 90.32 \; kW \\ 16.03 + 90.32 &= -54.52 + \dot{E}x_{dest,e} \\ \dot{E}x_{dest,e} &= 160.9 \; kW \end{split}$$

The mass balance equation of the weak solution expansion valve is written as

$$\dot{m}_{16} = \dot{m}_{15} = 0.7139 \text{ kg/s}$$

$$h_{16} = h_{15}$$

$$P_{16} = P_1$$

$$x_{16} = x_{38}$$

$$T_{16} = 287.9 \text{ K}$$

$$s_{16} = 0.1453 \text{ kJ/kg K}$$

$$\dot{E}x_{16} = 0.7139((-126.5 - (-102.5)) + 291.2(0.1453 - 0.1906)) = -7.728 \text{ kW}$$

The exergy destruction rate of the weak solution expansion valve is calculated as

$$-7.326 = -7.728 + \dot{E}x_{dest,evs}$$
$$\dot{E}x_{dest,evs} = 0.4 \text{ kW}$$

The mass balance equation of the absorber is written as

$$\dot{m}_1 = \dot{m}_{11} + \dot{m}_{16}$$

The amount of heat rejected by the absorber is calculated using formula

$$\dot{m}_1 h_1 + \dot{Q}_a = \dot{m}_{11} h_{11} + \dot{m}_{16} h_{16}$$

$$1(-180.1) + \dot{Q}_a = 0.2861(1251) + 0.7139(-126.5)$$

$$\dot{Q}_a = 447.7 \text{ kW}$$

The thermal exergy rate of the absorber is calculated as

$$\dot{E}x_{th,a} = \left(1 - \frac{291.2}{259.7}\right)447.7 = -54.4 \text{ kW}$$

The rate of exergy destroyed by the absorber is calculated as

$$-54.52 - 7.728 = -11.62 - 54.4 + \dot{E}x_{dest,a}$$

 $\dot{E}x_{dest,a} = 3.765 \text{ kW}$

The weak solutions at states 30 and 40 are mixed to leave at state 41. The mass balance equation of this mixing process is then written as

$$\dot{m}_{41} = \dot{m}_{30} + \dot{m}_{40}$$

 $\dot{m}_{41} = 0.0731 + 0.2924 = 0.3655 \text{ kg/s}$

The energy balance equation of the mixing process is written as

$$\begin{aligned} \dot{m}_{41}h_{41} &= \dot{m}_{30}h_{30} + \dot{m}_{40}h_{40} \\ 0.3655h_{41} &= 0.0731(-9.329) + 0.2924(-23.23) \\ h_{41} &= -20.45 \text{ kJ/kg} \\ h_{41} &= -20.45 \text{ kJ/kg} \\ P_{41} &= P_2 \\ x_{41} &= x_{38} \end{aligned}$$

$$T_{41} = 312.3 \text{ K} \\ s_{41} &= 0.497 \text{ kJ/kg K}$$

$$\dot{E}x_{41} = 0.3655((-20.45 - (-102.5)) + 291.2(0.497 - 0.1906)) = -2.631 \text{ kW}$$

The weak solutions at states 12 and 32 are mixed to leave at state 33. The mass balance equation of this mixing process is written as

$$\dot{m}_{33} = \dot{m}_{12} + \dot{m}_{32}$$

 $\dot{m}_{33} = 0.09138 + 0.3655 = 0.4569 \text{ kg/s}$

The energy balance equation of the mixing process is written as

$$\dot{m}_{33}h_{33} = \dot{m}_{12}h_{12} + \dot{m}_{32}h_{32}$$

$$0.4569h_{33} = 0.09138(-39.46) + 0.3655(-64.42)$$

$$h_{33} = -59.43 \text{ kJ/kg}$$

$$\left. \begin{array}{l} h_{33} = -59.43 \text{ kJ/kg} \\ P_{33} = P_2 \\ x_{33} = x_{38} \end{array} \right\} \quad \begin{array}{l} T_{33} = 303.3 \text{ K} \\ s_{33} = 0.3704 \text{ kJ/kg K} \end{array}$$

$$\dot{E}x_{33} = 0.4569((-59.43 - (-102.5)) + 291.2(0.3704 - 0.1906)) = -4.248 \text{ kW}$$

The weak solution at states 13 and 23 mix to leave at state 14. The mass balance equation of this mixing process is written as

$$\dot{m}_{14} = \dot{m}_{13} + \dot{m}_{23}$$

 $\dot{m}_{14} = 0.4569 + 0.257 = 0.7139 \text{ kg/s}$

The energy balance equation of the mixing process is written as

$$\begin{split} \dot{m}_{14}h_{14} &= \dot{m}_{13}h_{13} + \dot{m}_{23}h_{23} \\ 0.7139h_{14} &= 0.4569(-103.4) + 0.257(-69.61) \\ h_{14} &= -91.24 \text{ kJ/kg} \end{split}$$

$$\left. \begin{array}{l} h_{14} = -91.24 \; \mathrm{kJ/kg} \\ P_{14} = P_2 \\ x_{14} = x_{38} \end{array} \right\} \quad \begin{array}{l} T_{14} = 295.9 \; \mathrm{K} \\ s_{14} = 0.2642 \; \mathrm{kJ/kg} \; \mathrm{K} \end{array}$$

$$\dot{E}x_{14} = 0.7139((-91.24 - (-102.5)) + 291.2(0.2642 - 0.1906)) = -7.272 \text{ kW}$$

The energy and exergy COPs of the QEARS are calculated as

$$\begin{split} COP_{en} &= \frac{445.7}{290 + 1.971} = 1.527 \\ COP_{ex} &= \frac{90.32}{94.5 + 1.368} = 0.9363 \end{split}$$

The equipment cost of the QEARS is found using

$$\dot{Z}_{eq}(\$) = 1144.3(445.7)^{0.67} = \$68,142$$

The operation and maintenance cost of the QEARS are assumed to be 3 $\,\%$ of the equipment cost

$$\dot{C}_{\text{OPM}} = 0.03(68,142) = \$2044$$

The exergetic cost of cooling can then be calculated by using equipment cost, cost of operation and maintenance, and the thermal exergy rate of the evaporator as

$$c_{\text{Cool}} = \frac{68,142 + 2044}{90.32}$$
$$\mathbf{c_{\text{Cool}}} = 777.1 \text{ } \text{/kW}$$

The total rate of exergy entering the QEARS is calculated as

$$\dot{Ex}_{in} = 94.5 + 1.971 + 90.32 = 186.8 \text{ kW}$$

The total rate of exergy exiting the OEARS is calculated as

$$\dot{E}x_{out} = 54.4 + 122.7 = 177.1 \text{ kW}$$

The total rate of exergy destructed by the QEARS is calculated as

$$\dot{E}x_{dest,tot} = 186.8 - 177.1 = 9.644 \text{ kW}$$

The exergoenvironmental impact factor can then be calculated by dividing the total exergy destruction rate by total exergy supplied to the QEARS as

$$f_{\rm ei} = \frac{9.644}{186.8} = 0.05163$$

The exergoenvironmental impact coefficient is calculated by taking inverse of the exergetic COP as

$$C_{\rm ei} = \frac{1}{0.9363} = 1.068$$

The exergoenvironmental impact index is found by multiplying exergoenvironmental impact factor by exergoenvironmental impact factor as

$$\theta_{ei} = 0.05163 \times 1.068 = 0.05514$$

The exergoenvironmental impact improvement is then found by taking inverse of the exergoenvironmental impact index as

$$\theta_{\rm eii} = \frac{1}{0.05514} = 18.13$$

The exergetic stability factor is computed as

$$f_{\rm es} = \frac{177.1}{177.1 + 9.644} = 0.9484$$

The exergetic sustainability index is then calculated by multiplying exergetic stability factor with exergoenvironmental impact improvement as

$$\theta_{\rm est} = 0.9484 \times 18.13 = 17.2$$

The thermophysical properties at each state points of the QEARS are presented in Table 6.1.

Table 6.1 Thermophysical properties at each state points of the QEARS

State point	P (kPa)	T (K)	m (kg/s)	h (kJ/kg)	s (kJ/kg K)
0	100	291.2	_	-150	0.1034
1	200	286.5	1	-180.1	0.04011
2	700	286.9	1	-178.1	0.04481
3	700	293.9	0.8	-146.7	0.1532
4	700	303.8	0.1465	1327	4.617
5	700	304.5	0.1831	1329	4.624
6	700	287	0.1831	397.2	1.399
7	700	300.9	0.103	1318	4.587
8	700	288.2	0.103	1257	4.38
9	700	204.6	0.2861	-306.9	-1.278
10	200	204.7	0.2861	-306.9	-1.275
11	200	259.7	0.2861	1251	4.922
12	700	307.9	0.09138	-39.46	0.4357
13	700	293.1	0.4569	-103.4	0.2229
14	700	295.9	0.7139	-91.24	0.2642
15	700	287.8	0.7139	-126.5	0.1433
16	200	287.9	0.7139	-126.5	0.1453

(continued)

State point	P (kPa)	T (K)	m (kg/s)	h (kJ/kg)	s (kJ/kg K)
17	700	286.9	0.2	-178.1	0.04481
18	700	293.9	0.2	-146.7	0.1532
19	700	286.9	0.8	-178.1	0.04481
20	700	293.9	0.64	-146.7	0.1532
21	700	293.9	0.16	-146.7	0.1532
22	700	293.9	0.36	-146.7	0.1532
23	700	300.9	0.257	-69.61	0.3366
24	700	300.9	0.64	-115.3	0.2587
25	700	300.9	0.512	-115.3	0.2587
26	700	300.9	0.128	-115.3	0.2587
27	700	307.9	0.03662	1338	4.654
28	700	509.3	0.1172	1833	5.888
29	700	307.9	0.512	-83.87	0.3618
30	700	314.9	0.0731	-9.329	0.5325
31	700	314.9	0.0293	1356	4.711
32	700	302.1	0.3655	-64.42	0.3539
33	700	303.3	0.4569	-59.43	0.3704
34	700	307.9	0.1024	-83.87	0.3618
35	700	307.9	0.4096	-83.87	0.3618
36	700	314.9	0.4096	-52.42	0.4628
37	700	659	0.1172	2239	6.586
38	700	321.9	0.2924	20.82	0.6271
39	700	471.4	0.1465	1737	5.693
40	700	311.7	0.2924	-23.23	0.4881
			1	1	

Table 6.1 (continued)

Effects of the high temperature generator load

312.3

700

41

Figure 6.2 shows the impact of variation in very high temperature generator load on the cooling capacity and the cost of cooling of the QEARS. The rate of cooling produced is observed to decrease from 445.7 to 395.7 kW with an increase in very high temperature generator load from 290 to 340 kW. On the other hand, the cost of cooling produced by the QEARS is noted to increase from 777.1 to 1212 USD/kW with an increase in the very high temperature generator load. The cooling capacity is observed to decrease because the increse in the very high temperature generator load results in a higher exiting temperature of the ammonia vapor. This undesirable temperature increase for a particular condenser load results in the relatively higher temperature of the ammonia refrigerant entering the evaporator. As a consequence of this, the temperature difference between the inlet and exit of the evaporator decreases. The temperature difference, as the driving force for the heat transfer, is

0.3655

-20.45

0.497

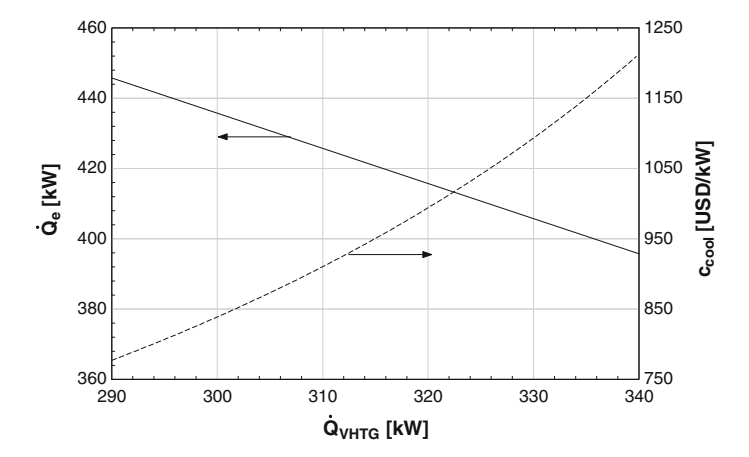


Fig. 6.2 Effects of the very high temperature generator load on cooling load and cost of cooling

critical and hence, smaller temperature difference in the evaporator results in the lower cooling capacity of the evaporator.

The cost of cooling is directly associated with the rate of cooling provided by the QEARS. As the rate of cooling supplied by the QEARS decreases with an increase in the very high temperature generator load, the cost of cooling decreases. The cost of cooling also shows that the QEARS performance degrades economically if an excess amount of energy is provided to the system because this excess energy is not translated into the additional cooling production due to the heat rejection limitations of the condenser. The effects of the rise in very high temperature generator load on the energy and exergy COPs of the QEARS are displayed in Fig. 6.3. The energy

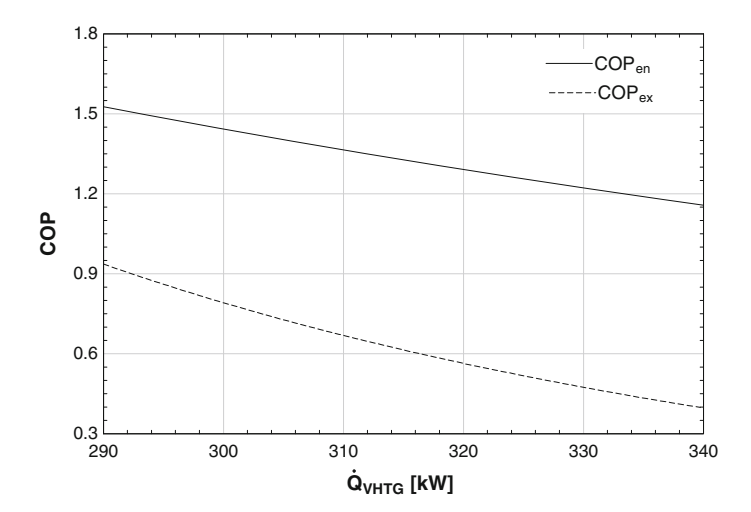


Fig. 6.3 Effects of the very high temperature generator load on energy and exergy COPs

and exergy COPs are observed to decrease from 1.527 to 1.157 and 0.936 to 0.396, respectively, with the rise in the very high temperature generator load from 290 kW to 340 kW. These decreases in the energy and exergy COPs of the quadruple effect absorption refrigeration system speak to the degrading performance of the system with the rise in the very high temperature generator load. The decrease in the cooling capacity with the increase in the very high temperature generator load negatively affects the performance of the system and because of that, both energy and exergy COPs decrease.

• Effects of the strong solution concentration

The concentration of the strong solution plays a vital role in the performance characteristics of any refrigeration system. This parameter defines how much refrigerant can be vaporized and supplied to the evaporator. The effects of the increase in concentration of the strong solution on the rate of cooling production and the cost of cooling are presented in Fig. 6.4. The rate of cooling production is observed to increase from 344.2 to 445.7 kW with the increase in the strong solution concentration from 0.45 to 0.55. However, the cost of cooling production is noticed to be decreasing from 778.3 to 777.1 USD/kW with the rise in the concentration of the strong solution. The increasing trend in the rate of cooling production is because the increase in the strong solution concentration results in a relatively higher amount of ammonia being vaporized from the very high temperature generator. This ammonia refrigerant then enters the evaporator where it can carry the most cooling load from the cooled space due to higher availability of the refrigerant passing through the evaporator. This increase in the cooling rate production for a fixed load also has a positive impact on the cost of cooling production. The increase in the rate of cooling production for the same system size results in

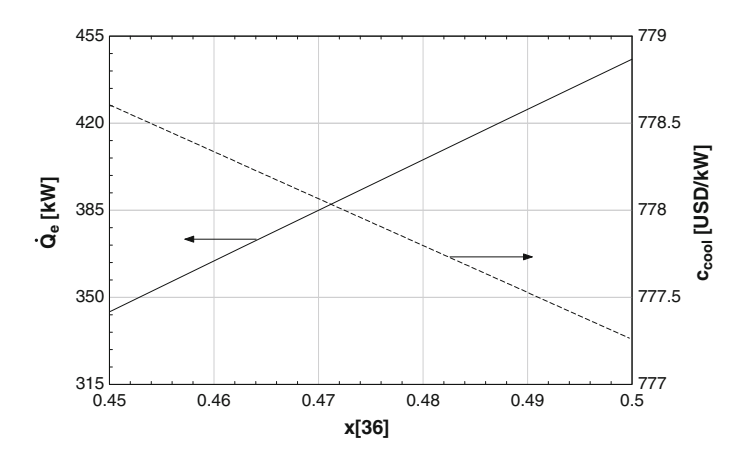


Fig. 6.4 Effects of strong solution concentration on cooling load and cost of cooling

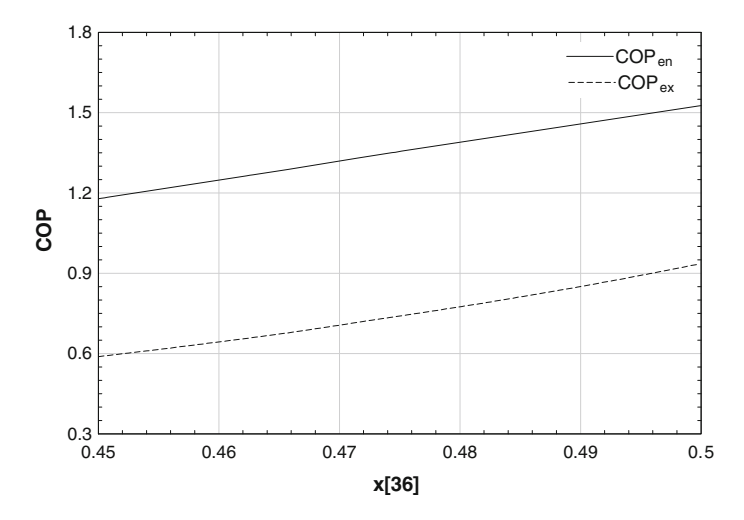


Fig. 6.5 Effects of strong solution concentration on energy and exergy COPs

lower cost of producing cooling, which can be viewed as an achievement for making the absorption refrigeration system more affordable. Moreover, it should also be noted that it is not possible to increase the strong solution concentration to very high levels as doing so might result in hampering system performance. Figure 6.5 displays the effects of the increase in concentration of the strong solution on the energy and exergy COPs of the QEARS. The energy and exergy COPs are noted to increase from 1.178 to 1.527 and 0.589 to 0.936, respectively with the rise in the strong solution concentration. This increasing behavior shows that the performance of the QEARS is indeed enhanced with the increase in the strong solution concentration. The energy and exergy COPs are directly related to the cooling production capacity of the system. As the rate of cooling production by the QEARS increases with the rise in the strong solution concentration for a constant load of very high temperature generator and condenser, the energetic and exergetic performance of the system increases as depicted by both COPs.

• Effects of ambient temperature

The performance of systems such as absorption refrigeration systems that rely mainly on high temperature heat transfer is greatly affected by variation in ambient temperature. The effects of the increase in ambient temperature on the QEARS energy and exergy are presented in Fig. 6.6. The energy COP is observed to remain constant at 1.53 whereas the exergy COP is noted to increas from 0.56 to 0.91 with an increase ambient temperature from 270 to 290 K. The constant behavior of the energy COP shows that the results obtained from energy analysis are not tampered with when variation in ambient temperature occurs. However, the increasing behavior of the exergy COP displays the importance of performing exergy analysis

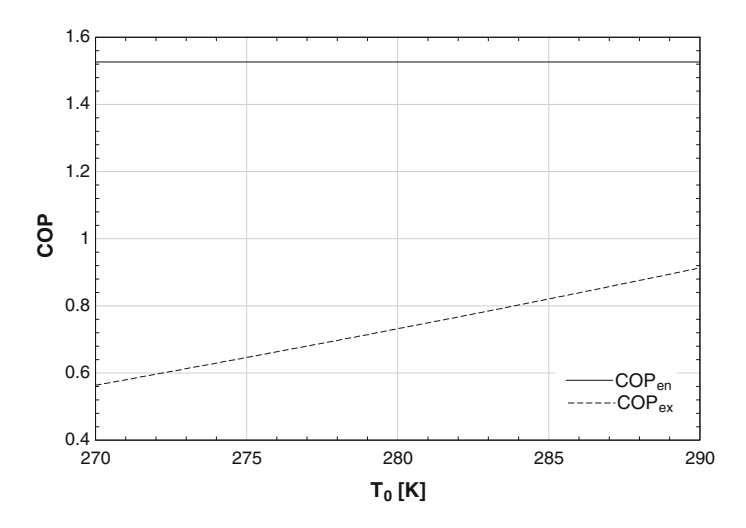


Fig. 6.6 Effects of ambient temperature on energy and exergy COPs

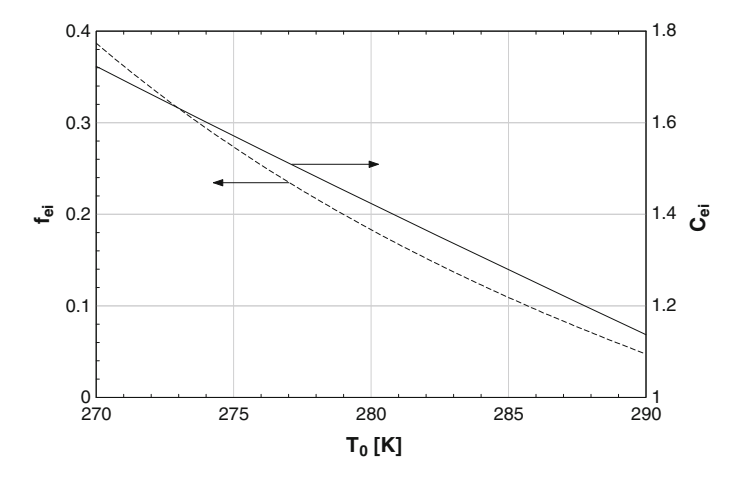


Fig. 6.7 Effects of ambient temperature on the exergoenvironmental impact factor and the impact coefficient

alongside energy analysis because exergy analysis, compared to energy analysis, is known to provide results more closer to real scenarios. The increasing behavior of exergy COP can be attributed to the lower exergetic heat loss from the system to the surrounding due to the lower temperature difference between the system and the surrounding. The effects of the increase in ambient temperature on the exergoenvironmental impact factor and the exergoenvironmental impact coefficient are shown in Fig. 6.7. The exergoenvironmental impact factor and the exergoenvironmental impact coefficient are noted to be decrease from 0.36 to 0.07 and 1.77 to

1.09, respectively with the increase in ambient temperature. The optimal value for exergoenvironmental impact factor is zero as it shows that the system is operating under ideal conditions from an environmental perspective. As the exergoenvironmental impact factor decreases with the increase in ambient temperature the QEARS becomes more and more environmentally friendly. This is caused by a decrease in the exergetic heat loss from the QEARS to the surrounding due to the smaller temperature difference between the QEARS and the surrounding. The reduction in the overall exergetic heat loss from the QEARS to surrounding also helps boost the exergetic COP of the system. As the exergetic COP of the system increases the exergoenvironmental impact coefficient decreases due to its dependence on the exergyCOP. This decreasing trend of the exergoenvironmental impact coefficient is a good sign for the OEARS because the ideal value for the exergoenvironmental impact coefficient is one. Figure 6.8 displays the effects of the increase in ambient temperature on the exergoenvironmental impact index and the exergoenvironmental impact improvement factor. The exergoenvironmental impact index is seen to decrease from 0.64 to 0.075, whereas, the exergoenvironmental impact improvement factor is noticed to increase from 1.56 to 13.34 with an increase in the ambient temperature from 270 to 290 K. The increase in ambient temperature helps to decrease the temperature difference between the OEARS and the surrounding. This lower temperature trigger a smaller amount of useful exergy loss from the system to the surrounding and helps bring down the value of the exergoenvironmental impact index. On the other hand, this reduction in exergetic heat loss in the form of useful exergy from the QEARS to the surrounding helps boost the exergoenvironmental impact improvement factor to as high as possible. The trend obtained in Fig. 6.8 indicates that the QEARS becomes more and more environmental friendly with the increasing ambient temperature.

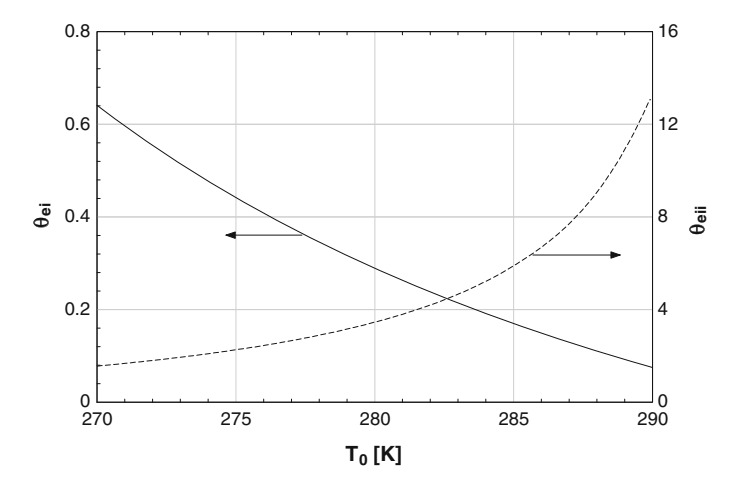


Fig. 6.8 Effects of ambient temperature on the exergoenvironmental impact index and the exergoenvironmental impact improvement

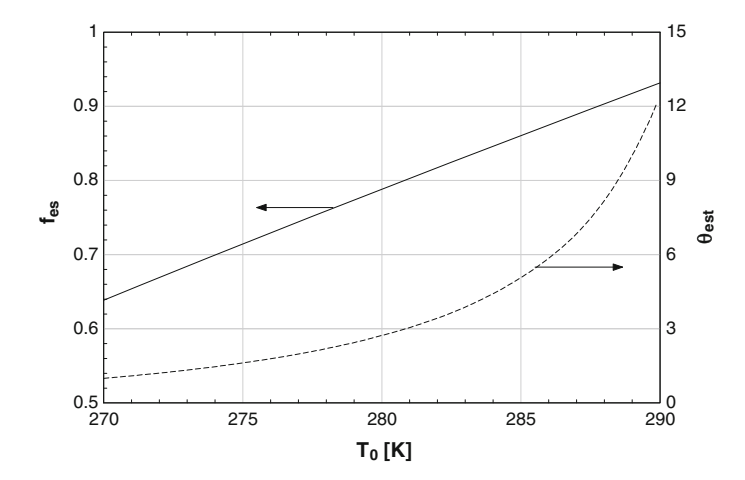


Fig. 6.9 Effects of ambient temperature on the exergetic stability and the exergetic sustainability index

Figure 6.9 displays the effects of the rise in ambient temperature on the exergetic stability factor and the exergetic sustainability index. The exergetic stability factor and the exergetic sustainability index are noted to increase from 0.64 to 0.93 and 0.99 to 12.42, respectively, with an increse in ambient temperature from 270 to 290 K. The growing trends of both parameters indicate that the QEARS becomes more stable and sustainable from an exergetic perspective due to a decrease in thermal exergy losses from the system to the surrounding with an increase in the ambient temperature. This additional stability and sustainability can be a useful tool for convincing individuals and governments situated in the hotter regions to install absorption refrigeration systems to help further control global warming and ever-rising temperatures.

Optimization results

Two optimization studies are carried out to obtain the optimum values for the exergetic COP, exergetic cost of cooling, and exergetic sustainability index based on the selected operating parameter ranges. Table 6.2 presents the constraints associated with the optimization study of the QEARS. In the first optimization study, we try to maximize the exergetic COP and minimize the exergetic cooling cost based on the selected operating conditions. The results obtained from this study

Table 6.2 Constraints related to the optimization study of the QEARS

Parameter	Minimum value	Maximum value	
\dot{Q}_{VHTG} (kW)	290	340	
T_0 (K)	270	290	
<i>x</i> ₃₆	0.45	0.5	
<i>x</i> ₃₈	0.2	0.3	

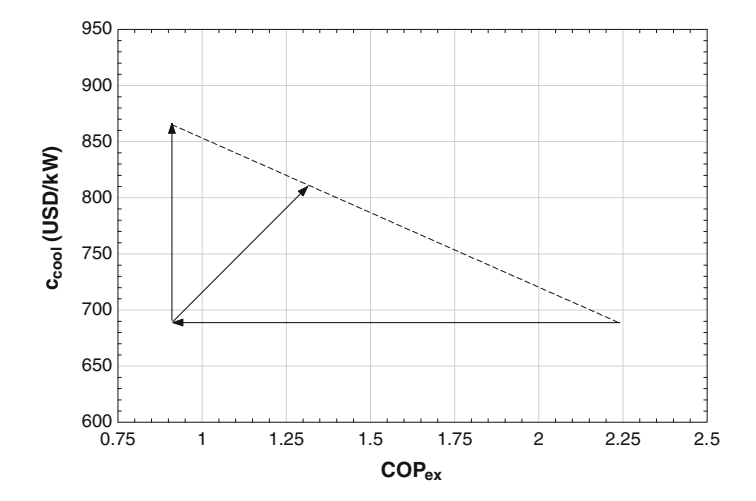


Fig. 6.10 Multi-objective optimization of the QEARS (exergetic cooling cost vs. exergetic COP)

are presented in Fig. 6.10. The Nelder-Mead simplex algorithm routine which comes with a built-in method in the engineering equation solver software is applied to perform multi-objective optimization study. The Nelder–Mead simplex algorithm makes use of N + 1 test points (where N represents the degrees of freedom), which is called a simplex. The algorithm evaluates every single point of the simplex, and the objective function is found at each of the points. The worst point in the simplex is then discarded, and a new point is found by reflecting away from the worst point about the axis formed by the other test points. The process is repeated several times until one of the stopping criteria are met, and then the objective function of the best point is taken to be the optimum. The results obtained from the first optimization study show that the highest exergetic COP obtained is 2.245 and the lowest cooling cost obtained is 867 USD/kW for the given constraints. It is worth noting that although all the points on the Pareto front are considered optimum, traditionally LINMAP is used to obtain the most desirable optimized points. LINMAP helps to find an imaginary point at which all the objective functions have their respective optimum location irrespective of other objective functions. The best exergetic COP and minimum exergetic cooling cost obtained using this method are 1.32 and 810 USD/kW, respectively.

The results obtained from the second optimization study related to maximizing exergetic sustainability index and minimizing the exergetic cost of cooling are presented in Fig. 6.11. The maximum exergetic sustainability index and minimum exergetic cooling cost obtained are 63.0 and 786 USD/kW, respectively. The best values obtained using LINMAP for the exergetic sustainability index, and the exergetic cost of cooling are 27.4 and 777.9 USD/kW, respectively.

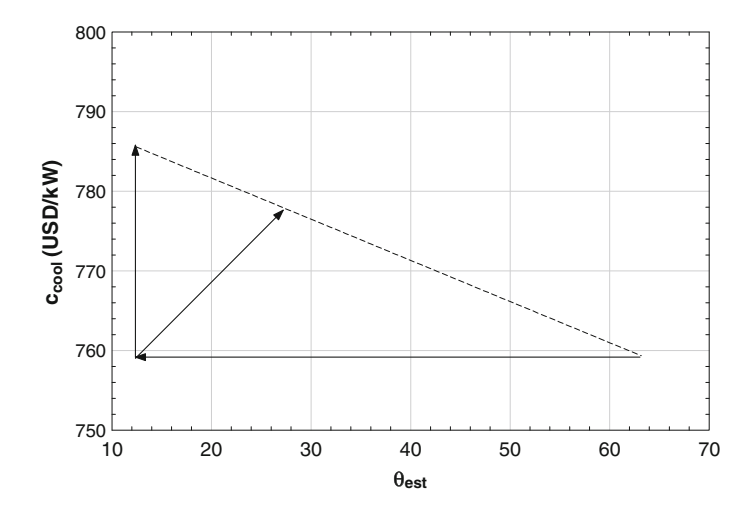


Fig. 6.11 Multi-objective optimization of the QEARS (exergetic cooling cost vs. exergetic sustainability index)

6.8 Closing Remarks

This chapter introduces a newly designed QEARS, which provides an additional benefit over conventional absorption refrigeration systems in terms of energy, exergy, thermal stability, environment and sustainability. These systems are proposed for better efficiency, greater cost effectiveness, less harm to the environment and hence better sustainability. A comprehensive case study is presented to cover energy, exergy, exergoeconomic, and exergoenvironmental analyses for a QEARS with thermodynamic data which are consistent with actual conditions. In addition, an optimization study is performed. Furthermore, a parametric study is undertaken to investigate how changing operating conditions, environmental conditions and state properties affects the performance of the system and its interactions with the environment.

Chapter 7

Integrated Absorption Refrigeration

Systems: Case Studies

7.1 Introduction

Absorption refrigeration systems provide an environmentally benign alternative to conventional vapour-compression refrigeration systems. The key benefit to using waste heat or low-grade heat to provide of cooling or heating, which gives an edge to absorption refrigeration systems over conventional air-conditioning systems. Absorption refrigeration systems can easily be integrated with renewable/alternative energy sources, such as solar, biomass, geothermal, to provide cooling in a cost effective, environmentally friendly and sustainable manner.

The present chapter focuses on energy and exergy analyses of several integrated absorption refrigeration systems for production of cooling or heating. Case studies are presented to integrate absorption refrigeration systems with geothermal and solar energy sources for generating multiple outputs. The last case study presented in this chapter provides a comprehensive investigation on how absorption refrigeration technique can be used to put an independent system in place for a sustainable community in the long-run. Some parametric studies are also presented in each case study to highlight the effects of variation in operating parameters on the performance of the integrated system.

7.2 Case Study 1: Geothermal-Based Power, Cooling, and Liquefied Hydrogen Generation System

• System description

The integrated system employed for analysis and performance assessments in the first case study is shown in Fig. 7.1. The first step in achieving liquefied hydrogen is to pre-cool the hydrogen in the quadruple effect absorption refrigeration system (QEARS) system which is driven by heat to provide cooling as it is supplied by

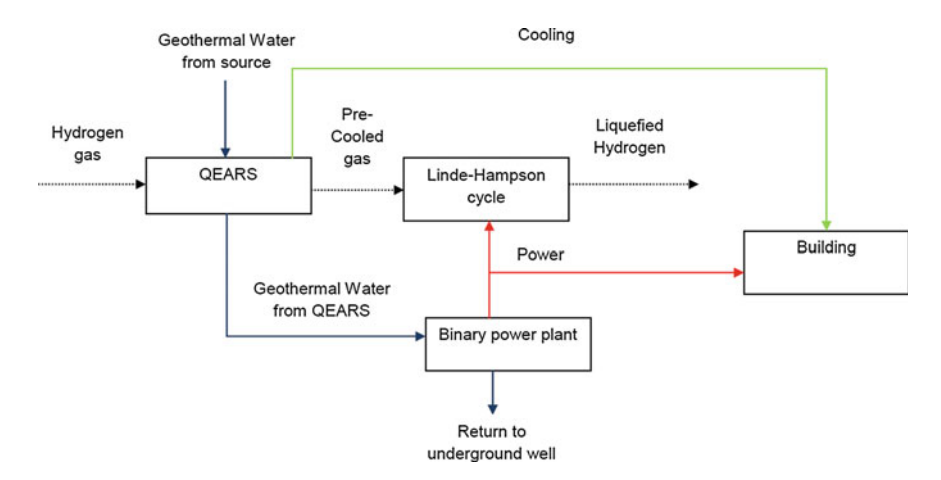


Fig. 7.1 Flow diagram of the integrated system

geothermal energy as shown in Fig. 7.2. The geothermal heat passes through the very high temperature generator (VHTG) before reaching the binary isobutane power plant. In the VHTG strong solution entering at state 36 is heated up to leave as a concentrated ammonia—water vapor at state 37 and as a weak solution at state 38. The stream coming out of the VHTG at state 38 enters the very high temperature heat exchanger (VHHX) to release heat to the stream from the absorber at state 35. After releasing heat in VHHX stream at state 40 mixes with the stream coming from the high temperature generator (HTG) at state 30 to leave at state 41. The process of releasing heat to the strong solution from a weak solution takes place

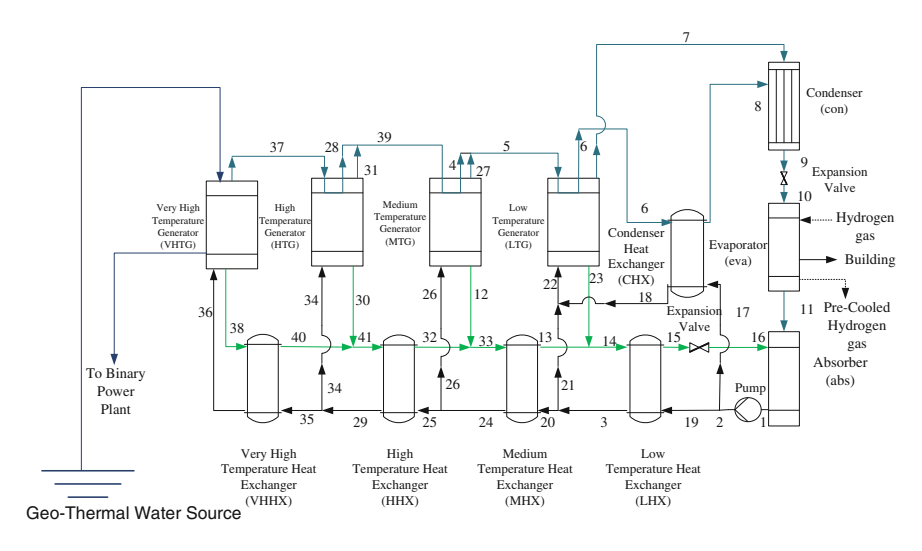


Fig. 7.2 Schematic of the QEARS

in the heat exchangers before the weak solution enters the expansion valve at state 15. The pressure of the weak solution at state 15 is then reduced by throttling it in the expansion valve. The low pressure weak solution leaves the expansion valve at state 16 to enter the absorber. The concentrated ammonia-water vapor at state 37 then enters the HTG. In the HTG, the stream at state 37 releases heat to exit at state 28. The heat released by the concentrated ammonia-water vapor at state 37 in the HTG is utilized to heat up the strong solution entering the HTG at state 34 to leave as a concentrated ammonia-water vapor at state 31 and as a weak solution at state 30. Then the concentrated ammonia-water vapor at state 28 and state 31 mixes to enter the medium temperature heat generator (MTG) at state 39. The process continues until the concentrated ammonia-water vapor leaving low temperature generator (LTG) at state 7 enters the condenser and the other ammonia-water vapor leaving the LTG at state 6 goes through the condenser heat exchanger (CHX). In the CHX, the concentrated ammonia-water vapor at state 6 rejects heats and leaves at state 8 to enter the condenser. In the condenser, concentrated ammonia-water vapor at state 7 and state 8 reject heat to the environment and leave at state 9 to enter the expansion valve. In the expansion valve pressure drops and concentrated ammonia water vapor leaving the expansion valve at state 10 enters the evaporator. In the evaporator, concentrated ammonia-water vapor at state 10 gains heat from the hydrogen and the return air from the building envelope to leave at a higher temperature at state 11. The ammonia-water mixture at state 11 and the weak solution at state 16 enter the absorber to reject heat and leave at state 1 as a strong solution in liquid form and enter the pump. The geothermal water leaving the VHTG is supplied to the binary isobutane cycle to produce power as seen in Fig. 7.3. The isobutane is then heated and vaporized using the geothermal water from the HTG. This vaporized isobutane flows through the turbine giving out power, is condensed, pumped, and supplied back to the heat exchanger. The part of the power produced by the binary cycle is used to compress hydrogen gas from state 1 to state 2 in the Linde-Hampson cycle, as shown in Fig. 7.4. The geothermal water coming out of

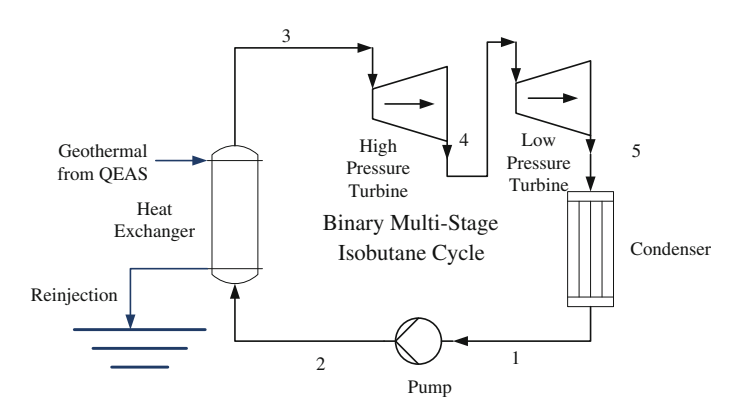


Fig. 7.3 Schematic of multi-stage binary power plant

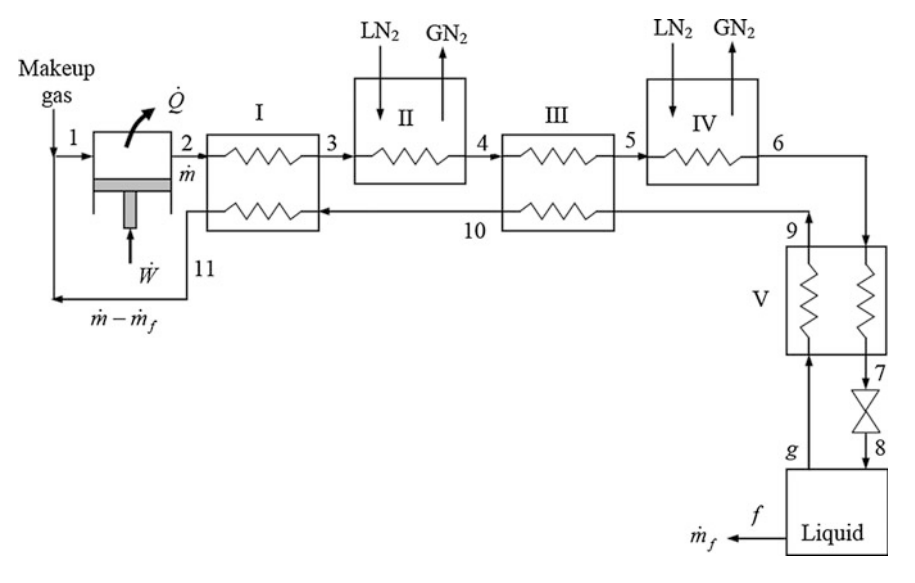


Fig. 7.4 Schematic of the Linde–Hampson cycle

the isobutane is injected back into the underground water well to maintain approximately its level. The first case study presented in this chapter is modified from Ratlamwala et al. (2012a).

• Energy and exergy analyses

To run an integrated system, mass and energy balance equations are written for the components of the OEARS, the isobutane binary multistage cycle, and Linde-Hampson cycle. Also, equations to calculate the efficiency of the binary multistage system, COPs of the OEARS, and ratios 'n', and 'v' are written. About 90 % of cooling produced by the QEARS is used to pre-cool the hydrogen from 25 °C and 101.3 kPa to −16.4 °C and 101.3 kPa in the evaporator. The remaining 10 % of the cooling is supplied to the building. In the Linde-Hampson cycle, hydrogen is compressed from 101 kPa to 10 MPa. The heat needed to operate the isobutane cycle is provided by geothermal water at 20 °C less than the geothermal source temperature. The pressure at the inlet and exit of the stage 1 turbine are taken to be 3600 and 1000 kPa, respectively, while, the temperature at the inlet of the stage 1 turbine is taken to be 15 °C lower than the geothermal temperature at the inlet of the binary power plant heat exchanger. However, the condenser pressure of the binary multi-stage power plant is taken to be 400 kPa. The 90 % of the power produced by the binary multistage plant is supplied to the Linde-Hampson cycle to compress hydrogen gas, and the remaining 10 % is supplied to the building. The strong solution concentration of ammonia-water, x[36] and the weak solution concentration of ammonia-water, x[38] are assumed to be 0.6 and 0.4, respectively, while concentration of ammonia–water vapor, x[39] varies from 0.999 to 0.9999.

• Quadruple effect absorption refrigeration system

The rate of heat to the VHTG of an absorption system is provided using the geothermal water source. The rate of heat transfer obtained from geothermal water source is calculated using

$$\dot{Q}_{\text{geo}} = \dot{m}_{\text{geo}} \times \left(h_{\text{geo}_{\text{source}}} - h_{\text{geo}_{\text{VHTG exit}}} \right) \tag{7.1}$$

$$\dot{Q}_{\rm VHTG} = \dot{Q}_{\rm geo}$$
 (7.2)

where \dot{Q} , \dot{m} , and h represent rate of heat transfer, mass flow rate, and specific enthalpy, respectively.

The mass balance equations of VHTG are given as follows

$$\dot{m}_{36}x_{36} = \dot{m}_{37}x_{37} + \dot{m}_{38}x_{38} \tag{7.3}$$

$$\dot{m}_{36} = \dot{m}_{37} + \dot{m}_{38} \tag{7.4}$$

To obtain the outlet conditions of the VHTG, the following equation is used

$$\dot{m}_{36}h_{36} + \dot{Q}_{VHTG} = \dot{m}_{37}h_{37} + \dot{m}_{38}h_{38} \tag{7.5}$$

The exergy destruction in VHTG becomes

$$\dot{E}x_{\text{dest.VHTG}} + \dot{E}x_{37} + \dot{E}x_{38} = \dot{E}x_{36} + \dot{E}x_{\text{th.VHTG}}$$
 (7.6)

where $\dot{E}x_{37} = \dot{m}_{37}((h_{37} - h_0) - T_0(s_{37} - s_0))$

Here, $\dot{E}x$, T, and s represent rate of exergy, temperature and specific entropy, respectively. The same relationship is employed for other states.

The energy balance equations for VHHX are given below

$$\dot{m}_{35}h_{35} + \dot{Q}_{\text{VHHX}} = \dot{m}_{36}h_{36} \tag{7.7}$$

$$\dot{m}_{38}h_{38} = \dot{m}_{40}h_{40} + \dot{Q}_{\text{VHHX}} \tag{7.8}$$

The mass and energy balance equations for the condenser are given below

$$\dot{m}_9 = \dot{m}_7 + \dot{m}_8 \tag{7.9}$$

$$\dot{m}_9 h_9 = \dot{m}_7 h_7 + \dot{m}_8 h_8 + \dot{Q}_{con} \tag{7.10}$$

The balance equations for mass and energy of the evaporato ae:r

$$\dot{m}_{10} = \dot{m}_{11} \tag{7.11}$$

$$\dot{m}_{10}h_{10} + \dot{Q}_{\text{eva}} = \dot{m}_{11}h_{11} \tag{7.12}$$

The following energy balance equation is used to calculate the heat rejected from the absorber:

$$\dot{m}_{11}h_{11} + \dot{m}_{16}h_{16} = \dot{m}_1h_1 + \dot{Q}_{abs} \tag{7.13}$$

The work done by the pump is calculated using the equation given below

$$\dot{W}_{p} = \dot{m}_{1}(h_{2} - h_{1}) \tag{7.14}$$

where \dot{W} represents power.

The energetic and exergetic COPs are defined as

$$COP_{en} = \frac{\dot{Q}_{eva}}{\dot{Q}_{geo} + \dot{W}_{P}} \tag{7.15}$$

$$COP_{ex} = \frac{\dot{E}x_{eva}}{\dot{E}x_{geo} + \dot{W}_{P}}$$
 (7.16)

where COP represents coefficient of performance.

• Binary power plant

The power that can be obtained from the turbines of binary multistage isobutane plant is calculated using

$$\dot{W}_{\text{turb}} = \dot{m}_{\text{iso}}(h_3 - h_4) + \dot{m}_{\text{iso}}(h_4 - h_5) \tag{7.17}$$

The power consumed by pump in the binary cycle is expressed as

$$\dot{W}_{p_{\rm iso}} = \dot{m}_{\rm iso}(h_2 - h_1) \tag{7.18}$$

To have the correct model, parasitic losses are also considered and are defined as

$$\dot{W}_{\text{parasitic}} = 0.2(\dot{W}_{\text{turb}} - \dot{W}_{\text{p}_{\text{ico}}}) \tag{7.19}$$

The actual net power that can be obtained from the binary isobutane plant running on geothermal energy source is expressed as

$$\dot{W}_{\text{net}_{\text{ego}}} = \dot{W}_{\text{turb}} - \dot{W}_{\text{p}_{\text{iso}}} - \dot{W}_{\text{parasitic}} \tag{7.20}$$

• Linde-Hampson liquefaction cycle

The specific ideal work required to compress hydrogen from P_1 = 101 kPa to P_2 = 10 MPa is given as

$$w_{\text{comp}_{\text{ideal}}} = R \times T_0 \times \ln \frac{P_2}{P_1}$$
 (7.21)

where w, R, and P represent specific work, gas constant, and pressure, respectively. However, the actual specific work input to liquefaction cycle per unit mass of hydrogen is stated as

$$w_{\text{comp}_{\text{actual}}} = \frac{w_{\text{comp}_{\text{ideal}}}}{\eta_{\text{comp}}} \tag{7.22}$$

where η_{comp} represents isentropic efficiency of the compressor and is taken to be 65 %. The amount of power needed for nitrogen is taken to be 5050 kJ/kg as used by Nandi and Saragani (1993).

A parameter 'y' is defined as a ratio of the work output from the power plant to the work input to the liquefaction cycle. This parameter also shows the mass of hydrogen liquefied per unit mass of geothermal water used. For reversible and irreversible operations, it is expressible as

$$y_{\text{rev}} = \frac{w_{\text{rev}_{\text{geo}}}}{w_{\text{rev}_{\text{I,inde-Hamnson}}}}$$
(7.23)

where

$$w_{\text{rev}_{geo}} = (h_2 - h_1) - T_0(s_2 - s_1)$$
 (7.24)

$$y_{\rm irr} = \frac{w_{\rm net_{geo}}}{w_{\rm total_{\rm Linde-Hampson}}}$$
 (7.25)

Here,

$$w_{\text{total}_{\text{Linde-Hampson}}} = \frac{w_{\text{comp}_{\text{actual}}} + w_{\text{Nitrogen}}}{f_{\text{liq}}}$$
(7.26)

$$f_{\rm liq} = \frac{h_9 - h_6}{h_9 - h_f} \tag{7.27}$$

where $f_{\rm liq}$ represents the fraction of liquefied hydrogen that is taken out of the cycle.

The amount of hydrogen liquefied is then calculated using

$$\dot{m}_{\rm H_{2_{\rm liq}}} = f_{\rm liq} \times \dot{m}_{\rm H_2} \tag{7.28}$$

· Results and discussion

In the current application domains, it has become highly important to design energy systems that are eco-friendly and sustainable to serve the environment and the struggling economies throughout the world. This section of the case study shows the impacts of the variation in operating conditions on system performance from energy and exergy perspective.

• Effects of geothermal mass flow rate

The variation in mass flow rate of geothermal water has a significant impact on the performance of the integrated system. Increase in mass flow rate of geothermal water ($\dot{m}_{\rm geo}$) results in higher energy input to the QEARS. This increase in energy input contributes to the lower output from the evaporator in form of cooling load for a fixed condenser load as can be seen in Fig. 7.5. The energy input to the VHTG increases from 60 to 120 kW with increase in $\dot{m}_{\rm geo}$ from 1.5 to 3.0 kg/s. For this increase in energy input to the QEARS, the cooling load is found to vary from 316.5 to 206.5 kW, for varying condenser load from 150 to 200 kW, respectively, and for a fixed geothermal source temperature of 573 K. It is noted that as the condenser load increases the evaporator load increases because more heat is removed in the condenser from the stream going into the evaporator. This higher heat rejection results in lower input temperature of the stream going into the evaporator and therefore, higher cooling load exists. The power and cooling load provided to the building are also found to vary with changes in mass flow rate of geothermal water and condenser load as seen in Fig. 7.6. Both power and cooling

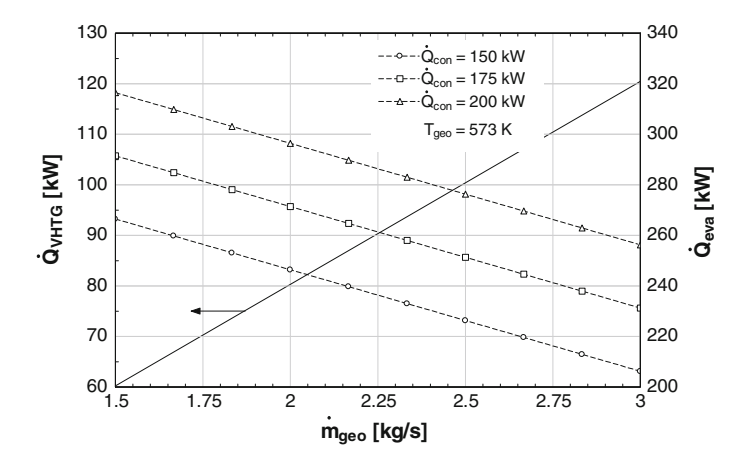


Fig. 7.5 Effects of geothermal mass flow rate on energy input to QEARS and cooling load

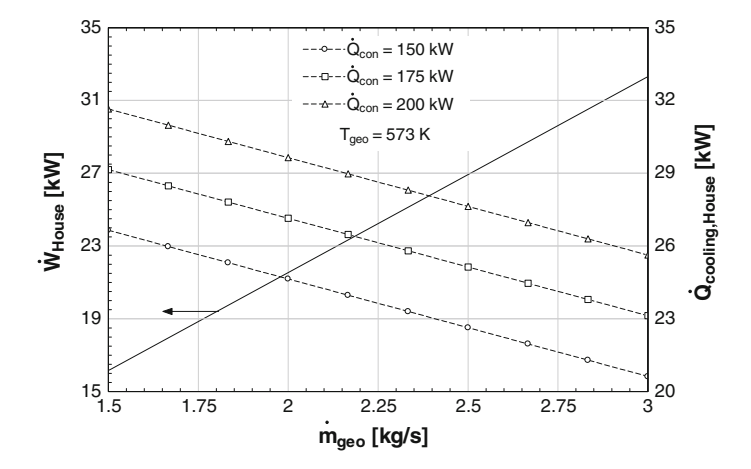


Fig. 7.6 Effects of geothermal mass flow rate on power and cooling supplied to building

load range from 16 to 32 kW and 31.6 to 20.6 kW, respectively. Also, the increase in the energy input to the QEARS and decrease in the cooling load with increasing $\dot{m}_{\rm geo}$ results in lower energetic and exergetic COPs of the QEARS as shown in Fig. 7.7. Both the COPs vary from 5.0 to 1.7 and 1.2 to 0.4, respectively, with increase in $\dot{m}_{\rm geo}$. The decrease in the COPs is a direct result of higher energy input to the QEARS and lower output from the QEARS in the form of cooling load. The increase in $\dot{m}_{\rm geo}$ results in increase in reversible and irreversible amounts of hydrogen gas precooled in the evaporator which is defined as parameter 'n' as shown in Fig. 7.8. Both reversible and irreversible 'n' vary from 3.1 to 1.6 g/kg and 0.73 to 0.36 g/kg, with increase in $\dot{m}_{\rm geo}$, respectively. The decrease in performance of the QEARS due to increase in $\dot{m}_{\rm geo}$ also effects the rate of hydrogen precooled by the

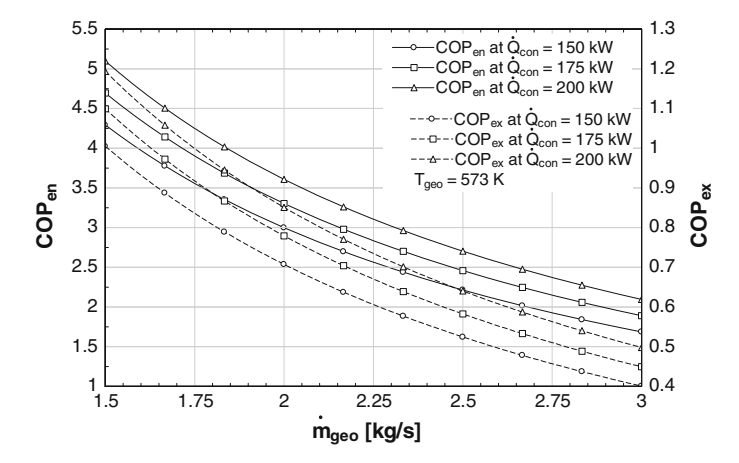


Fig. 7.7 Effects of geothermal mass flow rate on energetic and exergetic COPs

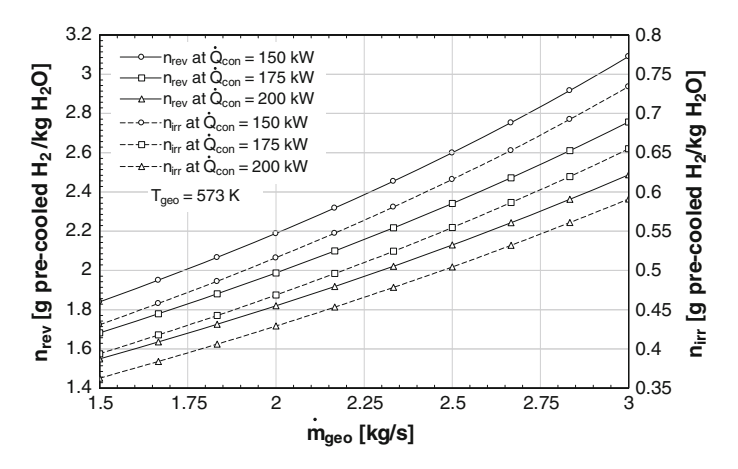


Fig. 7.8 Effects of geothermal mass flow rate on ratio 'n'

QEARS and liquefied by the LH system. Figure 7.9 shows that both the amount of hydrogen gas precooled and the amount of hydrogen gas liquefied decreases from 0.53 to 0.34 kg/s and 0.09 to 0.06 kg/s, with increase in the $\dot{m}_{\rm geo}$, respectively. By inspecting the results, we conclude that any increase in $\dot{m}_{\rm geo}$ affects the system in a negative way when it comes to cooling production, and hydrogen liquefaction. However, in the case of power production increase in $\dot{m}_{\rm geo}$ has a positive impact on the system and leads to higher power production.

• Effects of ambient temperature

The variation in ambient temperature plays a vital in the role in performance determination of any thermally driven system. The effects of the changes in ambient

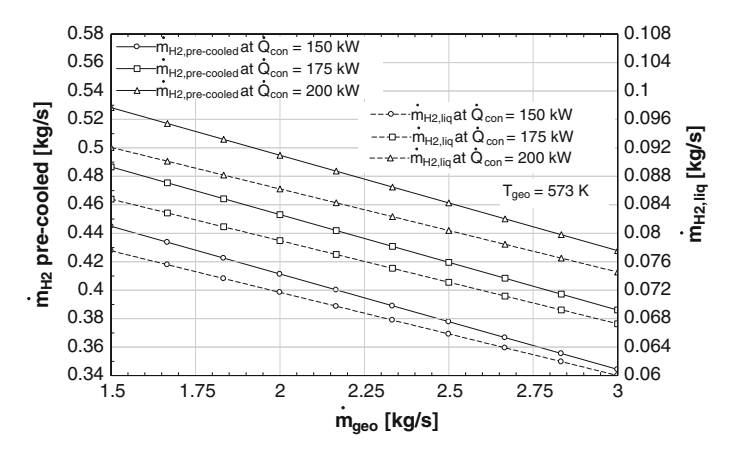


Fig. 7.9 Effects of geothermal mass flow rate on amount of hydrogen gas precooled and liquefied

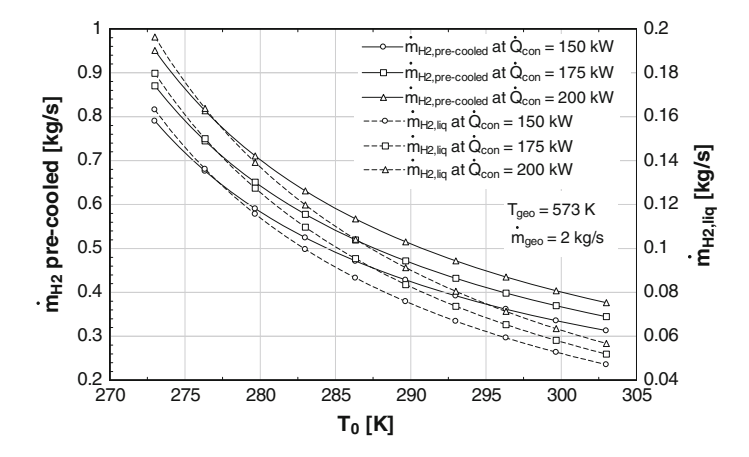


Fig. 7.10 Effects of ambient temperature on amount of hydrogen gas precooled and liquefied

temperature on the amount of hydrogen gas precooled and liquefied are shown in Fig. 7.10. Both the amount of hydrogen gas precooled and liquefied are found to decrease with an increase in ambient temperature. Both parameters are found to vary from 0.95 to 0.31 kg/s and 0.2 to 0.05 kg/s, respectively, for varying condenser loads of 150, 175, and 200 kW. This behavior is noted because any increase in ambient temperature decreases the natural cooling of the system from the ambient air. As the ambient temperature increases, the performance of the QEARS evaporator, as well as the performance of the LH system, decreases. This decrease is a result of the lower temperature difference between the surrounding and the system. Therefore, as the ambient temperature increases the system interacts in a negative way and its performance decreases.

7.3 Case Study 2: Solar-Based Integrated Absorption Refrigeration and Desalination System for Cooling and Fresh Water Production

• System description

The integrated hybrid system capable of producing cooling and fresh water while using solar energy analyzed in this case study is presented in Fig. 7.11. The process starts by producing thermal and electrical energy using a solar PV/T system. The solar irradiance falls onto the concentrated PV/T panel causing the electrons to vibrate in the panel and, therefore, producing power As air passes through the ducts of the concentrated PV/T system, it gains energy from the PV/T back surface and leaves the PV/T system at relatively higher temperature as seen in Fig. 7.11. This heated air along with power produced is supplied to the very high

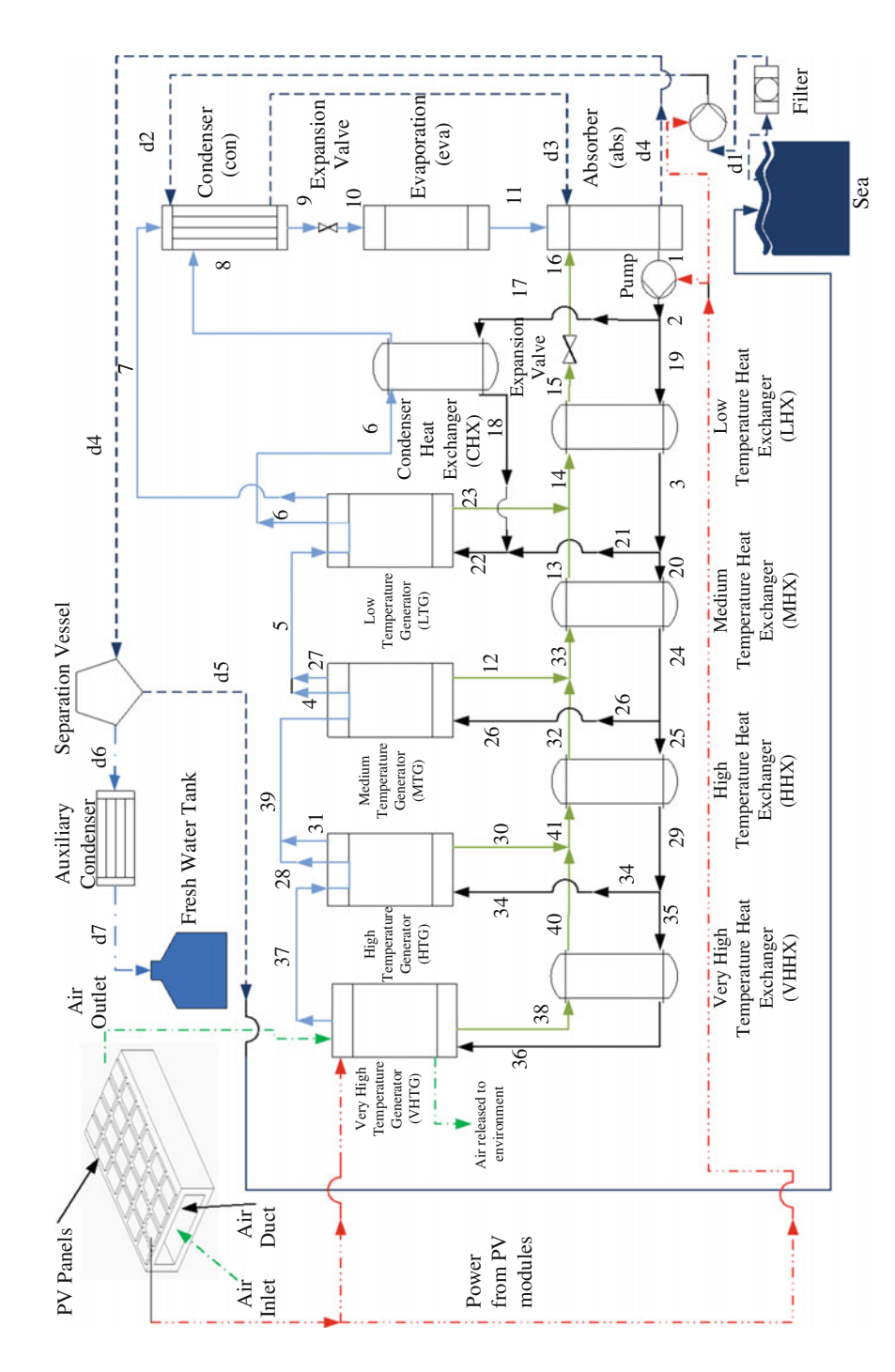


Fig. 7.11 Schematic of the integrated system for cooling and fresh water production

temperature generator (VHTG) of the OEARS to provide cooling and to heat seawater. A small amount of power generated by the PV/T system is fed to the pump of QEARS and desalination system. In the very high temperature generator, the strong solution from the absorber at state 36 is heated to leave as a weak solution at state 38 and ammonia-water vapor at state 37. The weak solution leaving the VHTG at state 38 enters the VHHX. The solution then rejects heat in the VHHX and combines with the weak solution from state 30 to leave at state 41 as a weak solution. This weak solution from state 41 then gives out the heat in the high temperature heat exchanger (HHX) and combines with the weak solution from state 12 to leave at state 33. This weak solution from state 33 then gives out heat in medium temperature heat exchanger (MHX) and mixes with the weak solution at state 23 to leave at state 14. This weak solution then enters the low temperature heat exchanger (LHX) where it heats up the strong solution from state 19. The weak solution at state 15 enters the expansion valve where its temperature and pressure drops and enters the absorber at state 16. The vapor from state 37 then enters the HTG where it heats up the strong solution from state 34 and leaves as an ammonia water vapor at state 28 and state 31. These two streams are combined together outside the HTG and leave as one stream at state 39 to enter the medium temperature generator (MTG) where it heats up the strong solution from state 26 and leaves as ammonia-water vapor at state 4 and state 27. These two ammonia-water vapors are mixed to leave at state 5. The ammonia-water vapor at state 5 enters the LTG and heats up the strong solution coming from state 22 and leaves as an ammonia-water vapor at state 6 and state 7. The stream at state 7 is directed to the condenser while state 6 is directed towards the CHX to lose heat to the liquid stream coming from the solution pump at state 17 and leaves the CHX at state 18. Ammonia-water vapor leaving the CHX at state 8 enters the condenser where it rejects heat and then leaves the condenser in the liquid phase at state 9. This stream then passes through the expansion valve and leaves at state 10 to enter the evaporator. In the evaporator (eva) heat is being gained by the refrigerant (ammonia) and the heated mixture leaves at stat 11 to enter the absorber. In the absorber, all three streams mix and reject heat to the cooling medium and leave the absorber at state 1 in liquid form. The rich solution is then pumped to the working VHTG pressure. The stream from the sea at state d1 passes through the filter to remove unwanted residuals. After passing through the filter, seawater is pumped to a higher pressure to enter the condenser at state d2. In the condenser, heat is absorbed by the seawater that leaves at state d3 as a preheated stream. The exit stream from condenser then enters the absorber to gain heat and leaves at state d4. This heated vapor-liquid mixture from d4 then enters the separation vessel. In the separation vessel, vapors are removed from the upper level to exit at state d6. The remaining brine solution in the separation vessel is then sent back to the sea and is marked as state d5. Vapors from state d6 then pass through the auxiliary condenser to reject heat and leaves as fresh water at state d7. Air in the concentrated solar PV/T system is used to cool down the PV panels. The flowing air in the solar PV/T duct absorbs heat from the back side of the panel and then exits the duct at a relatively high temperature to be later used in the absorption refrigeration system. The integrated system presented in this case study is modified from Ratlamwala et al. (2013).

Energy and exergy analyses

To analyze the hybrid system, mass and energy balance equations are written for the solar PV/T, the components of the QEARS, and the desalination system. Also, equations to calculate the efficiency of the solar system, COPs of the QEARS, utilization factors, and the performance ratio of the hybrid system are written. The following assumptions are made in the analysis

- The parameters considered for solar PV/T analysis are $A=100~\text{m}^2,\,b=0.45~\text{m},\,h_{\text{p1G}}=0.88,\,L=1.2~\text{m},\,\beta_{\text{c}}=0.83,\,\eta_{\text{c}}=0.12,\,\tau_{\text{g}}=0.95,\,U_{\text{b}}=0.62~\text{W m}^{-2}~\text{K}^{-1},\,U_{\text{t}}=2.8~\text{W m}^{-2}~\text{K}^{-1},\,\text{and}\,\,\alpha_{\text{c}}=0.90.$
- The concentrations of the ammonia—water mixture at states 36, 38, and 39 are 0.6, 0.4, and 0.999, respectively.
- The pressures at states 1, 2, d1, and d2 are 250, 400, 101, and 150 kPa, respectively.
- The mass flow rate of ammonia-water mixture at state 1 is 1 kg s⁻¹.
- The mass flow rate of sea water at state d1 is 2 kg s^{-1} .
- The mass flow rate of air flowing through the duct of solar PV/T is 1.15 kg s^{-1} .
- The isentropic efficiencies of the pumps are 95 %.
- The heat exchangers are modeled based on logarithm mean temperature difference model.
- The losses in pipes and connections are negligible.
- The ambient temperature and pressure are 291.2 K and 100 kPa, respectively.
 - Solar PV/T system

The equation used to calculate power produced by the PV module is given as

$$\dot{W}_{\text{solar}} = \eta_{\text{c}} \times \dot{I} \times \beta_{\text{c}} \times \tau_{\text{g}} \times A \tag{7.29}$$

where \dot{I} , β , τ , and A represent solar light intensity, packing factor, transmittance and area, respectively.

The rate of heat transferred to air is calculated as

$$\dot{Q}_{\text{solar}} = \frac{\dot{m}_{\text{a}} \times \text{cp}_{\text{a}}}{U_{\text{L}}} \times \left((h_{\text{p2G}} \times z \times \dot{I}) - U_{\text{L}} \times (T_{\text{ai}} - T_{0}) \right) \\
\times \left[1 - \exp(\frac{-b \times U_{\text{L}} \times L}{\dot{m}_{\text{a}} \times \text{cp}_{\text{a}}}) \right]$$
(7.30)

where

$$z = \alpha_{\rm b} \times \tau_{\rm g}^2 \times (1 - \beta_{\rm c}) + h_{\rm p1G} \times \tau_{\rm g} \times \beta_{\rm c} \times (\alpha_{\rm c} - \eta_{\rm c})$$

where cp, U, h, z, b, L, and α represent specific heat capacity, overall heat transfer coefficient, heat transfer coefficient, parameter, breadth, length and absorptance, respectively.

The rate of exergy of solar energy is calculated by

$$\dot{\mathbf{E}}\mathbf{x}_{\text{solar}} = \left[1 - \left(\frac{T_0 + 273.15}{T_{\text{sun}}}\right)\right] \times \dot{I} \times A \tag{7.31}$$

The electrical efficiency of the PV panel is defined as

$$\eta_{\rm el} = \eta_{\rm c} \times (1 - 0.0045 \times (T_{\rm c} - 25))$$
(7.32)

where

$$\begin{split} T_{\rm c} &= \frac{\tau_{\rm g} \times \beta_{\rm c} \times \dot{I} \times (\alpha_{\rm c} - \eta_{\rm c}) + U_{\rm t} \times T_{\rm 0} + h_{\rm t} \times T_{\rm bs}}{U_{\rm t} + h_{\rm t}} \\ T_{\rm bs} &= \frac{z \times \dot{I} + (U_{\rm t} + U_{\rm tb}) \times T_{\rm 0} + h_{\rm ba} \times T_{\rm air}}{U_{\rm b} + h_{\rm ba} + U_{\rm tb}} \\ T_{\rm air} &= \left[T_{\rm 0} + \frac{h_{\rm p2G} \times z \times \dot{I}}{U_{\rm L}} \right] \times \left[1 - \frac{1 - \exp\left(\frac{-b \times U_{\rm L} \times L}{\dot{m}_{\rm a} \times {\rm cp}_{\rm a}}\right)}{\frac{b \times U_{\rm L} \times L}{\dot{m}_{\rm a} \times {\rm cp}_{\rm a}}} \right] + T_{\rm ai} \times \left[\frac{1 - \exp\left(\frac{-b \times U_{\rm L} \times L}{\dot{m}_{\rm a} \times {\rm cp}_{\rm a}}\right)}{\frac{b \times U_{\rm L} \times L}{\dot{m}_{\rm a} \times {\rm cp}_{\rm a}}} \right] \end{split}$$

The thermal efficiency of solar PV/T is defined as

$$\eta_{\rm th} = \frac{\dot{Q}_{\rm solar}}{\dot{I} \times b \times L} \tag{7.33}$$

QEARS system

After receiving the heat and power output from the solar PV/T, the equations for the VHTG are written so that the QEARS achieves the cooling load. The amount of energy given to the VHTG can be found as:

$$\dot{Q}_{\text{VHTG}} = \dot{W}_{\text{solar}} + \dot{Q}_{\text{solar}} - \dot{W}_{\text{p}} - \dot{W}_{\text{dP}}$$
 (7.34)

The mass balance equations are given as follows:

$$\dot{m}_{36}x_{36} = \dot{m}_{37}x_{37} + \dot{m}_{38}x_{38} \tag{7.35}$$

$$\dot{m}_{36} = \dot{m}_{37} + \dot{m}_{38} \tag{7.36}$$

To obtain the outlet conditions of the VHTG, the following equation is used:

$$\dot{m}_{36}h_{36} = \dot{Q}_{\text{VHTG}} = \dot{m}_{37}h_{37} + \dot{m}_{38}h_{38} \tag{7.37}$$

The exergy destruction in VHTG becomes

$$\dot{E}x_{dest,VHTG} + \dot{E}x_{37} + \dot{E}x_{38} = \dot{E}x_{36} + \dot{E}x_{th,VHTG}$$
 (7.38)

where $\dot{E}x_{37} = \dot{m}_{37}((h_{37} - h_0) - T_0(s_{37} - s_0))$

The same relationship is applied to other states.

The energy balance equations for VHHX are given below:

$$\dot{m}_{35}h_{35} + \dot{Q}_{\text{VHHX}} = \dot{m}_{36}h_{36} \tag{7.39}$$

$$\dot{m}_{38}h_{38} = \dot{m}_{40}h_{40} + \dot{Q}_{\text{VHHX}} \tag{7.40}$$

The mass and energy balance equations for the condenser are given below:

$$\dot{m}_9 = \dot{m}_7 + \dot{m}_8 \tag{7.41}$$

$$\dot{m}_9 h_9 = \dot{m}_7 h_7 + \dot{m}_8 h_8 + \dot{Q}_{con} \tag{7.42}$$

The balance equations for mass and energy of the evaporator:

$$\dot{m}_{10} = \dot{m}_{11} \tag{7.43}$$

$$\dot{m}_{10}h_{10} + \dot{Q}_{\text{eva}} = \dot{m}_{11}h_{11} \tag{7.44}$$

The following energy balance equation is used to calculate the heat rejected from the absorber:

$$\dot{m}_{11}h_{11} + \dot{m}_{16}h_{16} = \dot{m}_1h_1 + \dot{Q}_{abs} \tag{7.45}$$

The work done by the pump is calculated using the equation given below

$$\dot{W}_{p} = \dot{m}_{1}(h_{2} - h_{1}) \tag{7.46}$$

The energetic and exergetic COPs are found using

$$COP_{en} = \frac{\dot{Q}_{eva} + \dot{Q}_{con} + \dot{Q}_{abs}}{\dot{Q}_{VHTG}}$$
(7.47)

$$COP_{ex} = \frac{\dot{E}x_{eva,th} + \dot{E}x_{con,th} + \dot{E}x_{abs,th}}{\dot{E}x_{VHTG,th} + \dot{W}_{P}}$$
(7.48)

• Desalination system

After studying solar PV/T and QEARS, the following equations are written to analyze desalination system thermodynamically.

The power required for the desalination pump to function is calculated by

$$\dot{W}_{\rm dP} = \dot{m}_{\rm sw} \nu_{\rm d1} \left[\frac{P_{\rm d2} - P_{\rm d1}}{\eta_{\rm dP}} \right] \tag{7.49}$$

where v represents specific volume.

The sea water passes through a condenser and then an evaporator to reach vapor state. Then a separation vessel is used to separate fresh water and brine. Mass and energy balance equations for the separation vessel are:

$$\dot{m}_{\rm sw} = \dot{m}_{\rm fw} + \dot{m}_{\rm sw,o} \tag{7.50}$$

$$\dot{m}_{\rm sw}h_{\rm d4} = \dot{m}_{\rm fw}h_{\rm d6} + \dot{m}_{\rm sw.o}h_{\rm d5} \tag{7.51}$$

The fresh water obtained from the separation vessel is then cooled in the auxiliary condenser. Energy balance for auxiliary condenser is defined as

$$\dot{m}_{\rm fw}h_{\rm d6} = \dot{m}_{\rm fw}h_{\rm d7} + \dot{Q}_{\rm aux.con}$$
 (7.52)

Performance ratio of the system is defined as the amount of fresh water produced per amount of air used and is calculated as

Performance Ratio =
$$\frac{\dot{m}_{\text{fw}}}{\dot{m}_{\text{a}}}$$
 (7.53)

Both energetic and exergetic utilization factors of the hybrid system are defined as

$$\varepsilon_{\text{overall,en}} = \frac{\dot{m}_{\text{fw}} h_{\text{d7}} + \dot{Q}_{\text{eva}}}{I \times A} \tag{7.54}$$

$$\varepsilon_{\text{overall,ex}} = \frac{\dot{E}x_{d7} + \dot{E}x_{\text{eva}}}{\dot{E}x_{\text{solor}}}$$
(7.55)

where ε represents utilization factor.

· Results and discussion

As the world looks towards renewable/alternative energy sources, it has become highly important to develop a system that can provide fresh water and cooling in a sustainable and eco-friendly manner. In this case study, a noble system that integrates concentrated solar PV/T to a quadruple effect absorption refrigeration and desalination system for fresh water and cooling production is assessed. The thermodynamic properties of each state point of the QEARS and desalination system are presented in Tables 7.1 and 7.2, respectively.

Table 7.1 Thermodynamic properties of QEARS at each state point

0 − 291.2 100 291.5 5.675 − − − 1 1 279.7 250 −199.5 −0.06288 0.6 1181 0 2 1 280.1 400 −197.6 −0.06288 0.6 1181 − 3 0.8 292.1 400 −197.6 −0.06288 0.6 144.4 − 4 0.171 271.4 400 996.6 3.672 0.999 225.7 0.2283 5 0.2137 271.3 400 281.8 1.05 0.999 285.7 0.2283 7 0.1202 276.4 400 1272 4.682 0.999 152.6 0.999 8 0.2137 271.3 400 29.87 0.1255 0.999 289.4 0.03068 9 0.3339 259.5 250 335.9 1.31 0.999 445.2 0.2707 10 0.3339 259.6 25	State points	m (kg/s)	T (K)	P (kPa)	h (kJ/kg)	s (kJ/kg K)	x (kg/kg)	Ėx (kW)	Quality
1 1 279.7 250 -199.5 -0.06834 0.6 1181 0 2 1 280.1 400 -197.6 -0.06288 0.6 1181 - 3 0.8 292.1 400 -142.8 0.129 0.6 944.4 4 0.171 271.4 400 917.6 3.383 0.999 221.1 0.7269 5 0.2137 271.3 400 281.8 1.05 0.999 285.7 0.2283 7 0.1202 276.4 400 1272 4.682 0.999 152.6 0.9944 8 0.2137 271.3 400 29.87 0.1255 0.999 289.4 0.0309 9 0.3339 271.3 400 29.87 0.1255 0.999 445.2 0.2707 10 0.3339 259.5 250 335.9 1.31 0.999 445.8 0.7591 10 0.3339 259.6 250 </td <td>0</td> <td>-</td> <td>291.2</td> <td>100</td> <td>291.5</td> <td>5.675</td> <td>_</td> <td>_</td> <td>_</td>	0	-	291.2	100	291.5	5.675	_	_	_
2 1 280.1 400 -197.6 -0.06288 0.6 1181 - 3 0.8 292.1 400 -142.8 0.129 0.6 944.4 - 4 0.171 271.4 400 917.6 3.383 0.999 221.1 0.7269 5 0.2137 271.3 400 98.8 1.05 0.999 285.7 0.2283 7 0.1202 276.4 400 1272 4.682 0.999 152.6 0.9949 8 0.2137 271.3 400 29.87 0.1255 0.999 289.4 0.03068 9 0.3339 271.3 400 335.9 1.249 0.999 445.2 0.2707 10 0.3339 259.6 250 934.9 3.608 0.999 415.8 0.7591 12 0.08526 330.1 400 122.7 0.9925 0.4 101.8 0.06351 13 0.4263 <t< td=""><td></td><td>1</td><td>_</td><td></td><td></td><td></td><td>0.6</td><td>1181</td><td>0</td></t<>		1	_				0.6	1181	0
3 0.8 292.1 400 -142.8 0.129 0.6 944.4 - 4 0.171 271.4 400 917.6 3.383 0.999 221.1 0.7269 5 0.2137 271.3 400 986.6 3.672 0.999 285.7 0.2283 7 0.1202 276.4 400 1272 4.682 0.999 152.6 0.9949 8 0.2137 271.3 400 29.87 0.1255 0.999 289.4 0.03068 9 0.3339 251.3 400 335.9 1.31 0.999 445.2 0.2707 10 0.3339 259.5 250 335.9 1.31 0.999 445.2 0.2707 10 0.3339 259.5 250 335.9 1.31 0.999 493.1 0.3034 11 0.3339 259.6 250 934.9 3.608 0.999 415.8 0.7591 12 0.08526			_						_
4 0.171 271.4 400 917.6 3.383 0.999 221.1 0.7269 5 0.2137 271.3 400 986.6 3.672 0.999 275.3 0.7887 6 0.2137 271.3 400 281.8 1.05 0.999 285.7 0.2283 7 0.1202 276.4 400 1272 4.682 0.999 285.7 0.2283 8 0.2137 271.3 400 29.87 0.1255 0.999 289.4 0.03068 9 0.3339 251.3 400 335.9 1.31 0.999 445.2 0.2707 10 0.3339 259.5 250 934.9 3.608 0.999 445.8 0.7501 11 0.3339 259.6 250 934.9 3.608 0.999 445.8 0.7591 12 0.08526 330.1 400 -657.9 -2.042 0.4 101.8 0.6651 13 0.4			_					_	_
5 0.2137 271.4 400 996.6 3.672 0.999 275.3 0.7887 6 0.2137 271.3 400 281.8 1.05 0.999 285.7 0.2283 7 0.1202 276.4 400 1272 4.682 0.999 152.6 0.9944 8 0.2137 271.3 400 29.87 0.1255 0.999 289.4 0.03068 9 0.3339 271.3 400 335.9 1.31 0.999 445.2 0.2707 10 0.3339 259.5 250 335.9 1.31 0.999 445.2 0.2707 11 0.3339 259.6 250 934.9 3.608 0.999 415.8 0.7591 12 0.08526 330.1 400 122.7 0.9925 0.4 101.8 0.06351 13 0.4263 190.7 400 -500 -1.265 0.4 818.7 16 0.6661 217.			_	400					0.7269
6 0.2137 271.3 400 281.8 1.05 0.999 285.7 0.2283 7 0.1202 276.4 400 1272 4.682 0.999 152.6 0.9949 8 0.2137 271.3 400 29.87 0.1255 0.999 289.4 0.03068 9 0.3339 271.3 400 335.9 1.31 0.999 445.2 0.2707 10 0.3339 259.5 250 335.9 1.31 0.999 445.2 0.2707 11 0.3339 259.6 250 934.9 3.608 0.999 415.8 0.7591 12 0.08526 330.1 400 122.7 0.9925 0.4 101.8 0.06351 13 0.4263 190.7 400 -657.9 -2.042 0.4 818.7 - 14 0.6661 217.2 400 -434.1 -0.9688 0.4 805.4 - 15 0.6661 <td></td> <td></td> <td></td> <td></td> <td></td> <td></td> <td></td> <td>_</td> <td></td>								_	
7 0.1202 276.4 400 1272 4.682 0.999 152.6 0.9949 8 0.2137 271.3 400 29.87 0.1255 0.999 289.4 0.03068 9 0.3339 271.3 400 335.9 1.249 0.999 445.2 0.2707 10 0.3339 259.6 250 335.9 1.31 0.999 445.8 0.7591 12 0.08526 330.1 400 122.7 0.9925 0.4 101.8 0.6551 13 0.4263 190.7 400 -657.9 -2.042 0.4 553.1 - 14 0.6661 229.7 400 -500 -1.265 0.4 818.7 - 15 0.6661 217.2 250 -500 -1.264 0.4 818.6 - 17 0.2 280.1 400 -197.6 -0.06288 0.6 252.5 - 18 0.2 300	-		_				0.999	_	
8 0.2137 271.3 400 29.87 0.1255 0.999 289.4 0.03068 9 0.3339 271.3 400 335.9 1.249 0.999 445.2 0.2707 10 0.3339 259.5 250 335.9 1.31 0.999 439.1 0.3034 11 0.3339 259.6 250 934.9 3.608 0.999 415.8 0.7591 12 0.08526 330.1 400 122.7 0.9925 0.4 101.8 0.06351 13 0.4263 190.7 400 -657.9 -2.042 0.4 553.1 - 14 0.6661 217.2 400 -500 -1.265 0.4 818.7 - 15 0.6661 217.2 250 -500 -1.264 0.4 818.6 - 17 0.2 280.1 400 -197.6 -0.06288 0.6 252.5 - 18 0.2			_	400			0.999	_	
9 0.3339 271.3 400 335.9 1.249 0.999 445.2 0.2707 10 0.3339 259.5 250 335.9 1.31 0.999 439.1 0.3034 11 0.3339 259.6 250 934.9 3.608 0.999 415.8 0.7591 12 0.08526 330.1 400 122.7 0.9925 0.4 101.8 0.06351 13 0.4263 190.7 400 -657.9 -2.042 0.4 553.1 - 14 0.6661 229.7 400 -434.1 -0.9698 0.4 805.4 - 15 0.6661 217.2 250 -500 -1.264 0.4 818.7 - 16 0.6661 217.2 250 -500 -1.264 0.4 818.6 - 17 0.2 280.1 400 -197.6 -0.06288 0.6 252.5 - 18 0.2 300.1			_				0.999	_	0.03068
10 0.3339 259.5 250 335.9 1.31 0.999 439.1 0.3034 11 0.3339 259.6 250 934.9 3.608 0.999 415.8 0.7591 12 0.08526 330.1 400 122.7 0.9925 0.4 101.8 0.06351 13 0.4263 190.7 400 -657.9 -2.042 0.4 553.1 - 14 0.6661 217.2 400 -500 -1.265 0.4 818.7 - 15 0.6661 217.2 250 -500 -1.264 0.4 818.6 - 17 0.2 280.1 400 -197.6 -0.06288 0.6 252.5 - 18 0.2 300.1 400 -197.6 -0.06288 0.6 945.2 - 20 0.64 292.1 400 -142.8 0.129 0.6 755.5 - 21 0.16 292.1							0.999	_	
11 0.3339 259.6 250 934.9 3.608 0.999 415.8 0.7591 12 0.08526 330.1 400 122.7 0.9925 0.4 101.8 0.06351 13 0.4263 190.7 400 -657.9 -2.042 0.4 553.1 - 14 0.6661 229.7 400 -500 -1.265 0.4 818.7 - 15 0.6661 217.2 250 -500 -1.264 0.4 818.6 - 16 0.6661 217.2 250 -500 -1.264 0.4 818.6 - 17 0.2 280.1 400 -197.6 -0.06288 0.6 252.5 - 18 0.2 300.1 400 -197.6 -0.06288 0.6 945.2 - 20 0.64 292.1 400 -142.8 0.129 0.6 188.9 - 21 0.16 292.1	10	0.3339	_			1.31	0.999	439.1	0.3034
13 0.4263 190.7 400 -657.9 -2.042 0.4 553.1 - 14 0.6661 229.7 400 -434.1 -0.9698 0.4 805.4 - 15 0.6661 217.2 400 -500 -1.265 0.4 818.7 - 16 0.6661 217.2 250 -500 -1.264 0.4 818.6 - 17 0.2 280.1 400 -197.6 -0.06288 0.6 252.5 - 18 0.2 300.1 400 71.51 0.849 0.6 237 0.1294 19 0.8 280.1 400 -142.8 0.129 0.6 945.2 - 20 0.64 292.1 400 -142.8 0.129 0.6 188.9 - 21 0.16 292.1 400 -36.35 0.5054 0.4 282.3 - 22 0.36 296.4 400			_				0.999	_	
13 0.4263 190.7 400 -657.9 -2.042 0.4 553.1 - 14 0.6661 229.7 400 -434.1 -0.9698 0.4 805.4 - 15 0.6661 217.2 400 -500 -1.265 0.4 818.7 - 16 0.6661 217.2 250 -500 -1.264 0.4 818.6 - 17 0.2 280.1 400 -197.6 -0.06288 0.6 252.5 - 18 0.2 300.1 400 71.51 0.849 0.6 237 0.1294 19 0.8 280.1 400 -197.6 -0.06288 0.6 945.2 - 20 0.64 292.1 400 -142.8 0.129 0.6 188.9 - 21 0.16 292.1 400 -142.8 0.129 0.6 188.9 - 22 0.36 296.4 400	12	0.08526	330.1	400	122.7	0.9925	0.4	101.8	0.06351
14 0.6661 229.7 400 -434.1 -0.9698 0.4 805.4 - 15 0.6661 217.2 400 -500 -1.265 0.4 818.7 - 16 0.6661 217.2 250 -500 -1.264 0.4 818.6 - 17 0.2 280.1 400 -197.6 -0.06288 0.6 252.5 - 18 0.2 300.1 400 -197.6 -0.06288 0.6 237 0.1294 19 0.8 280.1 400 -197.6 -0.06288 0.6 945.2 - 20 0.64 292.1 400 -142.8 0.129 0.6 188.9 - 21 0.16 292.1 400 -142.8 0.129 0.6 188.9 - 22 0.36 296.4 400 -23.72 0.5313 0.6 425.7 0.07258 23 0.2398 316.4 <td< td=""><td></td><td></td><td>_</td><td></td><td></td><td></td><td></td><td>_</td><td>†</td></td<>			_					_	†
15 0.6661 217.2 400 -500 -1.265 0.4 818.7 - 16 0.6661 217.2 250 -500 -1.264 0.4 818.6 - 17 0.2 280.1 400 -197.6 -0.06288 0.6 252.5 - 18 0.2 300.1 400 71.51 0.849 0.6 237 0.1294 19 0.8 280.1 400 -197.6 -0.06288 0.6 945.2 - 20 0.64 292.1 400 -142.8 0.129 0.6 755.5 - 21 0.16 292.1 400 -142.8 0.129 0.6 188.9 - 22 0.36 296.4 400 -23.72 0.5313 0.6 425.7 0.07258 23 0.2398 316.4 400 275.2 1.514 0.6 765 0.2426 25 0.512 310.1 400<	14	0.6661	+		-434.1	-0.9698			_
16 0.6661 217.2 250 -500 -1.264 0.4 818.6 - 17 0.2 280.1 400 -197.6 -0.06288 0.6 252.5 - 18 0.2 300.1 400 71.51 0.849 0.6 237 0.1294 19 0.8 280.1 400 -197.6 -0.06288 0.6 945.2 - 20 0.64 292.1 400 -142.8 0.129 0.6 755.5 - 21 0.16 292.1 400 -142.8 0.129 0.6 188.9 - 22 0.36 296.4 400 -23.72 0.5313 0.6 425.7 0.07258 23 0.2398 316.4 400 -36.35 0.5054 0.4 282.3 - 24 0.64 310.1 400 275.2 1.514 0.6 612 0.2426 25 0.512 310.1 400<	15	0.6661			-500	-1.265			_
17 0.2 280.1 400 -197.6 -0.06288 0.6 252.5 - 18 0.2 300.1 400 71.51 0.849 0.6 237 0.1294 19 0.8 280.1 400 -197.6 -0.06288 0.6 945.2 - 20 0.64 292.1 400 -142.8 0.129 0.6 755.5 - 21 0.16 292.1 400 -142.8 0.129 0.6 188.9 - 22 0.36 296.4 400 -23.72 0.5313 0.6 425.7 0.07258 23 0.2398 316.4 400 -36.35 0.5054 0.4 282.3 - 24 0.64 310.1 400 275.2 1.514 0.6 612 0.2426 25 0.512 310.1 400 275.2 1.514 0.6 612 0.2426 26 0.128 310.1 40	16	0.6661	+			<u> </u>		 	_
18 0.2 300.1 400 71.51 0.849 0.6 237 0.1294 19 0.8 280.1 400 -197.6 -0.06288 0.6 945.2 - 20 0.64 292.1 400 -142.8 0.129 0.6 755.5 - 21 0.16 292.1 400 -142.8 0.129 0.6 188.9 - 22 0.36 296.4 400 -23.72 0.5313 0.6 425.7 0.07258 23 0.2398 316.4 400 -36.35 0.5054 0.4 282.3 - 24 0.64 310.1 400 275.2 1.514 0.6 612 0.2426 25 0.512 310.1 400 275.2 1.514 0.6 612 0.2426 26 0.128 310.1 400 275.2 1.514 0.6 612 0.2426 27 0.04274 290.1 <td< td=""><td></td><td>0.2</td><td></td><td></td><td></td><td>-0.06288</td><td></td><td></td><td>_</td></td<>		0.2				-0.06288			_
19 0.8 280.1 400 -197.6 -0.06288 0.6 945.2 - 20 0.64 292.1 400 -142.8 0.129 0.6 755.5 - 21 0.16 292.1 400 -142.8 0.129 0.6 188.9 - 22 0.36 296.4 400 -23.72 0.5313 0.6 425.7 0.07258 23 0.2398 316.4 400 -36.35 0.5054 0.4 282.3 - 24 0.64 310.1 400 275.2 1.514 0.6 612 0.2426 25 0.512 310.1 400 275.2 1.514 0.6 612 0.2426 26 0.128 310.1 400 275.2 1.514 0.6 153 0.2426 27 0.04274 290.1 400 1312 4.823 0.999 175.8 0.8179 29 0.512 333.1	18	0.2		400	71.51	1	0.6		0.1294
20 0.64 292.1 400 -142.8 0.129 0.6 755.5 - 21 0.16 292.1 400 -142.8 0.129 0.6 188.9 - 22 0.36 296.4 400 -23.72 0.5313 0.6 425.7 0.07258 23 0.2398 316.4 400 -36.35 0.5054 0.4 282.3 - 24 0.64 310.1 400 275.2 1.514 0.6 612 0.2426 25 0.512 310.1 400 275.2 1.514 0.6 612 0.2426 26 0.128 310.1 400 275.2 1.514 0.6 153 0.2426 27 0.04274 290.1 400 1034 3.809 0.999 175.8 0.8179 29 0.512 333.1 400 618.4 2.578 0.6 629 0.4064 30 0.06821 353.1	19	0.8		400	-197.6	-0.06288	0.6	945.2	-
22 0.36 296.4 400 -23.72 0.5313 0.6 425.7 0.07258 23 0.2398 316.4 400 -36.35 0.5054 0.4 282.3 - 24 0.64 310.1 400 275.2 1.514 0.6 765 0.2426 25 0.512 310.1 400 275.2 1.514 0.6 612 0.2426 26 0.128 310.1 400 275.2 1.514 0.6 153 0.2426 27 0.04274 290.1 400 1312 4.823 0.999 54.23 0.9991 28 0.1368 271.4 400 1034 3.809 0.999 175.8 0.8179 29 0.512 333.1 400 618.4 2.578 0.6 629 0.4064 30 0.06821 353.1 400 1369 5.01 0.999 43.45 1.00 31 0.03419 31	20	0.64	1	400	-142.8	0.129	0.6	755.5	-
23 0.2398 316.4 400 -36.35 0.5054 0.4 282.3 - 24 0.64 310.1 400 275.2 1.514 0.6 765 0.2426 25 0.512 310.1 400 275.2 1.514 0.6 612 0.2426 26 0.128 310.1 400 275.2 1.514 0.6 153 0.2426 27 0.04274 290.1 400 1312 4.823 0.999 54.23 0.9991 28 0.1368 271.4 400 1034 3.809 0.999 175.8 0.8179 29 0.512 333.1 400 618.4 2.578 0.6 629 0.4064 30 0.06821 353.1 400 491.9 2.069 0.4 85.28 0.2269 31 0.03419 313.1 400 1369 5.01 0.999 43.45 1.00 32 0.341 309<	21	0.16	292.1	400	-142.8	0.129	0.6	188.9	-
24 0.64 310.1 400 275.2 1.514 0.6 765 0.2426 25 0.512 310.1 400 275.2 1.514 0.6 612 0.2426 26 0.128 310.1 400 275.2 1.514 0.6 153 0.2426 27 0.04274 290.1 400 1312 4.823 0.999 54.23 0.9991 28 0.1368 271.4 400 1034 3.809 0.999 175.8 0.8179 29 0.512 333.1 400 618.4 2.578 0.6 629 0.4064 30 0.06821 353.1 400 491.9 2.069 0.4 85.28 0.2269 31 0.03419 313.1 400 1369 5.01 0.999 43.45 1.00 32 0.341 309 400 -68.61 0.4023 0.4 400.8 - 33 0.4263 317.7<	22	0.36	296.4	400	-23.72	0.5313	0.6	425.7	0.07258
25 0.512 310.1 400 275.2 1.514 0.6 612 0.2426 26 0.128 310.1 400 275.2 1.514 0.6 153 0.2426 27 0.04274 290.1 400 1312 4.823 0.999 54.23 0.9991 28 0.1368 271.4 400 1034 3.809 0.999 175.8 0.8179 29 0.512 333.1 400 618.4 2.578 0.6 629 0.4064 30 0.06821 353.1 400 491.9 2.069 0.4 85.28 0.2269 31 0.03419 313.1 400 1369 5.01 0.999 43.45 1.00 32 0.341 309 400 -68.61 0.4023 0.4 400.8 - 33 0.4263 317.7 400 -30.35 0.5244 0.4 379.3 - 34 0.1024 333.1	23	0.2398	316.4	400	-36.35	0.5054	0.4	282.3	_
25 0.512 310.1 400 275.2 1.514 0.6 612 0.2426 26 0.128 310.1 400 275.2 1.514 0.6 153 0.2426 27 0.04274 290.1 400 1312 4.823 0.999 54.23 0.9991 28 0.1368 271.4 400 1034 3.809 0.999 175.8 0.8179 29 0.512 333.1 400 618.4 2.578 0.6 629 0.4064 30 0.06821 353.1 400 491.9 2.069 0.4 85.28 0.2269 31 0.03419 313.1 400 1369 5.01 0.999 43.45 1.00 32 0.341 309 400 -68.61 0.4023 0.4 400.8 - 33 0.4263 317.7 400 -30.35 0.5244 0.4 379.3 - 34 0.1024 333.1	24	0.64	310.1	400	275.2	1.514	0.6	765	0.2426
27 0.04274 290.1 400 1312 4.823 0.999 54.23 0.9991 28 0.1368 271.4 400 1034 3.809 0.999 175.8 0.8179 29 0.512 333.1 400 618.4 2.578 0.6 629 0.4064 30 0.06821 353.1 400 491.9 2.069 0.4 85.28 0.2269 31 0.03419 313.1 400 1369 5.01 0.999 43.45 1.00 32 0.341 309 400 -68.61 0.4023 0.4 400.8 - 33 0.4263 317.7 400 -30.35 0.5244 0.4 379.3 - 34 0.1024 333.1 400 618.4 2.578 0.6 125.8 0.4064 35 0.4096 362.1 400 1072 3.877 0.6 534.3 0.5969 37 0.1368	25	0.512	1	400	275.2	1.514	0.6	612	0.2426
28 0.1368 271.4 400 1034 3.809 0.999 175.8 0.8179 29 0.512 333.1 400 618.4 2.578 0.6 629 0.4064 30 0.06821 353.1 400 491.9 2.069 0.4 85.28 0.2269 31 0.03419 313.1 400 1369 5.01 0.999 43.45 1.00 32 0.341 309 400 -68.61 0.4023 0.4 400.8 - 33 0.4263 317.7 400 -30.35 0.5244 0.4 379.3 - 34 0.1024 333.1 400 618.4 2.578 0.6 125.8 0.4064 35 0.4096 362.1 400 1072 3.877 0.6 534.3 0.5969 37 0.1368 271.6 400 1158 4.265 0.999 174.7 0.9153 38 0.2728 3	26	0.128	310.1	400	275.2	1.514	0.6	153	0.2426
29 0.512 333.1 400 618.4 2.578 0.6 629 0.4064 30 0.06821 353.1 400 491.9 2.069 0.4 85.28 0.2269 31 0.03419 313.1 400 1369 5.01 0.999 43.45 1.00 32 0.341 309 400 -68.61 0.4023 0.4 400.8 - 33 0.4263 317.7 400 -30.35 0.5244 0.4 379.3 - 34 0.1024 333.1 400 618.4 2.578 0.6 125.8 0.4064 35 0.4096 333.1 400 618.4 2.578 0.6 503.2 0.4064 36 0.4096 362.1 400 1072 3.877 0.6 534.3 0.5969 37 0.1368 271.6 400 1158 4.265 0.999 174.7 0.9153 38 0.2728 38	27	0.04274	290.1	400	1312	4.823	0.999	54.23	0.9991
30 0.06821 353.1 400 491.9 2.069 0.4 85.28 0.2269 31 0.03419 313.1 400 1369 5.01 0.999 43.45 1.00 32 0.341 309 400 -68.61 0.4023 0.4 400.8 - 33 0.4263 317.7 400 -30.35 0.5244 0.4 379.3 - 34 0.1024 333.1 400 618.4 2.578 0.6 125.8 0.4064 35 0.4096 333.1 400 618.4 2.578 0.6 503.2 0.4064 36 0.4096 362.1 400 1072 3.877 0.6 534.3 0.5969 37 0.1368 271.6 400 1158 4.265 0.999 174.7 0.9153 38 0.2728 382.1 400 1117 3.757 0.4 377.5 0.4912 39 0.171 2	28	0.1368	271.4	400	1034	3.809	0.999	175.8	0.8179
31 0.03419 313.1 400 1369 5.01 0.999 43.45 1.00 32 0.341 309 400 -68.61 0.4023 0.4 400.8 - 33 0.4263 317.7 400 -30.35 0.5244 0.4 379.3 - 34 0.1024 333.1 400 618.4 2.578 0.6 125.8 0.4064 35 0.4096 333.1 400 618.4 2.578 0.6 503.2 0.4064 36 0.4096 362.1 400 1072 3.877 0.6 534.3 0.5969 37 0.1368 271.6 400 1158 4.265 0.999 174.7 0.9153 38 0.2728 382.1 400 1117 3.757 0.4 377.5 0.4912 39 0.171 271.5 400 1101 4.055 0.999 219 0.8704 40 0.2728 349	29	0.512	333.1	400	618.4	2.578	0.6	629	0.4064
32 0.341 309 400 -68.61 0.4023 0.4 400.8 - 33 0.4263 317.7 400 -30.35 0.5244 0.4 379.3 - 34 0.1024 333.1 400 618.4 2.578 0.6 125.8 0.4064 35 0.4096 333.1 400 618.4 2.578 0.6 503.2 0.4064 36 0.4096 362.1 400 1072 3.877 0.6 534.3 0.5969 37 0.1368 271.6 400 1158 4.265 0.999 174.7 0.9153 38 0.2728 382.1 400 1117 3.757 0.4 377.5 0.4912 39 0.171 271.5 400 1101 4.055 0.999 219 0.8704 40 0.2728 349.5 400 435.2 1.908 0.4 338.4 0.2029	30	0.06821	353.1	400	491.9	2.069	0.4	85.28	0.2269
33 0.4263 317.7 400 -30.35 0.5244 0.4 379.3 - 34 0.1024 333.1 400 618.4 2.578 0.6 125.8 0.4064 35 0.4096 333.1 400 618.4 2.578 0.6 503.2 0.4064 36 0.4096 362.1 400 1072 3.877 0.6 534.3 0.5969 37 0.1368 271.6 400 1158 4.265 0.999 174.7 0.9153 38 0.2728 382.1 400 1117 3.757 0.4 377.5 0.4912 39 0.171 271.5 400 1101 4.055 0.999 219 0.8704 40 0.2728 349.5 400 435.2 1.908 0.4 338.4 0.2029	31	0.03419	313.1	400	1369	5.01	0.999	43.45	1.00
34 0.1024 333.1 400 618.4 2.578 0.6 125.8 0.4064 35 0.4096 333.1 400 618.4 2.578 0.6 503.2 0.4064 36 0.4096 362.1 400 1072 3.877 0.6 534.3 0.5969 37 0.1368 271.6 400 1158 4.265 0.999 174.7 0.9153 38 0.2728 382.1 400 1117 3.757 0.4 377.5 0.4912 39 0.171 271.5 400 1101 4.055 0.999 219 0.8704 40 0.2728 349.5 400 435.2 1.908 0.4 338.4 0.2029	32	0.341	309	400	-68.61	0.4023	0.4	400.8	_
35 0.4096 333.1 400 618.4 2.578 0.6 503.2 0.4064 36 0.4096 362.1 400 1072 3.877 0.6 534.3 0.5969 37 0.1368 271.6 400 1158 4.265 0.999 174.7 0.9153 38 0.2728 382.1 400 1117 3.757 0.4 377.5 0.4912 39 0.171 271.5 400 1101 4.055 0.999 219 0.8704 40 0.2728 349.5 400 435.2 1.908 0.4 338.4 0.2029	33	0.4263	317.7	400	-30.35	0.5244	0.4	379.3	_
36 0.4096 362.1 400 1072 3.877 0.6 534.3 0.5969 37 0.1368 271.6 400 1158 4.265 0.999 174.7 0.9153 38 0.2728 382.1 400 1117 3.757 0.4 377.5 0.4912 39 0.171 271.5 400 1101 4.055 0.999 219 0.8704 40 0.2728 349.5 400 435.2 1.908 0.4 338.4 0.2029	34	0.1024	333.1	400	618.4	2.578	0.6	125.8	0.4064
37 0.1368 271.6 400 1158 4.265 0.999 174.7 0.9153 38 0.2728 382.1 400 1117 3.757 0.4 377.5 0.4912 39 0.171 271.5 400 1101 4.055 0.999 219 0.8704 40 0.2728 349.5 400 435.2 1.908 0.4 338.4 0.2029	35	0.4096	333.1	400	618.4	2.578	0.6	503.2	0.4064
38 0.2728 382.1 400 1117 3.757 0.4 377.5 0.4912 39 0.171 271.5 400 1101 4.055 0.999 219 0.8704 40 0.2728 349.5 400 435.2 1.908 0.4 338.4 0.2029	36			400	1072	1	0.6		<u> </u>
39 0.171 271.5 400 1101 4.055 0.999 219 0.8704 40 0.2728 349.5 400 435.2 1.908 0.4 338.4 0.2029	37	0.1368	271.6	400	1158	4.265	0.999	174.7	0.9153
40 0.2728 349.5 400 435.2 1.908 0.4 338.4 0.2029	38	0.2728	382.1	400	1117	3.757	0.4	377.5	0.4912
	39	0.171	271.5	400	1101	4.055	0.999	219	0.8704
41 0.341 350.2 400 446.5 1.941 0.4 423.7 0.2077	40	0.2728	349.5	400	435.2	1.908	0.4	338.4	0.2029
	41	0.341	350.2	400	446.5	1.941	0.4	423.7	0.2077

State points	m (kg/s)	T (°C)	P (kPa)	h (kJ/kg)	Salinity (g/kg)	Ėx (kW)
0	_	25	101	104.8	35	_
d1	2	25	101	99.77	35	0
d2	2	25.4	150	101.4	35	0.0023
d3	2	31.22	150	124.9	35	0.459
d4	2	53.53	150	214.2	35	10.22
d5	1.962	53.53	150	214	35	10.03
d6	0.03759	53.53	150	224.2	0.7491	0.2037
d7	0.03759	25	150	104.9	0.3669	0.00184

Table 7.2 Thermodynamic properties of the desalination system at each state point

• Effects of solar irradiance

The amount of solar irradiance available for production of power and rate of heat plays a significant role in the sizing of the system. Figure 7.12 displays that increase in solar radiation affects the performance of the QEARS in a negative manner.

Both energetic and exergetic COPs are found to decrease from 22.07 to 17.84 and from 7.01 to 6.18, respectively, with an increase in solar radiation from 550 to 650 W/m². This behavior is seen because an increase in solar radiation increases the power and rate of heat production of the solar PV/T system. This increase in output results in a decrease in the performance of the QEARS for a fixed cooling load. For a fixed cooling load provision of more energy to the system than its required results in degrading performance of the system, as this extra energy is not required by the system to achieve its target. The increase in solar radiation results in degrading performance of the desalination system as seen in Fig. 7.13.

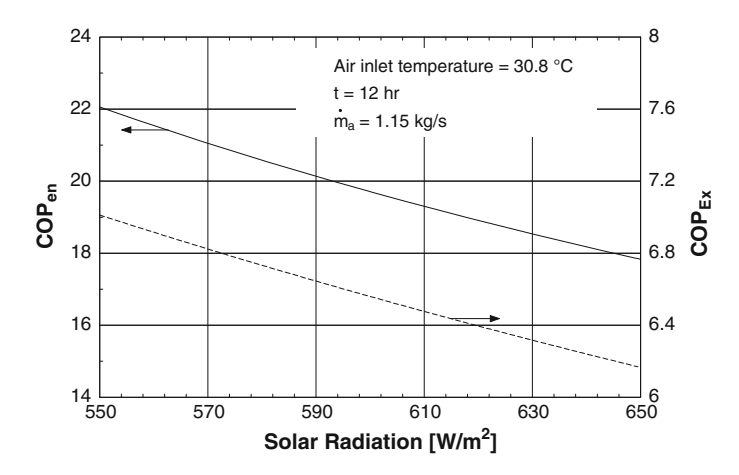


Fig. 7.12 Effects of solar irradiance on energetic and exergetic COPs

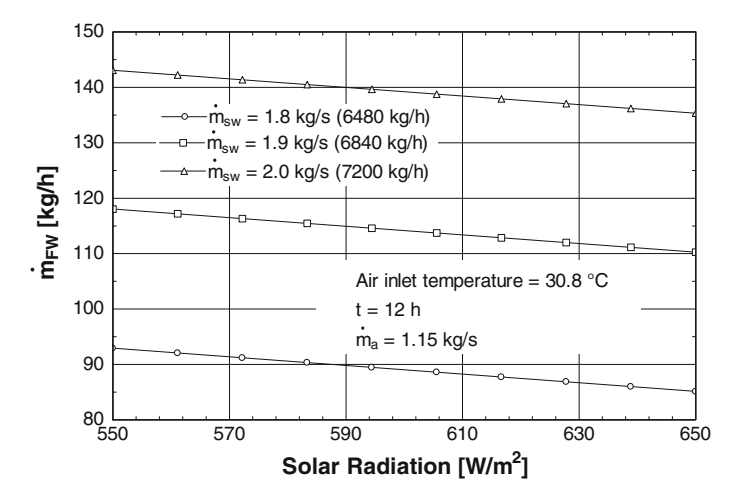


Fig. 7.13 Effects of solar irradiance on freshwater production for different flow rate of sea water

The increase in solar radiation results in a decrease in production of fresh water for a different flow rate of sea-water. The production rate of fresh water decreases from 143.1 to 85.1 kg/h to vary the flow rate of sea-water from 6480 to 7200 kg/h. As a result of the degrading performance of the QEARS and desalination system, the energetic and exergetic utilization factors and performance ratio of the system are also noted to decrease as shown in Figs. 7.14 and 7.15. The utilization factors and the performance ratio decrease from 3.7 to 3.1, 0.5 to 0.38, and 0.035 to 0.021, respectively. The results show that for a fixed cooling load, the increase in solar radiation is not recommended for the performance of the overall integrated system.

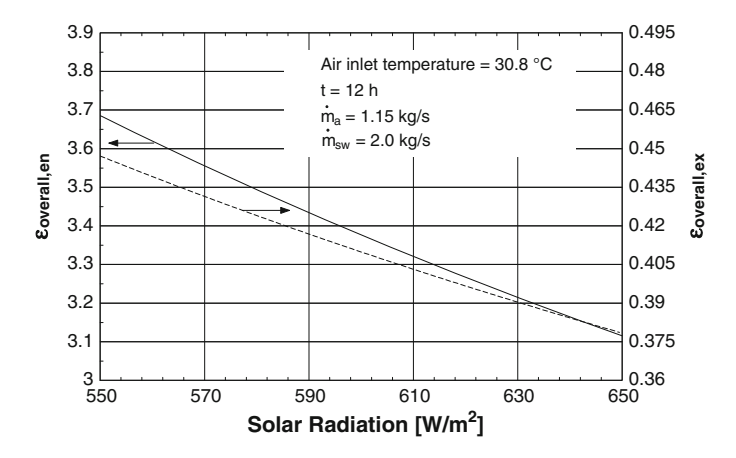


Fig. 7.14 Effects of solar irradiance on the energetic and exergetic utilization factors

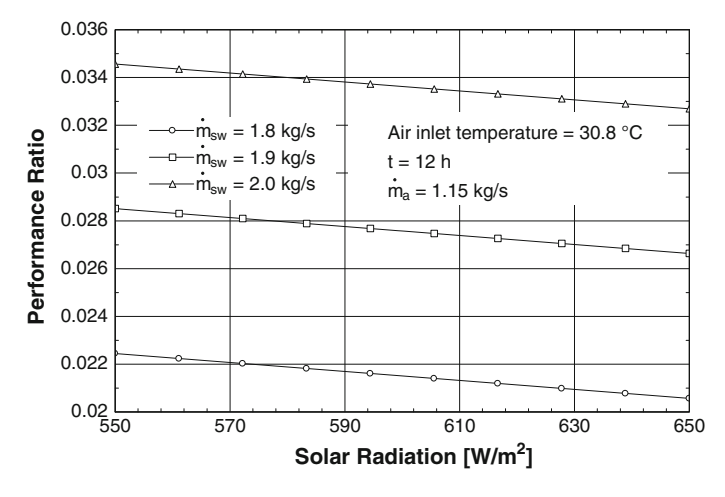


Fig. 7.15 Effects of solar irradiance on performance ratio of the system

• Effects of seawater salinity

The salinity of seawater plays a significant role in designing the solar-based integrated system. As shown in Fig. 7.16, an increase in salinity and temperature of the seawater results in a strange behavior of the system. The production of freshwater first increases with increase in temperature of sea water at a fixed salinity, but as the salinity increases the production of fresh water starts to decrease with

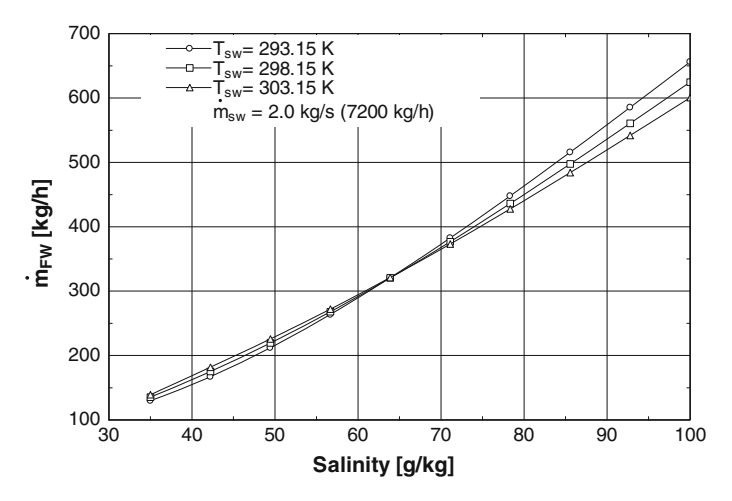


Fig. 7.16 Effects of salinity of seawater on freshwater production

increase in temperature of the sea water. The amount of freshwater produced varies from 130 to 656 kg/h with an increase in salinity from 35 to 100 g/kg, respectively. These results are obtained for seawater temperatures of 298, 303, and 308 K, respectively. This behavior is because increasing salinity until a certain level, and an increase in temperature of sea- water results in an increase in the amount of water vaporized to produce freshwater as it passes through the condenser and absorber of the QEARS. The increase in sea water temperature makes it possible to attain a higher temperature that is closer to the condition of superheated vapor.

The increase in vapor production then results in a higher rate of fresh water production. However, when the salinity of sea water crosses a certain threshold, the effect of sea-water temperature of sea water on the production of fresh water takes a secondary role and salinity of seawater is important to determination of the trend of the system behavior. Such irregular behavior of the system also reflects on the performance ratio of the system as displayed in Fig. 7.17. The performance ratio varies from 0.03 to 0.16, with an increase in salinity and temperature of sea water from 35 to 100 g/kg and 293.15 to 303.15 K, respectively. This behavior shows that there is a salinity limit to which an increase in seawater affects the performance of the system in a positive way. However, crossing the threshold limit results in domination of the salinity effect on the performance evaluation of the system as compared to the secondary role of seawater temperatures.

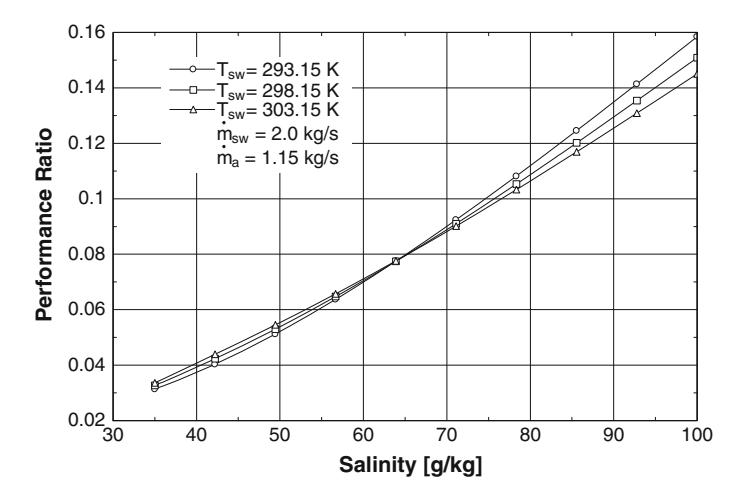


Fig. 7.17 Effects of salinity of seawater on performance ratio of the system

7.4 Case Study 3: Geothermal-Based Multigeneration System

System description

Figure 7.18 presents a novel integrated system capable of generating power, cooling, heating, hot water, and hydrogen while using geothermal water as an energy source. The first step towards achieving these multiple outputs from the proposed system is to provide energy to the very high temperature generator (VHTG) using high temperature geothermal water from an underground reservoir as shown in Fig. 7.19. The strong solution enters the VHTG at state 36 where it is heated to leave as a weak solution at state 38 and ammonia-water vapor at state 37 as shown in Fig. 7.19. The weak solution exiting the VHTG at state 38 releases heat in the VHHX to the incoming strong solution at state 35 before exiting the VHHX at state 40. This weak solution at state 40 then mixes with the weak solution from state 30 to leave at state 41. This weak solution from state 41 then gives out heat in the HHX and combines with a weak solution from state 12 to leave at state 33. The weak solution from state 33 then gives out heat in the MHX and combines with a weak solution from state 23 to leave at state 14. The weak solution then enters the LHX where it heats the strong solution coming from state 19. After releasing heat, the weak solution at state 15 enters the expansion valve where its pressure and temperature drops to that of the absorber before entering the absorber at state 16. The vapor from state 37 then enters the HTG where it heats up the strong solution from state 34 and leaves as an ammonia-water vapor at state 28 and state 31. These two streams mix and leave at state 39 to enter the MTG where it heats up the strong solution from state 26 and leaves as ammonia-water vapor at state 4 and state 27. These two ammonia-water vapors are then combined and leave at state 5. The

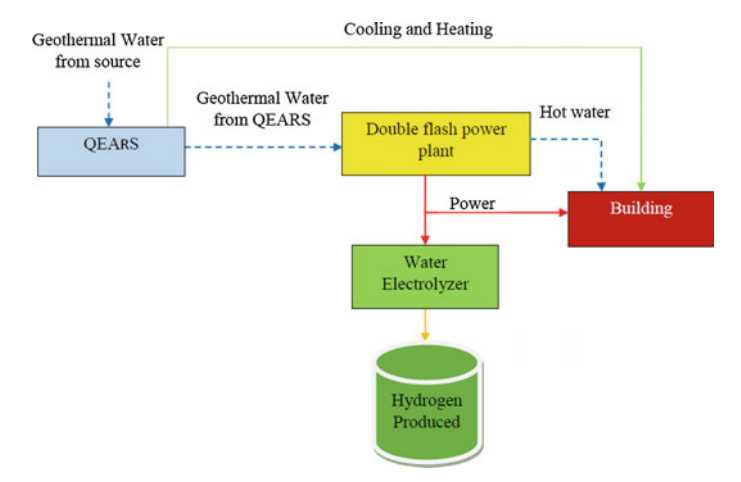


Fig. 7.18 Flow diagram of the multigeneration system

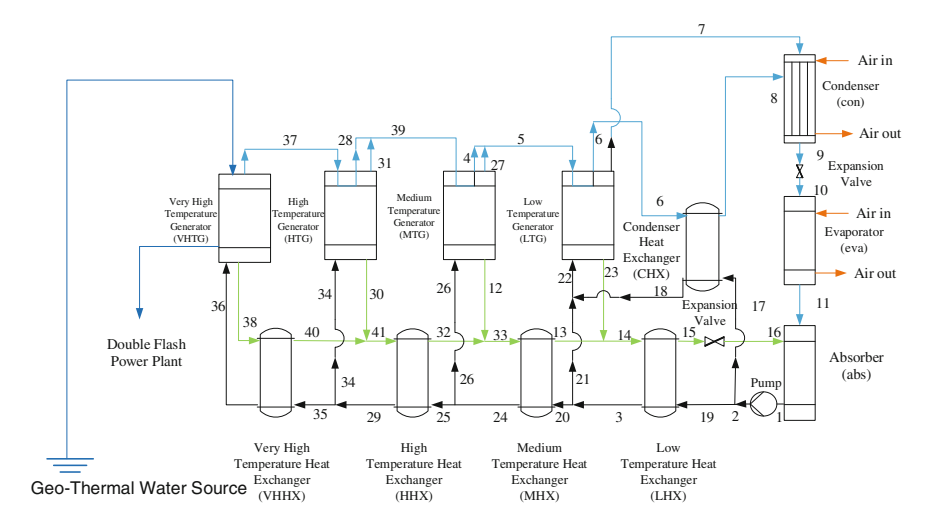


Fig. 7.19 Schematic of the geothermal source driven quadruple effect absorption refrigeration system

ammonia-water vapor at state 5 enters the LTG and heats up the strong solution coming from state 22 and leaves as an ammonia-water vapor at state 6 and state 7. The stream at state 7 goes directly into the condenser while state 6 is directed to the CHX to release heat to part of the liquid that is fed backward by the pump at state 17. The liquid gains heat and leaves the condenser at state 18. The ammonia-water vapor leaving CHX at state 8 enters the condenser, gives out heat, and then leaves at state 9. The air is used to cool the stream in the condenser. This air stream is heated up in the process and is then supplied to the building for heating purposes. The ammonia-water stream then passes through the expansion valve and leaves at state 10 to enter the evaporator. In the evaporator, heat is gained by the system from the returning air from the building. The air is cooled and supplied to the user for cooling. The ammonia-water vapor that is heated in the evaporator leaves at stat 11 to enter the absorber. In the absorber, all three streams mix and give out heat to the surrounding and leave at state 1 in liquid form to enter the pump. After providing energy to the QEARS, geothermal water enters the double flash power plant as shown in Fig. 7.20. The entering geothermal temperature is assumed to be 15 °C less than the source temperature. In the double flash power plant, the geothermal stream enters the expansion valve at state 1. Here, the pressure of the stream decreases to produce additional steam before entering the first flash chamber at state 2. In the flash chamber, steam is extracted from the upper half at state 3, and saturated mixture is allowed to leave from the bottom at state 8. The steam extracted at state 3 then enters the high pressure turbine and expands to state 4 to produce power. However, stream from state 8 enters second expansion valve to enter the second flash chamber at reduced pressure at state 9. In the second flash chamber, steam is extracted at state 10 which then mixes with state 4 to enter the low pressure turbine. The geothermal liquid from the flash chamber is reinjected to the source

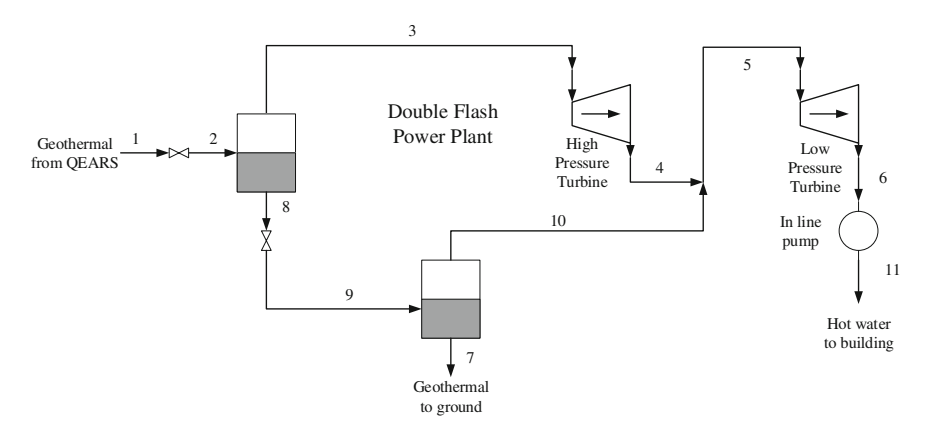


Fig. 7.20 Schematic of the geothermal double flash power plant

well at state 7. In the low pressure turbine, steam from state 5 expands to state 6 to produce power. Power generated by a high pressure turbine (HPT) and low pressure turbine (LPT) is then supplied to the building (80 %) and the electrolyzer (20 %). However, the geothermal liquid leaving the LPT at state 6 is pumped to the atmospheric pressure and is supplied to the building to meet its hot water needs. The power supplied to the electrolyzer is used to break the water bond to produce hydrogen. Hydrogen produced is stored in the tanks for later use. The system and analysis presented in this case study are obtained from the work done by Ratlamwala et al. (2012b).

• Thermodynamic analysis

To analyze and assess the integrated system studied, mass, energy, and exergy balance equations are written for the components of the QEARS, double flash power plant, and an electrolyzer. All systems are assumed to be running under thermodynamic equilibrium and steady state conditions. Heat losses and pressure drops in all components and connecting piping system are negligible. Parasitic losses caused by the pumps and turbines are considered while calculating the net power output from the plant.

QEARS system

The rate of heat supplied to the QEARS VHTG is provided using the geothermal water source. The rate of heat transfer obtained from the geothermal water source is calculated as follows:

$$\dot{Q}_{\text{geo}} = \dot{m}_{\text{geo}} \times \left(h_{\text{geo}_{\text{source}}} - h_{\text{geo}_{\text{VHTG exit}}} \right) \tag{7.56}$$

$$\dot{Q}_{\rm VHTG} = \dot{Q}_{\rm geo} \tag{7.57}$$

The mass balance equations of VHTG are given as follows:

$$\dot{m}_{36}x_{36} = \dot{m}_{37}x_{37} + \dot{m}_{38}x_{38} \tag{7.58}$$

$$\dot{m}_{36} = \dot{m}_{37} + \dot{m}_{38} \tag{7.59}$$

To obtain the outlet conditions of the VHTG, the following equation is used:

$$\dot{m}_{36}h_{36} + \dot{Q}_{VHTG} = \dot{m}_{37}h_{37} + \dot{m}_{38}h_{38} \tag{7.60}$$

The exergy destruction in VHTG becomes

$$\dot{E}x_{dest,VHTG} + \dot{E}x_{37} + \dot{E}x_{38} = \dot{E}x_{36} + \dot{E}x_{th,VHTG}$$
 (7.61)

where $\dot{E}x_{37} = \dot{m}_{37}((h_{37} - h_0) - T_0(s_{37} - s_0))$ and the same relationship is employed for other states.

The energy balance equations for VHHX are given below

$$\dot{m}_{35}h_{35} + \dot{Q}_{\text{VHHX}} = \dot{m}_{36}h_{36} \tag{7.62}$$

$$\dot{m}_{38}h_{38} = \dot{m}_{40}h_{40} + \dot{Q}_{\text{VHHX}} \tag{7.63}$$

The mass and energy balance equations for the condenser are given below

$$\dot{m}_9 = \dot{m}_7 + \dot{m}_8 \tag{7.64}$$

$$\dot{m}_9 h_9 = \dot{m}_7 h_7 + \dot{m}_8 h_8 + \dot{Q}_{\rm con} \tag{7.65}$$

The balance equations for mass and energy of the evaporator:

$$\dot{m}_{10} = \dot{m}_{11} \tag{7.66}$$

$$\dot{m}_{10}h_{10} + \dot{Q}_{\text{eva}} = \dot{m}_{11}h_{11} \tag{7.67}$$

The following energy balance equation is used to calculate the heat rejected from the absorber:

$$\dot{m}_{11}h_{11} + \dot{m}_{16}h_{16} = \dot{m}_1h_1 + \dot{Q}_{abs} \tag{7.68}$$

The work done by the pump is calculated using the equation given below

$$\dot{W}_{\rm p} = \dot{m}_1 (h_2 - h_1) \tag{7.69}$$

The energetic and exergetic COPs are defined as

$$COP_{en} = \frac{\dot{Q}_{eva} + \dot{Q}_{con}}{\dot{Q}_{geo} + \dot{W}_{P}}$$

$$(7.70)$$

$$COP_{ex} = \frac{\dot{E}x_{eva} + \dot{E}x_{con}}{\dot{E}x_{eeo} + \dot{W}_{P}}$$
(7.71)

• Double flash power plant

The power that can be obtained from the turbines of double flash power plant is calculated using

$$\dot{W}_{\text{turb}} = \dot{m}_3(h_3 - h_4) + \dot{m}_5(h_5 - h_6) \tag{7.72}$$

The power consumed by pump in is expressed as

$$\dot{W}_{\text{pump}} = \dot{m}_6(h_{11} - h_6) \tag{7.73}$$

To have the correct model, parasitic losses are also considered and are defined as

$$\dot{W}_{\text{parasitic}} = 0.1 \left(\dot{W}_{\text{turb}} - \dot{W}_{\text{pump}} - \dot{W}_{\text{p}} \right) \tag{7.74}$$

The actual net power that can be obtained from the double flash plant running on geothermal is expressed as

$$\dot{W}_{\text{net}_{\text{geo}}} = \dot{W}_{\text{turb}} - \dot{W}_{\text{pump}} - \dot{W}_{\text{p}} - \dot{W}_{\text{parasitic}} \tag{7.75}$$

The power supplied to the building is calculated as

$$\dot{W}_{\text{building}} = 0.8 \times \dot{W}_{\text{net}_{\text{geo}}} \tag{7.76}$$

The energetic and exergetic contents of hot water supplied to building are defined as

$$\dot{\mathbf{E}}\mathbf{n}_{\text{hw}} = \dot{m}_{11}(h_{11}) \tag{7.77}$$

$$\dot{\mathbf{E}}\mathbf{x}_{\text{hw}} = \dot{m}_{11}((h_{11} - h_0) - T_0(s_{11} - s_0)) \tag{7.78}$$

Electrolyzer

The amount of hydrogen produced by the electrolyzer is calculated as

$$\eta_{\text{electrolyzer}} = \frac{\dot{m}_{\text{H}_2} \times \text{HHV}}{\dot{W}_{\text{electrolyzer}}}$$
(7.79)

where $\eta_{\text{electrolyzer}}$ is assumed to be 60 % and $\dot{W}_{\text{electrolyzer}} = 0.2 \times \dot{W}_{\text{net}_{\text{geo}}}$.

• Energetic and exergetic utilization factors

The single generation energetic and exergetic utilization factors are defined as

$$\varepsilon_{\rm en,s} = \frac{\dot{Q}_{\rm eva}}{\dot{Q}_{\rm geo}} \tag{7.80}$$

$$\varepsilon_{\text{ex,s}} = \frac{\dot{E}x_{\text{eva}}}{\dot{E}x_{\text{geo}}} \tag{7.81}$$

The double generation energetic and exergetic utilization factors are defined as

$$\varepsilon_{\rm en,d} = \frac{\dot{Q}_{\rm eva} + \dot{Q}_{\rm con}}{\dot{Q}_{\rm geo}} \tag{7.82}$$

$$\varepsilon_{\text{ex,d}} = \frac{\dot{E}x_{\text{eva}} + \dot{E}x_{\text{con}}}{\dot{E}x_{\text{geo}}}$$
 (7.83)

The triple generation energetic and exergetic utilization factors are defined as

$$\varepsilon_{\text{en,t}} = \frac{\dot{Q}_{\text{eva}} + \dot{Q}_{\text{con}} + \dot{E}n_{\text{hw}}}{\dot{Q}_{\text{geo}}}$$
(7.84)

$$\varepsilon_{\text{ex,t}} = \frac{\dot{E}x_{\text{eva}} + \dot{E}x_{\text{con}} + \dot{E}x_{\text{hw}}}{\dot{E}x_{\text{geo}}}$$
(7.85)

The quadruple generation energetic and exergetic utilization factors are defined as

$$\varepsilon_{\text{en,q}} = \frac{\dot{Q}_{\text{eva}} + \dot{Q}_{\text{con}} + \dot{E}n_{\text{hw}} + \dot{E}n_{\text{H}_2}}{\dot{Q}_{\text{geo}}}$$
(7.86)

$$\varepsilon_{\text{ex,q}} = \frac{\dot{E}x_{\text{eva}} + \dot{E}x_{\text{con}} + \dot{E}x_{\text{hw}} + \dot{E}x_{\text{H}_2}}{\dot{E}x_{\text{eeo}}} \tag{7.87}$$

The pentuple generation energetic and exergetic utilization factors are defined as

$$\varepsilon_{\text{en,p}} = \frac{\dot{Q}_{\text{eva}} + \dot{Q}_{\text{con}} + \dot{E}n_{\text{hw}} + \dot{E}n_{\text{H}_2} + \dot{W}_{\text{bld}}}{\dot{Q}_{\text{geo}}}$$
(7.88)

$$\varepsilon_{\text{ex,p}} = \frac{\dot{E}x_{\text{eva}} + \dot{E}x_{\text{con}} + \dot{E}x_{\text{hw}} + \dot{E}x_{\text{H}_2} + \dot{W}_{\text{bld}}}{\dot{E}x_{\text{geo}}}$$
(7.89)

· Results and discussion

In present case study, we analyze a novel geothermal based integrated system for provision of pentuple outputs namely power, cooling, heating, hot water, and hydrogen production in a cost-effective, environmental friendly and sustainable manner. The effects of variation in geothermal source temperature and ambient temperature on the rate of cooling production, power generation, and energy and exergy utilization factors are then studied.

• Effects of geothermal source temperature

The geothermal water source temperature plays a vital role in the functioning of the proposed integrated system. This is a parameter that lets us know whether the geothermal water source has the capabilities to produce power or if it can only be used for direct purposes such as cooling or heating. The increase in the geothermal source temperature has positive effects on the rate of heat supplied to the QEARS and adverse effects on the rate of cooling produced by the QEARS as shown in Fig. 7.21. The rate of heat supplied to the QEARS is observed to increase from 64.9 to 68.9 kW with the rise in geothermal water source temperature from 440 to

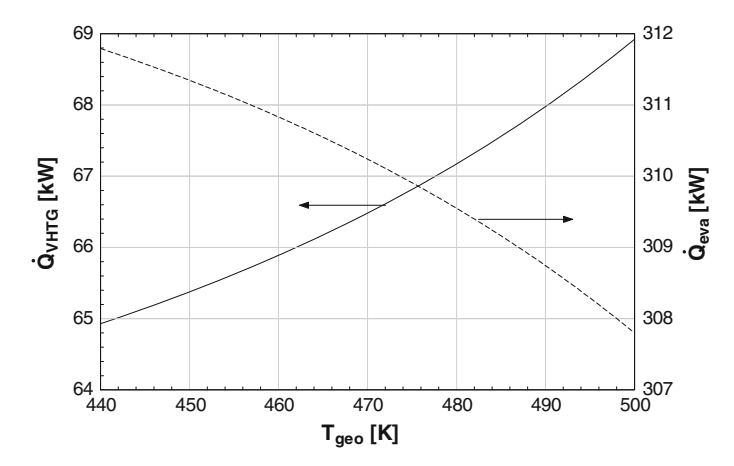


Fig. 7.21 Effects of geothermal source temperature on the rate of heat supplied to the VHTG and rate of cooling produced

500 K. The rate of cooling produced by the OEARS is noted to decrease from 311.8 to 307.8 kW with an increase in geothermal water source temperature. The increasing trend of the heat supplied to the QEARS is observed because the increase in the geothermal water source temperature supplies an additional amount of heat. The driving force for any heat related problem is temperature, and as the temperature difference increases, the heat supplied increases. This increase in the rate of heat supplied to the very high temperature generator of the OEARS hurts the performance of the refrigeration system due to the fixed condenser load. The fixed condenser load of the refrigeration system does not allow the extra heat to be converted into useful output because the condenser is incapable of rejecting this excess heat. This results in a relatively higher temperature refrigerant entering the evaporator. As the temperature difference between the inlet and outlet of the evaporator decreases, the rate of cooling produced by the evaporator decreases. The effects of a rise in geothermal water source temperature on the power supplied to the building, and electrolyzer are presented in Fig. 7.22. The power supplied to the building and the electrolyzer is observed to increase from 20.25 to 63.04 kW and 5.06 to 15.76 kW, respectively, with an increase in geothermal water source temperature from 440 to 500 K. The increasing trends of power supplied to the building, and the electrolyzer are noted because the increase in geothermal water source temperature results in relatively higher temperature geothermal water entering the double flash power plant. The rise in the supply temperature of the geothermal water temperature helps to generate additional high temperature steam in the flash chamber. This steam is then supplied to the turbine, producing relatively higher power provided to the building and the electrolyzer. The effects of an increase in geothermal water source temperature on the energy and exergy utilization factors are displayed in Fig. 7.23. The energy utilization factors for single,

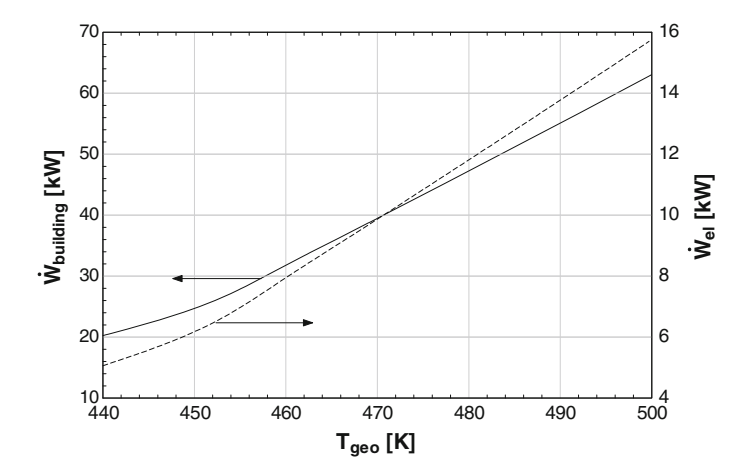


Fig. 7.22 Effects of geothermal source temperature on the power supplied to the building and electrolyzer

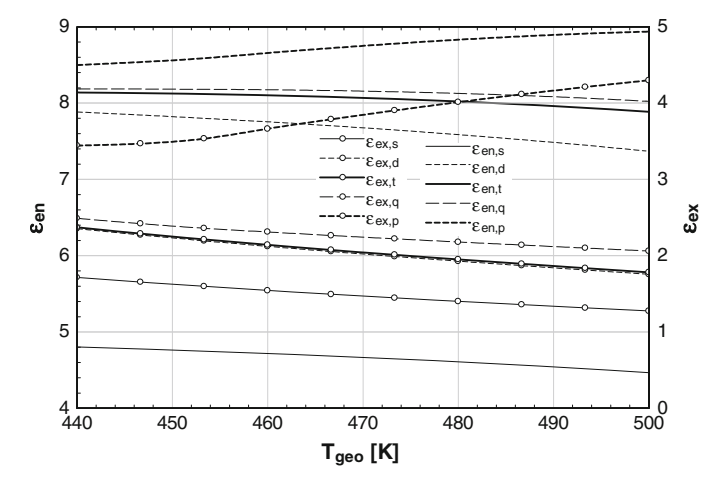


Fig. 7.23 Effects of geothermal source temperature on energy and exergy utilization factors

double, triple, quadruple, and pentuple generation are noticed to be varying from 4.8 to 4.5, 7.8 to 7.4, 8.1 to 7.9, 8.2 to 8.0, and 8.5 to 9.0, respectively, with increase in geothermal water source temperature from 440 to 500 K. The exergy utilization factors for single, double, triple, quadruple, and pentuple generation are noted to vary from 1.7 to 1.3, 2.3 to 1.8, 2.4 to 1.8, 2.5 to 2.0, and 3.4 to 4.3, respectively with increase in the geothermal water source temperature. The utilization factor trends show that as the number of generations increase, the system performance is enhanced as the system can better utilize the energy source by recovering as much energy as possible internally.

• Effects of ambient temperature

The fluctuation in the ambient temperature can play a significant role in the performance of any mainly heat driven system. The effect or rise in ambient temperature on the energy and exergy utilization factors is presented in Fig. 7.24. The energy utilization factors for single, double, triple, quadruple, and pentuple generation are noted to remain constant at 4.4, 7.3, 7.8, 8.0, and 8.9, respectively, with an increase in ambient temperature from 273 to 305 K. The exergy utilization factors for single, double, triple, quadruple, and pentuple generation are noted to increase from 0.46 to 1.92, 0.47 to 2.79, 0.54 to 2.80, 0.82 to 3.12, and 2.98 to 5.65, respectively, with an increase in ambient temperature. The constant behavior of the energy utilization factors shows that energy analysis is not capable of capturing the fluctuation in system performance due to variation in ambient temperature. On the other hand, the increasing trend of exergy utilization factors shows that the increase in ambient temperature is beneficial for performance enhancement of the system. The proposed system being mainly high temperature heat driven, the increase in the ambient temperature results in a lower temperature difference between the system and the surrounding. As the temperature difference decreases, the exergetic heat lost

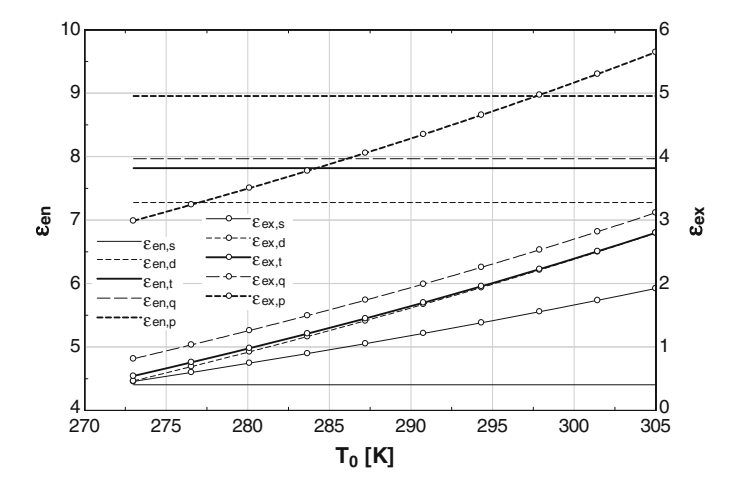


Fig. 7.24 Effects of ambient temperature on energy and exergy utilization factors

from the system to the surrounding drops and the system is better able to utilize the exergy provided to the system in terms of high temperature geothermal water. The analysis also shows that the exergy utilization factor increases with an increase in the number of useful outputs, hence indicating that with every additional useful output the system input exergy is better utilized.

7.5 Case Study 4: Geothermal-Based Integrated System for Standalone Building Needs

System description

The integrated system consisting of a quadruple flash power plant (QFPP), an electrolyzer, a quadruple effect absorption refrigeration system and an airconditioning process presented in this case study is illustrated in Fig. 7.25. The integrated system studied is capable of producing hextuple useful outputs that are power, hot water, heating, cooling, hydrogen and conditioned air (dry air). The high temperature geothermal water source is used as an energy carrier and is first passed through the QFPP to produce power and hot water. The net power generated by the QFPP is then supplied to the building, the QEARS, and the hydrogen production unit. The heat load produced by the condenser of the QFPP is used to provide hot water for domestic use. The low to moderate temperature geothermal liquid stream leaving the QFPP at state 20 is provided to the QEARS for heating and cooling production. The heating produced by the QEARS is supplied to the building to meet domestic heating loads whereas the cooling produced is divided into two parts. Part of the cooling produced is provided to the buildings for domestic purposes, and

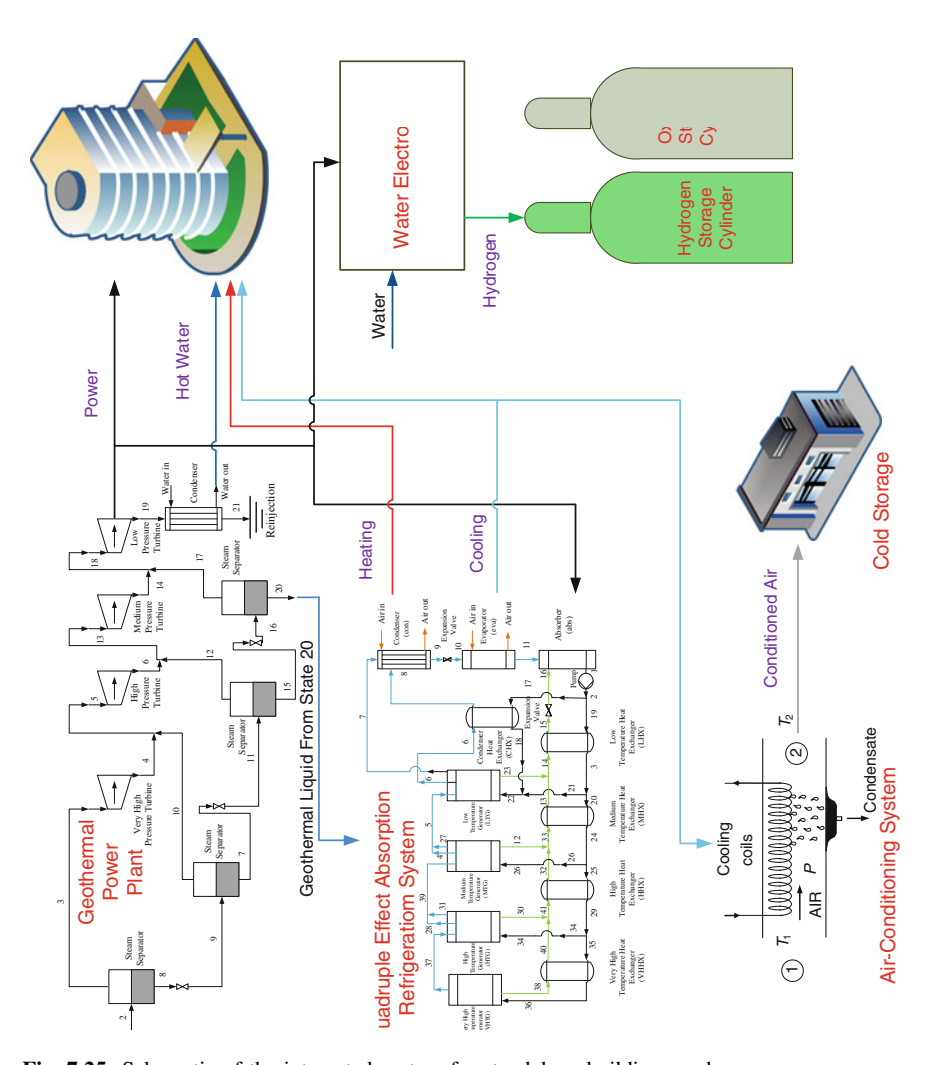


Fig. 7.25 Schematic of the integrated system for standalone building needs

another part is supplied to the air-conditioning system for provision of cooled dry air to cold storages. A detailed working principal and system description of QFPP and QEARS can be found in studies conducted by Ratlamwala and Dincer (2012) and Ratlamwala et al. (2012c), respectively. The part of the power produced by the QFPP is supplied to the water electrolyzer, its bonds are broken into hydrogen and oxygen. The hydrogen produced is stored in the cylinder that can be used later as per consumer need. The air-conditioned process considered in the present study is a cooling with dehumidification process for supply of cooled dry air. The moist air entering at state 1 passes through the cooling coil where it comes in contact with

low temperature coils. The low temperature coils help condensing the air and helps with moisture loss. The relatively dry air then leaves the air-conditioning process to be supplied to the cold, dry storage facility. The system and analysis presented in this case study are obtained from the work done by Ratlamwala and Dincer (2013).

• Thermodynamic analysis

This section provided energy and exergy modeling of the integrated system presented in this case study.

The net power produced by the QFPP is expressed as

$$\dot{W}_{\text{net}_{\text{geo}}} = \dot{W}_{\text{turb}} - \dot{W}_{\text{p}} - \dot{W}_{\text{parasitic}} \tag{7.90}$$

where

$$\dot{W}_{\text{turb}} = \dot{m}_3(h_3 - h_4) + \dot{m}_5(h_5 - h_6) + \dot{m}_{13}(h_{13} - h_{14}) + \dot{m}_{18}(h_{18} - h_{19})$$
 $\dot{W}_{\text{parasitic}} = 0.2(\dot{W}_{\text{turb}} - \dot{W}_{\text{p}}) \text{ and}$
 $\dot{W}_{\text{p}} = \dot{m}_1(h_2 - h_1)$

Here, $\dot{W}_{\rm net_{geo}}$ represents net power produced by the QFPP, $\dot{W}_{\rm turb}$ represents total power produced by the turbines, $\dot{W}_{\rm parasitic}$ represents parasitic loses occurring in the system and is assumed to be 20 % based on a study conducted by Ratlamwala and Dincer (2013), $\dot{W}_{\rm p}$ represents power consumed by the QEARS, h represents specific enthalpy, and \dot{m} represents mass flow rate.

In the present study, half of the power produced is supplied to the building and the remaining half is supplied to the electrolyzer. In the electrolyzer, power supplied is used to generate hydrogen, and the rate of hydrogen production is then calculated as

$$\eta_{\text{elec}} = \frac{\dot{m}_{\text{H}_2} \times \text{HHV}}{\dot{W}_{\text{electrolyzer}}} \tag{7.91}$$

where $\eta_{\rm elec}$ is assumed to be 56 %, HHV represents higher heating value of hydrogen, $\dot{W}_{\rm elec}$ represents power supplied to the electrolyzer, and $\dot{m}_{\rm H_2}$ represents hydrogen production rate in kg/s.

The exergy content of hydrogen produced is calculated as follows:

$$\dot{E}x_{H_2} = \dot{m}_{H_2} [ex_{H_2,ch} + ex_{H_2,ph}]$$
 (7.92)

where

$$\operatorname{ex}_{\mathrm{H_2,ch}} = \frac{236.1 \times 1000}{\mathrm{MW_{H_2}}}$$
 and $\operatorname{ex}_{\mathrm{H_2,ph}} = [(h_{\mathrm{H_2}} - h_0) - T_0(s_{\mathrm{H_2}} - s_0)].$

Here, the value of 235.15 kJ/g-mol is taken as the exergy content of hydrogen as given by Dincer and Rosen (2007). $\dot{E}x_{H_2}$, $ex_{H_2,ch}$, $ex_{H_2,ph}$, MW_{H_2} , T_0 and s, represent exergy rate of hydrogen produced, specific chemical exergy of hydrogen, specific physical exergy of hydrogen, molecular weight of hydrogen, ambient temperature and specific entropy, respectively.

The energy and exergy contents of the hot water supplied to the buildings are defined as

$$\dot{E}n_{hw} = \dot{m}_{hw}(h_{hw,o} - h_{hw,i})$$
 (7.93)

$$\dot{E}x_{hw} = \dot{m}_{hw} ((h_{hw,o} - h_{hw,i}) - T_0 (s_{hw,o} - s_{hw,i}))$$
(7.94)

where $\dot{E}n_{hw}$ and $\dot{E}x_{hw}$ represent energy rate of hot water and exergy rate of hot water, respectively.

The rate of heat supplied to the QEARS by the QFPP is calculated as

$$\dot{Q}_{\text{VHTG}} = \dot{m}_{20} \times \left(h_{20,\text{QFPP}} - h_{\text{QEARS,o}} \right) \tag{7.95}$$

where $\dot{Q}_{\rm VHTG}$ represents the rate of heat supplied to the very high temperature generator of the QEARS, \dot{m}_{20} represents mass flow rate of geothermal liquid at state 20 of the QFPP, $h_{20,\rm QFPP}$ represents specific enthalpy at state 20 of the QFPP, and $h_{\rm QEARS,o}$ represents the specific enthalpy of stream leaving the QEARS.

The mass balance and energy balance equations for the VHTG are given as follows:

$$\dot{m}_{36}x_{36} = \dot{m}_{37}x_{37} + \dot{m}_{38}x_{38} \tag{7.96}$$

$$\dot{m}_{36} = \dot{m}_{37} + \dot{m}_{38} \tag{7.97}$$

$$\dot{m}_{36}h_{36} + \dot{Q}_{\text{VHTG}} = \dot{m}_{37}h_{37} + \dot{m}_{38}h_{38} \tag{7.98}$$

where \dot{m} , x, h and \dot{Q}_{VHTG} represent mass flow rate, concentration of ammonia—water mixture, specific enthalpy and rate of heat supplied to the very high temperature generator of the QEARS, respectively.

The thermal exergy content of the VHTG is calculated using

$$\dot{\mathbf{E}}\mathbf{x}_{\text{VHTG}} = \left(1 - \frac{T_0}{T_{\text{VHTG}}}\right) \times \dot{Q}_{\text{VHTG}} \tag{7.99}$$

where

$$T_{\rm VHTG} = \frac{T_{36} + T_{37} + T_{38}}{3}$$

The energy balance equation for the condenser is given below

$$\dot{m}_9 h_9 = \dot{m}_7 h_7 + \dot{m}_8 h_8 + \dot{Q}_{\rm con} \tag{7.100}$$

The exergy content of condenser is calculated using

$$\dot{\mathbf{E}}\mathbf{x}_{\text{con}} = \left(1 - \frac{T_0}{T_{\text{con}}}\right) \times \dot{Q}_{\text{con}} \tag{7.101}$$

where

$$T_{\rm con}=\frac{T_7+T_8+T_9}{3}$$

The energy balance equation of evaporator is written as

$$\dot{m}_{10}h_{10} + \dot{Q}_{\text{eva}} = \dot{m}_{11}h_{11} \tag{7.102}$$

The exergy content of evaporator is calculated using

$$\dot{\mathbf{E}}\mathbf{x}_{\text{eva}} = \left(1 - \frac{T_0}{T_{\text{eva}}}\right) \times \dot{Q}_{\text{eva}} \tag{7.103}$$

where

$$T_{\text{eva}} = \frac{T_{10} + T_{11}}{2}$$

The mass balance equations for air-conditioning process is written as

$$\dot{m}_{a1} = \dot{m}_{a2} \tag{7.104}$$

$$\dot{m}_{w1} = \dot{m}_{w2} + \dot{m}_{w} \rightarrow \dot{m}_{a1}\omega_{1} = \dot{m}_{a2}\omega_{2} + \dot{m}_{w}$$
 (7.105)

The energy balance equation is written as

$$\dot{m}_{a1}h_1 = \dot{Q}_{out} + \dot{m}_{a2}h_2 + \dot{m}_{w}h_{w} \tag{7.106}$$

where \dot{Q}_{out} is supplied by QEARS

The exergy balance equation is written as

$$\dot{m}_{a1} ex_1 - \dot{Q}_{out} \left(1 - \frac{T_0}{T} \right) - \dot{m}_{a2} ex_2 - \dot{m}_{w} ex_w - \dot{E}x_{dest} = 0$$
 (7.107)

Here,

$$\dot{E}x_{\text{dest}} = T_0 \left[\dot{m}_{\text{a2}} s_2 + \dot{m}_{\text{w}} s_{\text{w}} + \frac{\dot{Q}_{\text{out}}}{T} - \dot{m}_{\text{a1}} s_1 \right]$$
(7.108)

The energy and exergy efficiencies equations are written on the principal of useful output over required input. The single generation energy and exergy efficiencies are defined as

$$\eta_{\text{en,s}} = \frac{\dot{W}_{\text{net,geo}}}{\dot{m}_{1,\text{qf}} h_{1,\text{qf}} - \dot{m}_{21,\text{qf}} h_{21,\text{qf}} - \dot{m}_{20,\text{qf}} h_{20,\text{qf}}}$$
(7.109)

$$\eta_{\text{ex,s}} = \frac{\dot{W}_{\text{net,geo}}}{\dot{E}x_{1,qf} - \dot{E}x_{21,qf} - \dot{E}x_{20,qf}}$$
(7.110)

where $\eta_{\rm en,s}$ and $\eta_{\rm ex,s}$ represent energy and exergy efficiencies of the single generation system.

The double generation energy and exergy efficiencies are defined as

$$\eta_{\text{en,d}} = \frac{\dot{W}_{\text{net,geo}} + \dot{E}n_{\text{hw}}}{\dot{m}_{1,\text{qf}}h_{1,\text{qf}} - \dot{m}_{21,\text{qf}}h_{21,\text{qf}} + \dot{m}_{\text{w}}h_{\text{w,in}}}$$
(7.111)

$$\eta_{\text{ex,d}} = \frac{\dot{W}_{\text{net,geo}} + \dot{E}x_{\text{hw}}}{\dot{E}x_{1\text{ of}} - \dot{E}x_{21\text{ of}} + \dot{E}x_{\text{hw in}}}$$
(7.112)

where $\eta_{\rm en,d}$ and $\eta_{\rm ex,d}$ represent energy and exergy efficiencies of the double generation system.

The triple generation energy and exergy efficiencies are defined as

$$\eta_{\text{en,t}} = \frac{\dot{W}_{\text{bld}} + \dot{E}n_{\text{hw}} + \dot{m}_{\text{H}_2}h_{\text{H}_2}}{\dot{m}_{1,\text{qf}}h_{1,\text{qf}} - \dot{m}_{21,\text{qf}}h_{21,\text{qf}} + \dot{m}_{\text{w}}h_{\text{w,in}}}$$
(7.113)

$$\eta_{\text{ex,t}} = \frac{\dot{W}_{\text{bld}} + \dot{E}x_{\text{hw}} + \dot{E}x_{\text{H}_2}}{\dot{E}x_{1,\text{of}} - \dot{E}x_{21,\text{of}} + \dot{E}x_{\text{hw,in}}}$$
(7.114)

where $\eta_{\text{en,t}}$ and $\eta_{\text{ex,t}}$ represent energy and exergy efficiencies of the triple generation system.

The quadruple generation energy and exergy efficiencies are defined as

$$\eta_{\text{en,q}} = \frac{\dot{W}_{\text{bld}} + \dot{E}n_{\text{hw}} + \dot{m}_{\text{H}_2}h_{\text{H}_2} + \dot{Q}_{\text{eva}}}{\dot{m}_{\text{1 of}}h_{\text{1 of}} - \dot{m}_{\text{21 of}}h_{\text{21 of}} + \dot{m}_{\text{w}}h_{\text{w in}} + \dot{m}_{\text{a eva}}h_{\text{a in eva}}}$$
(7.115)

$$\eta_{\text{ex,q}} = \frac{\dot{W}_{\text{bld}} + \dot{E}x_{\text{hw}} + \dot{E}x_{\text{H}_2} + \dot{E}x_{\text{eva}}}{\dot{E}x_{1,\text{of}} - \dot{E}x_{21,\text{of}} + \dot{E}x_{\text{hw,in}} + \dot{E}x_{\text{a,in,eva}}}$$
(7.116)

where $\eta_{\rm en,q}$ and $\eta_{\rm ex,q}$ represent energy and exergy efficiencies of the quadruple generation system. $\dot{Q}_{\rm eva}$ and $\dot{\rm Ex}_{\rm eva}$ represent rate of cooling produced by the QEARS and rate of exergy carried by cooling produced by the QEARS, respectively.

The pentuple generation energy and exergy efficiencies are defined as

$$\eta_{\text{en,p}} = \frac{\dot{W}_{\text{bld}} + \dot{E}n_{\text{hw}} + \dot{m}_{\text{H}_2}h_{\text{H}_2} + \dot{Q}_{\text{eva}} + \dot{Q}_{\text{con}}}{\dot{m}_{1,\text{qf}}h_{1,\text{qf}} - \dot{m}_{21,\text{qf}}h_{21,\text{qf}} + \dot{m}_{\text{w}}h_{\text{w,in}} + \dot{m}_{\text{a,eva}}h_{\text{a,in,eva}} + \dot{m}_{\text{a,con}}h_{\text{a,in,con}}}$$
(7.117)

$$\eta_{\text{ex,p}} = \frac{\dot{W}_{\text{bld}} + \dot{E}x_{\text{hw}} + \dot{E}x_{\text{H}_2} + \dot{E}x_{\text{eva}} + \dot{E}x_{\text{con}}}{\dot{E}x_{1,\text{of}} - \dot{E}x_{21,\text{of}} + \dot{E}x_{\text{hw,in}} + \dot{E}x_{\text{a,in,eva}} + \dot{E}x_{\text{a,in,con}}}$$
(7.118)

where $\eta_{\rm en,p}$ and $\eta_{\rm ex,p}$ represent energy and exergy efficiencies of the pentuple generation system.

The hextuple generation energy and exergy efficiencies are defined as

$$\eta_{\text{en,h}} = \frac{\dot{W}_{\text{bld}} + \dot{E}n_{\text{hw}} + \dot{m}_{\text{H}_2}h_{\text{H}_2} + \dot{Q}_{\text{eva}} + \dot{Q}_{\text{con}} + \dot{m}_{\text{2,d}}h_{\text{2,d}}}{\dot{m}_{1,\text{qf}}h_{1,\text{qf}} - \dot{m}_{21,\text{qf}}h_{21,\text{qf}} + \dot{m}_{\text{a,eva}}h_{\text{a,in,eva}} + \dot{m}_{\text{a,con}}h_{\text{a,in,con}} + \dot{m}_{\text{w}}h_{\text{w,in}}}$$
(7.119)

$$\eta_{\text{ex,h}} = \frac{\dot{W}_{\text{bld}} + \dot{E}x_{\text{hw}} + \dot{E}x_{\text{H}_2} + \dot{E}x_{\text{eva}} + \dot{E}x_{\text{con}} + \dot{m}_{2,\text{d}}ex_{2,\text{d}}}{\dot{E}x_{1,\text{of}} - \dot{E}x_{21,\text{of}} + \dot{E}x_{\text{a.in.eva}} + \dot{E}x_{\text{a.in.con}} + \dot{E}x_{\text{hw}}}$$
(7.120)

where $\eta_{en,h}$ and $\eta_{ex,h}$ represent energy and exergy efficiencies of the hextuple generation system. $ex_{2,d}$ represents specific exergy carried by conditioned air (dry air).

• Results and discussion

In present case study, we present in-depth energy and exergy analyses of an integrated system consisting of the QFPP, the QEARS, an electrolyzer and an air-conditioning process (cooling with dehumidification) for provision of power, hot water, heating, cooling, hydrogen and dry air. Several operating parameters are varied to observe their effects on the performance of the system, and the results obtained are discussed below.

• Effects of geothermal pressure at state f2

The geothermal liquid pressure plays a significant role in studies concerning geothermal flash systems because the amount of steam produced due to flashing is highly dependent on the pressure of geothermal fluid exiting the first expansion valve. The effect of an increase in geothermal liquid pressure at state f2 on net power produced by the QFPP and the hydrogen production rate is displayed in

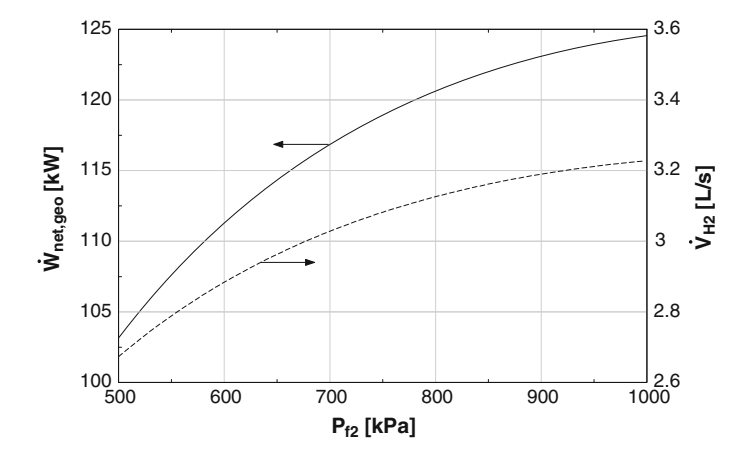


Fig. 7.26 Effects of geothermal liquid pressure at state f2 on net power generation and rate of hydrogen production

Fig. 7.26. The net power generated by the QFPP and the rate of hydrogen production increases from 103.2 to 124.6 kW and 2.7 to 3.2 L/s, respectively, with increase in pressure at state f2 from 500 to 1000 kPa. Such behavior is because the increase in the pressure of stream exiting the first expansion valve helps generae more steam out of the same amount of water as compared to stream exiting at a lower pressure. As the amount of steam in the exit stream increases the power produced by the turbine also increases and as a result, the net power generated by the QFPP increases. The portion of net power produced by the QFPP is supplied to the electrolyzer for hydrogen production, so there is a direct relation between the increase in net power generated and hydrogen production rate. With increase in net power generated, a greater amount of power is supplied to the electrolyzer and with increase in power; the bond dissociation capability of the electrolyzer increases, resulting in a higher rate of hydrogen produced.

• Effects of geothermal source temperature

The geothermal liquid temperature is important in the integrated systems that use geothermal liquid as an energy source. The impact of an increase in geothermal source temperature on the net power output of the QFPP and the hydrogen produced by the system can be seen in Fig. 7.27. The net power produced and rate of hydrogen produced are found to increase from 46.2 to 111 kW and 1.2 to 2.9 L/s, respectively, with an increase in geothermal source temperature from 450 to 500 K. Such behavior is because an increase in geothermal source temperature results in higher content of energy carried by the stream and as the energy content of the geothermal liquid being provided to the QFPP increases, the power production capacity of the QFPP also increases. The portion of power produced by the QFPP supplied to the water electrolyzer results in a higher rate of hydrogen production

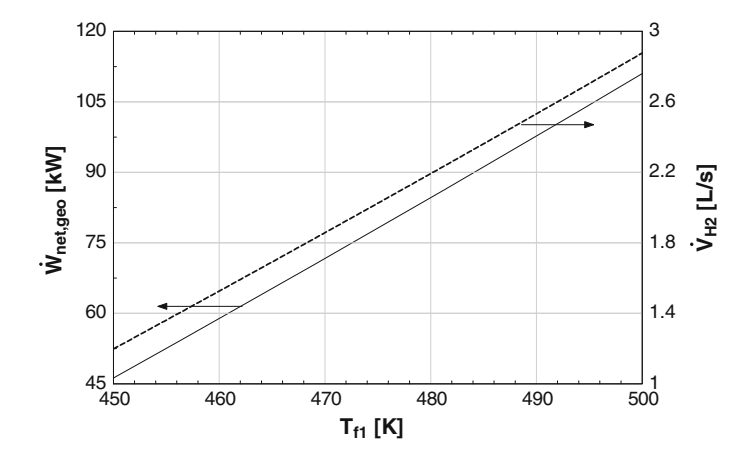


Fig. 7.27 Effects of geothermal source temperature on net power generation and rate of hydrogen production

because the water electrolyzers require power to break the water bond in order to produce hydrogen.

• Effects of cooling load

The integrated system studied in this paper is capable of providing cooling as per the demand, makeing it necessary to explore the impact of fluctuation in cooling demand on the performance of the integrated system. The consequences of variation in cooling load along with different evaporator temperatures on the provision of the rate of heating are studied as shown in Fig. 7.28. The rate of heating provided by the condenser of the QEARS is found to increase from 199.4 to 349.4 kW, 186.8 to

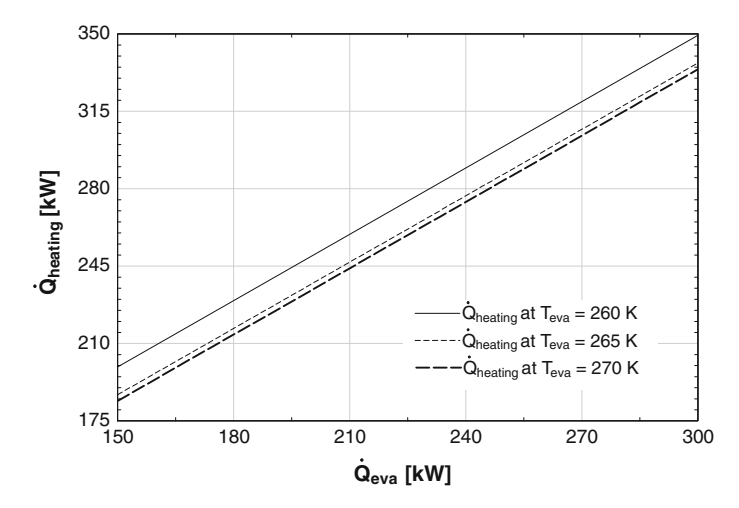


Fig. 7.28 Effects of evaporator load and temperature on rate of heating

336.8 kW, and 184 to 334 kW, respectively with increasing cooling demand from 150 to 300 kW for evaporator temperature of 260, 265 and 270 K. It is observed that increasing cooling demand results in an increase in the rate of heating for a particular evaporator temperature because increasing cooling demand for a specific evaporator temperature can only be met by provision of comparatively lower stream temperature entering the evaporator for steady mass flow rate. To reduce further the temperature of the steam entering the evaporator, more heat needs to be rejected through the condenser that is used for provide heating to the customers. The rise in evaporator temperature decreases the rate of heating provided because for higher evaporator temperature and fixed cooling load, lower amount of heat needs to be rejected by the stream entering the evaporator in the condenser to meet the evaporator load.

• Effects of multigeneration

This subsection sheds light on the performance improvement of the integrated system due to multigeneration. It is known that deploying a multigeneration system that uses a single source of energy enhances the performance of the system in terms of efficiency. In the present study a hextuple generation integrated system is examined that is capable of producing power, hot water, heating, cooling, hydrogen, and conditioned air (dry air). Figure 7.29 displays the effects of an increase in geothermal source temperature on the exergy efficiencies of the multigeneration systems. The exergy efficiency of the single, double, triple, quadruple, pentuple, and hextuple generations is found to increase from 0.20 to 0.23, 0.13 to 0.24, 0.15 to 0.25, 0.17 to 0.26, 0.20 to 0.28, and 0.21 to 0.28, respectively with an increase in

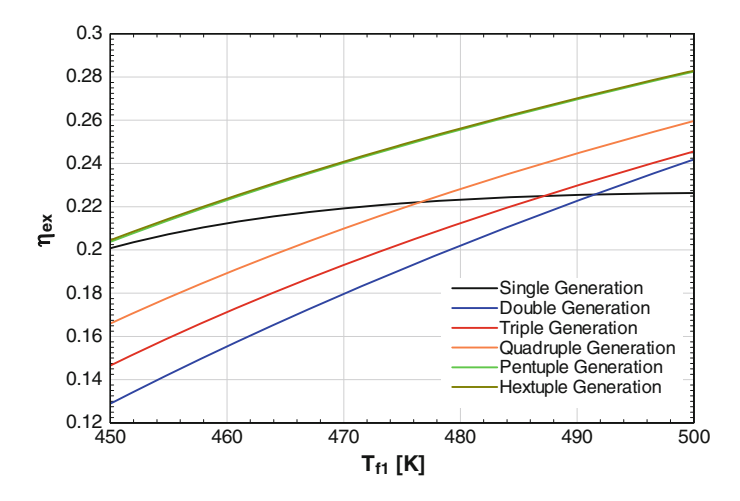


Fig. 7.29 Effects of geothermal source temperature on exergy efficiencies of the multigeneration systems

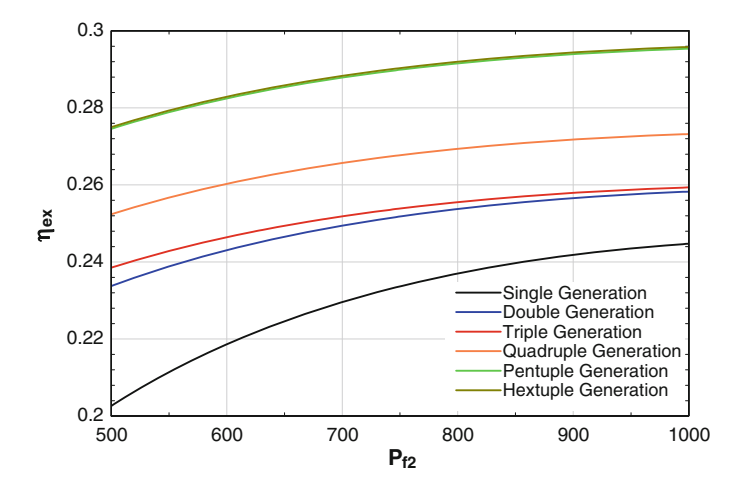


Fig. 7.30 Effects of geothermal liquid pressure at state f2 on exergy efficiencies of the multigeneration systems

geothermal source temperature from 450 to 500 K. It is observed that for higher geothermal source temperature above 475 K, the increase in number of generation leads to higher exergy efficiency. The effect of an increase in the number of generations fades out with each additional generation and for the pentuple and hextuple generations the exergy efficiencies are almost similar. The effects of an increase in geothermal liquid pressure at state f2 on the exergy efficiencies of the multigeneration systems are presented in Fig. 7.30. The exergy efficiency of the single, double, triple, quadruple, pentuple, and hextuple generations is found to increase from 0.20 to 0.24, 0.23 to 0.25, 0.24 to 0.26, 0.25 to 0.27, 0.27 to 0.29, and 0.27 to 0.29, respectively, with an increase in geothermal liquid pressure at state f2 from 500 to 1000 kPa. The trend seen in Fig. 7.30 shows that increase in a number of generations is beneficial in terms of exergy efficiency until it reaches pentuple generation then it becomes almost similar to the hextuple generation system. Another point observed is that as the number of generations increase, the difference in exergy efficiency with the previous generation decreases gradually until it reaches pentuple generation and then the difference between efficiencies become negligible. Other potential benefits of multigeneration systems include reduced environmental, reduced cost, reduced payback time, increased efficiency, and greater effectiveness.

7.6 Closing Remarks

The current chapter presents the number of case studies pertaining to the integrated absorption refrigeration systems with renewable energy sources for multigeneration purposes. Energy and exergy analyses of each system are also presented to familiarize the reader with the thermodynamic model of the integrated systems. The parametric studies are carried out to demonstration the effects of variation in operating parameters on the performance of the integrated systems. Also presented in this chapter, is the efficiency analysis of the multigeneration system which shows the effect of an increase in the number of generations on the efficiency of the system.

Chapter 8 Developments in Absorption Refrigeration Systems

8.1 Introduction

At present, the dominant technology in refrigeration systems around the globe is the conventional vapor-compression cycle, known for heavy electricity consumption due to the presence of a compressor and to the high peak loads during hot days (Zeyghami et al. 2015; Hassan et al. 2012). Using solar energy to produce refrigeration and air-conditioning can provide a sustainable and an environmentally friendly alternative to the conventional air-conditioning system (Baniyounes et al. 2013). The concept of a solar assisted refrigeration system was first presented in the 1970, during an energy crisis (Qu et al. 2010; Maidment and Paurine 2012; Kim 2008). However, with the sudden decrease in fossil fuel prices, interest in this idea has dwindled. The only driving force currently is the environmental consequence.

An International Energy Agency (2013) report highlighted that until 2011 only about 750 solar cooling systems were operational worldwide. Although, the number of installed solar cooling systems is minuscule at present, recently we have again seen a gain in interest in the solar cooling systems due to public awareness of the need to reduce greenhouse and ozone depleting gasses coupled with an increase in fossil fuel prices (Baniyounes et al. 2013).

The present chapter highlights the recent developments and potential applications in the area of absorption refrigeration systems. This chapter provides an overview of the studies carried out concerning advanced multigeneration systems, novel ARS mixtures and novel ARS designs.

8.2 Advanced Solar-Based Absorption Refrigeration Systems

This section deals with advancements in the area of solar driven absorption refrigeration systems. Sauceda et al. (2011) carried out a numerical design and simulation study of a parabolic trough solar collector assisted absorption cooling system and found out that under particular design conditions, the COP of the integrated system and the global efficiency of the system are 0.87 and 0.54, respectively. A dynamic model of a novel integrated parabolic trough collector and double effect absorption chiller for solar heating and cooling were presented by Calise (2012). The results obtained from the analysis highlighted that the combined system can give tough competition to the conventional systems in the majority of the locations studied. However, the hottest climates provide the best economic profitability. A mathematical model for the optimal COP prediction of a solar refrigeration system for ice production using a different technique was presented by Hernandez et al. (2012). A dynamic simulation study of a solar collector assisted single effect absorption cooling system coupled to a hot storage tank was presented by Eicker et al. (2012). The results obtained were validated by comparing the simulated results with the experimental data obtained from an installed 15 kW solar cooling system and office building. Islam et al. (2015) presented a novel solar-based multigeneration system including thermoelectric generator as shown in Fig. 8.1. A unique cooling system of PV (photovoltaics) panels incorporating thermoelectric generator and cooler was developed to improve the efficiency. The heat rejected

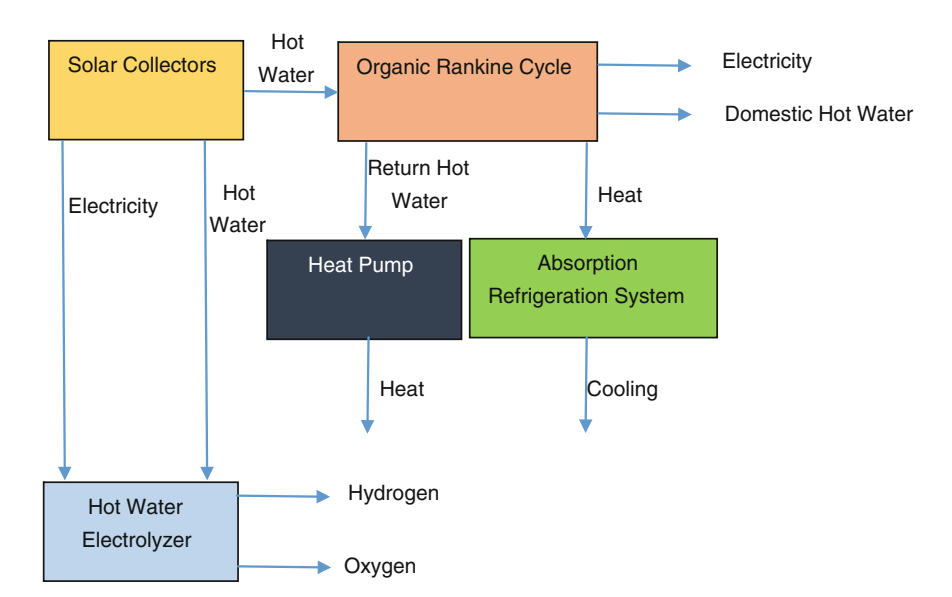


Fig. 8.1 Flow diagram of a solar based integrated system for multigeneration (modified from Islam et al. 2015)

while the operation of thermoelectric devices was conserved through innovative design of fluid flow across the low and high temperature junctions. The operating conditions and their influence on energy and exergy efficiency of the overall system and PV panels, and work done by thermoelectric devices were examined. The energy and exergy efficiencies of the PV panels and the overall system improved significantly, after incorporating thermoelectric generation. The maximum work done by the thermoelectric generator and cooler was increased considerably, by increasing the temperature of solar heat transfer fluid.

A dynamic simulation model of a solar driven absorption chiller was applied successfully to a Rotartica chiller that differs in design from a conventional absorption chiller by Evola et al. (2013). An innovative solar-based small-cooled absorption diffusion chiller working with light hydrocarbon was modeled and studied by Sayadi et al. (2013). In this study, the authors found that the total cost of the proposed system was 1.6 €/kWh produced which is very reasonable in the current scenario. Several researchers have carried out modeling and analysis of a solar driven single-stage absorption cooling system for building cooling, and refrigeration needs around the world while using LiBr/water (Parene et al. 2011; Fong et al. 2012; Molero-Villar et al. 2012; Sarabia et al. 2011) and ammonia/water (Ozgoren et al. 2012; Al-Alili et al. 2012; Said et al. 2012) as working fluids. Suleman et al. (2014) in their paper proposed a new integrated, solar and geothermal energy-based system for multigeneration applications, which comprises two ORC (organic Rankine cycles) for power generation, an absorption chiller cycle for cooling production and a drying system to dry wet products. Also, some useful heat is recovered from the condensers of the ORC for heating applications. To determine the irreversibility, almost all system components are examined energetically and exergetically. The overall energy and exergy efficiencies of the system are found to be 54.7 and 76.4 %, respectively. Moreover, to analyze the system efficiently, parametric studies are also performed to observe the effects of different substantial parameters namely inlet pressure and temperature of the ORC turbine, and reference environment temperature to investigate the variations in the system performance regarding the energy and exergy efficiencies. A novel parabolic trough collector driven organic Rankine cycle and absorption cooling system capable of producing cooling, heating and power was presented by Al-Sulaiman et al. (2012) as shown in Fig. 8.2. The proposed novel system used a portion of waste heat in a heat exchanger to provide heating and the other portion in an absorption cooling system for cooling production. Three modes of operation, namely, a solar mode, a solar and storage mode and a storage mode were considered in the analysis. The results obtained showed that the maximum electrical efficiency achieved for the solar mode, the solar and storage mode, and the storage mode was 15, 7, and 6.5 %, respectively.

At Carnegie Mellon University, a solar driven cooling and heating system working with LiBr/water mixture was developed by Qu et al. (2010). The experimental result obtained showed that the system is capable of meeting 39 % cooling and 20 % heating energy needs of the building space. An outdoor solar driven absorption cooling system with a cold storage was evaluated by Agyenim et al. (2010) and found

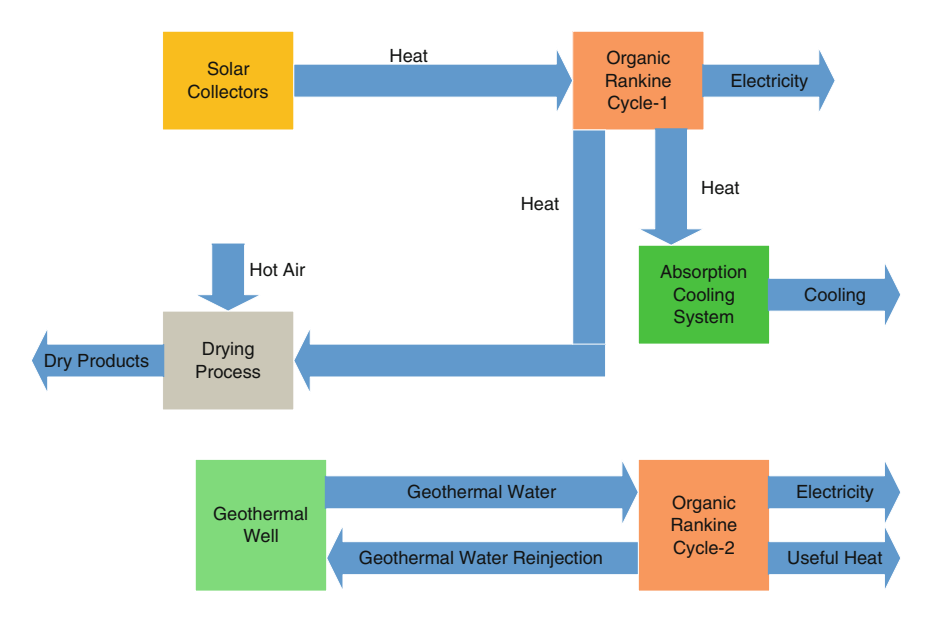


Fig. 8.2 Flow diagram of an integrated renewable energy system for multigeneration (modified from Suleman et al. 2014)

that the system can provide chilled water at 7.4 °C with an average COP of 0.58. Monne et al. (2011) presented the operation of a solar driven absorption cooling system design to solve the overheating problems of already installed solar fields. For an averaged cooling load of 3.5–5.8 kW, the schieved COP of the system was around 0.5. A performance analysis of a commercial solar cooling facility using absorption cooling system for one summer season was performed by Venegas et al. (2011). The results obtained showed that the solar irradiance, wind velocity, and wind direction played a pivotal role in the daily cooling produced and the daily average solar COP. A compact solar cooling system capable of meeting small cooling needs was fabricated by Achuthan et al. (2011). The COP of the system was improved from 0.3 to 0.6 by the introduction of the micro-nozzles in the evaporator and the absorber. The experimental analysis of a direct air-cooled absorption cooling system for solar air-conditioning was performed by Gonzalez-Gil et al. (2011). Moreno-Quintanar et al. (2012) carried out a comparative experimental analysis of a solar absorption cooling system for ice production working with ammonia/lithium nitrite and ammonia/lithium nitrite/water solution. The analysis showed that the system is capable of providing cooling at as low as 8 °C while the COP of the ternary mixture is up to 24 % higher than that obtained for binary mixtures. An innovative prototype of a solar-based direct air-cooled absorption cooling system for residential use was developed and studied by Lizarte et al. (2012). The system provided a lowest cooling temperature of 14.3 °C at a COP of 0.53. An experimental analysis of a mini-type absorption cooling system with a capacity of 4.6 kW and a COP of 0.31 during continuous 9 h of operation was presented by Yin et al. (2012). A COP of 0.8 for an

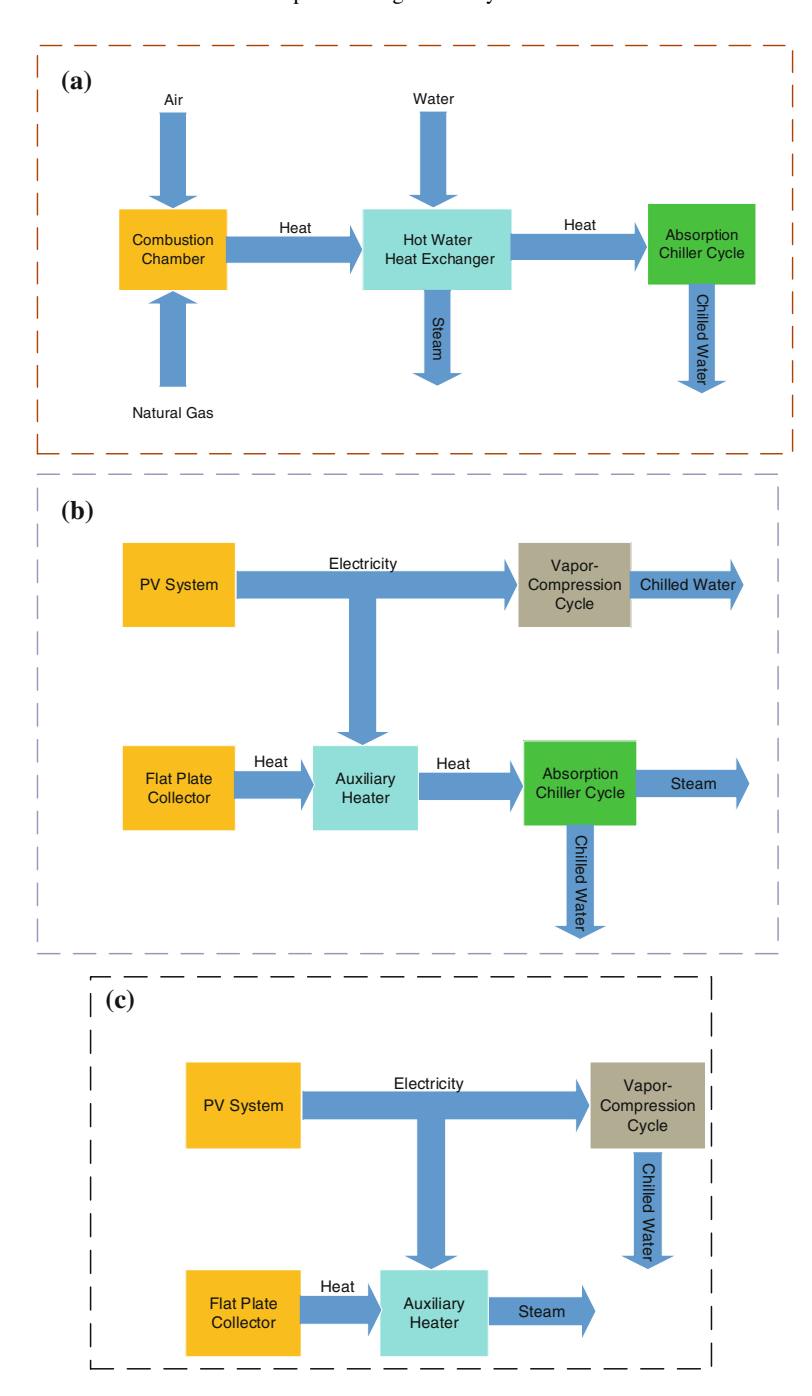


Fig. 8.3 Flow diagram of three proposed systems for cooling and heating (modified from Khalid et al. 2015a)

enhanced solar driven open absorption cooling system for dehumidification and air-conditioning purposes was obtained by Gommed and Grossman (2012). A comparative experimental performance evaluation of two solar-based air-cooled absorption cooling systems was carried out by Lizarte et al. (2013). The prototype and the commercial chiller provided cooling at 16 and 18 °C, respectively with mean daily COP of 0.62 and 0.55 for prototype and commercial chiller, respectively. Several researchers (Yin et al. 2013; Rosiek et al. 2012; Prasartkaewa and Kumar 2013; Le Lostec et al. 2012) have carried out an experimental evaluation of a commercial absorption cooling system using solar radiation as an energy source. Khalid et al. (2015a) studied three newly developed systems for heating and cooling applications in buildings as displayed in Fig. 8.3.

Energy and exergy analyses were performed to assess the performance of the heating, cooling and overall systems for each case. The overall system energy efficiency was found to be highest for the natural gas operated system with a vapor absorption chiller (system 1) at 27.5 % and lowest for the photovoltaic (PV) and solar thermal operated system with vapor-compression chiller (system 3) at 19.9 %. The overall system exergy efficiency was found to be highest for the PV and solar thermal operated system with vapor-compression chiller (system 3) at 3.9 % and lowest for the PV and solar thermal operated system with heat pump (system 2) at 1.2 %, respectively.

8.3 Solid Oxide Fuel Cell-Based Multigeneration Systems

Chitsaz et al. (2015) conducted greenhouse gas emission assessment and exergy analyses of an integrated trigeneration system driven by a solid oxide fuel cell (SOFC) as shown in Fig. 8.4. The results obtained showed that the maximum energy efficiency enhancement of 46 % is when the SOFC is used as the primary mover for the trigeneration system compared to the case when the SOFC is used as a standalone unit. The unit CO₂ emission (in kg/MWh) is considerably higher for the case in which only electrical power is generated. This parameter is reduced by half when the system is operated in a trigeneration mode. The main sources of irreversibility are observed to be the air heat exchanger, the SOFC, and the afterburner. Tippawan et al. (2015) examined an integrated SOFC (solid oxide fuel cell) system with an absorption chiller that uses heat recovery of the SOFC exhaust gas for combined cooling, heating, and power production (trigeneration) through energy, and exergy analyses as shown in Fig. 8.5. The system consists of an ethanol reformer, SOFCs, an air preheater, a steam generator, and a double effect LiBr/H2O absorption chiller. To assess the system performance and determine the irreversibility in each component, a parametric study of the effects of changing the current density, SOFC temperature, fuel use ratio and SOFC anode recirculation ratio on the net electrical efficiency, and the efficiency of heating cogeneration, cooling cogeneration, and trigeneration were presented.

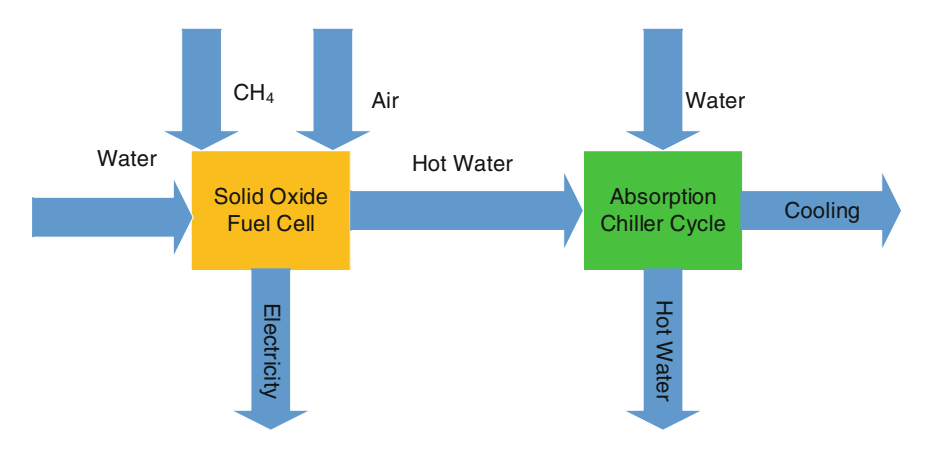
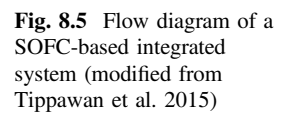
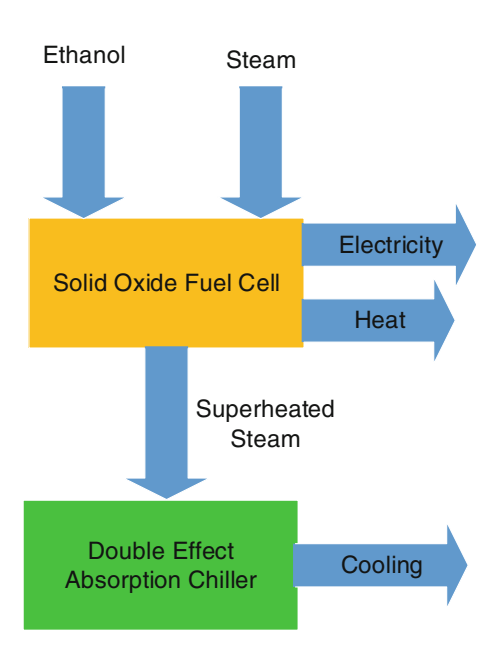


Fig. 8.4 Flow diagram of the integrated trigeneration system (modified from Chitsaz et al. 2015)





Their study shows that in the trigeneration plant, there was at least a 32 % gain in efficiency, compared to the conventional power cycle. This study also demonstrates that the proposed trigeneration system represents an attractive option to improve the heat recovery and enhance the exergetic performance of the SOFC-based systems. Ozcan and Dincer (2015) conducted thermodynamic analyses of an internal reforming solid oxide fuel cell (IR-SOFC) system using three different practical gasifier products as shown in Fig. 8.6.

The syngas products from bubbling fluidized bed (BFB), circulating fluidized bed (CFB), and dual fluidized bed (DFB) gasifiers were considered and comparatively

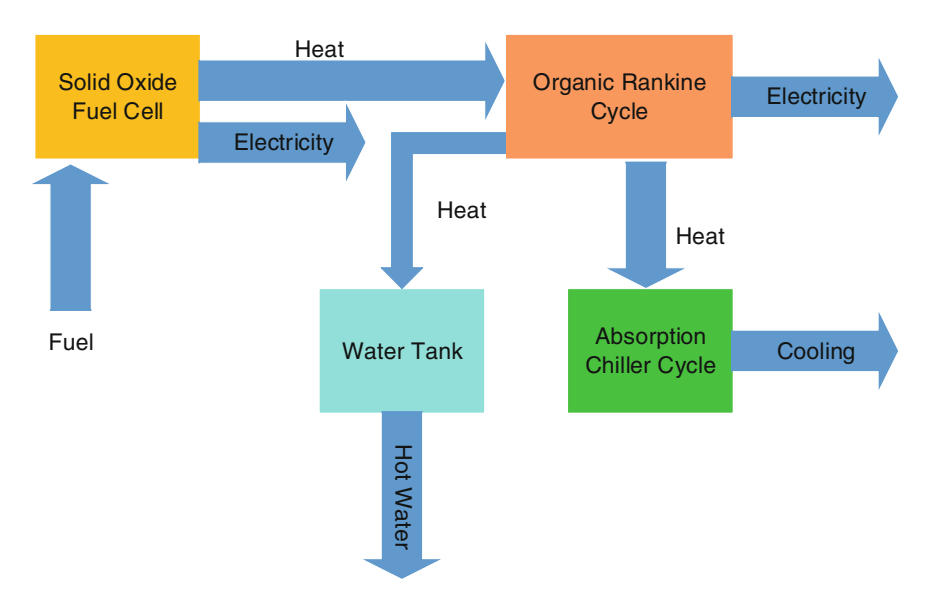


Fig. 8.6 Flow diagram of an integrated SOFC system for multigeneration (modified from Ozcan and Dincer 2015)

studied. Fuels from the ThermoChem bubbling fluidized bed gasifier (TRI), CUTEC circulating fluidized bed gasifier, and SilvaGas&Taylor dual fluidized bed gasifiers were also considered. An SOFC-based integrated system was then proposed to use relatively high temperature waste heat from SOFC unit by producing power, water heating, and space cooling. The proposed system consists of (a) an internal reforming SOFC unit, (b) an organic Rankine cycle (ORC) working with Toluene, (c) an absorption chiller cycle, and (d) a water heating unit connected to an ORC condenser. Energy and exergy efficiencies of subunits and overall system were comparatively evaluated considering irreversibility of the system components for the best fuel performance. The TRI-fueled SOFC system showed the best energy and exergy efficiencies with lowest exergy destructions throughout the trigeneration system. Energy and exergy efficiencies of the SOFC system were determined as 42.2 and 36.5 %, respectively. A 24.6 kW of additional power production from the ORCcycle, 69.9 kW of heating energy production from water heating, and 22.1 kW of cooling load from AC cycle are obtained by the system integration. Furthermore, the system integration for exhaust gas utilization enhances the energy and exergy efficiencies up to ~ 78 and ~ 50 %, respectively.

8.4 Biomass-Based Multigeneration Systems

Wang et al. (2015) performed energy and exergy analyses of an integrated combined cooling, heating, and power generation (CCHP) system with biomass air gasification as shown in Fig. 8.7. Operational flows for three work conditions:

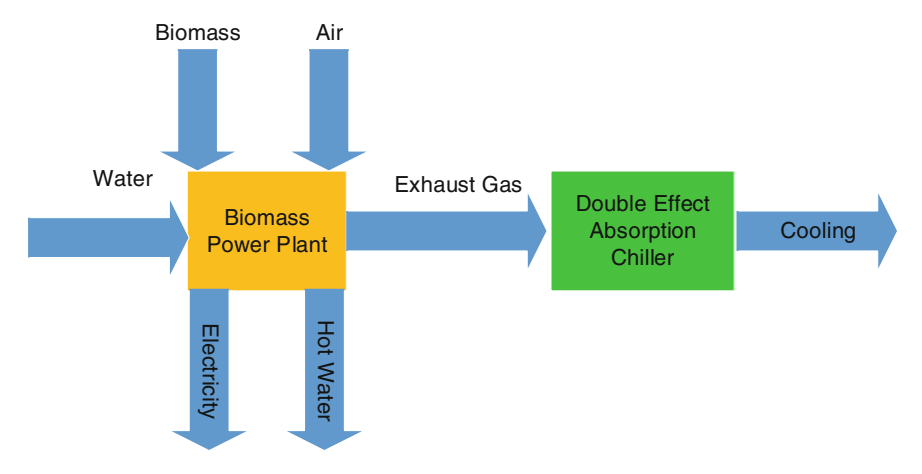


Fig. 8.7 Flow diagram of the biomass integrated gasification and combine generation system (modified from Wang et al. 2015)

summer, winter, and the transitional seasons were presented. The results obtained from the case studies demonstrated that the energy efficiencies in the three work conditions are 50.00, 37.77, and 36.95 %, whereas the exergy efficiencies are 6.23, 12.51, and 13.79 %, respectively. Destruction analyses of energy and exergy indicate that the largest destruction occurs in the gasification system, which accounts for more than 70 % of the total energy and exergy losses. Annual performance shows that the proposed biomass-fueled CCHP system reduces biomass consumption by 4 % compared with the non-use of a heat recovery system for high temperature product gas. Khalid et al. (2015b) studied a biomass and solar integrated system for multigeneration of useful outputs as presented in Fig. 8.8. Energy and exergy analyses were used to assess the performance of the cycle, and the effects of various system parameters on energy and exergy efficiencies of the overall system and its subsystems were examined. The overall energy and exergy efficiencies of the system were found to be 66.5 and 39.7 %, respectively. Furthermore, the effects of variation in the reference environment temperature on energy and exergy efficiencies for the system, when operated only on biomass and solar energy were investigated.

Malik et al. (2015) presented a renewable energy-based multigeneration system as shown in Fig. 8.9. Two renewable sources of energy, biomass and geothermal, are combined to deliver five useful outputs for residential applications. The energy products from the biomass sources are used to drive an organic Rankine cycle and a vapor absorption chiller and further used to dry the wet material in an industrial dryer.

The outlet water flows from the separators and the steam turbine were used to heat water used in households. Liquefied gas was produced through the Linde–Hampson liquefaction cycle, in which the compressor was directly coupled to the organic Rankine cycle turbine. The energy efficiency of the system was found to be

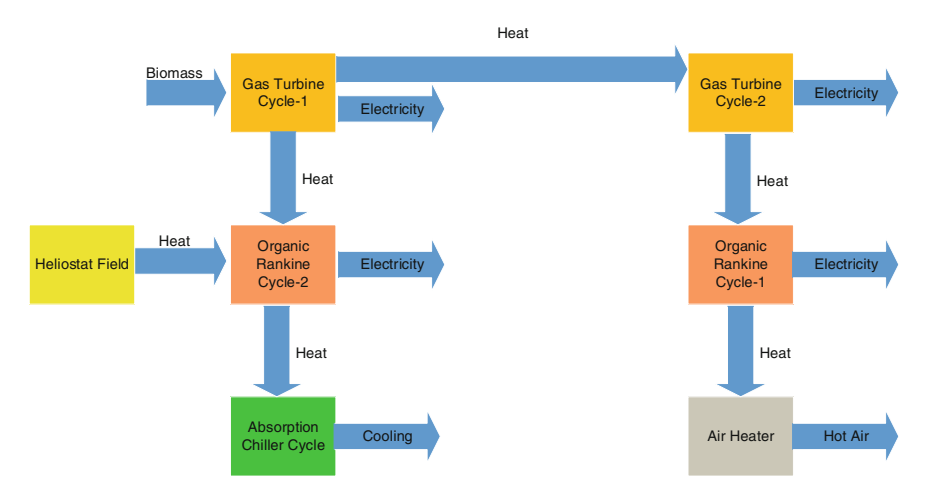


Fig. 8.8 Flow diagram of a solar-biomass integrated cycle for multigeneration (modified from Khalid et al. 2015b)

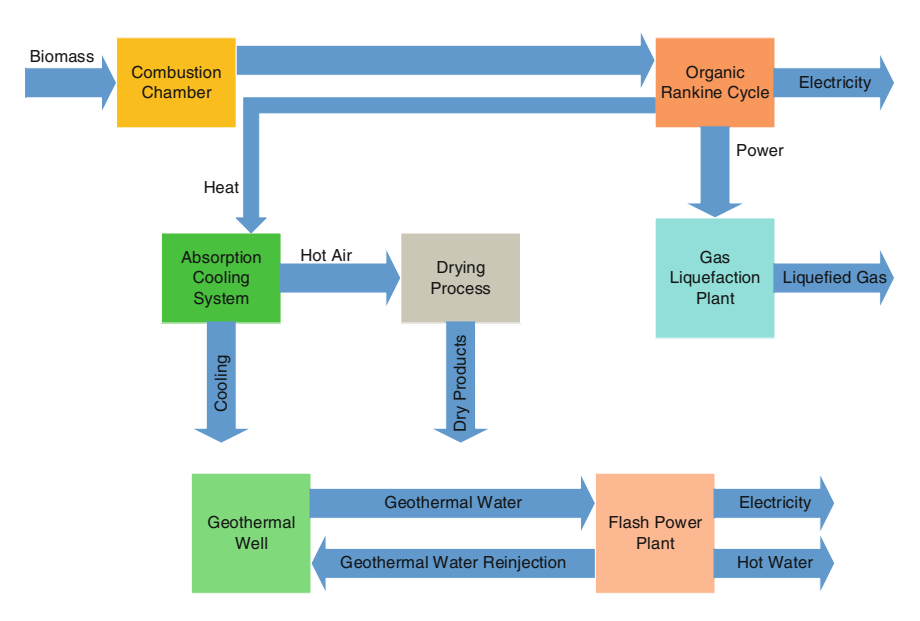


Fig. 8.9 Flow diagram of the developed multigeneration system (modified from Malik et al. 2015)

56.5 % and the exergy efficiency 20.3 %. The largest exergy destructions were found to occur in both the combustion chamber and the boiler. The variations in exergy efficiencies and exergy destructions for the system components were determined with respect to the changes in the reference environment temperature and other major system parameters.

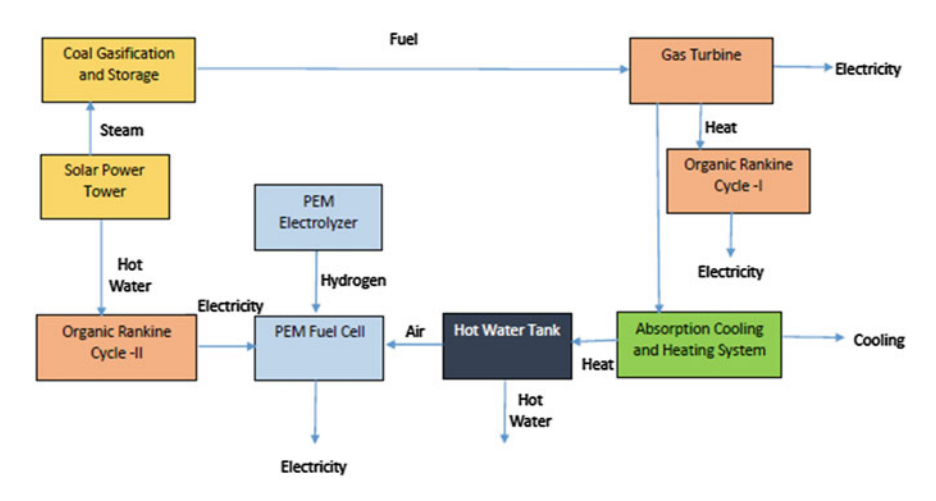


Fig. 8.10 Flow diagram of the multigeneration energy production system (modified from Ozturk and Dincer 2013)

8.5 Fossil Fuels-Based Multigeneration System

Ozturk and Dincer (2013) proposed multigeneration energy production system allows higher efficiency by integration of different systems for recovering the highest possible exergy of the energy input as displayed in Fig. 8.10. The coal gasification system was integrated with a solar power tower to use the concentrating solar energy. The clean syngas produced from the system was stored for the continuous power production. Energy and exergy efficiencies of each subsystem were studied to show the system performance under the chosen conditions and also how to approach the ideal case. The results obtained from their study show that the energy and exergy efficiencies of the subsystems vary between 19.43–46.05 % and 14.41–46.14 %, respectively, and the multigeneration system has the maximum energy and exergy efficiencies of 54.04 and 57.72 %, respectively.

8.6 Novel ARS-Based Combined Heating and Power Generation Systems

A parametric analysis of an integrated organic Rankine and absorption refrigeration cycle capable of producing both power and cooling was presented by Padilla et al. (2010). In this study, the maximum energy and exergy efficiencies for an absorber temperature of 30 °C were obtained to be 20 and 72 %, respectively, for variation in heat source temperature from 90 to 170 °C. Several combined cooling, heating, and power generation systems integrated with renewable energy sources to meet the energy needs of a grid isolated island in Singapore were studied by Chua et al. (2014).

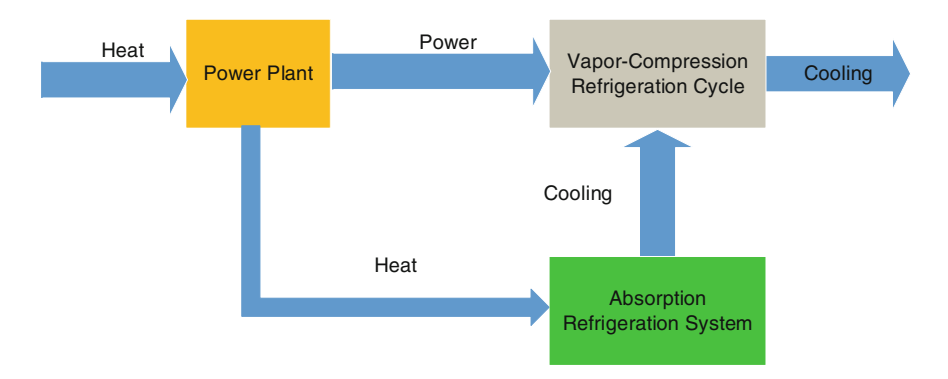


Fig. 8.11 Flow diagram of the novel absorption–compression refrigeration system (modified from Chen et al. 2015)

A vast range of prime movers such as microturbines, solar photovoltaics, solar Stirling dish, fuel cell, and biomass integrated with absorption cooling systems were studied at differing levels of renewable energy penetration. The primary energy was reduced for each case, and high renewable penetration (40 %) corresponded to the largest potential reduction in CO₂ emissions, but the increased capital costs, in this case, resulted in a net projected economic loss (Cho et al. 2014). Fong and Lee (2015) presented technical effectiveness investigation of the separate or integrated provision of solar cooling and heating for use in a typical low-rise residential building in subtropical Hong Kong. Through results obtained year-round, the dynamic simulation showed that the integrated provision could have annual primary energy saving of 13.5 % against the separate provision. The effectiveness of the integrated provision was further verified through two energy-saving scenarios, with energy reduction by 17.7 and 18.0 %, correspondingly, as compared to the separate provision. Under the synergistic effect of centralized thermal harness and storage, the integrated solar cooling and heating is more appropriate for typical low-rise residential application in Hong Kong and other countries with the same weather as Hong Kong. Chen et al. (2015) presented a thermodynamic analysis of a novel absorption-compression refrigeration system using a mid-temperature heat source for freezing applications, as shown in Fig. 8.11. The results obtained from the analysis showed that the coefficient of performance of the proposed system was 0.277, which was approximately 50 % higher than that of a conventional two-stage absorption refrigeration system.

Chaiyat and Kiatsiriroat (2015) presented an experimental analysis of a combined cooling heating and power generation from organic Rankine cycle and absorption system as shown in Fig. 8.12. The study was focussed on feasibilities of energy, economic, and environment of a method to enhance an organic Rankine cycle (ORC) efficiency by combined cooling heating and power generation from an absorption system for reducing the ORC condenser temperature. The analysis showed that the ORC with the absorption system gave higher total efficiency compared with the normal ORC. The ORC efficiency could be increased by 7 %, with 15 °C of water cooled temperature supplied from the absorption system. But,

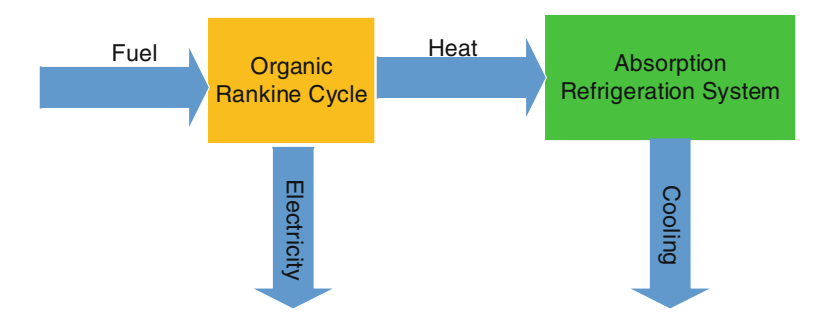


Fig. 8.12 Flow diagram of an integrated organic Rankine cycle and absorption refrigeration system (modified from Chaiyat and Kiatsiriroat 2015)

in terms of the economic result, an LEC (levelized electricity cost) of the modified system was around 0.0891~USD/kWh, which was higher than that of the normal system at around 0.0669~USD/kWh. In terms of the environmental impact, a released carbon dioxide intensity of the new unit was lower than the normal unit at around $0.203~and~0.216~kg~CO_2~eq/kWh$, respectively.

8.7 Novel ARS Designs

Che et al. (2015) performed an energy analysis of an absorption–compression refrigeration system driven by a mid-temperature heat source for low temperature applications. The results obtained from the analysis showed that the coefficient of performance and the cooling capacity per unit mass of flue gas reached 0.357 and 84.18 kJ/k, respectively. The results of a process energy analysis showed that the cycle coupling configuration of the proposed system enhances its cascade energy use. A comprehensive comparison with a heat-driven double-stage compression refrigeration system was also carried out to display the advantages of the proposed system. In the area of an advanced absorption cooling systems, a low temperature-based half-effect absorption cooling systems was studied by Kim and Ferreira (2009). This study was aimed at developing an air-cooled absorption cooling system capable of integrated with low-cost flat plate solar collector for the provision of solar cooling in dry and hot regions. The results obtained reflected that the system is capable of providing cooling at 7.0 °C with a COP of 0.37.

A novel absorber–generator heat exchanger-based absorption cooling system was proposed by Xu et al. (2013). The result obtained from the simulation depicted that the innovative cycle can work in single effect, 1.n effect, and double effect mode with generator temperatures in the ranges of 85–93 °C, 93–140 °C, and 140–150 °C, while having COPs of 0.75, 0.75–1.08, and 1.08–1.25, respectively. A thermodynamic analysis of multi effect absorption cooling system was performed by Gomri (2010), in which it was found that the COP of double effect system can be

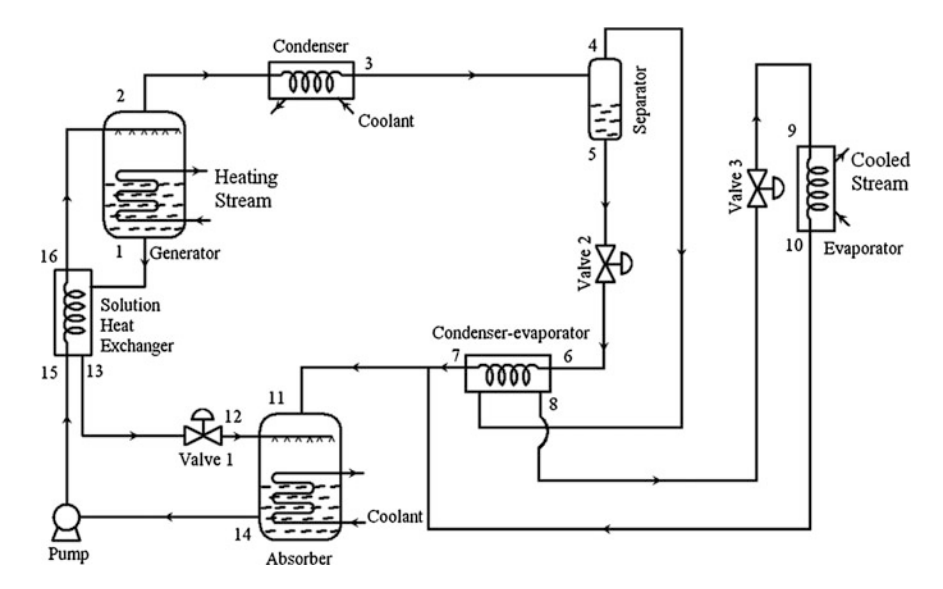


Fig. 8.13 Schematic diagram of the novel auto-cascade absorption refrigeration system (adapted from He et al. 2015)

approximately twice the COP of the single effect system, and the COP of the triple effect system can be almost be three times the COP of the single effect system. He et al. (2015) presented simulation study of a novel auto-cascade absorption refrigeration (ACAR) system for precooling of LNG liquefaction as shown in Fig. 8.13. Under the actuating heat with a temperature of 122.5 °C, a minimum refrigeration temperature of -52.9 °C is obtained by the ACAR system. An experimental coefficiency of performance value of the ACAR system reaches 0.011 with a refrigeration temperature of -52.9 °C. For an absorption refrigeration system, used for reliquefaction of a LNG bulk gas carrier by using engine exhaust heat with a temperature of 145 °C, the required minimum value of COP is about 0.05 with a refrigeration temperature of -30 °C. However, under the actuating heat with a temperature of 120 °C, the minimum value becomes about 0.023 with a refrigeration temperature of -53 °C. Therefore, the performance of the experimental ACAR prototype is approaching the basic requirements for reliquefaction of a LNG bulk gas carrier, which could utilize engine exhaust heat. Based on the theoretical COP values of the ACAR system, it is found that its energy saving could be equivalent to that of an ammonia/water absorption refrigeration system for precooling of LNG liquefaction. The experimental analysis of a novel solar pump-free lithium bromide absorption refrigeration system with a second generator was presented by Yaxiu et al. (2008). The innovative system significantly enhanced the performance of the conventional absorption cooling system with the help of the increase in the temperature drop of the chilled water and decrease in the outlet temperature of the chilled water while providing COP close to 0.8. A solar/gas cooling plant at the Engineering School of Seville (Spain) was evaluated by

Bermejo et al. (2010). The system consisted of 174 kW capacity double effect absorption cooling system integrated with Fresnel solar collectors. The system operated with an average daily COP of 1.1–1.25 while gaining 75 % of required heat from the solar energy. Du et al. (2012) developed and analyzed a prototype of 2 kW an air-cooled solar double-stage absorption cooling system. The experimental results indicated that the prototype operates smoothly and steadily and provides COP of 0.21 when it is driven by 85 °C hot water with an evaporating temperature of 8 °C and an ambient air temperature of 29 °C, respectively.

8.8 Advanced Numerical and Optimization Studies of ARS

Jain et al. (2015) performed the thermodynamic analysis and parametric study of a low temperature vapor-compression-absorption system (VCAS) based on modified Gouy-Stodola equation. The results obtained showed that the optimum cascade condenser temperature is found to be −13 °C for 175 kW refrigeration capacity at an evaporator temperature of -45 °C and condenser temperature of 35 °C. A comparative study of a two-stage vapor-compression system (TSVCS) used for low temperature refrigeration applications with VCAS shows that at the design point, primary energy consumption is reduced by 60.6 % and electrical COP is improved by 153.6 % in VCAS as compared to conventional TSVCS. But the total irreversibility rate of VCAS is 38.4 % higher than the TSVCS due to the use of low-grade energy in vapor absorption system and hence the rational efficiency of VCAS is 14 % low. Gebreslassie et al. (2012) performed a multi-objective optimization study of a solar driven absorption cooling system with an aim of reducing the total cost of the cooling and its contribution to the global warming. Hu and Cho (2014) proposed new a stochastic multi-objective optimization model to optimize the operation strategy of combined cooling, heating and power generation systems for variable climate conditions using operational cost, primary energy consumption, and carbon dioxide emissions. In this mode, they inserted the probability constraints into the stochastic model to guarantee that the proposed optimized operation strategy is reliable to satisfy the stochastic energy demand. Xu et al. (2015) developed a stochastic multi-objective optimization model to improve the design robustness and validate the usage of deterministic approaches used in the optimization of solar absorption cooling and heating generation systems. Xu et al. (2015) applied this proposed model to optimize a cogeneration system with respect to the life-cycle energy, economic, and environment performances as uncertain parameters. The comparative analysis showed that the results are very close within 10 % of the maximum variation between deterministic and stochastic optimizations. Ajib and Günther (2013) developed two prototypes of absorption cooling systems of small capacity. After measuring the first prototype, the chillers were redesigned to reduce internal heat losses and make the heat and mass transfer over the surfaces of the shell and tube heat exchangers more effective. A comparative study of the performance assessment of the absorption refrigeration systems with internal and external storages was presented by Soutullo et al. (2011). The results obtained showed that similar solar fractions can be reached for both the systems, but the conventional storage technique requires a larger storage space. Marc et al. (2012) suggested a simplified numerical model capable of assessing the performance and controlling the operation condition of a solar assisted absorption chiller. The reasonable agreement achieved between the presented model and the experimental results in the study paves the way for the use of model not only to design an installation, but also to follow and control its performances. A dynamic distributed generation dispatch strategy was proposed by Flores et al. (2014) to lower the cost of building energy. The proposed technique was applied to simulate several modes of operation, such as electric load, thermal load, peak shaving, peak shifting, or base-load operation. The results obtained showed that the proposed dispatch technique is more effective than more traditional dispatch techniques. Palacin et al. (2011) presented an improvement in an existing solar driven absorption cooling system by employing multi-regression fit and dynamic simulation. Du et al. (2015) presented an intuitional graphical analysis to identify the characteristics of different cycles with different internal heat recovery strategies and to find out the key points that have a significant influence on internal heat recovery. The results obtained from the advanced analysis show that the saturated feed condition is the optimal feed condition due to the minimum irreversible loss of heat and mass transfer and reducing the heat flow rate in the pocket of the background process contributes to the heat integration between the column and background processes. The two key points on internal heat recovery can be the operating direction of internal heat recovery for system performance improvement.

8.9 Novel Working Mixtures

Apart from innovative designs and integrations, several researchers have focussed on introduction new working mixtures to avoid some of the drawbacks associated with the conventional LiBr/water and ammonia/water-based absorption cooling systems. Alvarez et al. (2015) carried out performance analysis of a triple effect absorption cooling cycle using aqueous (lithium, potassium, sodium) nitrate solution as a working pair. Results show that the Alkitrate triple effect cycle has a slightly higher efficiency as compared to the H₂O/LiBr triple effect cycle at generator temperatures of over 180 °C. Moreover, the practical operation of a H₂O/LiBr triple effect cycle at temperatures higher than 180 °C is observed to suffer from problems related to thermal stability and corrosion of the working pair. An evaluation of a monomethyl amine/water-based solar absorption cooling system for milk cooling was performed by Pilatowsky et al. (2004) and found that the system provided cooling at reasonable COPs while operating at low generator temperatures. He et al. (2009) performed a comparative analysis of a single-stage absorption cooling system working with

refrigerant-dimethyl fumarate mixtures at low generator temperatures. The results show that the system operating with R134-dimethyl fumarate presented the best results for those mixtures studied in the paper. A solar-based diffusion-absorption cooling system using R124-dimethylacetmaide as working solution was investigated by Ben Ezzine et al. (2010). The results obtained from the analysis showed that the proposed solution can deliver cooling at high COP and can be an attractive alternative to the ammonia/water mixture. A numerical and experimental analysis of a horizontal tube falling film generator working with ammonia/lithium nitrite mixture was carried out by Herrera et al. (2010). Zhang and Hu (2011) performed thermodynamic analysis of an absorption cooling system working with water and ionic liquid 1-ethyl-3- methylimidazoliumdimethyl phosphate. The results obtained showed that the COP of the proposed system was slightly lower than that of a LiBr/water system but with the benefit of working with low generator temperatures. With an advancement in technologies, the researcher have begun performing experimental investigations of absorption cooling systems working with innovative mixtures. An innovative ammonia/lithium nitrate-based solar absorption cooling system with the capacity to deliver 8 kg of ice/day was developed and studied by Rivera et al. (2011). The system consisted of a cylindrical parabolic collector behaving as a generator absorber was capable of delivering evaporator temperature as low as 11 °C with a COP of 0.08. A novel diffusion-absorption cooling system operating with ammonia/helium/lithium nitrate-based ternary mixture was developed by Wang (2011). An experimental investigation of a bubble pump operated diffusion-absorption cooling system using light hydrocarbons as working fluid for solar cooling applications was performed by Ezzine et al. (2010). The system was capable of producing cold at temperatures ranging between -10 and 10 °C for a generator temperature ranges of 120-150 °C which have COPs ranging from 0.1 to 0.17. The heat and mass transfer analysis of a compact generator of R134a/dimethyl fumarate absorption refrigeration system was performed by Balamurugan and Mani (2012) in which they proposed empirical correlations for the Nusselt and Sherwood numbers.

8.10 Closing Remarks

The current chapter presents an overview of recent advancements and developments taking place in the area of absorption refrigeration systems and their potential applications in various sectors ranging from residential to industrial. This chapter also discusses the introduction of advanced fluids and innovative novel designs in the field of absorption refrigeration system for various systems and applications. Furthermore, several multigeneration systems are also presented to highlight the usefulness of the ARS for producing multi-commodities, beyond cooling, with power generation, heating, hot water, desalination, hydrogen and synthetic fuels.

References

- Achuthan, M., Venkataraman, A., & Rathnasamy, R. (2011). Experimental analysis on the performance and characteristics of compact solar refrigeration system. *Journal of Distribution and Generation of Alternative Energy*, 26(3), 66–80.
- Agyenim, F., Knight, I., & Rhodes, M. (2010). Design and experimental testing of the performance of an outdoor LiBr/H₂O solar thermal absorption cooling system with a cold store. *Solar Energy*, 84, 735–774.
- Ajib, S., & Günther, W. (2013). Solar thermally driven cooling systems: Some investigation results and perspectives. *Energy Conversion and Management*, 65, 663–669.
- Al-Alili, A., Islam, M. D., Kubo, I., Hwang, Y., & Radermacher, R. (2012). Modeling of a solar powered absorption cycle for Abu Dhabi. Applied Energy, 93, 160–167.
- Al-Sulaiman, F. A., Hamdullahpur, F., & Dincer, I. (2012). Performance assessment of a novel system using parabolic trough solar collectors for combined cooling, heating, and power production. *Renewable Energy*, 48, 161–172.
- Alvarez, M. E., Esteve, X., & Bourouis, M. (2015). Performance analysis of a triple-effect absorption cooling cycle using aqueous (lithium, potassium, sodium) nitrate solution as a working pair. *Applied Thermal Engineering*, 79, 27–36.
- Ameel, A., Gee, K. G., & Wood, B. D. (1995). Performance predictions of alternative, low cost absorbents for open-cycle absorption solar cooling. *Solar Energy*, 54(2), 65–73.
- Balamurugan, P., & Mani, A. (2012). Heat and mass transfer studies on compact generator of R134a/DMF vapour absorption refrigeration system. *International Journal of Refrigeration*, 35, 506–517.
- Baniyounes, A. M., Ghadi, Y. Y., Rasul, M. G., & Khan, M. M. K. (2013a). An overview of solar assisted air conditioning in Queensland's sub-tropical regions, Australia. *Renewable and Sustainable Energy Reviews*, 26, 781–804.
- Baniyounes, A. M., Liu, G., Rasul, M. G., & Khan, M. M. K. (2013b). Comparison study of solar cooling technologies for an institutional building in subtropical Queensland, Australia. *Renewable and Sustainable Energy Reviews*, 23, 421–430.
- Ben Ezzine, N., Garma, R., & Bellagi, A. (2010). A numerical investigation of a diffusion absorption refrigeration cycle based on R124-DMAC mixture for solar cooling. *Energy*, *35*, 1874–1883.
- Bermejo, P., Pino, F. J., & Rosa, F. (2010). Solar absorption cooling plant in Seville. *Solar Energy*, 84, 1503–1512.
- Calise, F. (2012). High temperature solar heating and cooling systems for different Mediterranean climates: Dynamic simulation and economic assessment. Applied Thermal Engineering, 32, 108–124.
- Chaiyat, N., & Kiatsiriroat, N. (2015). Analysis of combined cooling heating and power generation from organic Rankine cycle and absorption system. *Energy*, 91, 363–370.
- Chen, Y., Han, W., Sun, L., & Jin, H. (2015). A new absorption-compression refrigeration system using a mid-temperature heat source for freezing application. *Energy Procedia*, 75, 560–565.

Chitsaz, A., Mahmoudi, S. M. S., & Rosen, M. A. (2015). Greenhouse gas emission and exergy analyses of an integrated trigeneration system driven by a solid oxide fuel cell. *Applied Thermal Engineering*, 86, 81–90.

- Cho, H., Smith, A. D., & Mago, P. (2014). Combined cooling, heating and power: A review of performance improvement and optimization. Applied Energy, 136, 168–185.
- Chua, K. J., Yang, W. M., Er, S. S., & Ho, C. A. (2014). Sustainable energy systems for a remote island community. *Applied Energy*, 113, 1752–1763.
- Critoph, R. E. (1993). Laboratory testing of van ammonia carbon solar refrigerator. *Solar world congress* (pp. 23–26). Hungary: Budapest.
- Dincer, I., & Rosen, M. A. (2007). Exergy; energy environment and sustainable development. Oxford: Springer.
- Du, S., Wang, R. Z., Lin, P., Xu, Z. Z., Pan, Q. W., & Xu, S. C. (2012). Experimental studies on an air-cooled two-stage NH₃-H₂O solar absorption air-conditioning prototype. *Energy*, 45, 581–587.
- Du, S., Wang, R. Z., & Xia, Z. Z. (2015). Graphical analysis on internal heat recovery of a single stage ammonia–water absorption refrigeration system. *Energy*, 80, 687–694.
- Eicker, U., Pietruschka, D., & Pesch, R. (2012). Heat rejection and primary energy efficiency of solar driven absorption cooling systems. *International Journal of Refrigeration*, 35, 729–738.
- Evola, G., Le Pierres, N., Boudehenn, F., & Papillon, P. (2013). Proposal and validation of a model for the dynamic simulation of a solar-assisted single-stage LiBr/water absorption chiller. *International Journal of Refrigeration*, 36, 1015–1028.
- Ezzine, N. B., Garma, R., Bourouis, M., & Bellagi, A. (2010). Experimental studies on bubble pump operated diffusion absorption machine based on light hydrocarbons for solar cooling. *Renewable Energy*, *35*, 464–470.
- Flores, R. J., Shaffer, B. P., & Brouwer, J. (2014). Dynamic distributed generation dispatch strategy for lowering the cost of building energy. *Applied Energy*, 123, 196–208.
- Fong, K. F., & Lee, C. K. (2015). Investigation of separate or integrated provision of solar cooling and heating for use in typical low-rise residential building in subtropical Hong Kong. *Renewable Energy*, 75, 847–855.
- Fong, K. F., Lee, C. K., & Chow, T. T. (2012). Comparative study of solar cooling systems with building-integrated solar collectors for use in sub-tropical regions like Hong Kong. *Applied Energy*, 90, 189–195.
- Gebreslassie, B. H., Guillen-Gosalbez, G., Jimenez, L., & Boer, D. (2012). Solar assisted absorption cooling cycles for reduction of global warming: A multi-objective optimization approach. *Solar Energy*, 86, 2083–2094.
- Gommed, K., & Grossman, G. (2012). Investigation of an improved solar-powered open absorption system for cooling, dehumidification and air conditioning. *International Journal of Refrigeration*, 35, 676–684.
- Gomri, R. (2010). Investigation of the potential of application of single effect and multiple effect absorption cooling systems. *Energy Conversion and Management*, 51, 1629–1636.
- Gonzalez-Gil, A., Izquierdo, M., Marcos, J. D., & Palacios, E. (2011). Experimental evaluation of a direct air-cooled lithium bromide-water absorption prototype for solar air conditioning. *Applied Thermal Engineering*, 31, 3358–3368.
- Hassan, H. Z., & Mohamad, A. A. (2012). A review on solar-powered closed physisorption cooling systems. Renewable and Sustainable Energy Reviews, 15, 2516–2538.
- He, L. J., Tang, L. M., & Chen, G. M. (2009). Performance prediction of refrigerant-DMF solutions in a single-stage solar-powered absorption refrigeration system at low generating temperatures. Solar Energy, 83, 2029–2038.
- He, Y., Li, R., Chen, G., & Wang, Y. (2015). A potential auto-cascade absorption refrigeration system for pre-cooling of LNG liquefaction. *Journal of Natural Gas Science and Engineering*, 24, 425–430.
- Hernandez, J. A., Rivera, W., Colorado, D., & Moreno-Quintanar, G. (2012). Optimal COP prediction of a solar intermittent refrigeration system for ice production by means of direct and inverse artificial neural networks. *Solar Energy*, 86, 1108–1117.

References 261

Herrera, J. V., García-Valladares, O., Gomez, V. H., & Best, R. (2010). Numerical simulation and experimental results of horizontal tube falling film generator working in a NH₃-LiNO₃ absorption refrigeration system. *Applied Thermal Engineering*, *30*, 1751–1763.

- Hu, M., & Cho, H. (2014). A probability constrained multi-objective optimization model for CCHP system operation decision support. Applied Energy, 116, 230–242.
- International Energy Agency. (2013). Tracking clean energy progress 2013. www.iea.org
- Islam, S., Dincer, I., & Yilbas, B. S. (2015). Energetic and exergetic performance analyses of a solar energy-based integrated system for multigeneration including thermoelectric generators. *Energy*, 93, 1246–1258.
- Jain, V., Sachdeva, G., & Kachhwaha, S. S. (2015). Thermodynamic modelling and parametric study of a low temperature vapour compression-absorption system based on modified Gouy-Stodola equation. *Energy*, 79, 407–418.
- Khalid, F., Dincer, I., & Rosen, M. A. (2015a). Development and analysis of sustainable energy systems for building HVAC applications. Applied Thermal Engineering, 87, 389–401.
- Khalid, F., Dincer, I., & Rosen, M. A. (2015b). Energy and exergy analyses of a solar-biomass integrated cycle for multigeneration. *Solar Energy*, 112, 290–299.
- Kim, D. S., & Ferreira, C. A. I. (2008). Solar refrigeration options-a state-of-the-art review. International Journal of Refrigeration, 31, 3–15.
- Kim, D. S., & Ferreira, C. A. I. (2009). Air-cooled LiBr-water absorption chillers for solar air conditioning in extremely hot weathers. *Energy Conversion and Management*, 50, 1018–1025.
- Klein, S. A. (2014). Engineering equation solver (EES): Academic commercial. F-Chart Software. www.fChart.com
- Le Lostec, B., Galanis, N., & Millette, J. (2012). Experimental study of an ammonia-water absorption chiller. *International Journal of Refrigeration*, 35, 2275–2286.
- Lizarte, R., Izquierdo, M., Marcos, J. D., & Palacios, E. (2012). An innovative solar-driven directly air-cooled LiBr-H₂O absorption chiller prototype for residential use. *Energy and Buildings*, 47, 1-11.
- Lizarte, R., Izquierdo, M., Marcos, J. D., & Palacios, E. (2013). Experimental comparison of two solar-driven air-cooled LiBr/H₂O absorption chillers: Indirect versus direct air-cooled system. *Energy and Buildings*, 62, 323–334.
- Lof, G. O. C. (1955). Cooling with solar energy. Proceedings of the 1955 congress on solar energy (pp. 171–189). AZ: Tucson.
- Luo, H. L., Wang, R. Z., Dai, Y. J., Wu, J. Y., Shenand, J. M., & Zhang, B. B. (2007). An efficient solar powered adsorption chiller and its application in low temperature grain storage. *Solar Energy*, 81(5), 607–613.
- Maidment, G. G., & Paurine, A. (2012). Solar cooling and refrigeration systems. *Comprehensive Renewable Energy*, 3, 481–494.
- Malik, M., Dincer, I., & Rosen, M. A. (2015). Development and analysis of a new renewable energy-based multi-generation system. *Energy*, 79, 90–99.
- Marc, O., Anies, G., Lucas, F., & Castaing-Lasvignottes, J. (2012). Assessing performance and controlling operating conditions of a solar driven absorption chiller using simplified numerical models. Solar Energy, 86, 2231–2239.
- Moler, C. (2014). Matlab: Academic. Mathworks. www.mathworks.com
- Molero-Villar, N., Cejudo-Lopez, J. M., Domínguez-Munoz, F., & Carrillo-Andes, A. (2012). A comparison of solar absorption system configurations. Solar Energy, 86, 242–252.
- Monne, C., Alonso, S., Palacín, F., & Guallar, J. (2011). Stationary analysis of a solar LiBr-H₂O absorption refrigeration system. *International Journal of Refrigeration*, 34, 518–526.
- Moreno-Quintanar, G., Rivera, W., & Best, R. (2012). Comparison of the experimental evaluation of a solar intermittent refrigeration system for ice production operating with the mixtures NH₃/LiNO₃ and NH₃/LiNO₃/H₂O. *Renewable Energy*, 38, 62–68.
- Nandi, T. K., & Sarangi, S. (1993). Performance and optimization of hydrogen liquefaction cycles. *International Journal of Hydrogen Energy*, 18(2), 131–139.

Otanicar, T., Taylor, R. A., & Phelan, P. E. (2012). Prospects for solar cooling—an economic and environmental assessment. *Solar Energy*, 86, 1287–1299.

- Ozcan, H., & Dincer, I. (2015). Performance evaluation of an SOFC based trigeneration system using various gaseous fuels from biomass gasification. *International Journal of Hydrogen Energy*, 40, 7798–7807.
- Ozgoren, M., Bilgili, M., & Babayigit, O. (2012). Hourly performance prediction of ammonia—water solar absorption refrigeration. *Applied Thermal Engineering*, 40, 80–90.
- Ozturk, M., & Dincer, I. (2013). Thermodynamic assessment of an integrated solar power tower and coal gasification system for multi-generation purposes. *Energy Conversion and Management*, 76, 1061–1072.
- Padilla, R. V., Demirkaya, G., Goswami, D. Y., Stefanakos, E., & Rahman, M. M. (2010). Analysis of power and cooling cogeneration using ammonia-water mixture. *Energy*, 35, 4649–4657.
- Palacín, F., Monne, C., & Alonso, S. (2011). Improvement of an existing solar powered absorption cooling system by means of dynamic simulation and experimental diagnosis. *Energy*, 36, 4109–4118.
- Pilatowsky, I., Rivera, W., & Romero, J. R. (2004). Performance evaluation of a monomethylamine–water solar absorption refrigeration system for milk cooling purposes. *Applied Thermal Engineering*, 24, 1103–1115.
- Praene, J. P., Marc, O., Lucas, F., & Miranville, F. (2011). Simulation and experimental investigation of solar absorption cooling system in Reunion Island. *Applied Energy*, 88, 831–839.
- Prasartkaewa, B., & Kumar, S. (2013). Experimental study on the performance of a solar biomass hybrid air-conditioning system. *Renewable Energy*, *57*, 86–93.
- Qu, M., Yin, H., & Archer, D. H. (2010). A solar thermal cooling and heating system for a building: Experimental and model based performance analysis and design. *Solar Energy*, 84, 166–182.
- Ratlamwala, T. A. H., & Dincer, I. (2012). Comparative efficiency assessment of novel multi-flash integrated geothermal systems for power and hydrogen production. *Applied Thermal Engineering*, 48, 359–366.
- Ratlamwala, T. A. H., & Dincer, I. (2013). Development of a geothermal based integrated system for building multigenerational needs. *Energy and Buildings*, 62, 496–506.
- Ratlamwala, T. A. H., Dincer, I., & Gadalla, M. A. (2012a). Thermodynamic analysis of a novel integrated geothermal based power generation-quadruple effect absorption cooling-hydrogen liquefaction system. *International Journal of Hydrogen Energy*, *37*, 5840–5849.
- Ratlamwala, T. A. H., Dincer, I., & Gadalla, M. A. (2012b). Performance analysis of a novel integrated geothermal-based system for multi-generation applications. *Applied Thermal Engineering*, 40, 71–79.
- Ratlamwala, T. A. H., Dincer, I., & Gadalla, M. A. (2012c). Energy and exergy analyses of an integrated solar-based desalination quadruple effect absorption system for freshwater and cooling production. *International Journal of Energy Research*, 37(13), 1569–1579.
- Ratlamwala, T. A. H., Dincer, I., & Gadalla, M. A. (2013). Energy and exergy analyses of an integrated solar-based desalination quadruple effect absorption system for freshwater and cooling production. *International Journal of Energy Research*, 37, 1569–1579.
- Rivera, W., Moreno-Quintanar, G., Rivera, C. O., Best, R., & Martínez, F. (2011). Evaluation of a solar intermittent refrigeration system for ice production operating with ammonia/lithium nitrate. *Solar Energy*, 85, 38–45.
- Rosiek, S., & Garrido, F. J. B. (2012). Performance evaluation of solar-assisted air-conditioning system with chilled water storage (CIESOL building). *Energy Conversion and Management*, 55, 81–92.
- Said, S. S. M., El-Shaarawi, M. A. I., & Siddiqui, M. U. (2012). Alternative designs for a 24-h operating solar-powered absorption refrigeration technology. *International Journal of Refrigeration*, 35, 1967–1977.

References 263

Sarabia, E. J., Lamas Sivila, E. V., & Soto Frances, V. M. (2011). Air conditioning production by a single effect absorption cooling machine directly coupled to a solar collector field. Application to Spanish climates. Solar Energy, 85, 2108–2121.

- Sauceda, D., Velazquez, N., García-Valladares, O., & Beltran, R. (2011). Numerical simulation and design of a parabolic trough solar collector used as a direct generator in a solar-GAX cooling cycle. *Journal of Mechanical Science and Technology*, 25(6), 1399–1408.
- Sayadi, Z., Thameur, N. B., Bourouis, M., & Bellagi, A. (2013). Performance optimization of solar driven small-cooled absorption-diffusion chiller working with light hydrocarbons. *Energy Conversion and Management*, 74, 299–307.
- Soutullo, S., San Juan, C., & Heras, M. R. (2011). Comparative study of internal storage and external storage absorption cooling systems. *Renewable Energy*, *36*, 1645–1651.
- Suleman, F., Dincer, I., & Chaan, M. A. (2014). Development of an integrated renewable energy system for multigeneration. *Energy*, 78, 196–204.
- Tippawan, P., Arpornwichanop, A., & Dincer, I. (2015). Energy and exergy analyses of an ethanol-fueled solid oxide fuel cell for a trigeneration system. *Energy*, 87, 228–239.
- Vella, G. J., Harris, L. B., & Goldsmid, H. J. (1976). A solar thermoelectric refrigerator. Solar Energy, 18(4), 355–359.
- Venegas, M., Rodríguez-Hidalgo, M. C., Salgado, R., Lecuona, A., Rodríguez, P., & Gutierrez, G. (2011). Experimental diagnosis of the influence of operational variables on the performance of a solar absorption cooling system. *Applied Thermal Engineering*, 88, 1447–1454.
- Wang, H. D. (2011). Experimental study on LiNO₃–NH₃ diffusion-absorption refrigeration system. *Key Engineering Materials*, 474–476, 2335–2340.
- Wang, J. J., Yang, K., Xu, Z. L., & Fu, C. (2015). Energy and exergy analyses of an integrated CCHP system with biomass air gasification. *Applied Energy*, 142, 317–327.
- Xu, D., Qu, M., Hang, Y., & Zhao, F. (2015). Multi-objective optimal design of a solar absorption cooling and heating system under life-cycle uncertainties. Sustainable Energy Technologies and Assessments, 11, 92–105.
- Xu, Z. Y., Wang, R. Z., & Xia, Z. Z. (2013). A novel variable effect LiBr-water absorption refrigeration cycle. *Energy*, 60, 457–463.
- Yaxiu, G., Yuyuan, W., & Xin, K. (2008). Experimental research on a new solar pump-free lithium bromide absorption refrigeration system with a second generator. Solar Energy, 82, 33–42.
- Yin, Y. L., Song, Z. P., Li, Y., Wang, R. Z., & Zhai, X. Q. (2012). Experimental investigation of a mini-type solar absorption cooling system under different cooling modes. *Energy and Buildings*, 47, 131–138.
- Yin, Y. L., Zhai, X. Q., & Wang, R. Z. (2013). Experimental investigation and performance analysis of a mini-type solar absorption cooling system. Applied Thermal Engineering, 59, 267–277.
- Zeyghami, A., Goswami, D. Y., & Stefanakos, E. (2015). A review of solar thermo-mechanical refrigeration and cooling methods. *Renewable and Sustainable Energy Reviews*, 51, 1428–1445.
- Zhang, X., & Hu, D. (2011). Performance simulation of the absorption chiller using water and ionic liquid 1-ethyl-3-methylimidazolium dimethyl phosphate as the working pair. *Applied Thermal Engineering*, *31*, 3316–3321.

Note: Page numbers followed by f and t refer to figures and tables, respectively

```
A
                                                        multigeneration system, 227-228, 228f
Absorbents, 2-4
                                                        power, cooling, and liquefied hydrogen
                                                           generation system, 206-207, 207f
Absorber, 7, 7f, 30t
                                                 Ammonia-water absorption refrigeration
   absorption refrigeration system
       double effect, 79
                                                           system, 3-4, 48, 72-73, 108-109
       quadruple effect, 161
                                                 Auto-cascade absorption refrigeration (ACAR)
       single effect, 52–53
                                                           system, 254, 254f
       triple effect, 117
   energy and exergy analyses, 36-37
Absorption
                                                 Binary power plant, 198f
   defined, 2
                                                    energy and exergy analyses, 202
   process, 2, 2f
                                                    multi-stage, schematic of, 199f
Absorption heat pumps, 23–24, 24f
                                                 Biomass based multigeneration systems,
Absorption refrigeration system (ARS), 2
                                                           248-250, 249f, 250f
   advantages and disadvantages of, 18
                                                 Bubbling fluidized bed (BFB) gasifier, 247
   classification of, 4-5, 4f
                                                 Building needs, geothermal-based integrated
   comparison with other cooling systems,
                                                           system for, 228-238, 229f
          18 - 23
                                                    cooling load effects, 236-237, 236f
   components of, 5-10, 6f
                                                    geothermal effects
   developments in, 241-257
                                                        pressure effects, at state f2, 234-235,
   heat sources, 17–18
                                                           235f
   operating principle, 10
                                                        source temperature effects, 235–236,
   types of, 10-17
                                                           236f
                                                    multigeneration effects, 237-238, 237f,
Adsorption cooling system, 22–23, 23t
Advanced single effect absorption refrigeration
                                                           238f
          system, 242-246, 242f, 244f, 245f
                                                    system description, 228-230
Air, dry. See Dry air
                                                    thermodynamic analysis, 230-234
Air-conditioning system, 2
   vapor-compression, 20
                                                 \mathbf{C}
                                                 Chiller, 242, 243, 246
Ambient temperature effects
   absorption refrigeration system
                                                 Circulating fluidized bed (CFB) gasifier, 247
       double effect, 100-103, 101-103f
                                                 Coal gasification system, 251
       quadruple effect, 191–194, 192–194f
                                                 Coefficient of performance (COP), 1, 4, 5, 21,
       single effect, 65–67, 65–68f
                                                           22-23, 23t, 38-39, 54, 57, 81, 118,
       triple effect, 143–146, 144–146f
                                                           121, 122, 163, 166, 202, 223
   geothermal-based
                                                 Cold storage, 22, 229, 243
```

[©] Springer International Publishing Switzerland 2016
I. Dincer and T.A.H. Ratlamwala, *Integrated Absorption Refrigeration Systems*, Green Energy and Technology, DOI 10.1007/978-3-319-33658-9

Combustion chamber, 250	cost, 1, 71, 196, 197, 225
Condenser, 8, 8 <i>f</i> , 29 <i>t</i>	Efficiency, 28
absorption refrigeration system	energy, 246, 249–250
double effect, 77–78	exergy, 42, 45, 74, 110, 152, 200, 210, 238,
quadruple effect, 160	246, 250
single effect, 51–52	isentropic, 30, 203
triple effect, 115–116	organic Rankine cycle, 252
energy and exergy analyses, 33–34	of solar PV/T, 211
Condenser heat exchanger	Electricity, 18, 19, 47, 241
double effect absorption refrigeration	levelized cost, 253
system, 80–81	Electrolyzer, 226, 230
quadruple effect absorption refrigeration	geothermal-based multigeneration system,
system, 162–163	224
triple effect absorption refrigeration system,	quadruple flash power plant (QFPP), 228
118	Energy analyses, 27–39
Cooling load	absorption refrigeration system
effects, geothermal-based integrated	double effect, 73–81
system, 236–237, 236 <i>f</i>	quadruple effect, 152–163
effects of generator load on, 62, 62f	single effect, 49–54
Cooling system	triple effect, 109–118
adsorption, 22–23, 23 <i>t</i>	geothermal-based
desiccant, 21–22	multigeneration system, 224–225
geothermal-based, 206–207, 207f	power, cooling, and liquefied hydrogen
solar-based diffusion-absorption, 257	generation system, 200–204
solar PV, 19–20, 19 <i>f</i>	solar-based integrated absorption
solar thermoelectric, 20–21, 20 <i>f</i>	refrigeration and desalination
	system, 210–213
D	Environmentally-benign, 21, 24, 66, 101, 145,
Desalination system, 213	197
thermodynamic properties of, 215t	Ethanol, 246
Desiccant cooling systems, 21–22	Evaporator, 8, 9f, 29t
Domestic heating loads, 228	absorption refrigeration system
Domestic thermoelectric cooling systems,	double effect, 78
20–21	quadruple effect, 160–161
Double effect absorption refrigeration system	single effect, 52
(DEARS), 5, 12–13, 12f, 71–105,	triple effect, 116
72 <i>f</i> , 242	energy and exergy analyses, 35–36
energy and exergy analyses, 73-81	Exchanger. See also Condenser heat
exergoeconomic analysis, 81–82	exchanger; Heat exchanger
exergoenvironmental analysis, 82–83	double effect absorption refrigeration
illustrative example, 83–105	system, 74–75, 80–81
optimization, 83	Exergetic stability factor, 43, 56, 83, 121, 165
system description, 72–73	Exergetic sustainability index, 43, 56, 83, 121,
Double flash power plant, 220, 226	165
geothermal-based multigeneration system,	Exergoeconomic analysis, 39–41, 40 <i>f</i>
223	absorption refrigeration system
schematic of, 221f	double effect, 81–82
Dry air, 22, 228, 229, 230, 234, 237	quadruple effect, 163–164
Drying, 243, 244f, 250f	single effect, 54–55
	<u> </u>
Dual fluidized bed (DFB) gasifier, 247	triple effect, 119 Exergenvironmental analysis, 41, 44
E	Exergoenvironmental analysis, 41–44
E	absorption refrigeration system
Effectiveness of absorption refrigeration	double effect, 82–83
systems, 252, 256	quadruple effect, 164–165

single effect, 55–56	absorption refrigeration system
triple effect, 120–121	double effect, 76–77
Exergoenvironmental impact coefficient, 42,	quadruple effect, 156–159
55, 82, 120, 165	single effect, 50–51
Exergoenvironmental impact factor, 41–42, 55,	triple effect, 112–115
82, 120, 164–165	energy and exergy analyses, 31–33
Exergoenvironmental impact improvement,	Generator absorber heat recovery heat
42–43, 56, 83, 120, 165	exchanger (GAX), 5
Exergoenvironmental impact index, 42, 56,	Generator load effects
82–83, 120, 165	double effect absorption refrigeration
Exergy analyses, 27–39	system, 97–98, 98 <i>f</i> , 99 <i>f</i>
absorption refrigeration system	quadruple effect absorption refrigeration
double effect, 73–81	system, 188–190, 189 <i>f</i>
quadruple effect, 152–163	single effect absorption refrigeration
single effect, 49–54	system, 62–63, 62 <i>f</i> , 63 <i>f</i>
triple effect, 109–118	triple effect absorption refrigeration system,
geothermal-based	140–142, 141 <i>f</i>
multigeneration system, 224–225	Genetic algorithm technique, 44
power, cooling, and liquefied hydrogen	Geothermal-based multigeneration system,
generation system, 200–204	219–228, 219–221 <i>f</i>
solar-based integrated absorption	ambient temperature effects, 227–228, 228f
refrigeration and desalination	geothermal source temperature effects,
system, 210–213	225–227, 225–227 <i>f</i>
Expansion valve, 9–10, 10 <i>f</i> , 30 <i>t</i>	system description, 219–221
absorption refrigeration system	thermodynamic analysis, 221–225
double effect, 79–80	Geothermal-based power, cooling, and
quadruple effect, 161–162	liquefied hydrogen generation
single effect, 53–54	system, 197–207, 199 <i>f</i>
triple effect, 117–118	ambient temperature effects, 206–207, 207f
energy and exergy analyses, 37–38	energy and exergy analyses, 200-204
	geothermal mass flow rate effects, 204–206,
F	204–206 <i>f</i>
First-law of thermodynamics, 27	Linde-Hampson liquefaction cycle, 199,
Flat plate, 17, 253	200, 200 <i>f</i> , 203–204
Fossil fuels-based multigeneration system, 251,	system description, 197-200
251 <i>f</i>	Geothermal source temperature effects
Fresh water production, solar-based integrated	geothermal-based multigeneration system,
absorption refrigeration and	225–227, 225 <i>f</i> , 226 <i>f</i> , 227 <i>f</i>
desalination system for, 207–218,	on exergy efficiencies of the
208f	multigeneration systems, 237–238,
energy and exergy analyses, 210-213	237f, 238f
seawater salinity effects, 217–218, 217f,	on net power generation and rate of
218 <i>f</i>	hydrogen production, 235–236, 236f
solar irradiance effects, 215–217, 215–217f	Gouy-Stodola equation, modified, 255
system description, 207–210	
thermodynamic properties of, 214t, 215t	Н
Fuel cell system	Half effect absorption refrigeration system, 4–5
internal reforming solid oxide fuel cell	Heat exchanger
(IR-SOFC) system, 247, 248 <i>f</i>	quadruple effect absorption refrigeration
solid oxide, 246–248, 247 <i>f</i>	system, 153–155, 162–163
	triple effect absorption refrigeration system,
G	110–112, 118
Gas turbine, 250f	Heat pumps, absorption, 23–24, 24 <i>f</i>
Generator, 5–7, 6 <i>f</i> , 29 <i>t</i>	Heat recovery heat exchanger, 5, 11, 12, 15, 48
Scherator, 5 1, 0j, 250	110at 1000 vory front exchanger, 3, 11, 12, 13, 40

single effect absorption refrigeration system, 50	Multiple effect absorption refrigeration system, 5, 15–17, 16 <i>f</i>
•	3, 13–17, 10j
Heat sources, 17–18	N
Heating	
loads, domestic, 228	Natural gas, 246
system, novel ARS-based, 251–253, 252 <i>f</i> , 253 <i>f</i>	Nelder–Mead simplex algorithm, 45, 68, 104, 146, 195
Heliostat, 250f	Novel ARS
Hextuple effect, 228, 234, 237, 237 <i>f</i> , 238	-based combined heating and power
Hot water, 219, 221, 223, 228, 231, 255	generation systems, 251–253, 252f,
Hydrogen, 229	253 <i>f</i>
Hydrogen generation system, liquefied,	designs, 253–255, 254f
197–207, 199 <i>f</i> , 200 <i>f</i> , 204–207 <i>f</i>	Novel working mixtures, 256–257
	Numerical studies, of absorption refrigeration
I	systems, 255–256
Integrated absorption refrigeration systems,	•
197–239, 198 <i>f</i>	0
geothermal-based	Optimization studies, 44–46, 45f, 46t, 255–256
integrated system, for standalone	absorption refrigeration system
building needs, 228–238, 229f, 235f,	double effect, 83, 104–105, 104 <i>f</i> , 104 <i>t</i> ,
236–238 <i>f</i>	105 <i>f</i>
multigeneration system, 219–228,	quadruple effect, 165, 194–196, 194 <i>t</i> ,
219–221 <i>f</i> , 225–228 <i>f</i>	195 <i>f</i> , 196 <i>f</i>
power, cooling, and liquefied hydrogen	single effect, 56, 67–69, 68f, 68t, 69f
generation system, 197–207, 199 <i>f</i> ,	triple effect, 121, 146–148, 146t, 147f
200f, 204–207f	Organic Rankine cycle (ORC), 243, 248, 249,
solar-based integrated absorption	251, 252, 253 <i>f</i>
refrigeration and desalination	Oxygen, 229
system, 207–218, 208f, 214t,	
215–218 <i>f</i> , 215 <i>t</i>	P
Internal reforming solid oxide fuel cell	Peltier effect, 20
(IR-SOFC) system, 247, 248, 248f	Pentuple effect, 225, 237f, 238
	Photovoltaic cooling system, solar, 19–20, 19f
L	Photovoltaic-thermal system, solar, 207, 209,
Levelized electricity cost (LEC), 253	210–211
Linde-Hampson liquefaction cycle, 199, 200,	Positive displacement pump, 9f
200f, 203–204, 249	Power generation systems
Linear programming technique for	geothermal-based, 197-207, 199f
multidimensional analysis	novel ARS-based, 251–253, 252f, 253f
(LINMAP), 68–69, 69f, 105,	Power plant
195–196, 195, 196 <i>f</i>	binary, 202
Liquefied hydrogen generation system,	double flash, 223
geothermal-based, 197–207, 199f,	quadruple flash, 228-229, 230, 231,
200f, 204–207f	234–235
Liquefied natural gas, 249, 250f	Prototype, 244, 246, 255
Lithium-bromide-water absorption	ACAR, 254
refrigeration system, 3, 4	Pump(s), 9, 29t
. g	absorption heat, 23–24, 24f
M	absorption refrigeration system
Methanol, 22, 23 <i>t</i>	double effect, 73–74
Mixtures, novel working, 256–257	quadruple effect, 152–153

single effect, 49–50	Solar-based diffusion—absorption cooling
triple effect, 110	system, 257
energy and exergy analyses, 28-31	Solar-based integrated absorption refrigeration
positive displacement, 9f	and desalination system, 207–218,
	208f
Q	energy and exergy analyses, 210-213
Quadruple effect absorption refrigeration	seawater salinity effects, 217–218, 217f,
system (QEARS), 5, 16, 16 <i>f</i> ,	218f
149–196, 150 <i>f</i> , 198 <i>f</i> , 225, 237 <i>f</i> , 238	solar irradiance effects, 215–217, 215–217f
ambient temperature effects, 211–212	system description, 207–210
energy and exergy analyses, 152–163	thermodynamic properties of, 214t, 215t
exergoeconomic analysis, 163–164,	Solar irradiance effects, 215–217, 215–217 <i>f</i>
201–202	Solar photovoltaic-thermal (PV/T) system, 207,
exergoenvironmental analysis, 164-165	209, 210–211
geothermal-based	Solar PV cooling system, 19–20, 19f
multigeneration system, 221–223	Solar-steam ejector system, 21, 22t
power, cooling, and liquefied hydrogen	Solar thermoelectric cooling system, 20–21,
generation system, 201–202,	20f
204–206	Solid oxide fuel cell (SOFC) system, 246, 247f
geothermal mass flow rate effects, 204–206,	internal reforming, 247, 248, 248f
204–206 <i>f</i>	Stability, exergetic, 43, 56, 83, 121, 165
illustrative example, 166–196, 187–188 <i>t</i> ,	Standalone building needs, geothermal-based
189–196 <i>f</i> , 194 <i>t</i>	integrated system for, 228–238, 229f
optimization of, 165	cooling load effects, 236–237, 236f
seawater salinity effects, 218	geothermal effects
solar-based integrated, 210–213, 214 <i>t</i>	pressure effects, at state f2, 234–235,
solar irradiance effects, 215, 216	235 <i>f</i>
	source temperature effects, 235–236,
system description, 150–152 Quadruple flash power plant (QFPP), 228–229,	236 <i>f</i>
	•
230, 231, 234–235	multigeneration effects, 237–238, 237 <i>f</i> ,
ъ	238f
R Defricements 2.4	system description, 228–230
Refrigerants, 2–4	thermodynamic analysis, 230–234 Stochastic multi-chicative entimination model
classification of, 3f	Stochastic multi-objective optimization model,
Refrigeration system, absorption. See	255
Absorption refrigeration system	Strong solution concentration effects
(ARS)	double effect absorption refrigeration
Rotartica chiller, 243	system, 98–100, 99f, 100f
g	quadruple effect absorption refrigeration
S	system, 190–191, 190 <i>f</i> , 191 <i>f</i>
Seawater salinity effects, 217–218, 217f, 218f	single effect absorption refrigeration
Second-law of thermodynamics, 27	system, 63–64, 64 <i>f</i>
Single effect absorption refrigeration system	triple effect absorption refrigeration system,
(SEARS), 4, 11–12, 11 <i>f</i> , 47–69, 48 <i>f</i> ,	142–143, 142 <i>f</i> , 143 <i>f</i>
242	Sustainability, exergetic, 43, 56, 83, 121, 165
advanced, 242–246, 242f, 244f, 245f	Sustainable energy, 47, 67, 103, 107, 146, 149,
energy analysis, 49–54	194, 204, 213, 241
exergoeconomic analysis, 54–55	
exergoenvironmental analysis, 55–56	<u>T</u>
exergy analysis, 49–54	Thermodynamic analysis
illustrative example, 56–69, 62–69 <i>f</i> , 62 <i>t</i> ,	energy analysis, 27–39
68 <i>t</i>	exergoeconomic analysis, 39–41, 40f
optimization, 56	exergoenvironmental analysis, 41–44
system description, 48–49	exergy analysis, 27–39

optimization, 44–46, 45f, 46t	Two-stage vapor-compression system
Thermoelectric cooling system	(TSVCS), 255
domestic, 20	
solar, 20–21, 20 <i>f</i>	\mathbf{U}
Thermomechanical cooling system, 21, 21f, 22t	Unused fuel, 43
Triple effect absorption refrigeration system	
(TEARS), 13–15, 14 <i>f</i> , 17, 107–148,	V
108f	Vapor-compression-absorption system
energy and exergy analyses, 109-118	(VCAS), 255
exergoeconomic analysis, 119	Vapor-compression air-conditioning system,
exergoenvironmental analysis, 120-121	20
illustrative example, 121–148, 139–140 <i>t</i> ,	
141–147f	W
optimization, 121	Waste energy, 17
system description, 108–109	Waste exergy, 42, 67, 102
Turbine, gas, 250f	